Fermilab Proposal No. 394

Spokesman: J. Whitmore
Department of Physics
Michigan State University
East Lansing, Mich. 48824

Proposal for a High Statistics Study of Antiproton-Proton Interactions at 100 GeV/c with the Fermilab 30-inch Bubble Chamber

R. E. Ansorge, J. R. Carter, W. W. Neale and J. G. Rushbrooke
Cavendish Laboratory, Cambridge

and

W. Morris, B. Y. Oh, D. L. Parker, G. A. Smith and J. Whitmore
Michigan State University

ABSTRACT

We propose to continue our study of multiparticle production in 100 GeV/c antiproton-proton interactions using the 30-inch hydrogen bubble chamber with one of the downstream hybrid systems and, if possible, forward neutral particle detectors. We request an additional 400,000 pictures with the existing Cerenkov tagged $\bar{p}/\pi^-$ secondary beam. We would propose to take a bubble chamber picture whenever we have 2 or more $\bar{p}$'s/pulse or whenever there is a tagged antiproton interaction. The primary objects of this experiment are (a) a study of the low cross section processes such as several exclusive channels and strange particle production and (b) a detailed comparison with existing 100 GeV/c pp data in an attempt to investigate the annihilation contribution to the $\bar{p}p$ interaction.

I. Introduction

Our collaboration has recently completed (Jan. 27, 1975) the data taking for Experiment 311[1] -- a survey experiment of antiproton-proton interactions at 100 GeV/c using the Fermilab 30-inch bubble chamber-wide gap optical spark chamber hybrid system. The data analysis is progressing rapidly and preliminary results have already been presented[2] on elastic scattering and on the charged multiplicity distributions. We expect to have data soon on neutral particle production and on the inclusive distributions in $\bar{p}p$ interactions. These papers will be submitted in the near future as appendices to this proposal.

On the basis of the current analysis of the charged multiplicity distribution and the scanning results for neutral particle production in E-311, we are requesting an additional 400,000 pictures of a 100 GeV/c Cerenkov tagged enriched $\bar{p}$ beam in the 30-inch bubble chamber filled with hydrogen. Either the wide-gap optical spark chamber system or the proportional wire chamber system should be used downstream of the bubble chamber in order to achieve a more accurate momentum determination for the forward-going charged particles. A downstream neutral particle detector would also be highly desirable.

II. Beam

The results of E-311 have shown that an enriched $\bar{p}$ beam at 100 GeV/c is perfectly adequate for this current bubble chamber proposal. By selecting a 100 GeV/c negative particle beam from the target "halo" produced[3] by the decays of Λ, $\bar{\Lambda}$, and K°, we have obtained[2] 0.2 $\bar{p}$'s/negative beam particle. By using (a) a deflection trigger on a tagged $\bar{p}$ beam particle or (b) the requirement that there be 2 or more p's/pulse before taking a bubble chamber picture,

we have taken 98,000 pictures containing 0.32 $\bar{p}$'s/negative beam particle. By putting ~6 particles/pulse into the 30-inch bubble chamber we have obatined ~5,000 pp and 5000 π^-p interactions per 34,000 bubble chamber pictures in about 68,000 chamber expansions and 17,000 accelerator cycles. While some beam tests have been made and further tests could be made to investigate more optimum beam settings, we think that the beam used in E-311 is acceptable for this current proposal and would expect to take the 400,000 pictures in less than 200,000 accelerator cycles.

III. Physics Motivation

The primary motivation for requesting further pictures at 100 GeV/c is based on preliminary analyses of data from E-311:

(1) The $\bar{p}p$ topological cross sections, shown in Table I and Figure 1, show interesting differences when compared to pp data at 102 GeV/c. The trend seems to be for the lower multiplicity (i.e., 2 and 4 prong) cross sections to be smaller for $\bar{p}p$ than for pp, while the higher charged multiplicity (i.e., $\geq$ .14 prongs) cross sections are significantly larger than the corresponding pp values. With an increase in statistics by a factor of 5 we should be able to study this difference in much greater detail than will be possible in E-311.

(2) Based on scanning results from E-311, we estimate that in 400,000 pictures we would have 10,000 neutral particle events in which we detect at least one γ conversion or strange particle decay. Based on results from pp experiments[4], about one-half of these will be strange particle decays. With these statistics we should be able to make a comprehensive search for excited

states (charm??) which decay into a strange particle (K_S^o, Λ, $\bar{\Lambda}$) and between 1 and $\lesssim$ 18 charged pions. It is important to note that a bubble chamber is an excellent 4π detector for studying excited states decaying into $\geq$ 3 particles. The statistical level of this proposed experiment is about 60,000 $\bar{p}p$ events/42 mb $\approx$ 1.5 ev/μb.

We will also determine the single particle inclusive distributions for $\bar{p}p \rightarrow K_S^o$, $\Lambda/\bar{\Lambda}$ as well as the two particle correlations between strange and charged particle production.

With the ~5000 γ conversions we should be able to make a significant contribution to the knowledge of π^o-$\pi^\pm$ correlations at Fermilab energies. In addition, we may be able to study inclusive $\Sigma^o/\bar{\Sigma}^o$ production by directly observing the $\Lambda\gamma/\bar{\Lambda}\gamma$ decay mode. Similarly, we may be able to set limits on the inclusive η^o production by studying the $\gamma\gamma$ final state. The following topics are currently being investigated in E-311 and will benefit greatly from an increased number of events:

(3) <u>Exclusive processes</u>:

(a) Elastic scattering: We estimate[2] that in 400,000 pictures we will obtain ~10,000 elastic events with four-momentum transfer, t, between -0.02 and -0.7 $(GeV/c)^2$. While this cannot statistically compete with counter experiments investigating elastic scattering for $|t| < 0.1$ $(GeV/c)^2$, these data will be a useful check. We show in Fig. 2 preliminary t distributions for $\bar{p}p$ and π^-p elastic scattering from E-311.

(b) Assuming that the cross section for the reaction $\bar{p}p \rightarrow \bar{p}p\pi^+\pi^-$ is about 700 μb (as is[4] the $pp \rightarrow pp\pi^+\pi^-$ cross section) we will

obtain approximately 1000 4-constraint events. It will be interesting to study this final state to see if the $\Delta\bar{\Delta}$ final state continues to have a large contribution to this reaction at 100 GeV/c as is found at lower energies[5], or whether it is almost completely diffractive in nature as found in the corresponding pp reaction at Fermilab energies.[4]

(c) We would hope to be able to obtain a sample of the reaction

$$\bar{p}p \rightarrow \bar{p}p2\pi^+2\pi^-$$

which may have a cross section of ~300 μb if it is similar to the pp reaction.

(d) For all these exclusive channels, it will be important to have a downstream hybrid system available to provide better discrimination against single pion production. Furthermore, use can be made of the charge conjugate symmetry of the $\bar{p}p$ system.

(4) Diffractive processes:

Diffractive excitation has been extensively studied in πp and pp interactions between 100 and 400 GeV/c at Fermilab. With the statistics available in this experiment we will be able to make a detailed comparison of both target and projectile fragmention into $\pi^{\pm}$, $p/\bar{p}$ with similar data in pp and πp interactions. While pomeron factorization is often used to relate these processes, no detailed check at very high energies has been made other than in π^+p (and pp) $\rightarrow \pi^{\pm}$ + anything at 100 GeV/c. These results[6] indicated that factorization seems to work in π^+p (pp) $\rightarrow \pi^-$ + X reactions, but not for the π^+ production data. It will be of interest

to compare such data with those obtained from 100 GeV/c $\bar{p}p$ interactions.

(5) Inclusive distributions:

Because of the interest in $\bar{p}p$ annihilations, it is important to obtain a sample of events which are primarily $\bar{p}p$ annihilations. Since it will be difficult to do this on an event by event basis (although we can remove obvious nonannihilation interactions which have a final state proton, Λ, $\bar{\Lambda}$, or anti-proton -- defined as a negative track with laboratory momentum greater than ~80 GeV/c), we will need high statistics in order to make a more meaningful separation on a statistical basis. Similarly, high statistics will be required in order to make a detailed comparison (as functions of x, y, P_T, etc.) with inclusive $\pi^{\pm}$, p distributions as measured in pp interactions at 100 GeV/c.

(6) Two Particle correlations

Correlations between two charged particles will be studied as a function of their rapidity and transverse momentum separation. It will be of particular interest to compare these data with similar data in pp for events with high charged particle multiplicity, i.e., semi-inclusively for $n_c \gtrsim 14$ where one might expect (see Fig. 1) that the annihilation contribution is particularly enhanced. Differences between the $\bar{p}p$ and pp data might shed some light on the high energy annihilation process.

IV. Summary

(1) Exposure: We request an additional 400,000 pictures of a 100 GeV/c $\bar{p}/\pi^-$ Cerenkov-tagged beam in the 30-inch hydrogen bubble chamber. We

estimate that with either the interaction trigger or the $\gtrsim 2$ $\bar{p}$'s/pulse selection, we will obtain ~60,000 $\bar{p}p$ and another 60,000 $\pi^- p$ events. We will measure every $\bar{p}p$ event and would expect to analyze most of the $\pi^- p$ data as well, although at a lower priority.

(2) Primary objectives: The basis for requesting a high statistics bubble chamber exposure is (a) to study the low cross section processes such as $\bar{p}p \to \bar{p}p\pi^+\pi^-$ and neutral strange particle production (and a search for charmed states?) and (b) to make a detailed comparison, as a function of various kinematic variables and/or final states, with similar data from pp interactions. In this regard, it is worth noting the extent of existing ~100 GeV/c pp 30-inch bubble chamber data:

102 GeV/c E-252	Michigan-Rochester	33,000	pictures	100% pp
100 GeV/c E-121	U of Calif.-Davis	104,000	"	~60% pp,~40% π^+p
100 GeV/c E-2B	Purdue-Wisconsin	80,000	"	~60%pp,~40% π^+p
150 GeV/c E-299	MWPC Consortium	158,000	"	~50% pp,~50% π^+p

Thus our request for 400,000 pictures should permit a detailed comparison with comparable statistics for final states produced by pp and $\bar{p}p$ interactions.

(3) Other experiments: To the best of our knowledge, there are no other experiments planned to make a comprehensive study of $\bar{p}p$ interactions (except for a survey experiment, E-344 between 40-60 GeV/c at Fermilab) at momenta above 40 GeV/c. Furthermore, the only high statistics $\bar{p}p$ bubble chamber exposure above 7 GeV/c is a CERN experiment at 12 GeV/c. We feel that a large statistics $\bar{p}p$ experiment at Fermilab would be extremely useful for comparison with the 12 GeV/c data.

REFERENCES

1. Fermilab Experiment E-311: Cambridge, Fermilab, Michigan State University collaboration.
2. J. G. Rushbrooke, BAPS 20, 545 (1975); J. Whitmore, IV International Conference on $\bar{N}N$ Interactions, Syracuse, N.Y., May 1975.
3. W. W. Neale, Fermilab Report FN-259, June 24, 1974.
4. J. Whitmore, Phys. Rep. 10C, 273 (1974).
5. I. Borecka *et al.*, Nuovo Cimento 5A, 19 (1971).
6. J. Erwin *et al.*, Phys. Rev. Letters 33, 1352 (1974).

Table I

Topological Cross Sections for 100 GeV/c $\bar{p}p$ Interactions

Cambridge-Fermilab-MSU

(Experiment #311 - Preliminary Results)

Prong number	Number observed	Corrected number	Cross-section (mb)	102 GeV/c pp (2)
0	6	6	0.053 ± .022	
2	el. 498	829	7.39 ± .31	7.0 ± .4
	inel. 431	443	3.95 ± .36	4.5 ± .4
4	856	869	7.75 ± .24	7.9 ± .3
6	905	906	8.08 ± .24	7.5 ± .3
8	796	790	7.05 ± .23	5.8 ± .2
10	468	461	4.11 ± .18	3.7 ± .2
12	242	235	2.10 ± .13	1.6 ± .1
14	113	109	0.972 ± .090	0.62 ± .07
16	51	49	0.437 ± .061	0.21 ± .04
18	14	13	0.115 ± .031	0.05 ± .02
20	4	4	0.036 ± .018	0.016± .011
Total inelastic		3885	34.65 ± .23	31.9 ± 0.7
Total	4384	4714	42.04 ± .09 (1)	38.9 ± .8

(1) A. S. Carroll et al., Phys. Rev. Lett. 33, 928, 932 (1974).

(2) C. Bromberg et al., Phys. Rev. Lett. 31, 1563 (1973).

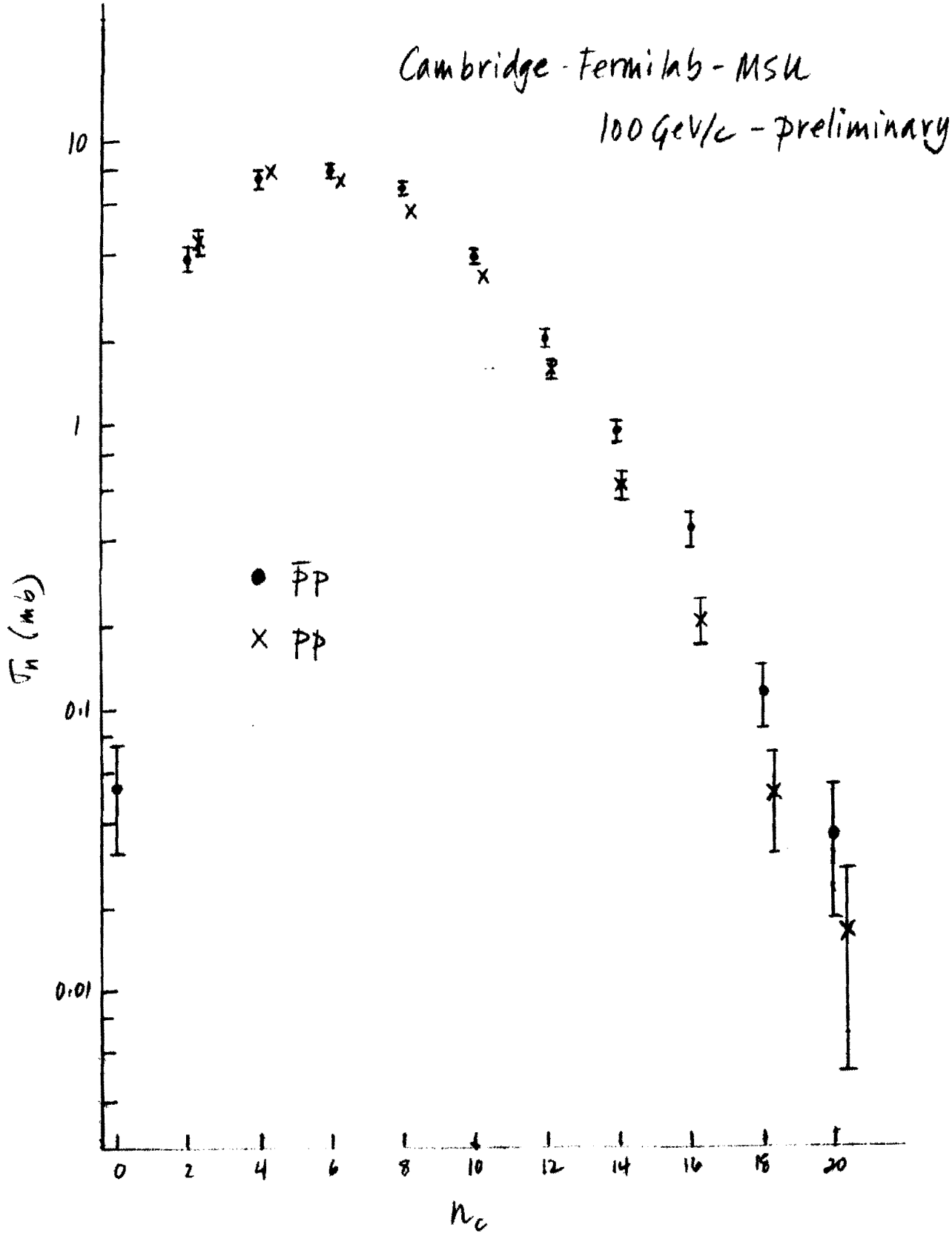
Cambridge - Fermilab - MSU
100 GeV/c - preliminary
10
1
0.1
0.01
σ_n (mb)
● $\bar{p}p$
× pp
0
2
4
6
8
10
12
14
16
18
20
n_c

Figure 1

CAMBRIDGE - FERMILAB - MSU

May 16, 1975

100 GeV/c Elastic scattering - Preliminary

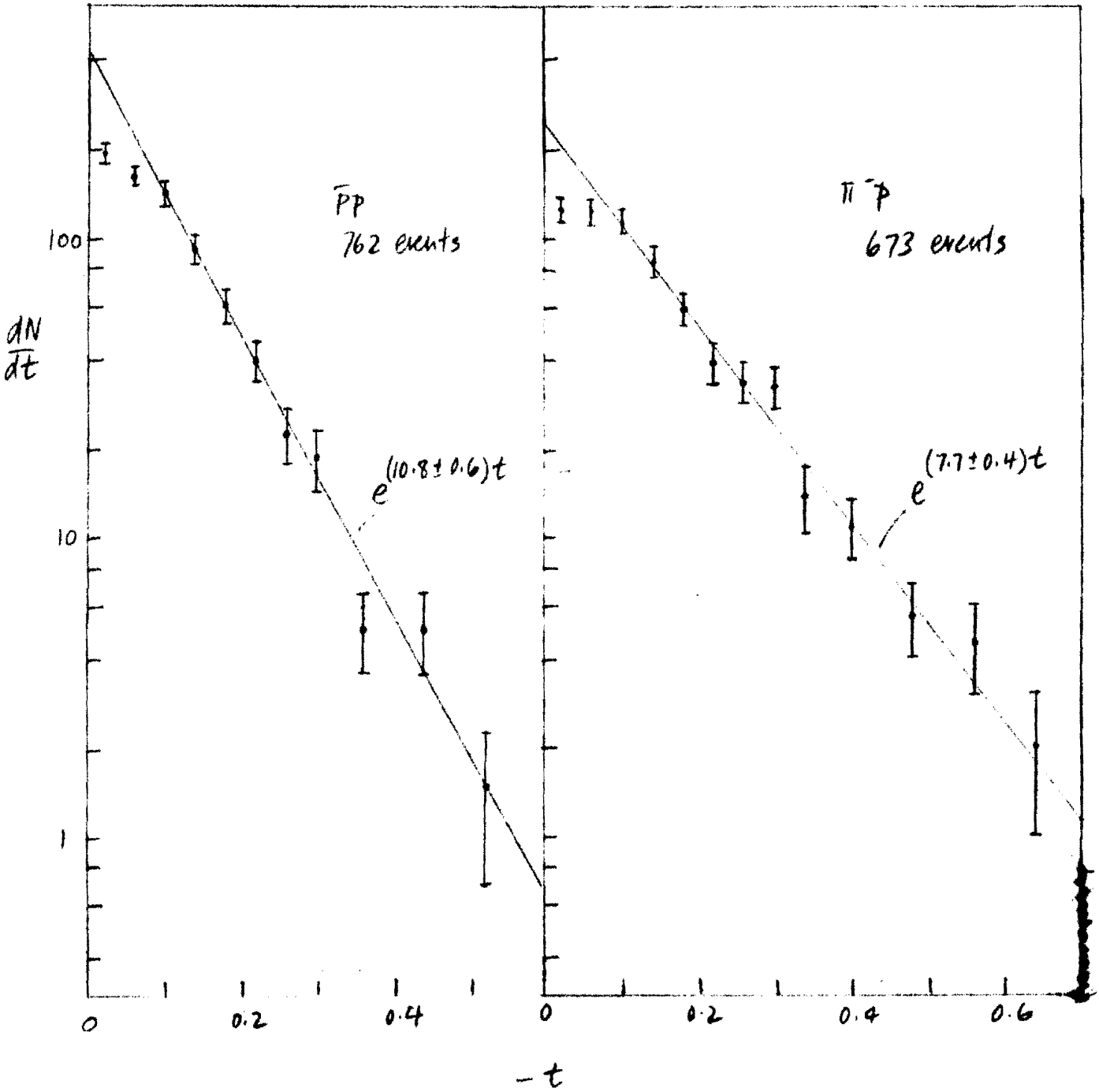

Figure 2

Spokesman: J. Whitmore
Department of Physics
Michigan State University
East Lansing, Mich. 48824
517-353-5180

Fermilab Proposal No. 394 (Rev.)

PROPOSAL FOR A HIGH STATISTICS STUDY OF ANTIPROTON-PROTON AND PROTON-PROTON INTERACTIONS AT 100 GeV/c WITH THE FERMILAB 30-INCH HYDROGEN BUBBLE CHAMBER SPECTROMETER AND EXTERNAL PARTICLE IDENTIFIER

R. E. ANSORGE, J R. CARTER, W. W. NEALE,
J. G. RUSHBROOKE, D. R. WARD and T. O. WHITE
Cavendish Laboratory, University of Cambridge, Cambridge, England

C. MOORE, R. RAJA, L. VOYVODIC and R. WALKER
Fermi National Accelerator Laboratory, Batavia, Illinois, U.S.A.

B. Y. OH, M. PRATAP, G. A. SMITH and J. WHITMORE
Department of Physics, Michigan State University, East Lansing, Michigan, U.S.A.

G. EKSPONG, S. O. HOLMGREN, S. NILSSON and N. YAMDAGNI
Institute of Physics, University of Stockholm, Stockholm, Sweden

plus additional U.S. and European institutions to be added later.

7 January 1976

ABSTRACT

We propose to continue our studies of multiparticle production at high energies by performing two high statistics experiments with 100 GeV/c antiproton-proton and proton-proton interactions using the Fermilab 30-inch hydrogen bubble chamber spectrometer with a downstream external particle identifier for $p/K/\pi$ separation. We request 10^6 pictures with a Cerenkov-tagged $\bar{p}/\pi^-$ secondary beam and a like number of pictures with a tagged p/π^+ beam. The primary goals of these experiments are: (a) a measurement of the $\bar{p}p$ annihilation cross section and a study of the multiparticle production in baryon annihilation events, (b) a study of the $K\pi$ correlations in both $\bar{p}p$ and pp interactions, (c) a study of the low cross section processes such as exclusive channels and neutral particle production, and (d) a high statistics comparison between $\bar{p}p$ and pp interactions.

Since there will be a large number of $\pi^{\pm}p$ interactions in this film, these events will permit a high statistics study of many of the above topics in $\pi^{\pm}p$ reactions. A separate proposal which will guarantee that the πp data will be analyzed will follow shortly.

1. INTRODUCTION

Our collaboration completed data taking for experiment 311 in January 1975. This experiment was a survey experiment of 100 K pictures of antiproton-proton interactions at 100 GeV/c using the Fermilab 30-inch bubble chamber-wide gap optical spark chamber hybrid system. The data analysis is progressing rapidly with most of the ~15,000 $\bar{p}p$ events having been measured. Two papers on the multiplicity distributions in $\bar{p}p$ and pp interactions are already published[1,2], and a paper on the annihilation effects in neutral particle production is nearing completion.[3]

On the basis of the current analysis of E-311 as well as other studies of high energy interactions at Fermilab, we are requesting 10^6 pictures of a 100 GeV/c Cerenkov-tagged enriched $\bar{p}$ beam and 10^6 pictures of a 100 GeV/c Cerenkov-tagged p/π^+ beam into the 30-inch bubble chamber filled with hydrogen. A novel feature of this proposal is the planned use of an External Particle Identifier (EPI) in order to identify the antiprotons and protons which emerge from the chamber. With such a device we expect to obtain a highly enriched sample of baryon annihilation events. Another extremely important use of the proposed system would be to identify a large fraction of the central region kaons. With this information, as well as the neutral kaon detection in the bubble chamber itself, one can study interesting topics such as the rapidity gap distribution for strangeness exchange and the two particle correlations between $K^-\pi^-$, $K^+\pi^+$ and $K^\mp\pi^\pm$ (and $K\bar{K}$). Since significant like-particle effects have been observed in $\pi^\pm\pi^\pm$ correlations[4], it would be most interesting to study other combinations such as $K^\pm\pi^\pm$ which are still exotic but do not consist of two identical particles.

2. BEAM AND BUBBLE CHAMBER

The results of E-311 have shown that an enriched $\bar{p}$ beam at 100 GeV/c is perfectly adequate for the current proposal. However, recent computer studies by Neale have shown that with a modification to the N3 beam line significant improvements should result in both the $\bar{p}/\pi^-$ ratio as well as the flux at the bubble chamber of $\bar{p}$'s per incident primary proton.

During the run of E-311 a negative beam containing 20 per cent $\bar{p}$'s at 100 GeV/c [5] was obtained from the target "halo" produced by the decays of Λ, $\bar{\Lambda}$ and K°. By using (a) a deflection trigger on a tagged $\bar{p}$ beam particle or (b) the requirement that there be 2 or more $\bar{p}$'s/pulse before taking a bubble chamber picture we took 98,000 pictures containing 0.32 $\bar{p}$'s/negative beam

particle. With the collimators wide open a flux of 30-40 $\bar{p}$'s/10" incident protons was obtained which was more than adequate for the quadruple pulsing of the bubble chamber.

The E-311 exposure was carried out with a 300 GeV incident proton beam. However, 400 GeV protons are now available on a regular basis and should lead to a factor of 2 increase in both the $\bar{p}$ flux and the $\bar{p}/\pi^-$ ratio. Several dipole and quadrupole magnets have been replaced since our run with magnets of significantly larger aperture which should lead to a further increase in the $\bar{p}$ flux. Simply by running with 400 GeV protons it should be possible to achieve the same number of $\bar{p}$ interactions per picture as in the E-311 experiment without triggering the bubble chamber flash.

Calculations[6] indicate that by closing down the horizontal aperture of the beam dump from 25 mm to 10 mm the $\bar{p}/\pi^-$ ratio could be improved by up to a factor 2 but at the expense of losing a factor 2 in flux. This would lead to a beam containing equal numbers of $\bar{p}$'s and π^-'s.

In summary, it seems most likely that we would no longer need to trigger the bubble chamber flash and we should be able to multipulse the 30-inch chamber. Hence, the 10^6 $\bar{p}p/\pi^-p$ pictures could be taken in $\sim 10^6$ chamber expansions and $\sim$250 K accelerator cycles assuming quadruple pulsing. The currently existing beam line is quite adequate for the proposed 50% pp/50% π^+p exposure and again multipulsing the chamber will be feasible.

We would plan to use the current upstream system of proportional wire chambers (PWC) and beam Cerenkov counter to tag each beam track entering the bubble chamber.

Finally, we should mention that we would request a beam spill of $\sim$1 msec because of the design features of the proposed EPI. To obtain such a spill would not appear to present any problems. We think that the proposed experiments

should be run as soon as possible and that a rapid cycling bubble chamber, while highly desirable, is not essential. In this regard, the above considerations show that we would expect ~4-6 $\bar{p}$'s per bubble chamber expansion assuming 10^{11} protons on target per accelerator cycle and 15 bubble chamber expansions per accelerator cycle.

3. EXTERNAL PARTICLE IDENTIFIER (EPI)

The primary object of the proposed experiment is to identify as many of the produced particles as possible, i.e. one wants to identify the leading particles (generally p, $\bar{p}$ or π) if they exist, as well as those particles produced in the central region (generally π's and K's). To do this, two possible systems could be used: (1) a system of multicell threshold Cerenkov counters, or (2) a particle identification system based on detecting the relativistic rise in ionization. Since no such Cerenkov system exists at the present time (although plans are being made for such a system for the CERN RCBC project) and since an EPI based on detecting the relativistic rise of the ionization loss in gaseous detectors does exist at CERN and encouraging tests have been made, we would propose to use the latter for this experiment. However, should this sytem (described below) not become available for use at Fermilab, detailed plans are currently underway to design a Cerenkov counter system which would identify leading particles (p/π) with momentum between 20 and 100 GeV/c and central region particles below 20 GeV/c (K/π)[7].

The system we would propose to use is the CERN EPI which was designed for use behind BEBC with the RF beam and which is currently under construction. Details of the system as well as the results of tests made at CERN are described in papers[8,9] included as Appendix A. Basically, the system consists of 128 layers (88 presently exist) of 32 (6 x 90 cm^2) individual proportional

counters (cells) each of which is 6 cm thick (see fig. 1). Ionization deposited in the detector is sampled by measuring the pulse height from each cell traversed by the charged particles. The circulating gas would be a 95% Ar-5% CH_4 mixture which gives a satisfactory relativistic rise. Monte Carlo calculations, substantiated by the tests, indicate that one can obtain 5.5% FWHM ionization resolution on a track which passes through all 128 layers.

To examine the suitability of the EPI for the proposed experiment, we have used ~4200 inelastic $\bar{p}p$ events (see fig. 2) obtained from E-311. To investigate the properties of the leading $\bar{p}$ (or p in pp collisions), we have identified slow protons and π's by ionization in the bubble chamber, transformed their laboratory 3-momenta into the center-of-mass system and reversed them, and then transformed them back into the laboratory system. Using these events we find the following:

(a) Typically ~50% of the tracks from a given event make their way into the EPI (see fig. 3). Many slow particles do not traverse the exit aperature of the bubble chamber magnet.

(b) For a sample of events examined in detail (see fig. 4 for examples), we estimate that the average resulting resolution on ionization, after folding in the probability of more than 1 track entering the same cell, is better than ~6% FWHM.

(c) As can be seen in fig. 4, the efficiency for finding the $\bar{p}$ alone in a large number of cells is extremely high.

A few minor modifications have to be made to use the existing system in the proposed configuration at Fermilab:

(d) Because of the horizontal magnetic field, the entire device would be rotated by 90°. This presents no technical difficulties, although a new support frame will have to be constructed.

(e) We would not make use of the existing beam hole, which is an insensitive area (6 x 36 cm^2) made necessary by the tight (~5 μsec) time structure of the RF beam into BEBC. The EPI would be centered on the beam axis and this insensitive area would then be at the bottom where the loss of solid angle would cause only a minimum loss of track information (see fig. 1).

(f) For BEBC the EPI electronics are triggered by a signal at the start of the RF beam spill. For our application, we will provide an interaction trigger signal. This trigger will be generated by two small PWC's upstream and downstream of the bubble chamber when an interaction (deflection) occurs in the beam.

(g) Minor electronics modifications would have to be made to decrease the dead time of the system from the present 255 μsec to $\lesssim$ 75 μsec. If we then have a 1 msec beam spill and 6 tracks, there is a $\lesssim$ 27% probability that a beam track will overlap an event in time. However if we also require that the 2 tracks (one beam, one produced) are in the same 6 cm cell, then the probability drops to $\lesssim$13% (see fig. 5). This represents an upper limit, is unbiased and only causes a possible loss of data concerning identification of very forward $\bar{p}$'s or p's, with no anticipated effect on the K/π separation in the central region.

To effectively use the information from the EPI requires that the momentum of the particle be known to ~7% and that one has information on the position of each track entering and leaving the EPI. With the proposed use of the EPI, three sets of PWC's would be required, one immediately behind the bubble chamber, one directly in front of the EPI and one directly behind the EPI. The latter two would have dimensions of 1 x 2 m^2 in order to fully cover

the EPI. Such a set of planes should yield the desired momentum resolution. With a straightforward shift of ~5 meters for apparatus downstream of the EPI, the above configuration is consistent with the improved 30-inch BC-Hybrid scheme of Plano and co-workers[10].

4. PHYSICS MOTIVATION

The primary objectives of this experiment are twofold: to study the baryon annihilation process at high energy and to investigate the central region correlations between kaons and pions. These and other topics will now be discussed in more detail.

(1) $\bar{p}p$ Annihilations

If one estimates that the total annihilation cross section is given by the difference between $\bar{p}p$ and pp total cross sections, then at 100 GeV/c σ_{ann} ~3.5 mb (see fig. 6). It is extremely important to measure the total annihilation cross section directly and to compare with the difference $\sigma_T(\bar{p}p) - \sigma_T(pp)$. Using the EPI we hope to be able to obtain a highly enriched sample of annihilation events because only the final states with both n and $\bar{n}$ cannot be found with this system. Estimates of these events may be made assuming that the 2 vertices can be factorized: i.e. from $\bar{p}p \to \bar{n}p + X$, $\bar{p}p \to \bar{p}n + X$ and $\bar{p}p \to \bar{p}p + X$ one can estimate the inclusive distributions for $\bar{p}p \to \bar{n}n + X$.

(2) Multiplicities

The $\bar{p}p$ topological cross sections, shown in the papers[1-2] from E-311 that have been included as Appendix B, show interesting differences when compared to pp at 100 GeV/c. The trend seems to be for the low multiplicity $\bar{p}p$ cross sections to be smaller than the pp ones, while the higher charged multiplicity (i.e. $\gtrsim$ 14 prongs) cross sections are significantly larger

than the corresponding pp values. This suggests that annihilations occur mainly in the high multiplicity events. (If this is true, it will be difficult to study these events in anything but a bubble chamber). With an increase in statistics by a factor of 10 for both $\bar{p}p$ and pp, we will be able to study this difference in much greater detail.

(3) Neutral and strange particle production

The results[3] from E-311, also included in Appendix B, show that the differences in single particle production spectra occur mainly in the central region suggesting that the annihilation process is a more central collision than the pp reaction. Clearly, a factor of 10 (again for both $\bar{p}p$ and pp) will make such studies more conclusive.

With the identification of K_S^o, $K^{\pm}$, Λ and $\bar{\Lambda}$ in a large number of events (see summary in table 1) one might expect to study the process of strangeness exchange in both pp and $\bar{p}p$ interactions. For example, what is the rapidity gap distribution between the 2 strange particles? How locally is strangeness conserved? The answers to these questions (along with the analogous questions relating to charge exchange) could be most revealing.

With such data it will also be possible to estimate how often annihilations occur which yield K's in the final state and to make a comprehensive search for excited states which decay into a strange particle and one or more pions.

(4) Single particle inclusive distributions

With the data that we obtain in this experiment we will be able to make detailed comparisons between $\bar{p}p$ and pp inelastic interactions and between $\bar{p}p$ annihilations and pp interactions. The latter comparison studied as a

function of x, y, p_T, etc., should yield information about the annihilation process. It will also be interesting to compare these data with similar $\bar{p}p$ data that already exist at incident momenta below ~20 GeV/c. For example, fig. 7 shows the cm rapidity distribution for $\bar{p}p \to \pi^+ +$ anything, for annihilation and nonannihilation interactions combined, at 4.6, 9.1, 14.8 and 100 GeV/c. In view of the strong energy dependence observed at $y = 0$ it would be most interesting to study such distributions separately for annihilations and nonannihilations.

(5) Two-particle correlations

One of the interesting features observed in $\pi^- p$ and pp interactions at Fermilab energies is the strong dependence of the two particle correlation function on the azimuthal angular separation for a pair of like pions.[4] Figure 8 shows a strong like-particle correlation for $\Delta\phi \sim 0$ and the absence of a correlation for $\Delta\phi \sim \pi$. It would be interesting to learn whether this effect is due to the bose statistics of two identical particles. One may be able to learn more about such effects by studying $K^{\pm}\pi^{\pm}$ correlations in a similar manner.

Another correlation which has been observed at lower energies is that between neutral and charged pions. Whereas a positive correlation is observed in $\bar{p}p$ interactions at 15 GeV/c where the annihilation-nonannihilation separation was not possible, the correlation for $\bar{p}p$ annihilations at 4.6 GeV/c has been found to be negative. By identifying events with a proton and/or antiproton we should be able to study the $\pi^o\pi^c$ correlation separately for annihilation and nonannihilation at 100 GeV/c.

Interesting results have been obtained from those pp events which have an identified slow proton. With such events, studies have been made of the charged multiplicity of the recoiling system as well as single

particle distributions of $\pi^{\pm}$ in the recoiling system. Interpretations of these data have been made in terms of Pomeron-particle interactions. By identifying both a slow proton as well as a fast leading proton or antiproton one may hope to learn about the diffractive excitation of the Pomeron as well as study the inclusive double Pomeron exchange process with high statistics.

(6) Exclusive channels

Figure 9 shows a summary of the 4 and 6 body final states in $\bar{p}p$ interactions. By extrapolation to 100 GeV/c, one can estimate the numbers of events expected for various annihilation and nonannihilation final states. These are given in table 1 along with similar values for the pp exposure. With the expected numbers of $\bar{p}p\pi^+\pi^-$ and $pp\pi^+\pi^-$ events one will be able to make interesting comparisons at 100 GeV/c. The number of annihilation events expected in the low ($\lesssim 6$) multiplicities will be too small to permit much analysis, but it could be that the cross sections for annihilations to 8π and up will be large enough to permit some interesting analysis.

5. SUMMARY

(1) Exposure: We request 10^6 pictures of a 100 GeV/c $\bar{p}/\pi^-$ and 10^6 pictures of a 100 GeV/c p/π^+ Cerenkov-tagged beam in the 30-inch hydrogen bubble chamber spectrometer. We would hope that a $\bar{p}/\pi^-$ ratio of about 0.6 could be obtained with minor modifications to the present beam line and that a p/π^+ ratio of about 0.6 could be used for the positive beam. We request that a beam spill of ~1 msec be provided to the bubble chamber.

(2) Downstream EPI: We would like to use the EPI that is currently being constructed at CERN. Such a system is expected to be able

to identify both leading particles as well as a large number of central region particles. With the improved 30-inch BC-Hybrid system proposed by Plano and co-workers[10] (modified somewhat to allow for the 8m long EPI) one should be able to measure fast forward secondaries with considerable precision, certainly well within the requirements for particle identification in the EPI. Figure 10a shows the proposed layout[10], with our suggested modifications to that plan shown in Figure 10b. It is our opinion based on a detailed study of requirements dictated by physics that additional space, beyond that allocated in Fig. 10a, is essential for adequate particle identification. Hence, we have found it necessary to displace the elements beyond the EPI by up to ~5 meters in some instances. We feel this will not result in any major changes in the physics capabilities of the spectrometer system.

(3) Equipment: The EPI system would come with its own NORD-10 computer and peripherals. The existing system including the PDP-11 for upstream and downstream tagging information will be utilized. A support frame for the EPI must be built upon completion of the design work at CERN.

(4) Time: It is expected that the full 128 layers of the EPI will become available in mid-1977.[11] We expect therefore that if approved these two large exposures could begin taking data at that time. We would also request a few weeks of time in the bubble chamber beam both to test fluxes for the $\bar{p}$ beam and for testing of the EPI.

REFERENCES AND FOOTNOTES

1. R. E. Ansorge et al., Physics Letters 59B, 299 (1975).
2. J. G. Rushbrooke et al., Physics Letters 59B, 303 (1975).
3. "Annihilation Effects in Neutral Particle Production in 100 GeV/c $\bar{p}p$ Interactions", D. R. Ward et al., Cambridge, Fermilab, Michigan State preprint, November, 1975.
4. B. Y. Oh et al., Physics Letters 56B, 400 (1975).
5. W. W. Neale, Fermilab Report FN-259, June, 1974.
6. W. W. Neale, private communication.
7. The CERN EPI, in the proposed configuration at Fermilab, would have outside dimensions of 1m (H) x 2m (V) x 8m long and is capable of separating π's and K's from ~3 to ~40 GeV/c, π's and $\bar{p}$'s (p's) from ~3 to ~100 GeV/c and K's and $\bar{p}$'s (p's) from ~6 to ~70 GeV/c on a single particle basis with efficiencies of >90%, >90% and >80% respectively. To do a comparable job with multicell threshold Cerenkov counters would require a set of five such counters in order to provide the same range of mass and momentum sensitivity. Such a system is being considered for the CERN RCBC project [CERN/D.Ph. II/RCBC 75-8, 75-12A, 75-24]. The estimated cost is 2 MSF (~$800,000) and the overall length of this system of counters is $\gtrsim$19m. As will be noted later, the CERN EPI is presently nearly completed at a total cost of ~0.9 MSF (~$400,000) (see reference 8). Hence, the above considerations of cost (funds already expended versus funds yet to be allocated), size (8m versus $\gtrsim$19m length) and proven technical performance make it clear that the CERN EPI is desired for external particle identification with the 30-inch bubble chamber spectrometer at Fermilab.

8. M. Aderholz et al., Nuclear Instruments and Methods 118, 49 (1974).

9. M. Aderholz et al., Nuclear Instruments and Methods 123, 237 (1975).

10. "Improved 30" BC-Hybrid System", R. J. Plano et al., September 27, 1974.

11. The technical features of the CERN EPI, as well as a possible schedule for use of the EPI at Fermilab, were explored by G. A. Smith (MSU) and J. Whitmore (MSU) on separate visits to CERN in November-December, 1975. Discussions were held with P. Lazeyras, I. Lehraus, L. Montanet, L. Van Hove, members of the CERN technical staff, and various physicists outside of CERN. To the best of our knowledge, at this time a formal decision to commit the EPI to a program of research at Fermilab has not been made. Based on the previously mentioned discussions, it is our opinion that the EPI could be available at Fermilab by mid-1977. This schedule would permit the completion of the construction of the EPI, possible further tests of the EPI at CERN and a possible 3-6 month research program of hadrons from the SPS into BEBC with the EPI.

TABLE I

ESTIMATES OF NUMBER OF EVENTS TO BE OBTAINED[a]

	Negative beam	Positive beam
Events/μb	$\bar{p}p$ 4.0	pp 4.0
Total events	168,000	154,000
Elastic	30,000	27,700
Inelastic 2 prong	14,400	17,800
" 4 "	32,200	31,300
" 6 "	33,000	29,700
" 8 "	27,700	23,000
" 10 "	16,400	14,600
" 12 "	8,800	6,300
" 14 "	3,600	2,500
" 16 "	1,400	830
" 18 "	480	200
" 20 "	160	63
" 22 "	40	--
K_S^o	7,700[b]	5,600
Λ	3,800[b]	4,900
$\bar{\Lambda}$	820[b]	220
γ	12,600[b]	11,500
$pp\pi^+\pi^-$	> 4,000	3,300
$pp2\pi^+2\pi^-$	> 1,300	1,300
$4\pi/6\pi/8\pi$	~10/~40/~40	--
Total Annihilation	14,000	--

(a) Based on 10^6 pictures of $\bar{p}/\pi^-$ and 10^6 pictures of p/π^+.
(b) Based on the data of E-311.

Fig. 1. Schematic Drawing (not to scale) of CERN EPI.

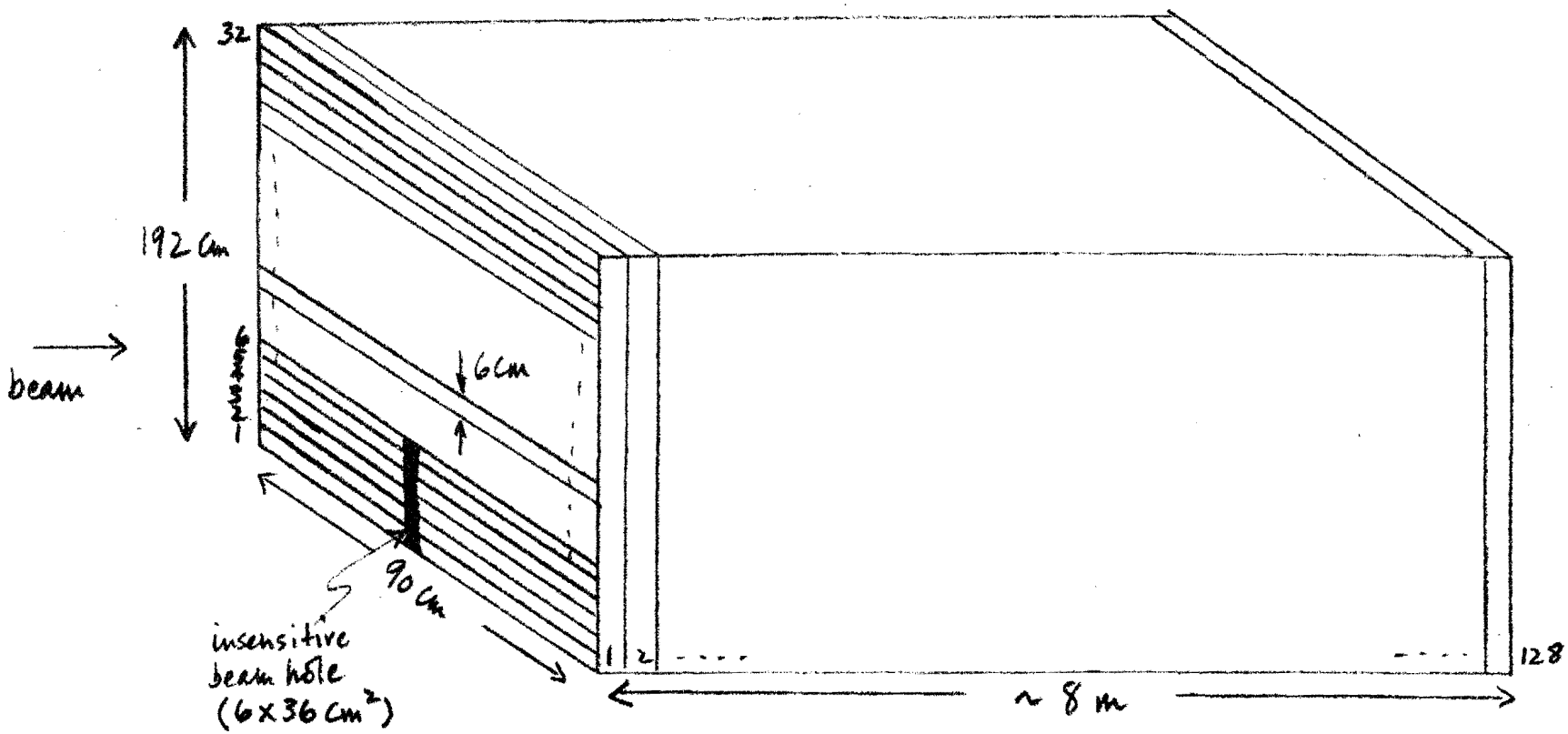

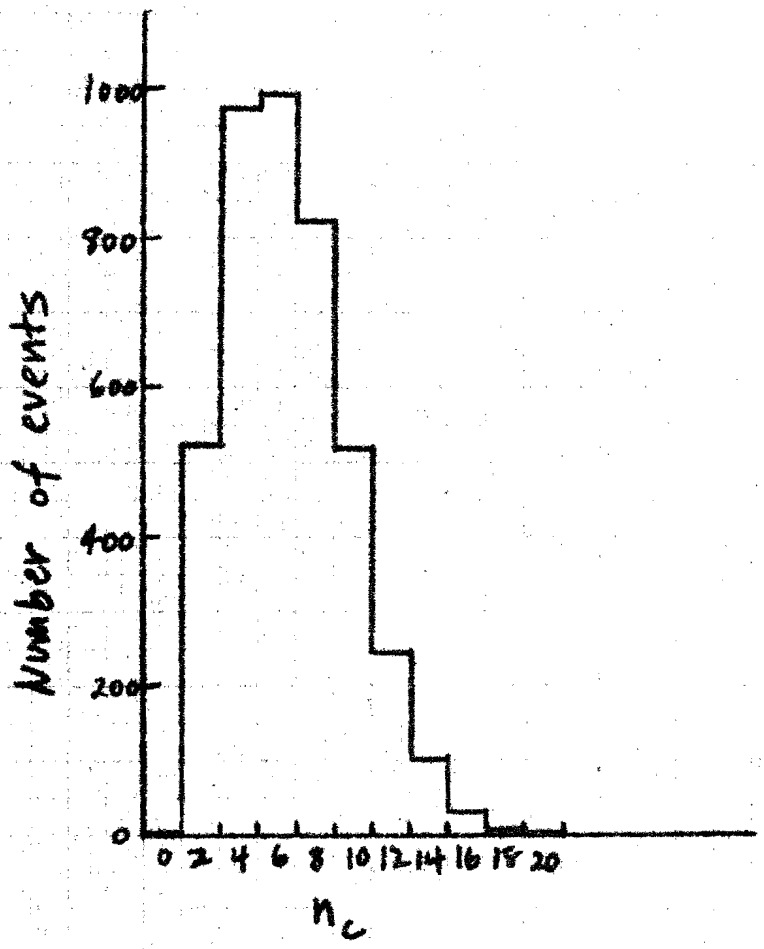

Fig. 2. $\bar{p}p$ Multiplicity distribution of events at 100 GeV/c used for study of the EPI.

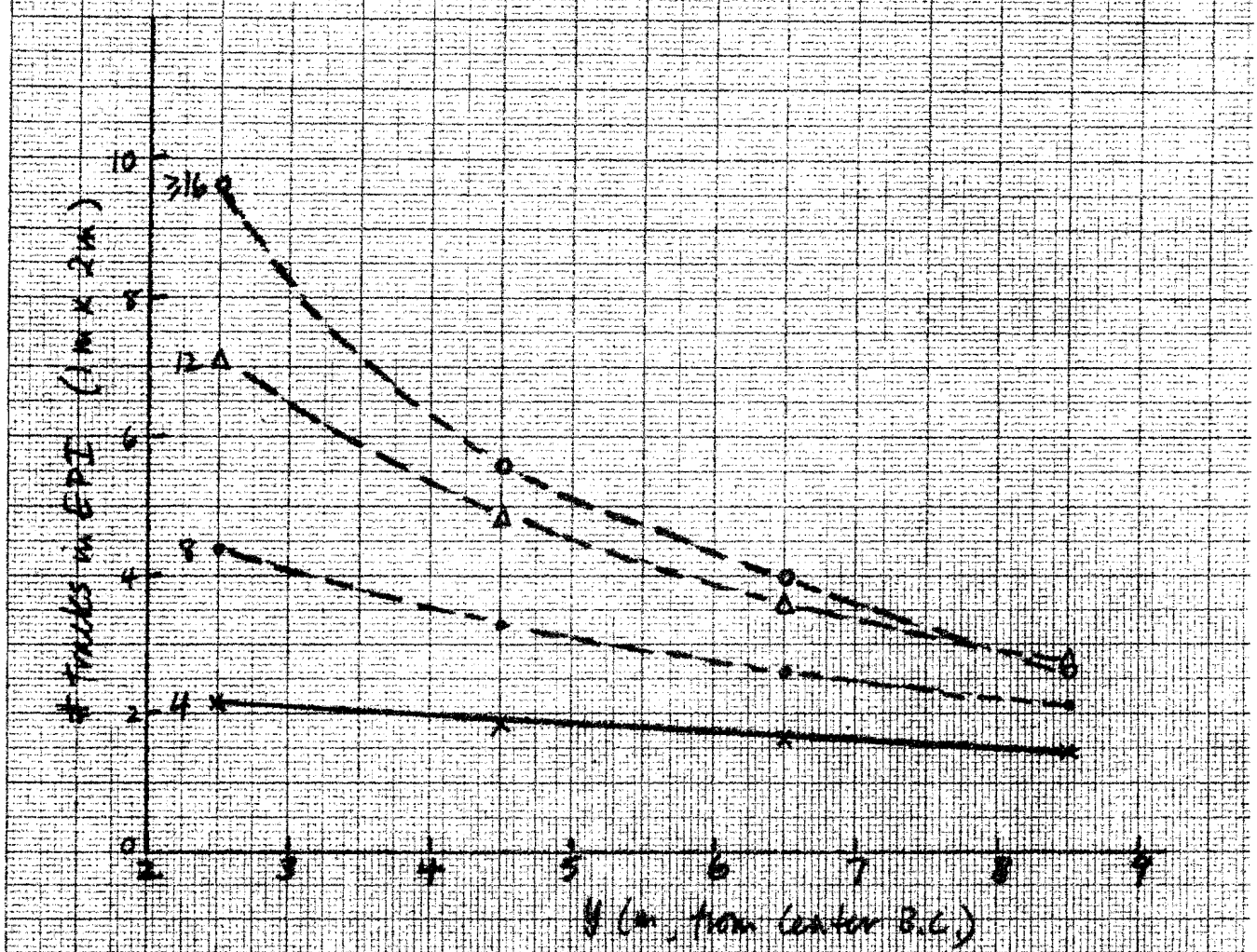

Fig. 3. Average number of tracks per event (for various multiplicity) that pass through the EPI (1m x 2m) as a function of the distance from the center of the 30-inch chamber.

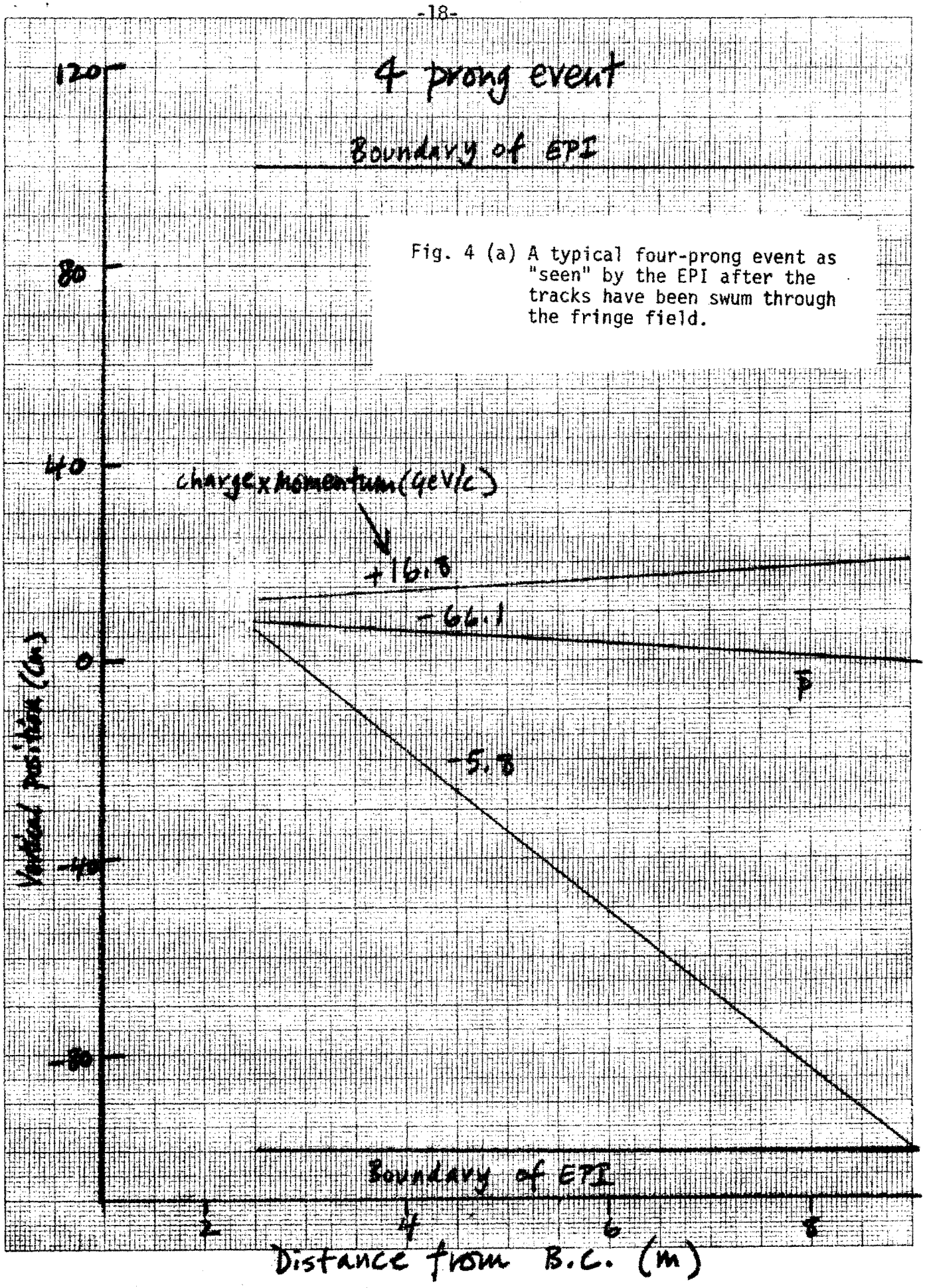

Fig. 4 (a) A typical four-prong event as "seen" by the EPI after the tracks have been swum through the fringe field.

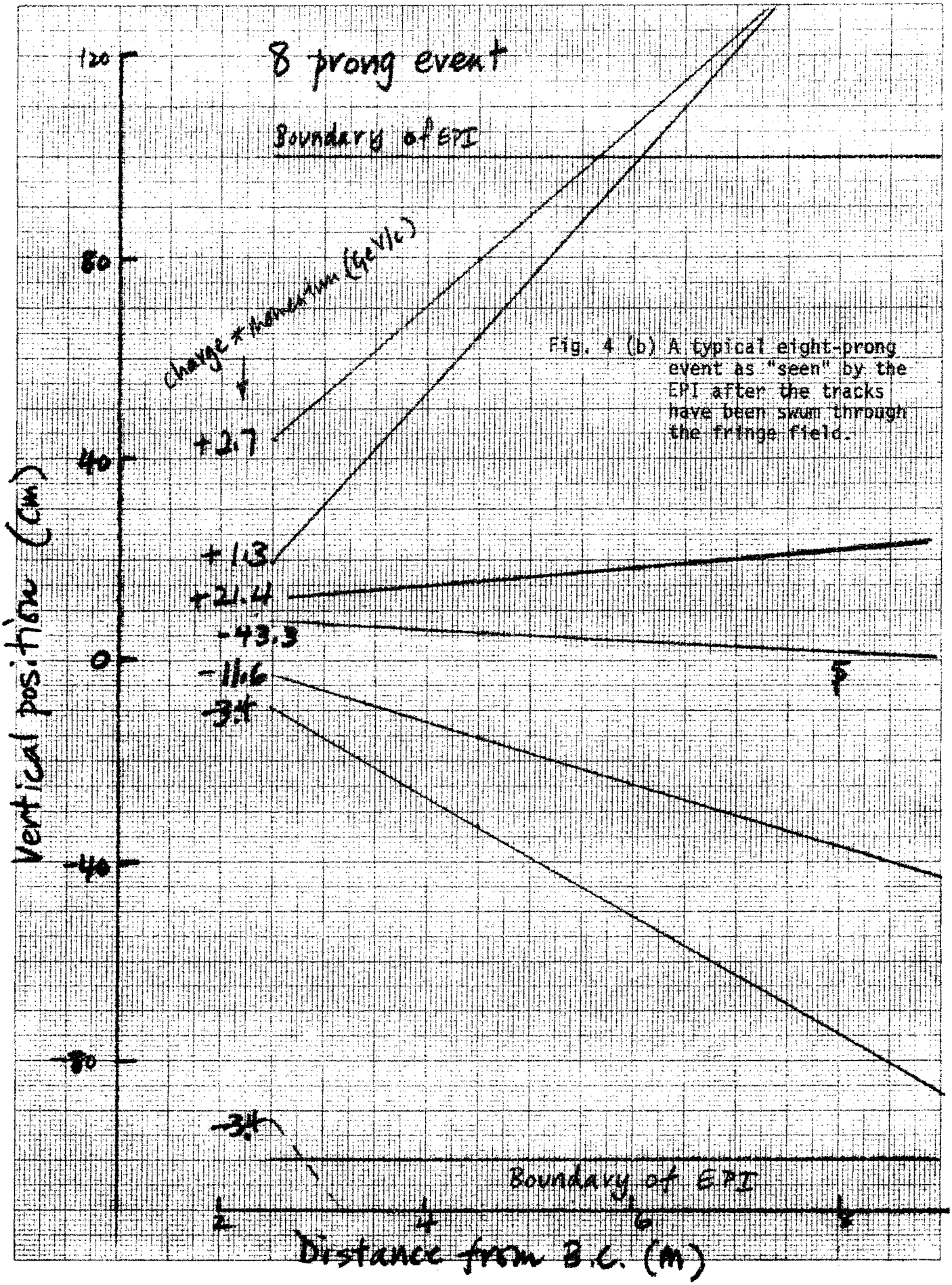

Fig. 4 (b) A typical eight-prong event as "seen" by the EPI after the tracks have been swum through the fringe field.

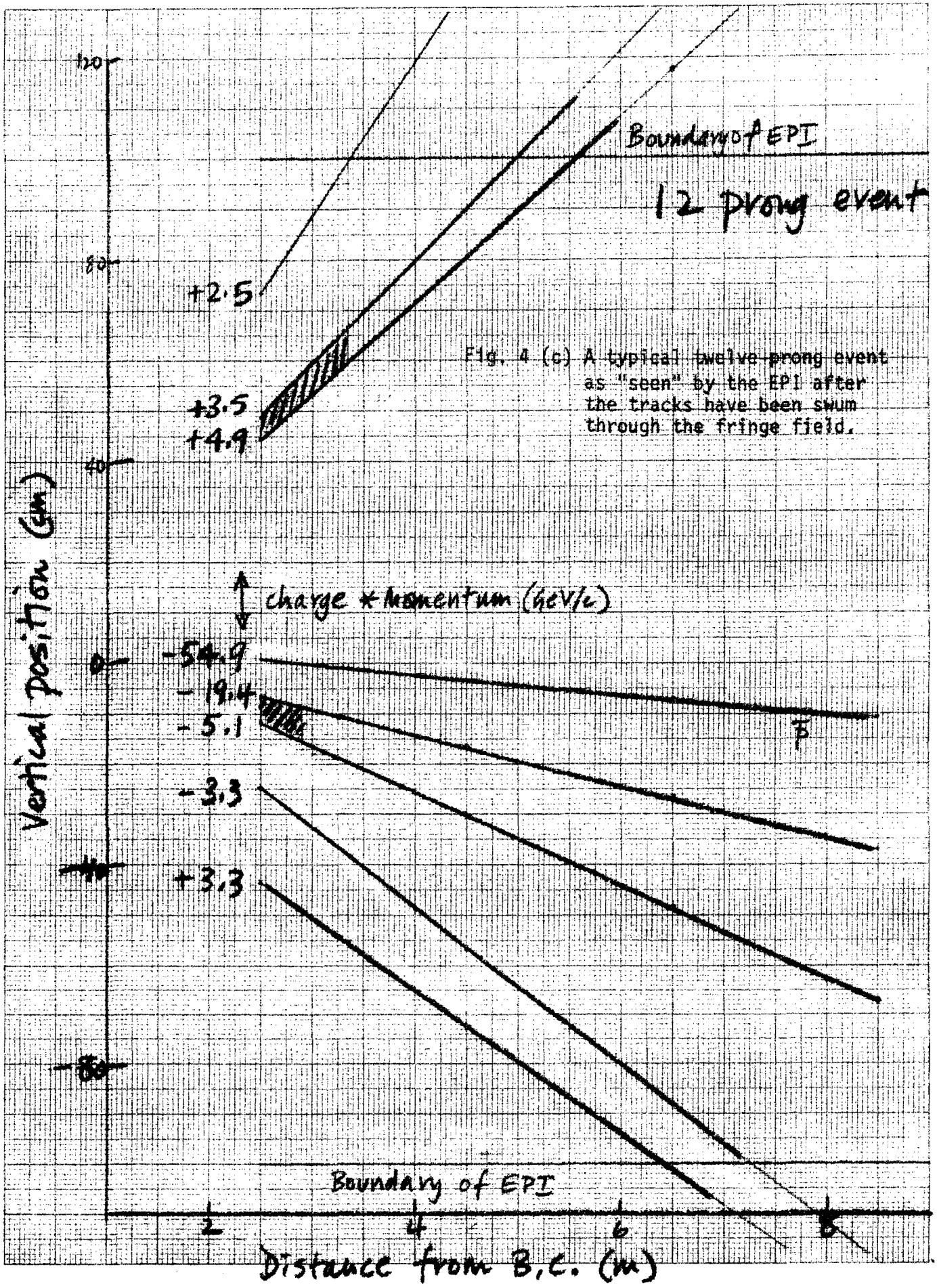

Fig. 4 (c) A typical twelve-prong event as "seen" by the EPI after the tracks have been swum through the fringe field.

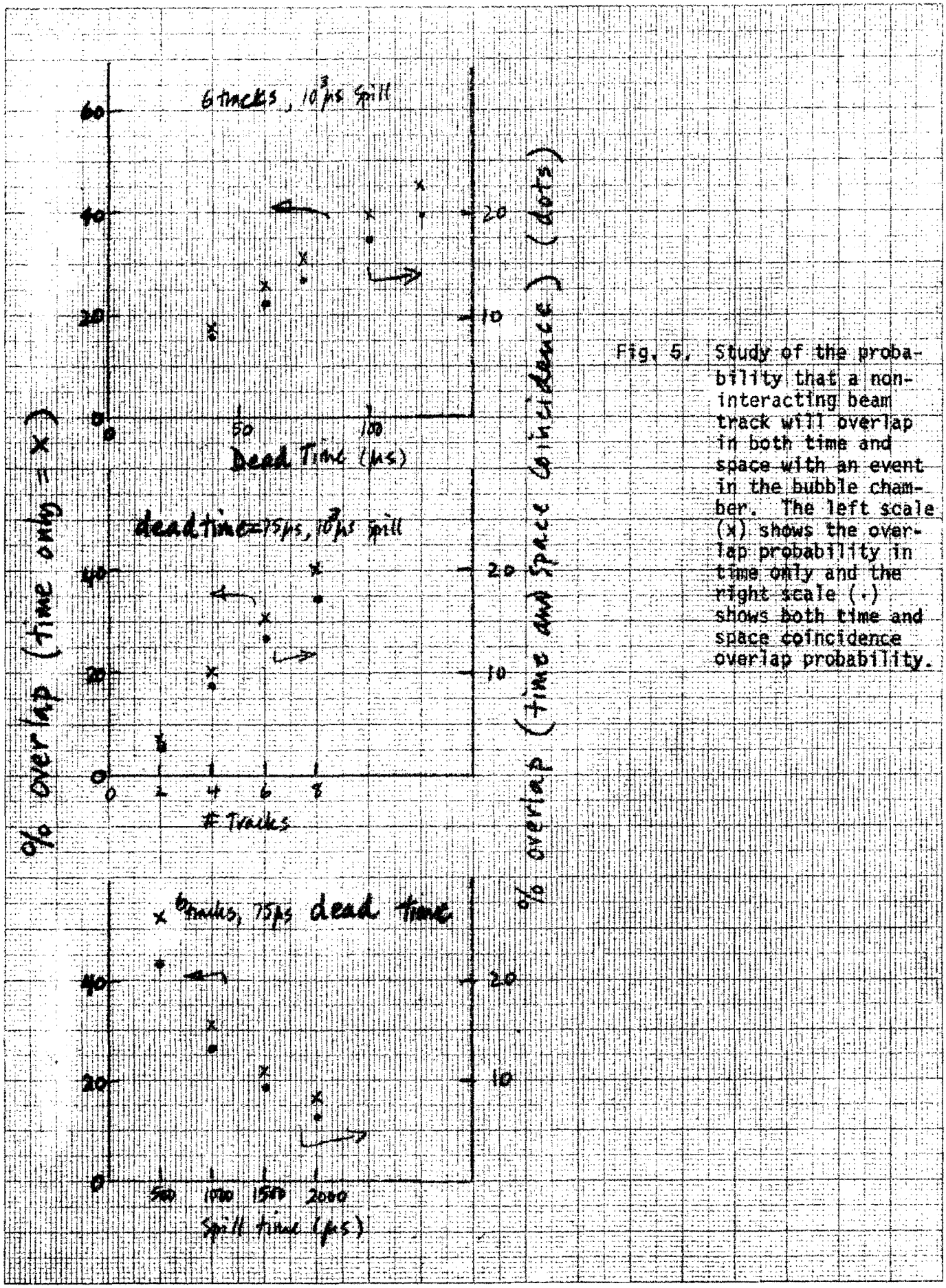

Fig. 5. Study of the probability that a non-interacting beam track will overlap in both time and space with an event in the bubble chamber. The left scale (x) shows the overlap probability in time only and the right scale (.) shows both time and space coincidence overlap probability.

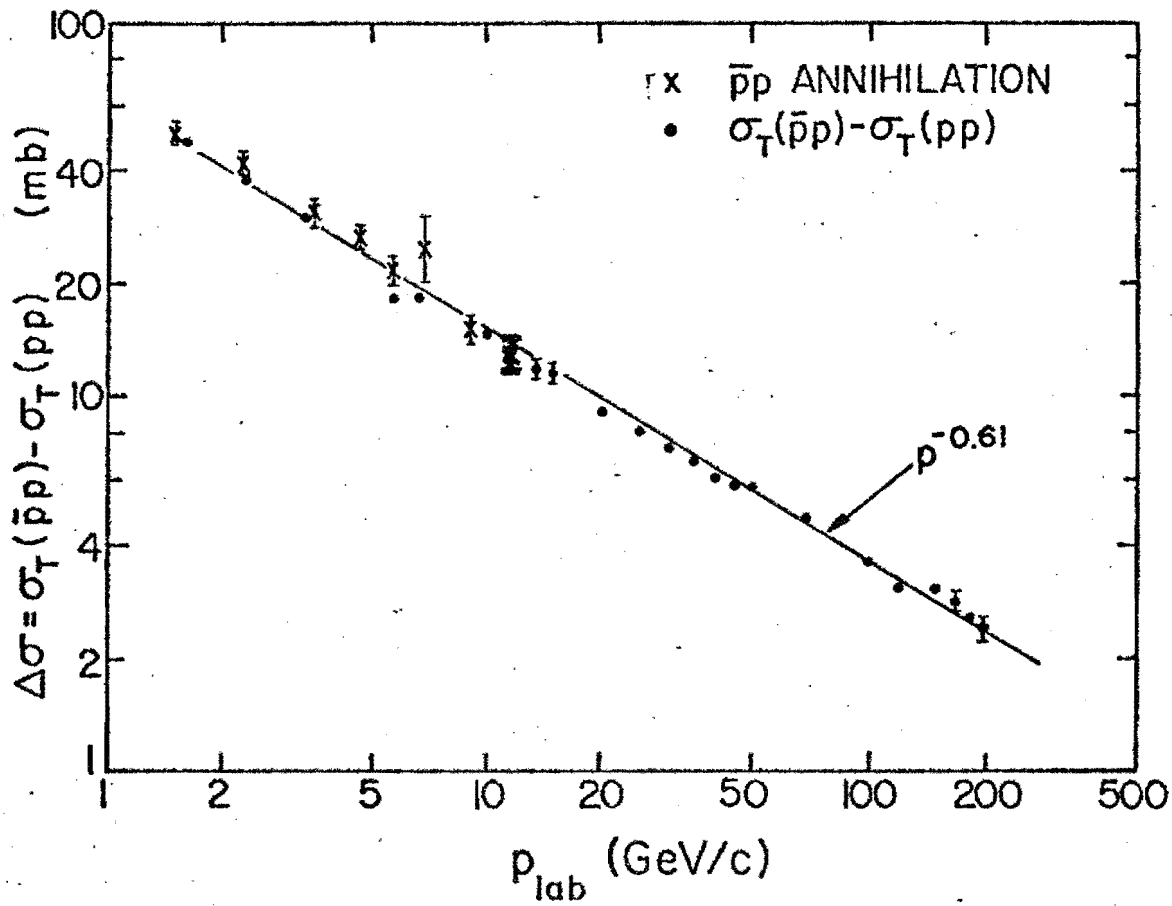

Fig. 6. Difference in total cross section for $\bar{p}p$ and pp interactions as a function of the incident beam momentum. Also shown as the measured annihilation cross section at low energies (see J. Whitmore, proceedings of the APS/DPF Meeting, Seattle, 1975).

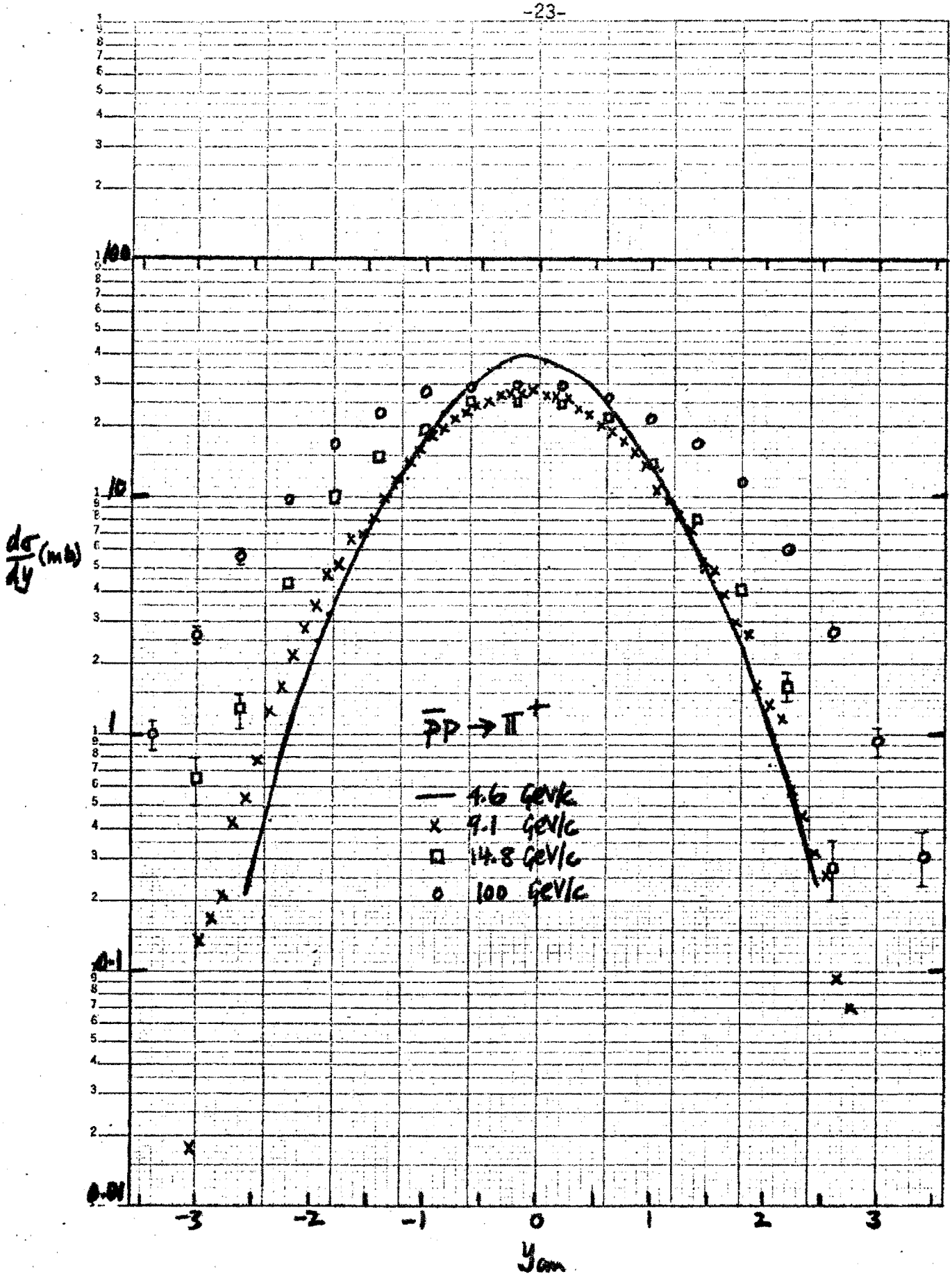

Fig. 7. Center of Mass rapidity distributions for $\bar{p}p \to \pi^+ +$ anything at 4.6, 9.1, 14.8 and 100 GeV/c.

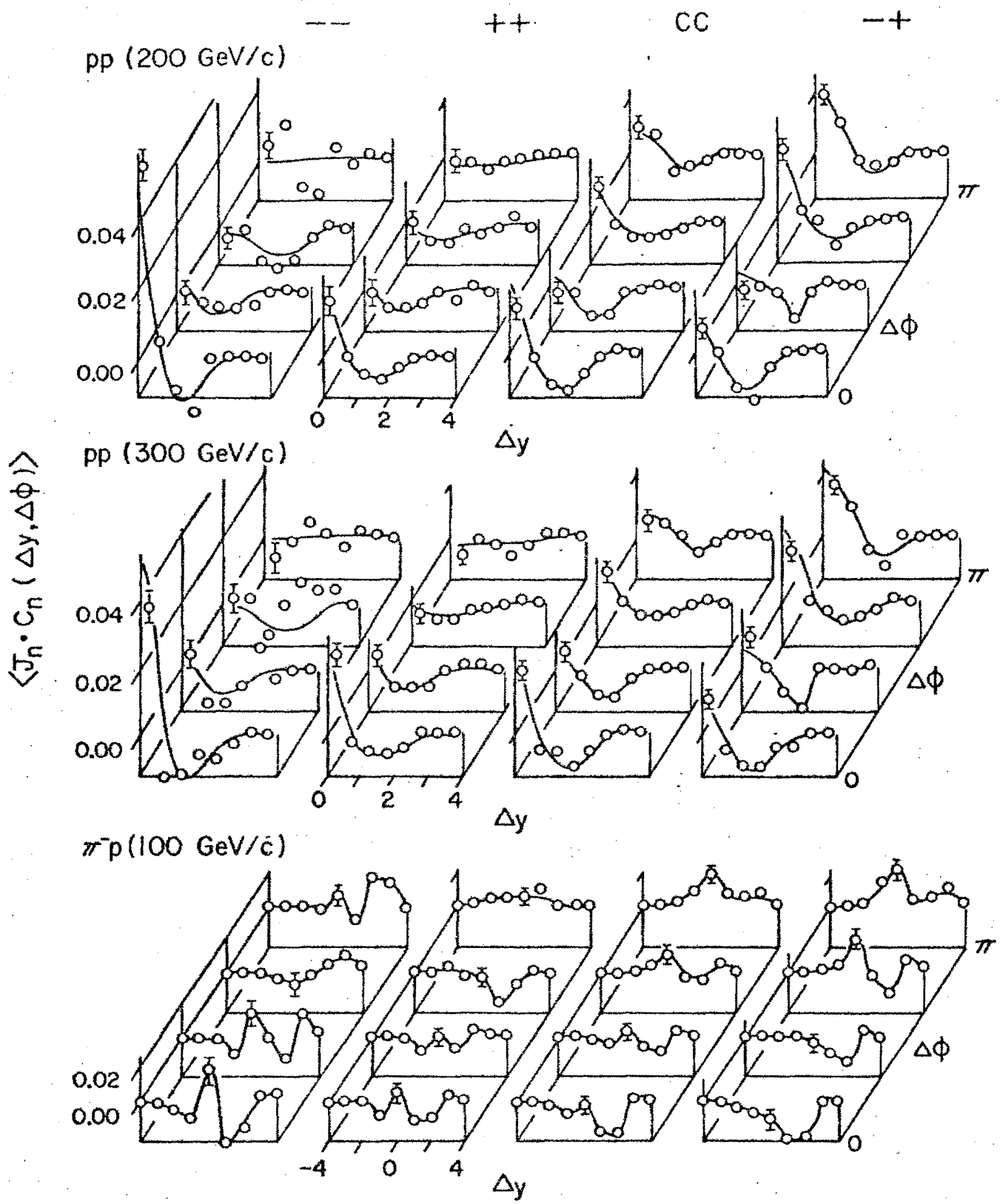

Fig. 8. The two-particle correlation function for various charge combinations from π^-p and pp collisions as a function of the rapidity separation and azimuthal angular separation (Ref. 4).

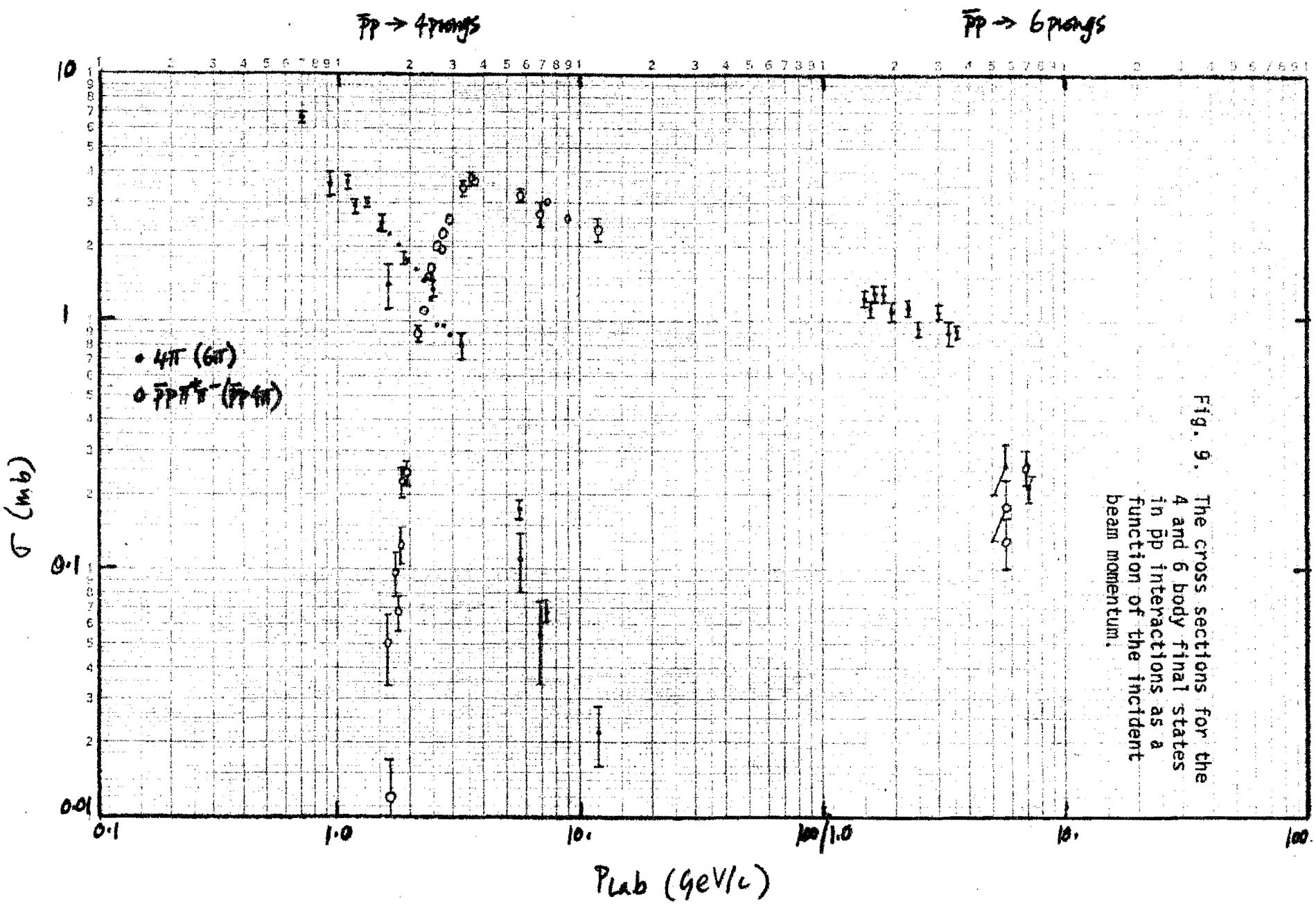

Fig. 9. The cross sections for the 4 and 6 body final states in $\bar{p}p$ interactions as a function of the incident beam momentum.

a) PROPOSED 30" BC-HYBRID SYSTEM (REF. 10)

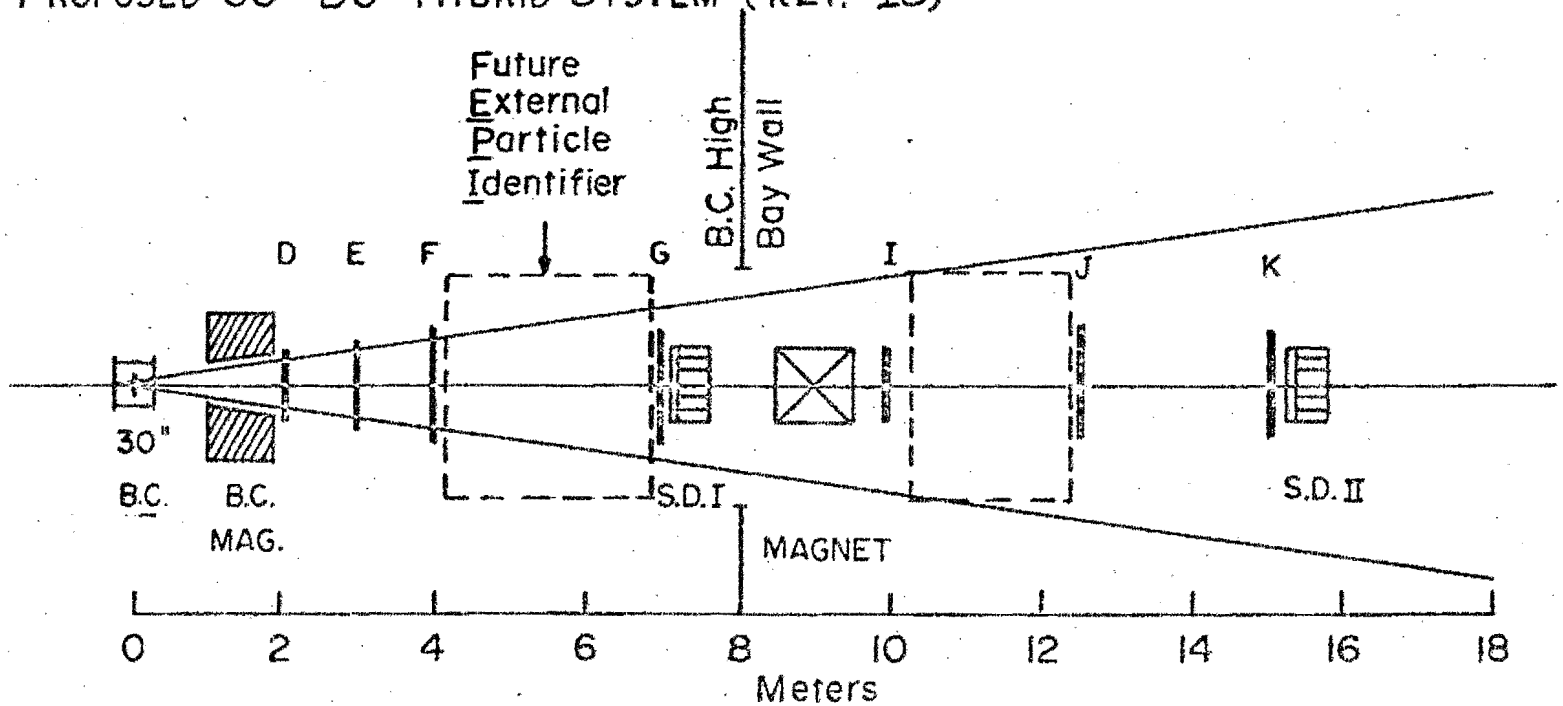

b) MODIFIED PLAN INCLUDING CERN EPI

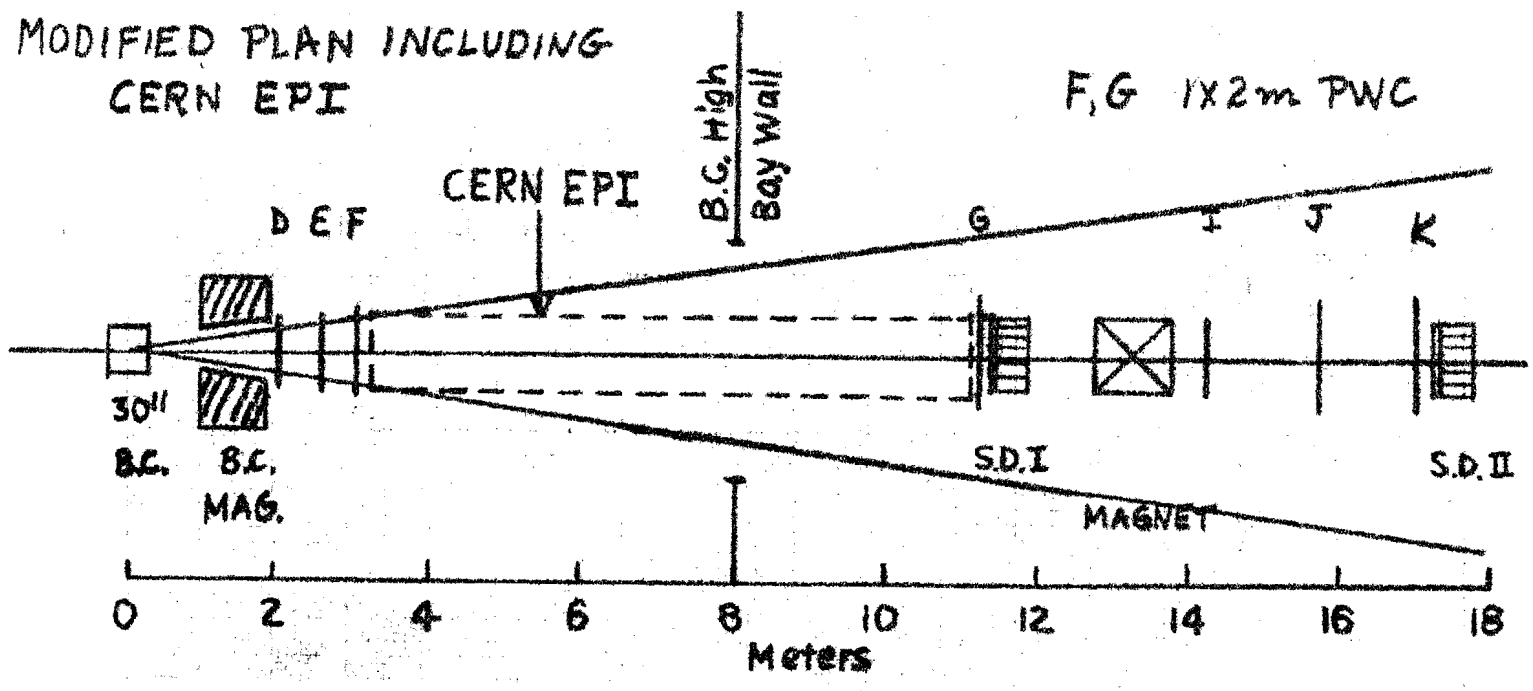

FIGURE 10

CERN/D.Ph.II/BEAM 74-1
3.1.1974

Nuclear Instruments and Methods
118, 49 (1974)

HIGH RESOLUTION IONIZATION MEASUREMENTS IN THE REGION OF THE RELATIVISTIC RISE

M. ADERHOLZ, P. LAZEYRAS, I. LEHRAUS,
R. MATTHEWSON, W. TEJESSY.

CERN, Geneva.

ABSTRACT

Results of a 62 layer gas proportional counters test at 9 GeV/c are given. The achieved resolution in the ionization was 9.4% FWHM for 4 cm layer thickness and Ar + 5% CH_4 gas mixture. The ionization ratio of pions and protons was 1.21 ± 0.01 for Argon at atmospheric pressure. Other gas mixtures were also tested. The results of the experiment were used for design improvements of a 128 layer ionization detector proposed for identification of fast secondaries emerging from the 3.7 m bubble chamber working at SPS energies.

IL/mk

1. INTRODUCTION

This paper represents another step in the development of a particle identification device proposed for the 3.7 m Hydrogen Bubble Chamber to work at the 400 GeV CERN SPS energies [1]. Previous work permitted the design characteristics of a 128 layer, 4096 - channels multilayer proportional counters system to be determined, which will be able to identify the fast secondary particles emerging from the bubble chamber. The detection area is assumed to be about 2 m wide and 0.75 m high. The detector should have a good multiparticle detection efficiency and it should be able to identify protons, pions and kaons at momenta corresponding to the design parameters of the proposed radio - frequency separated beam (6 μs spill time, maximum unseparated momentum 150 GeV/c). Several half-scale prototype modules were made and the equivalent of a single 32 - layer cell was tested at 16 GeV/c. Details of the experimental arrangement and the results of ionization measurements made in Argon in the region of the relativistic rise have been presented already in ref. [1].

This time, the measurements were extended to 62 layers and different gas mixtures. Also, the operational aspects (long - term stability etc.) of the detector were studied in detail and with great care. The results obtained during these tests, namely the surprising behaviour of the width of the single layer ionization loss distribution as a function of the layer thickness, were used to optimize the final detector design. A slightly modified version, therefore, is proposed, giving an improved resolution and better performance extended towards higher particle momenta.

2. GAS MIXTURES

An extensive study has been made in order to find a gas mixture which will give the steepest slope of the relativistic rise and narrowest width of the ionization loss distribution. The high voltage characteristics of different gas mixtures are shown on Fig. 1, where the peak P.H.A. channel of the 5.9 keV Fe^{55} X-ray source is plotted. The working range was limited by noise level at the lower end and by the degradation of

proportionality and resolution at the upper end of the characteristics. The main interest was to determine the influence of Helium admixtures on the performance and stability of operation. It was also very important to find out if an expensive heavy gas like Krypton or Xenon would improve the performance when small percentages were added to the Argon. Clearly, the "good" gas mixture should not have very steep high voltage characteristics, which practically excludes the first 5 gas mixtures (from the left) on Fig. 1. Fig. 1. alone is not sufficient, without taking into account also the possible degradation of the ionization resolution. Fig. 2 shows the spectra of the Fe^{55} source, as measured in different gas mixtures working near the middle region of the characteristics. All measurements were done under the same conditions at atmospheric pressure, when the gas filling (supplied from pre-mixed gas bottles) was perfectly stabilized and clean. Fig. 2a) shows the "standard" 95% Ar + 5% CH_4 mixture. Mixtures on Fig. 2b) and (c) contain 60% He. Their behaviour is essentially the same as for the "standard" mixture but the gas amplification is higher by a factor of approximately 14 in case (b) and by a factor of 5 in case (c). The explanation for this behaviour is probably the Penning effect. Further increase of Helium content in the mixture to 85% (Fig. 2d) leads to a visible degradation of the resolution and to a considerable reduction of the detection efficiency. Another two gas mixtures containing 95% He + 5% CH_4 and 90% He + 10% CH_4 did not work at all. Fig. 2e) shows 95% Ne + 5% CH_4 mixture which was very unstable in operation and therefore not suitable for reliable ionization measurements. 95% Kr + 5% CH_4 mixture (Fig. 2f) was satisfactory and stable, the gas amplification factor was about seven times lower than for the Ar + 5% CH_4 mixture. Adding 75% He (Fig. 2g) spoiled the resolution and the detection efficiency. Finally, Fig. 2h) shows the mixture of 85% He + 5% Xe + 10% CH_4 which is apparently not very satisfactory from the stability point of view. The comparison of the resolution (width of Fe^{55} spectrum) for individual gas mixtures is presented in Table 1.

TABLE 1

	Gas mixture	Fe^{55} peak FWHM [%]
a	95% Ar + 5% CH_4	17.7
b	60% He + 35% Ar + 5% CH_4	18.0
c	60% He + 30% Ar + 10% CH_4	17.7
d	85% He + 10% Ar + 5% CH_4	23.9
e	95% Ne + 5% CH_4	40.4
f	95% Kr + 5% CH_4	17.6
g	75% He + 20% Kr + 5% CH_4	20.9
h	85% He + 5% Xe + 10% CH_4	22.2

The choice of Methane as a quenching agent was determined mainly by its compressibility, without condensation, permitting a more efficient and economic filling of pre-mixed bottles, as compared with CO_2 or Propane. It is perhaps worth mentioning here that the unit volume cost ratios of Ar : He : Kr : Xe are roughly 1 : 2 : 35 : 170. This inevitably demands an installation of a closed recirculating gas system, with continuous purification and restitution of exact proportion of the quenching agent, in cases where either Krypton or Xenon (even in rather small percentages) were used.

3. EXPERIMENTAL ARRANGEMENT

The set-up used for the beam tests was similar to the one already described in detail in the Ref. [1]. Four half-scale prototype modules of 16 rectangular proportional counters each were placed one behind the other so as to form one "slice" of a 64 layer detector. The individual proportional counters of 4 x 4 cm^2 cross section and of 33 cm (frame - to - frame) length were formed by stretched thin wires with 1 cm spacing. Windows cut in the frames allowed an unimpeded passage for the beam particles. One 3 cm wide scintillation counter was fixed in front and another one behind and their coincidence was used to trigger the data acquisition chain.

The detector assembly was electrostatically shielded and thermally insulated. It was installed in the U7 high-energy beam in the CERN West Area, at a distance of about 150 m (Fig. 3) from the external target. The beam size in this region was 8 to 16 mm (FWHM) in both horizontal and vertical planes, safely within the detection area. The unseparated beam of $\frac{\Delta p}{p} < \pm 0.25\%$ was tuned for 9 GeV/c. One 10 ns long bunch of particles was ejected from the PS at 22 GeV and the beam intensity was drastically reduced by closing the acceptance defining collimators, so as to register one event in about 5 accelerator bursts. This was necessary to reduce simultaneous double particle events within tolerable limits. Under such circumstances the data taking is rather slow (some 200 to 300 events per hour), but corresponds closely to the real working conditions for which the detector is proposed.

To monitor the detector performance and stability, a Sr^{90} collimated source was fixed to one of the unused edge channels and the lower (steeper edge) half - maximum point of the electrons spectrum was recorded at regular intervals from a pulse - height analyser. Minimum ionizing particles traversing the full layer thickness must be used, otherwise the monitor would not react to the pressure changes.

Fig. 4 shows in the middle part the monitor data during the September 1973 run. Above the monitor there is a barometric pressure recording for the corresponding interval of time. The increase in the barometric pressure produces a decrease in the proportional counter output, as expected. Roughly, 0.1% of the barometric pressure change gives 1% change in the recorded output amplitude.

Another component in the monitor behaviour was observed - first an increasing and then a decreasing general trend - probably caused by a mechanical settling down of the detector frames and by outgassing inside the detector.

The lower part of Fig. 4 shows (as a monitor reliability check) the time variations of the π - mesons peak as accumulated over about 2 to 3 hour intervals during the run. The phase correlation between pressure, monitor and the beam data is correct, the monitor and the ionization peak follow almost exactly the same pattern. The very small difference was due to the rather long accumulation time necessary for collecting a significant statistical sample of the beam events, compared with about 15 minutes of accumulation time for the Sr^{90} spectrum.

The electronic circuitry and the data processing chain was again very similar to the one used in the Ref. [1]. Each signal wire was connected to a simple high-impedance low voltage gain amplifier mounted directly on the detector frame. The signals were integrated and stretched in a sample and hold circuit and processed in a set of 64 gated 8-bit ADC's situated near the detector. The pulse train outputs from the ADC's were sent to a set of 64 scalers in the beam control room. The content of the scalers was read into an on-line PDP-8 computer and transferred via a fast data link first onto the BEBC PDP-15 computer disc and then onto the DEC tape. The event trigger for the conversion and data taking was given by the scintillation counters fixed on the detector. The computer on-line system and the 64 channel analogue and digital electronics were borrowed from the beam tuning and control equipment.

The DEC tapes were immediately processed off-line (for quick checks of the data, verification of all channels etc.). Later they were copied onto a standard magnetic tape and the data processed on the CDC 7600 computer. Real time clock from the original event-by-event data taking was used for the monitor time correlation. The monitor data were introduced via punched cards at the stage of the CDC 7600 processing.

4. BEAM TESTS AND DETECTOR DESIGN OPTIMIZATION

Two of the 64 amplifiers failed during the run (bad contact inside the integrated circuit chips) but is was considered best not to effect reparations because of the need to remove the detector covers and hence disturbing the stable thermal conditions during the run. So Fig. 5 shows only a 62 layers detector result using Ar + 5% CH_4 gas mixture. 7061 true single π^- events are plotted. The μ^- contamination was estimated to be on the level of a few per cent only. The data were corrected for all systematic drifts using the Sr^{90} monitor. The response of the individual layers was adjusted by varying the corresponding amplifier gains to be equal within 10% limits. Further correction was made during the data processing, after the run, using the peak positions of each single layer ionization distribution. For the final result we could therefore assume that all the 62 layers are essentially identical. The histogram on Fig. 5 presents the result of a single parameter maximum likelihood fit, using the corrected "average" single layer ionization losses distribution as a reference. The parameter mentioned above is simply a linear shift of the reference curve along the channel number axis. Black circles show the result of a very simple and efficient cut-off method of taking a "mean of 40% smallest values" for each event. Crosses connected by a dashed curve indicate a Monte-Carlo simulation for the same number of events as taken in the experiment, using the same maximum likelihood method with the same reference curve and assuming all layers identical. The differences between the fake and the experimental distributions are negligible. They are probably due to occasional delta-electrons and associated intercorrelation effects, μ-meson and

other background, electrical noise etc.

The width of the experimental distribution is 9.4% FWHM for the maximum likelihood and 9.8% FWHM for the cut-off method. The errors shown on Fig. 5 are only the statistical ones. This result was much better than expected from the predictions of Ref. [1]. Fig. 6 shows the resolution as a function of the number of layers for the maximum likelihood and for the cut-off method. The experimental points for 4 cm layer thickness and Ar + 5% CH_4 gas mixture at atmospheric pressure are from the 9 GeV/c π^- run (corrected data). Monte-Carlo generated distributions facilitate reliable and exact predictions of a 128 layer detector performance.

The reason for the considerable improvement in the present experiment results, as compared with the results presented in the Ref. [1], is explained by the much narrower single layer distributions of the ionization losses. It is very likely due to the fact that during this experiment single particle events were in the majority, whereas in Ref.[1] they were a minority (simultaneous particle contamination was very high even in the best data samples). The dashed curve on Fig. 7 was used for optimization of the number of detector layers and layer thickness in Ref. [1]. It is clearly far too pessimistic. Most of the points on this curve were measured either by 1.3 MeV electrons or by cosmic ray μ-mesons [2-8]. Even with guard counters used against showers in cosmic rays and in accelerator beams it is rather difficult to eliminate completely the double particles. Presumed "single particle" events from Ref. [1] are plotted on Fig. 7 in full black circles. The experimental points were produced by summing up the values of a corresponding number of the individual layers, event by event. The first two layers gave 8 cm of detector thickness, first four gave 16 cm etc. up to 128 cm. The resulting distribution widths are all well below the above mentioned dashed curve. The present experimental results (black squares) produce a much better result, extended to 248 cm of equivalent total detector length of Argon at atmospheric pressure. This curve, above about 50 cm of detector length,

is in reasonable agreement with the theoretical Landau predictions [9,10]. Below about 50 cm length, of this detector, corrections for the electron binding should be applied to the Landau curve according to Blunck [11] (another dotted curve on Fig. 7). These corrections make the Landau distribution wider on the side of the lower ionization losses, for relatively thin detectors. Some of the delta-rays responsible for the big fluctuations in the ionization could escape from the detector, which is only 4 cm wide. This effect is probably responsible for a narrowing of the distribution width for large detector thicknesses, as compared with the theoretical predictions on Fig. 7.

Using the new results presented on Fig. 6 and Fig. 7 another optimization of the ionization detector was made concerning the number of layers, layer thickness and total detector length, for a desired resolution. The result is shown on Fig. 8 for Argon at atmospheric pressure, maximum likelihood method and all layers having identical response. Around 3 cm of layer thickness gives the shortest total detector length. Obviously, from economical considerations, it is preferable to choose the smallest possible number of rather thick layers, which will still lead to a tolerable total detector length. Crossing simultaneous particle tracks and particles passing from one detector "slice" into the adjacent one will reduce the effective number of layers. For this reason, on the contrary, it is preferable to keep the number of layers rather high. For the envisaged application a reasonable compromise seems to be to increase the layer thickness from 4 to 6 cm and conserve 128 layers. Such a detector will attain, in the best case, about 5.5% FWHM of ionization resolution for a total length of about 8 m. Updated estimation of the cost is some 220 SFr per channel for electronics and detector itself. The electronics represents roughly 73% of the total cost. Sacrificing to some extent the detection efficiency for the inclined and crossing tracks, about 20% saving could be achieved by halving the number of layers to 64. The layer thicknesss should be then about 16 cm in that case (see Fig. 8), which leads to a total detector length of 10.3 m. In this variant the

electronics represent only 60% of the total cost. Intermediate variants with e.g. 90 or 80 layers represent only a marginal savings of the order of 12% and they are therefore not worth the corresponding loss of detection efficiency.

The relativistic rise of the ionization was measured in the positive 9 GeV/c beam, containing protons and appropriate proportion of surviving π^+ mesons. The results for Ar + 5% CH_4 gas mixture and 62 layer detector are shown on Fig. 9, together with the π^- distributions plotted on the same scale. The data were corrected using the Sr^{90} monitor and the individual layers were equalized before the final data processing. The upper part of Fig. 9 shows the result of maximum likelihood and the lower part the "mean of 40% smallest values" cut-off method. 12698 events are plotted in the p, π^+ distributions. Note the exact coincidence of the π^+ and π^- peaks, which is an indication of a very reliable monitor. The negative and positive runs took a total time of about 110 hours.

The efficiency of the p/π separation can be estimated using the π^- peak width and a ratio of proton peak to valley between protons and π^+. Clearly the maximum likelihood method is the most efficient, giving 9.4% FWHM for π^- and about 7.4 for the peak to valley ratio. In order to establish the best cut-off parameters the proportion of values taken for the mean was varied from 20 to 60%. Other cuts were taken (e.g. mean of 10 to 50% smallest values, or just 20th value alone after consecutive ordering of all the 62 values per event). Table 2 shows the comparison of different methods for a 62 layer detector. The "mean of 40% smallest

TABLE 2

Method (62 layers; Ar + 5% CH_4)		FWHM[%] (π^- run)	Peak/valley (p; π^+ run)
Mean of smallest	20%	12.4	4.7
	30%	10.9	5.3
	40%	9.8	6.1
	50%	10.1	5.2
	60%	10.5 (asymmetric)	4.4
Mean of 10 to 50% smallest		10.4	3.6
20th value		12.0	3.2
Maximum likelihood		9.4	7.4

values" seems to be the most efficient cut-off method, which is in agreement with the predictions from Ref. [1]. This simple and fast method is only slightly less efficient than much more elaborate and computer time consuming maximum likelihood approach.

The ratio of ionization (peak positions) between protons and π^+ is 1.21 ± 0.01 for Ar + 5% CH_4 at atmospheric pressure. The errors emanate from the uncertainty of determination of the exact peak positions. This result was plotted on Fig. 10 together with the previously measured points from Ref. [1]. The solid curve represents a fit to all compiled proportional counter data (the experimental points are not shown, for the sake of clarity). The dashed curve represents a theoretical prediction of Steinheimer [12], including the density effect corrections. The relativistic rise curve seems to be established with a reasonable precision. The values near the bend towards the Fermi plateau and above cannot be measured at CERN PS energies. There is still some hope that future NAL or CERN SPS measurements will show higher absolute values for the plateau (the data existing at present in this region were all measured using a few hundred MeV electrons).

In the first half of December 1973 another run was made, using two more gas mixtures selected from the group presented on Fig. 1 according to the criteria of good stability of operation. Krypton + 5% Methane and 60% He + 30% Ar + 10% CH_4 mixtures were chosen for this test. It is obviously very interesting to search for a possibly steeper slope of the relativistic rise of ionization in a gas heavier than Argon and in a mixture containing considerable proportion of light Helium. Cloud chamber data [13,14,15] show some confusing and difficult to explain phenomena in similar gas mixtures. The results of this experiment are shown in Table 3.

TABLE 3

Gas mixture	π/p ionization ratio	Proton peak FWHM [%]
95% Ar + 5% CH_4	1.21 ± 0.01	10.7
60% He + 30% Ar + 10% CH_4	1.21 ± 0.012	11.3
95% Kr + 5% CH_4	1.26 ± 0.015	14.9

The targetting conditions were not exactly the same in the Ar + 5% CH_4 run as in the run for the other two gas mixtures, therefore the direct comparison of peak to valley ratios was not possible. Also, the proton peak width increased with the second and third mixture by the greater influence of the binning effect (the peak positions were lower than in the Ar + 5% CH_4 run). Nevertheless, the following general statements can be safely made:

a) Ar + 5% CH_4 mixture shows the best resolution;

b) the mixture containing 60% He + 30% Ar behaves almost exactly as "pure" Argon;

c) Kr + 5% CH_4 mixture gives by about 4% higher ionization ratio than Argon, but the resolution seems to be worse and might cancel the gain made by the 4% improvement.

In the light of the presented results it will be certainly interesting to investigate in more detail the resolution of the Krypton gas mixture and to measure the relativistic rise in Xenon. Such an experiment running without closed gas circulation might be, unfortunately, rather expensive.

A new approximation of the expected 128 (6 cm thick) layers detector performance was made in the following way: the relativistic rise of the ionization was taken from Fig. 10 and a 6% FWHM Monte-Carlo maximum likelihood distribution was used, shifted along the relativistic rise according to the particle momentum. Equal number of protons, kaons and pions was assumed. The result for 20 and 50 GeV/c is shown on Fig. 11. The muons cannot be obviously resolved from pions, but they cannot be resolved by threshold Cerenkov counters either. The overlapping area of the proton and kaon distributions is about 21% of the integral of the individual distributions and it remains unchanged to almost 60 GeV/c. The K/π overlap is about 1.7% at 20 GeV/c and it grows steadily to some 15.6% at 50 GeV/c. The p/π overlap of roughly 0.5% at 50 GeV/c does not present any serious problem.

Finally, Fig. 12 shows the separation efficiency of the proposed detector in terms of the non-overlapping parts of the distributions for p/π, p/K and K/π separation as a function of the particle momentum. The separation efficiency is still acceptable up to almost 100 GeV/c. A very important feature of particle identification by ionization measurements is that the loss of efficiency is purely statistical in origin and does not introduce any kinematical bias in the bubble chamber data evaluation. Note that an absolute limit for K/π separation by the atmospheric pressure threshold Cerenkov counters is at 60 GeV/c [16].

5. CONCLUSIONS

A slightly modified and improved version of a 128 (6 cm thick) layers 4096 proportional counters detector as proposed in Ref. [1] was given, using some new results obtained in a 62 layer test run at 9 GeV/c. The detector is designed to identify, by ionization, the fast secondary particles emerging from the 3.7 m bubble chamber (BEBC) operating in SPS beams of up to about 150 GeV/c momenta. The detector should achieve an ionization resolution of better than ± 3% with acceptable separation efficiency up to almost 100 GeV/c for p/K/π separation. The updated

cost estimation gives about 220 SFr per each of the 4096 channels, including both the electronics and the detector itself. It has been proved that a reliable monitor enables extremely stable and reproducible operation over extended periods of time.

A full-scale prototype of one (32 cells across the beam) double layer module has been made already (Fig. 13) and is undergoing an extensive series of tests. A final version of the electronics circuitry is being prepared, consisting of amplifier, stretcher, ramp comparison ADC, 8-bit C-MOS scaler and shift register read-out per channel. Definite choice of the gas mixture is still open within certain limits ("reasonable" gas amplification factor etc), but very likely Argon + 5% Methane will be used. The detector is totally insensitive to non-uniform magnetic field of a few hundred gauss, which is to be expected near the bubble chamber.

The non-interracting beam particles will pass through an insensitive region of appropriate dimensions. It is possible to form such a dead zone in the detector by simply covering the necessary few centimeters of the corresponding signal wires by thin glass tubes, which very efficiently prevents the electron avalanche in a region with sharply defined boundaries.

The reconstruction of the inclined and crossing tracks present no problem, since the individual proportional counters form a well defined geometrically fixed matrix.

A detailed study of the whole system, including the bubble chamber and its stray magnetic field, best beam size and position of the detector, detection losses due to crossing tracks and simultaneous multiparticle events etc. are just being finished and will be published soon.

The data handling facility will be determined later in connection with other planned equipment (MWPC system for the bubble chamber entry and exit angle labelling, external muon identifier for neutrino beam etc.).

We would like to thank all members of the TC beam group who helped in the preparation and during the experiments. Understanding and active support from Messrs. M. Demoulin and F. Perriollat (BEBC instrumentation and computer group) was greatly appreciated.

REFERENCES

[1] D. Jeanne, P. Lazeyras, I. Lehraus, R. Matthewson, W. Tejessy and M. Aderholz: Nucl. Instr. and Meth. 111 (1973) 287.

[2] D. West: Proc. Phys. Soc. A66 (1953) 306.

[3] B. Eiben, H. Faissner, M. Holder, J. König, K. Krisor and M. Umbach Nucl. Instr. and Meth. 73 (1969) 83.

[4] J.K. Parry, H.D. Rathgeber and J.L. Rouse: Proc. Phys. Soc. A66 (1953) 541.

[5] P.V. Ramana-Murthy and G.D. Demeester: Nucl. Instr. and Meth. 56 (1967) 93.

[6] P.V. Ramana-Murthy: Nucl. Instr. and Meth. 63 (1968) 77.

[7] E.D. Palmatier, J.T. Meers and C.M. Askey: Phys. Rev. 97 (1955) 486.

[8] F. Harris, T. Katsura, S. Parker, V.Z. Peterson, R.W. Ellsworth, G.B. Yodh, W.W.M. Allison, C.B. Brooks, J.H. Cobb and J.H. Mulvey: Nucl. Phys. Lab. Report 57/72 (Oxford Univ., 1972).

[9] L. Landau: J. Phys. USSR 8 (1944) 201.

[10] S.M. Seltzer and M.J. Berger: NAS-NRC Nucl. Sci. Report 39 (1964) 178.

[11] O. Blunck and K. Westphal: Z. Physik 130 (1951) 641.

[12] R.M. Sternheimer and R.F. Peierls: Phys. Rev. B3 (1971) 3681.

[13] R.G. Keppler, C.A.D'Andlau, W.B. Fretter and L.F. Hansen Nuovo Cim. VII (1958) No.1., 71.

REFERENCES (Cont'd)

[14] A. Rousset, A. Lagarrique, P. Musset, P. Rançon and X. Sauteron: Nuovo Cim. XIV (1959) No.2., 365.

[15] C. Ballario, A. De Marco, R.D. Fortune and C. Verkerk: Nuovo Cim. XIX (1961) No.6., 1142.

[16] M. Benot, J. Litt and R. Meunier: Nucl. Instr. and Meth. 105 (1972) 431.

FIGURE CAPTIONS

Fig. 1 High voltage characteristics for different gas mixtures.

Fig. 2 Fe^{55} spectrum in
a) 95% Ar + 5% CH_4
b) 60% He + 35% Ar + 5% CH_4
c) 60% He + 30% Ar + 10% CH_4
d) 85% He + 10% Ar + 5% CH_4
e) 95% Ne + 5% CH_4
f) 95% Kr + 5% CH_4
g) 75% He + 20% Kr + 5% CH_4
h) 85% He + 5% Xe + 10% CH_4

Fig. 3 Experimental arrangement of a 64-layer detector.

Fig. 4 Barometric pressure dependence of the ionization signal.

Fig. 5 9 GeV/c π^- result and Monte-Carlo distributions. (Ar + 5% CH_4).

Fig. 6 Ionization resolution as a function of number of layers.

Fig. 7 Single layer ionization losses distribution width as a function of the layer thickness.

Fig. 8 Optimum number of layers and layer thickness for a given resolution and total detector length.

Fig. 9 9 GeV/c positive run result.

Fig. 10 Relativistic rise of the ionization in Argon.

FIGURE CAPTIONS (Cont'd)

Fig. 11 Expected separation at 20 and 50 GeV/c assuming ionization resolution of 6% FWHM.

Fig. 12 Expected separation efficiency (non-overlapping parts of the distributions) as a function of the particle momentum.

Fig. 13 Full-scale prototype of a double layer module (32 channels 6 cm wide per layer).

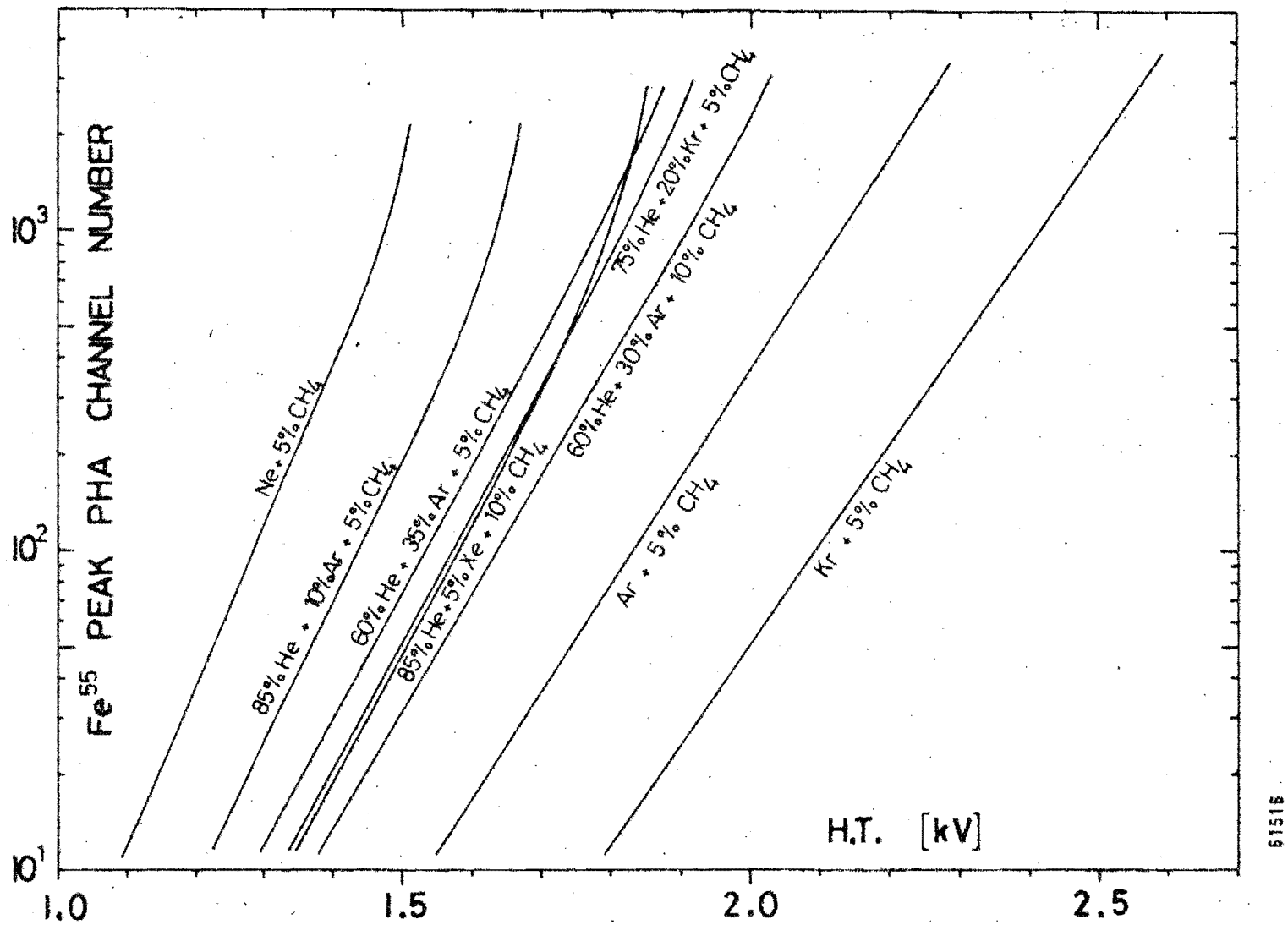
Fe55 PEAK PHA CHANNEL NUMBER
10^3
10^2
10^1
1.0
1.5
2.0
2.5
H.T. [kV]
Ne + 5% CH4
85% He + 10% Ar + 5% CH4
60% He + 35% Ar + 5% CH4
85% He + 5% Xe + 10% CH4
75% He + 20% Kr + 5% CH4
60% He + 30% Ar + 10% CH4
Ar + 5% CH4
Kr + 5% CH4
61516

fig. 1

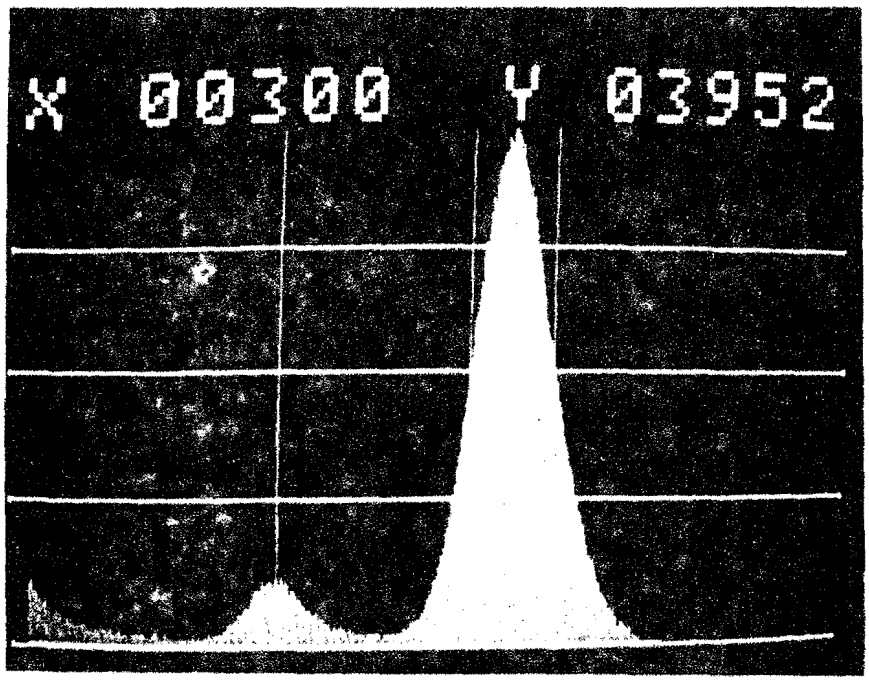

Fig. 2a)

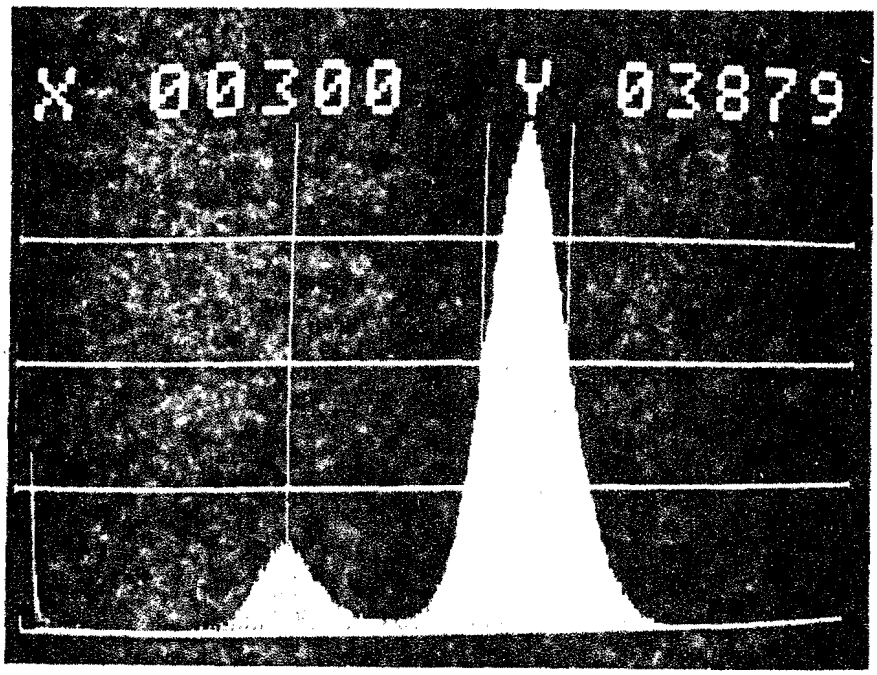

Fig. 2b)

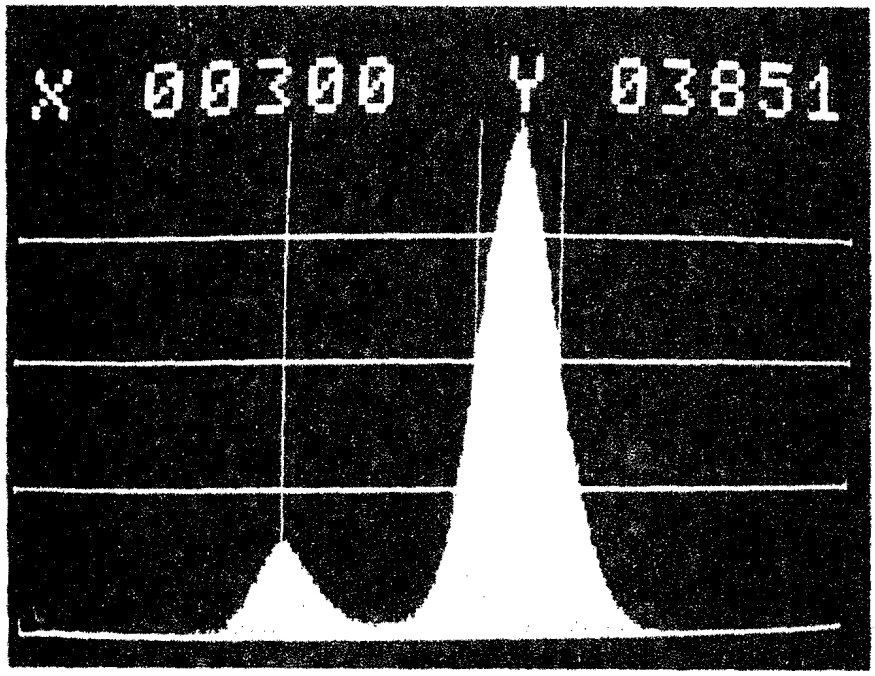

Fig. 2c)

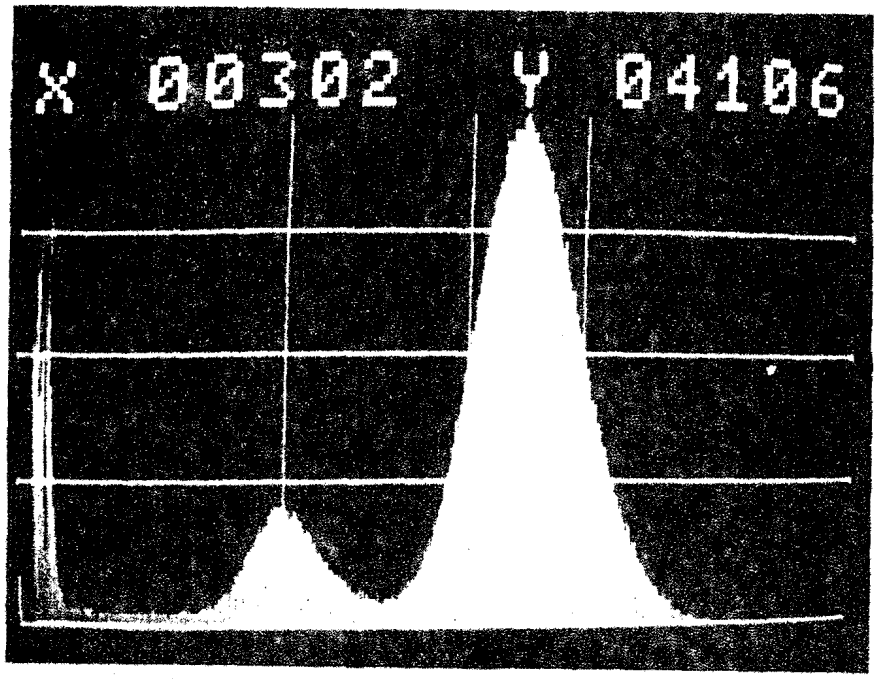

Fig. 2d)

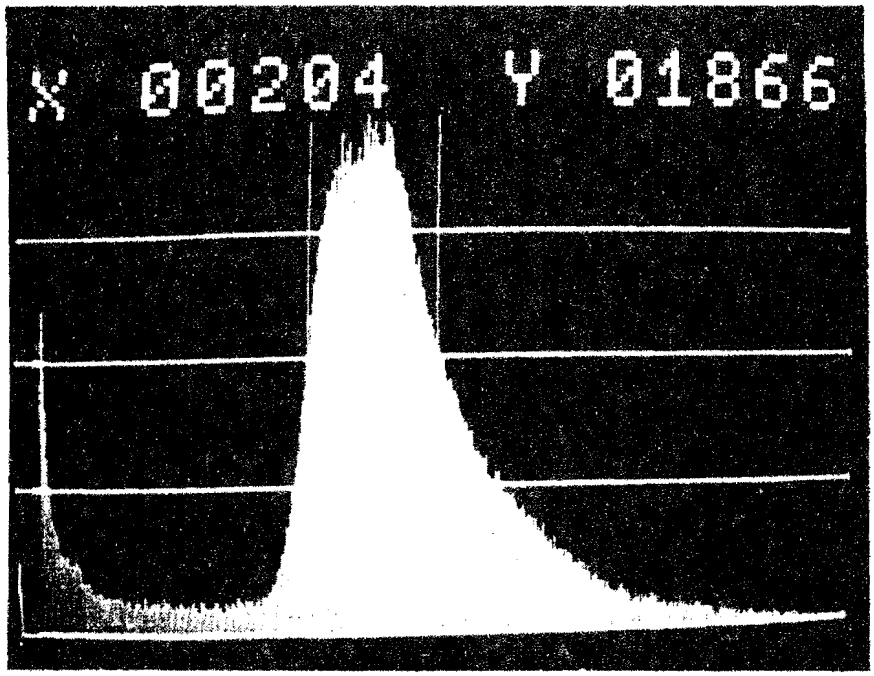

Fig. 2e)

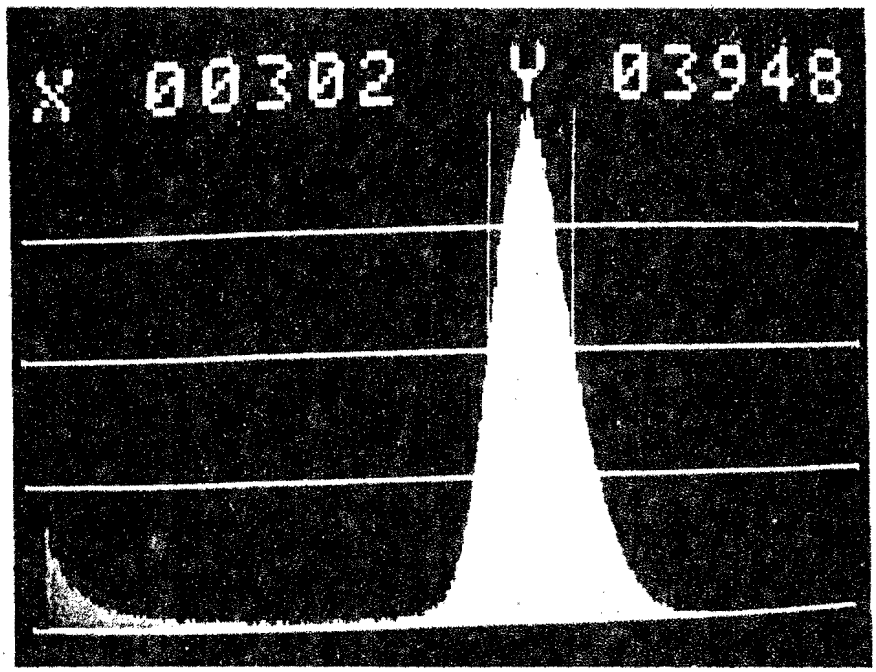

Fig. 2f)

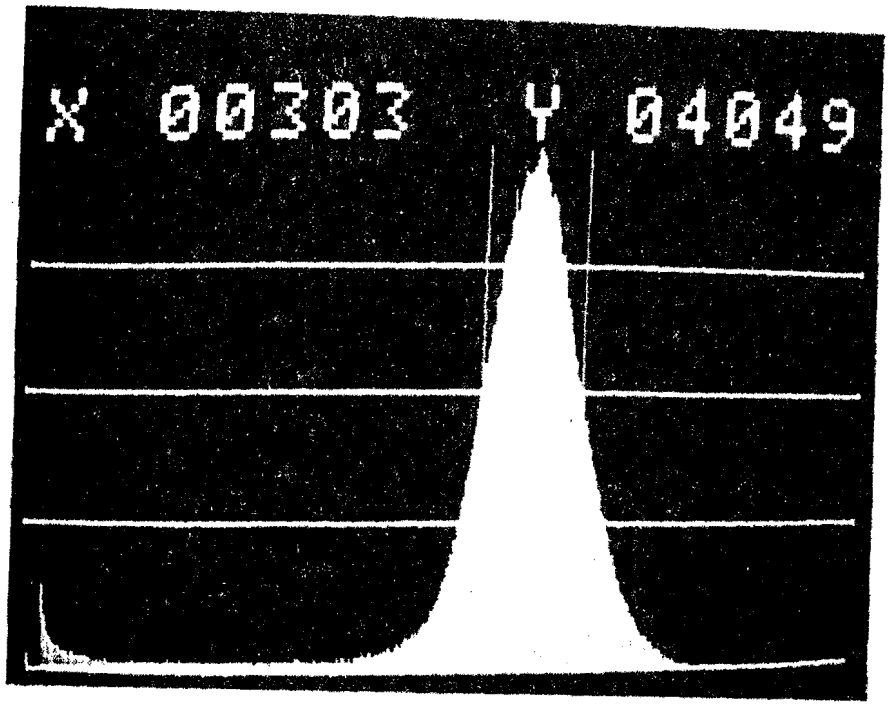

Fig. 2g)

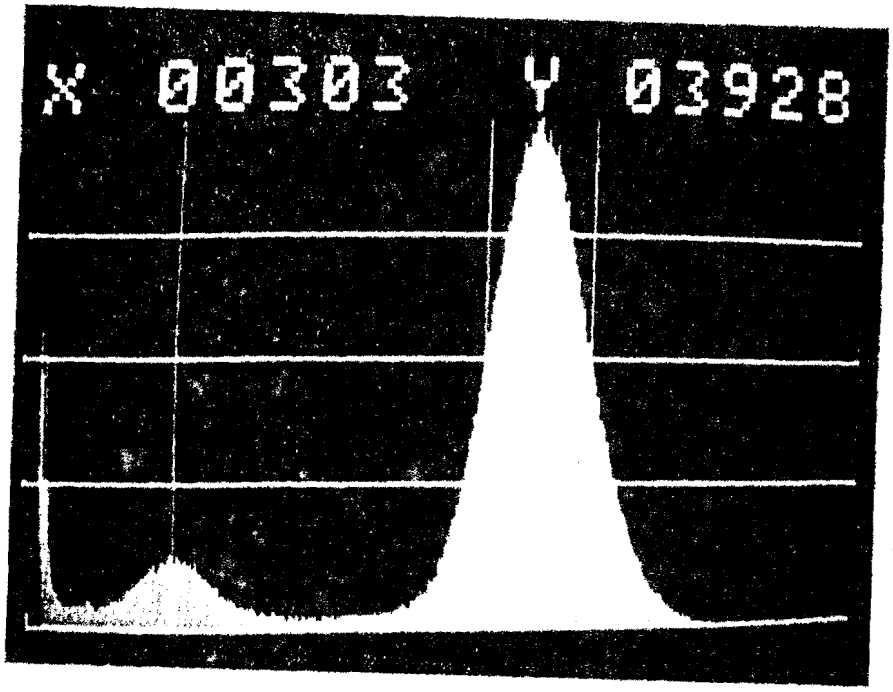

Fig. 2h)

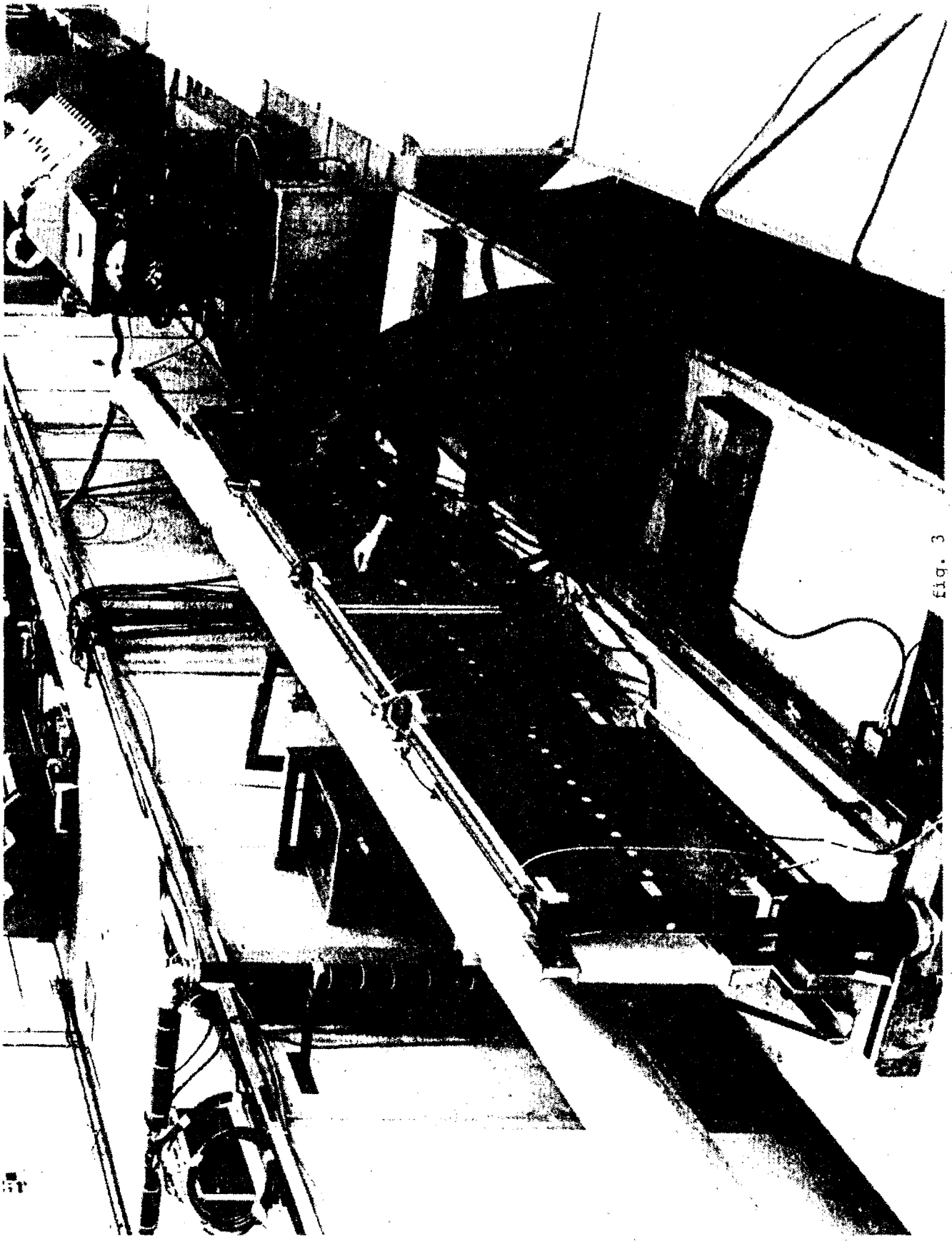

Fig. 3

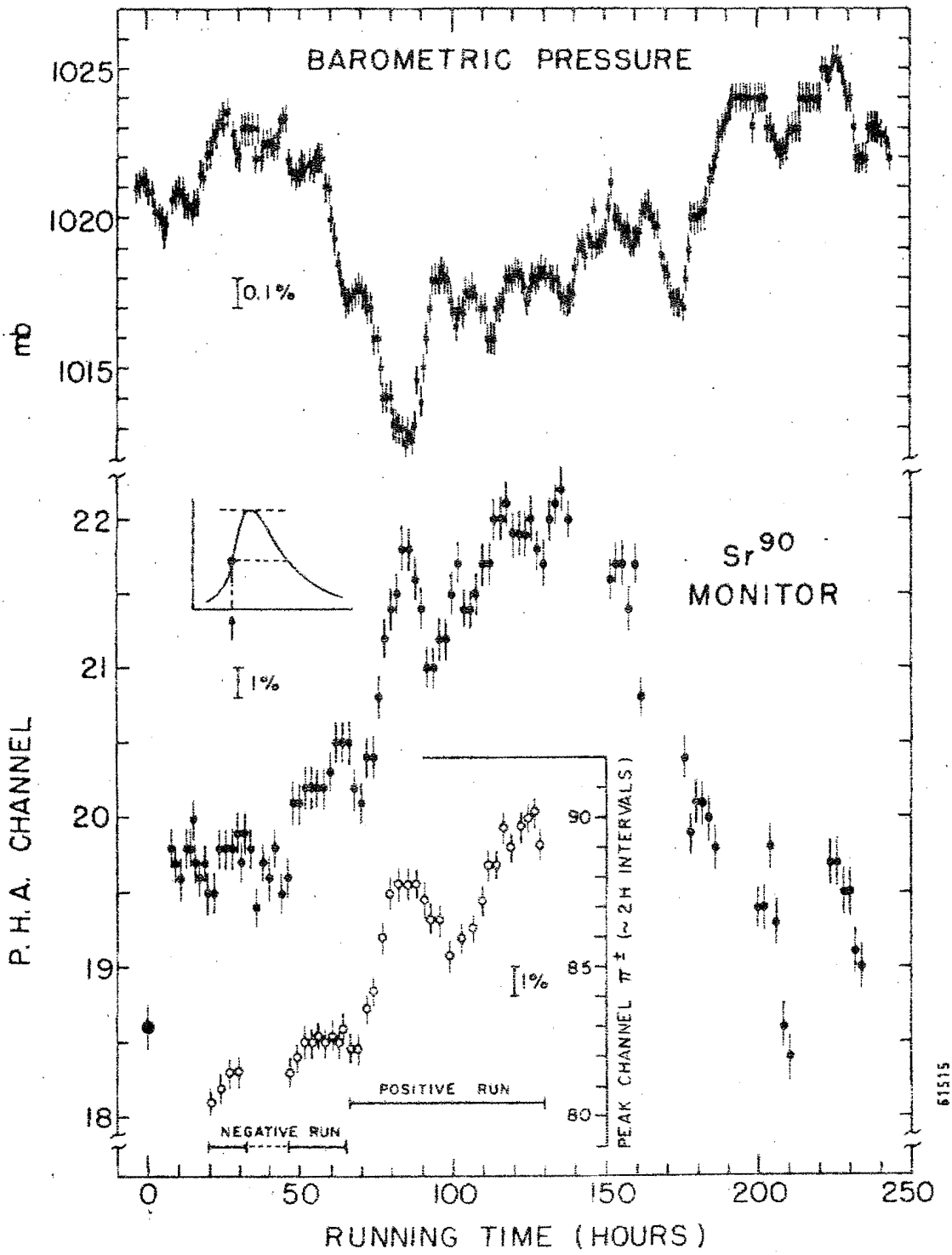
BAROMETRIC PRESSURE
1025
1020
1015
mb
0.1%
22
21
20
19
18
P.H.A. CHANNEL
1%
Sr90
MONITOR
90
85
80
PEAK CHANNEL π± (~ 2H INTERVALS)
1%
POSITIVE RUN
NEGATIVE RUN
0
50
100
150
200
250
RUNNING TIME (HOURS)
61515

fig. 4

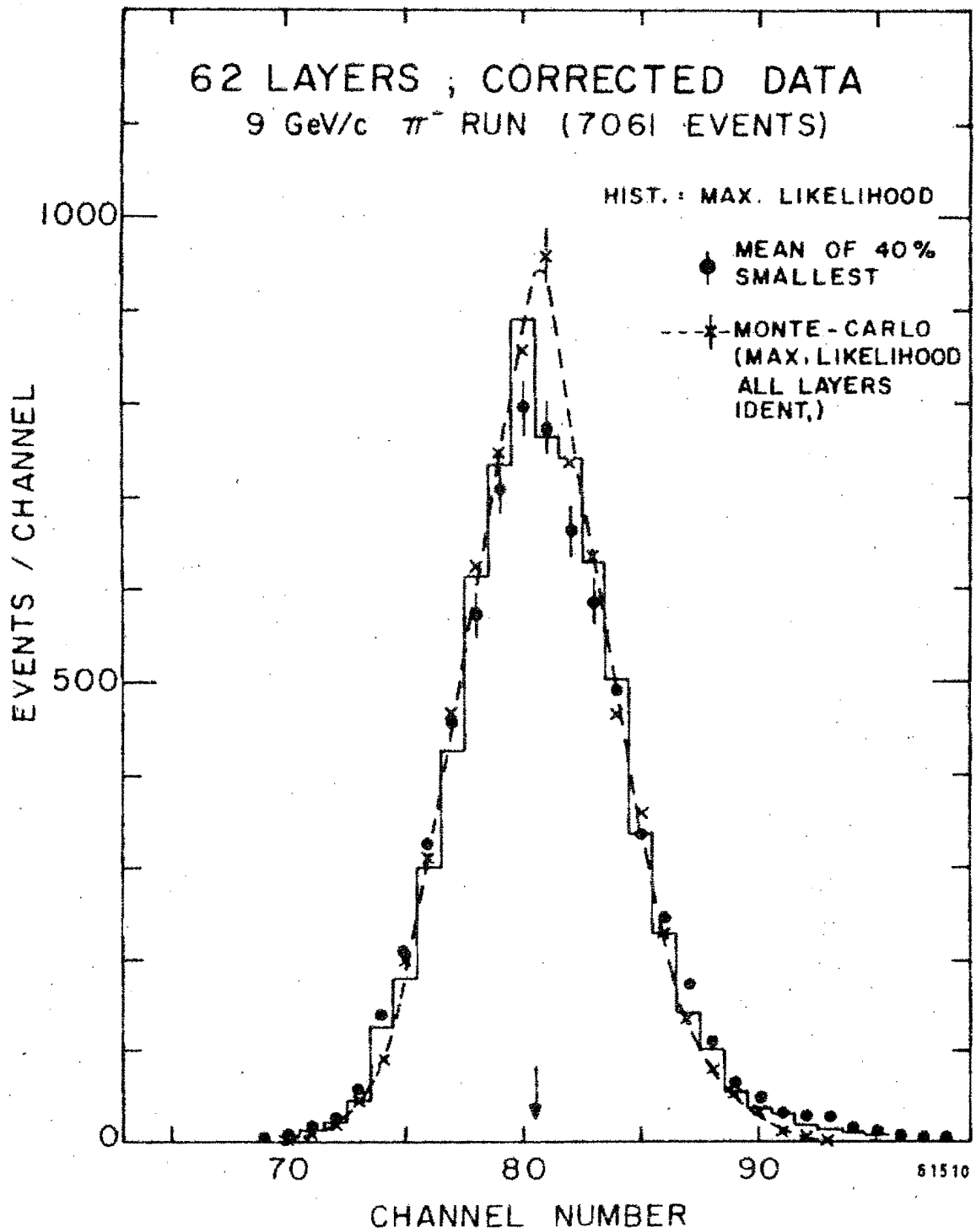
62 LAYERS ; CORRECTED DATA
9 GeV/c π⁻ RUN (7061 EVENTS)
HIST. : MAX. LIKELIHOOD
MEAN OF 40% SMALLEST
MONTE-CARLO (MAX. LIKELIHOOD ALL LAYERS IDENT.)
EVENTS / CHANNEL
1000
500
0
70
80
90
CHANNEL NUMBER
61510

fig. 5

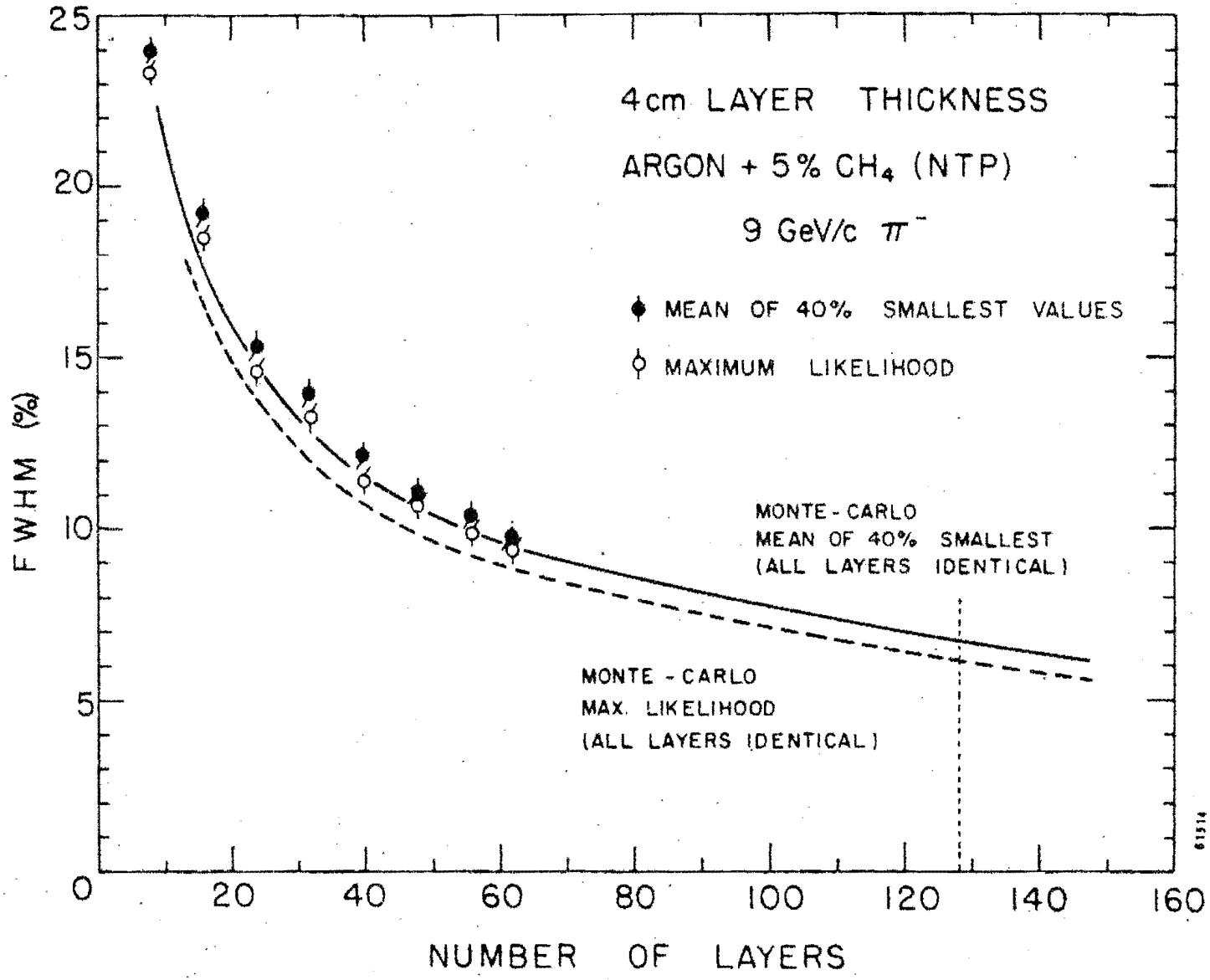
4cm LAYER THICKNESS
ARGON + 5% CH_4 (NTP)
9 GeV/c π^-
MEAN OF 40% SMALLEST VALUES
MAXIMUM LIKELIHOOD
MONTE-CARLO
MEAN OF 40% SMALLEST
(ALL LAYERS IDENTICAL)
MONTE-CARLO
MAX. LIKELIHOOD
(ALL LAYERS IDENTICAL)
FWHM (%)
NUMBER OF LAYERS
0
5
10
15
20
25
20
40
60
80
100
120
140
160

fig. 6

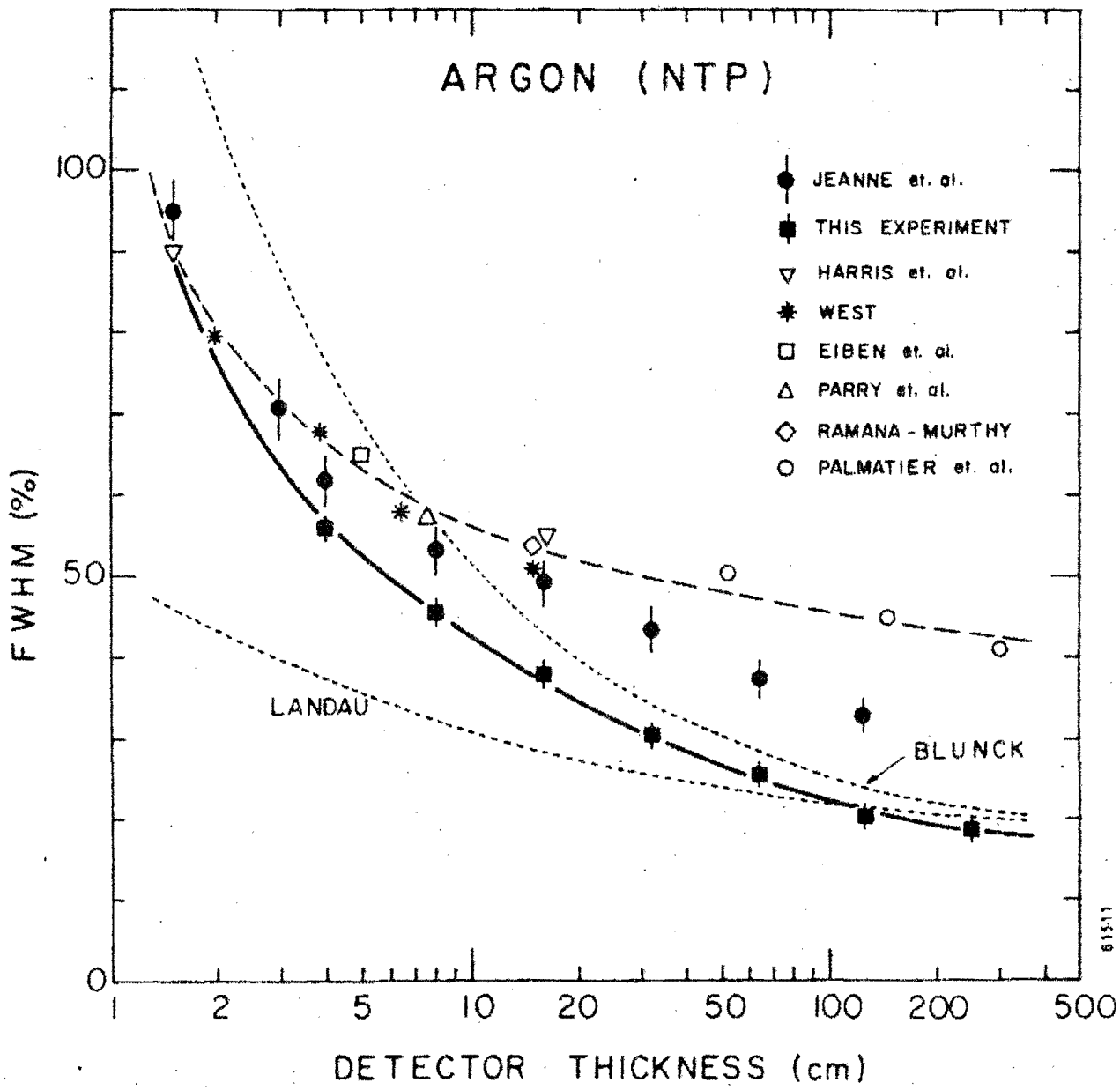
ARGON (NTP)
JEANNE et. al.
THIS EXPERIMENT
HARRIS et. al.
WEST
EIBEN et. al.
PARRY et. al.
RAMANA - MURTHY
PALMATIER et. al.
LANDAU
BLUNCK
FWHM (%)
100
50
0
1
2
5
10
20
50
100
200
500
DETECTOR THICKNESS (cm)

fig. 7

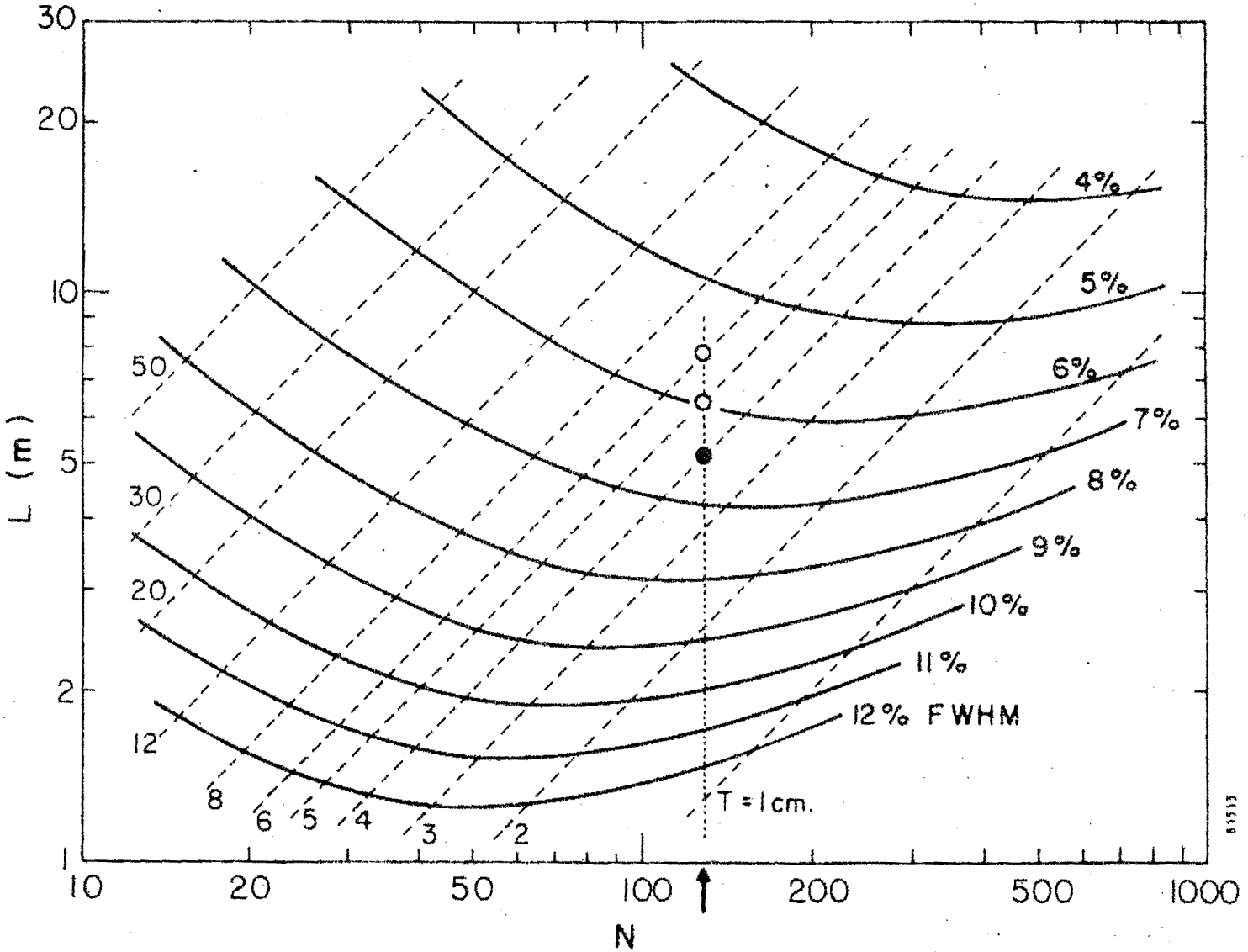
30
20
10
5
2
1
L (E)
10
20
50
100
200
500
1000
N
4%
5%
6%
7%
8%
9%
10%
11%
12% FWHM
50
30
20
12
8
6
5
4
3
2
T = 1cm.

fig. 8

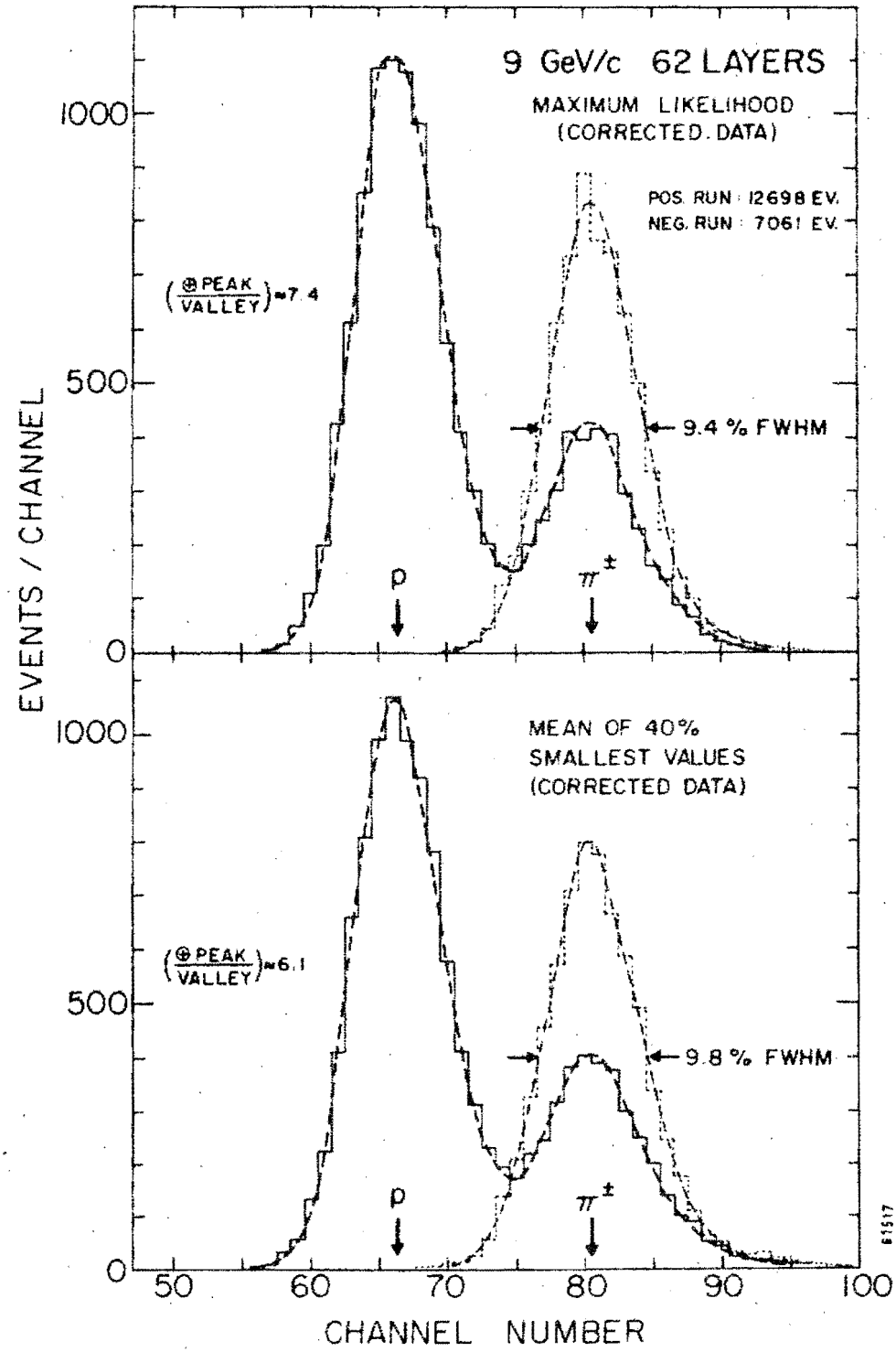
9 GeV/c 62 LAYERS
MAXIMUM LIKELIHOOD
(CORRECTED DATA)
POS. RUN : 12698 EV.
NEG. RUN : 7061 EV.
(⊕PEAK / VALLEY) ≈ 7.4
9.4 % FWHM
p
π±
MEAN OF 40%
SMALLEST VALUES
(CORRECTED DATA)
(⊕PEAK / VALLEY) ≈ 6.1
9.8 % FWHM
p
π±
EVENTS / CHANNEL
1000
500
0
50
60
70
80
90
100
CHANNEL NUMBER
61517

fig. 9

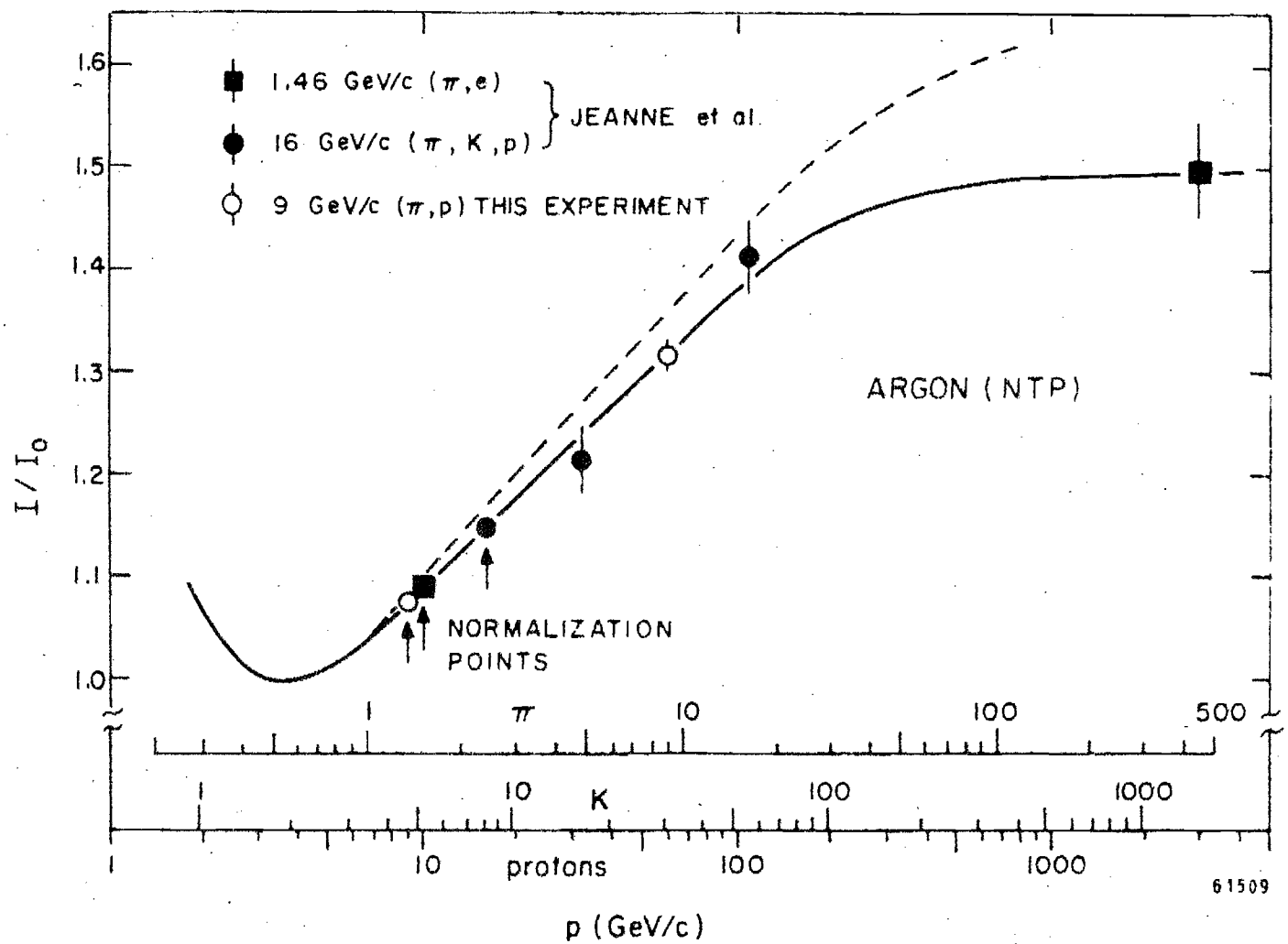
1.46 GeV/c (π,e)
16 GeV/c (π, K, p)
JEANNE et al.
9 GeV/c (π,p) THIS EXPERIMENT
ARGON (NTP)
NORMALIZATION POINTS
I / I₀
1.6
1.5
1.4
1.3
1.2
1.1
1.0
1
π
10
100
500
1
10
K
100
1000
1
10
protons
100
1000
61509
p (GeV/c)

fig.10

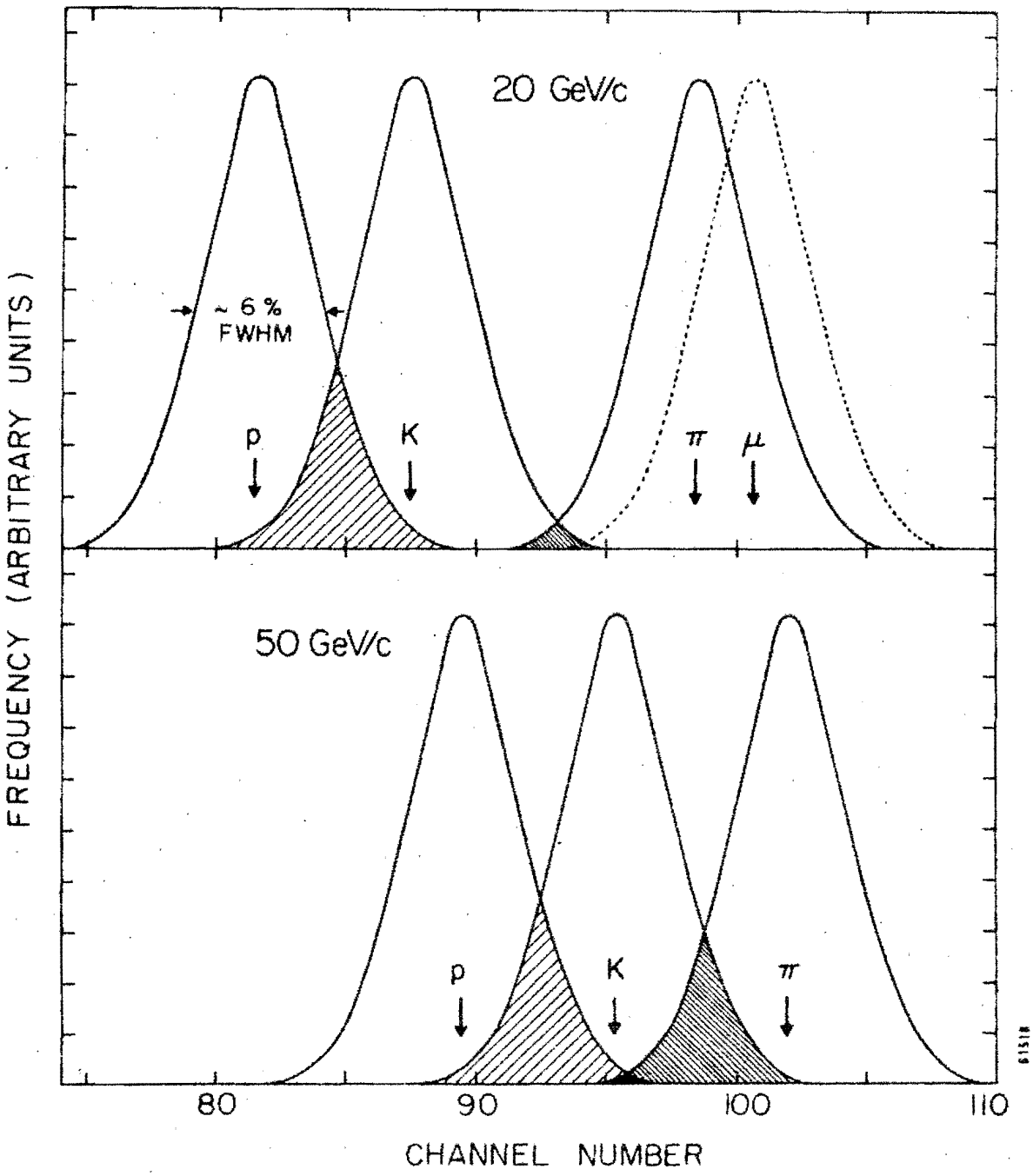
20 GeV/c
~ 6 %
FWHM
p
K
π
μ
50 GeV/c
p
K
π
FREQUENCY (ARBITRARY UNITS)
80
90
100
110
CHANNEL NUMBER

fig. 11

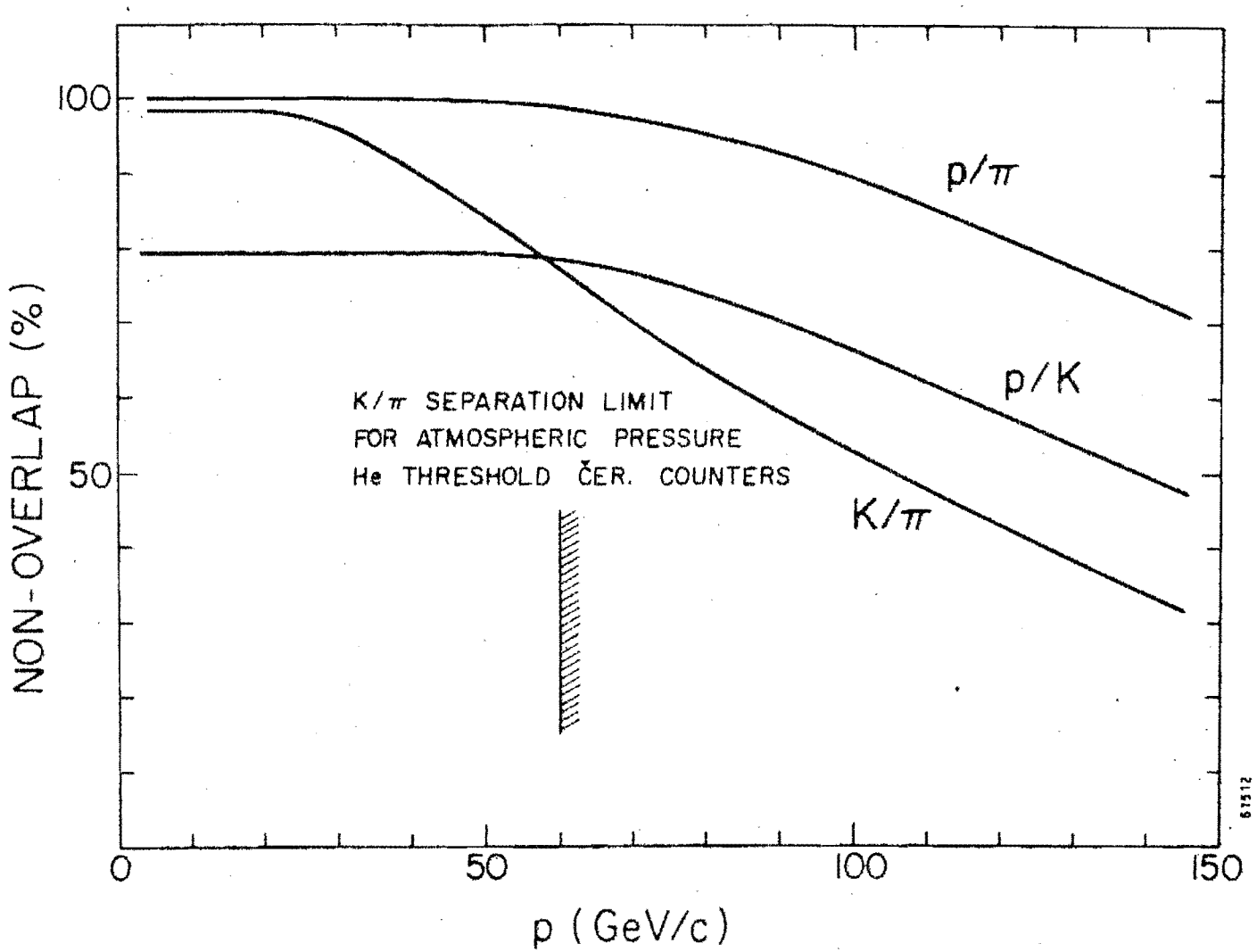
100
50
NON-OVERLAP (%)
0
50
100
150
p (GeV/c)
p/π
p/K
K/π
K/π SEPARATION LIMIT
FOR ATMOSPHERIC PRESSURE
He THRESHOLD ČER. COUNTERS
61512

fig.12

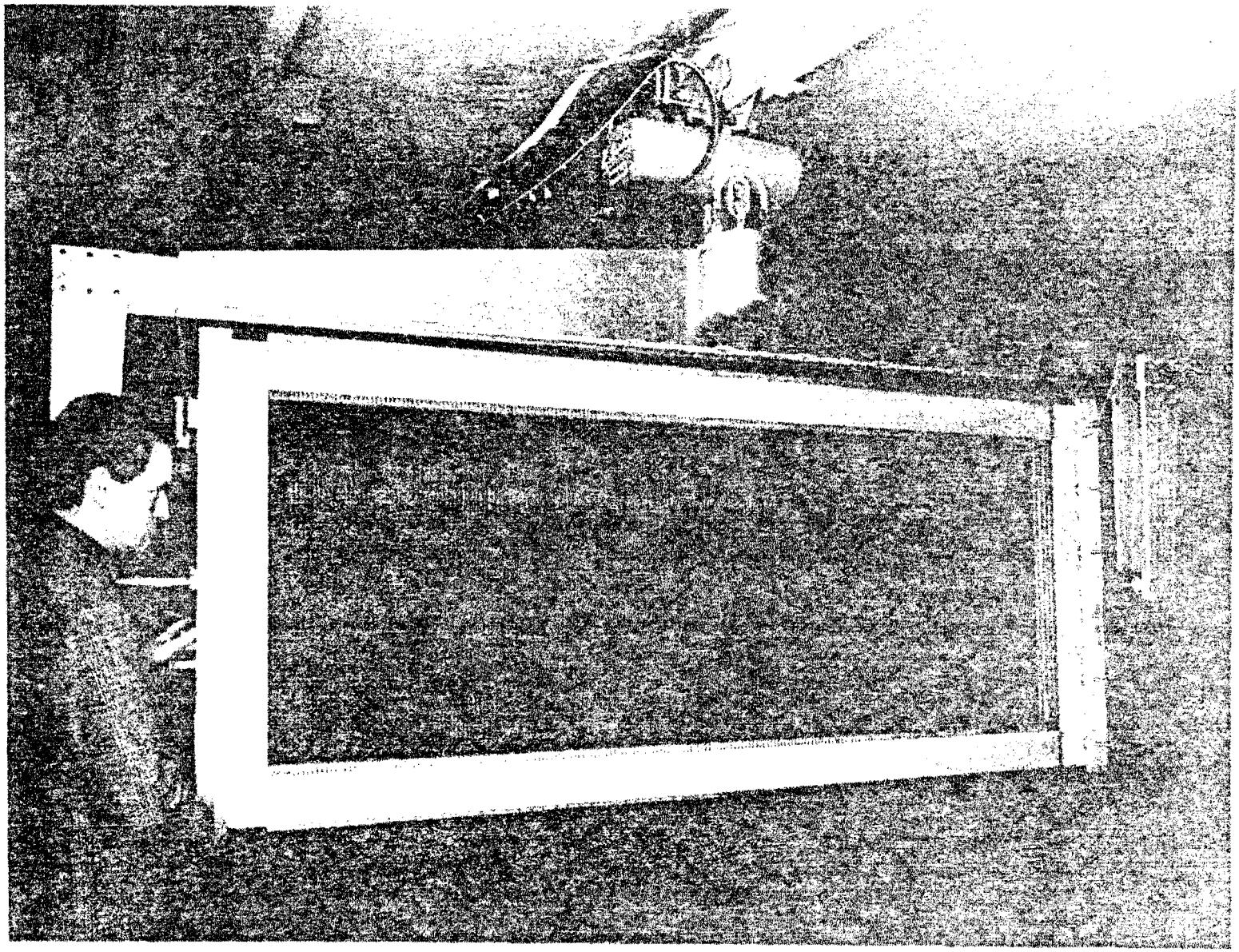

Fig. 13

CERN
SERVICE D'INFORMATION
SCIENTIFIQUE

NUCLEAR INSTRUMENTS AND METHODS 123 (1975) 237–254; © NORTH-HOLLAND PUBLISHING CO.

APPENDIX A-2

EXTERNAL PARTICLE IDENTIFIER (EPI) FOR THE BIG EUROPEAN BUBBLE CHAMBER (BEBC)

M. ADERHOLZ, P. LAZEYRAS, I. LEHRAUS, R. MATTHEWSON and W. TEJESSY

CERN, Geneva, Switzerland

Received 19 September 1974

A description of a multi-layer proportional counter system being built to identify fast charged secondary particles behind the 3.7 m bubble chamber is given in detail. The device consists of 128 layers, each with 32 (6×6 cm^2) cells across. It will be able to distinguish pions and kaons up to 70 GeV/c by sampling the ionization in the region of the relativistic rise.

1. Introduction

In this paper we describe the final version of a multi-layer proportional counter system[1–3]) designed for identification of fast charged secondary particles emerging from the 3.7 m bubble chamber. The External Particle Identifier (EPI) will efficiently distinguish between pions and kaons up to about 70 GeV/c, kaons and protons up to about 100 GeV/c and protons and pions up to about 150 GeV/c. This device, which is now under construction, consists of 128 layers with 32 (6×6 cm^2) individual proportional counters (cells) in each layer. Ionization deposited in the detector is sampled by measuring the pulse height from each cell traversed by the particles. The final ionization-resolution in the region of the relativistic rise will be about $\pm 3\%$ fwhm according to our measurements.

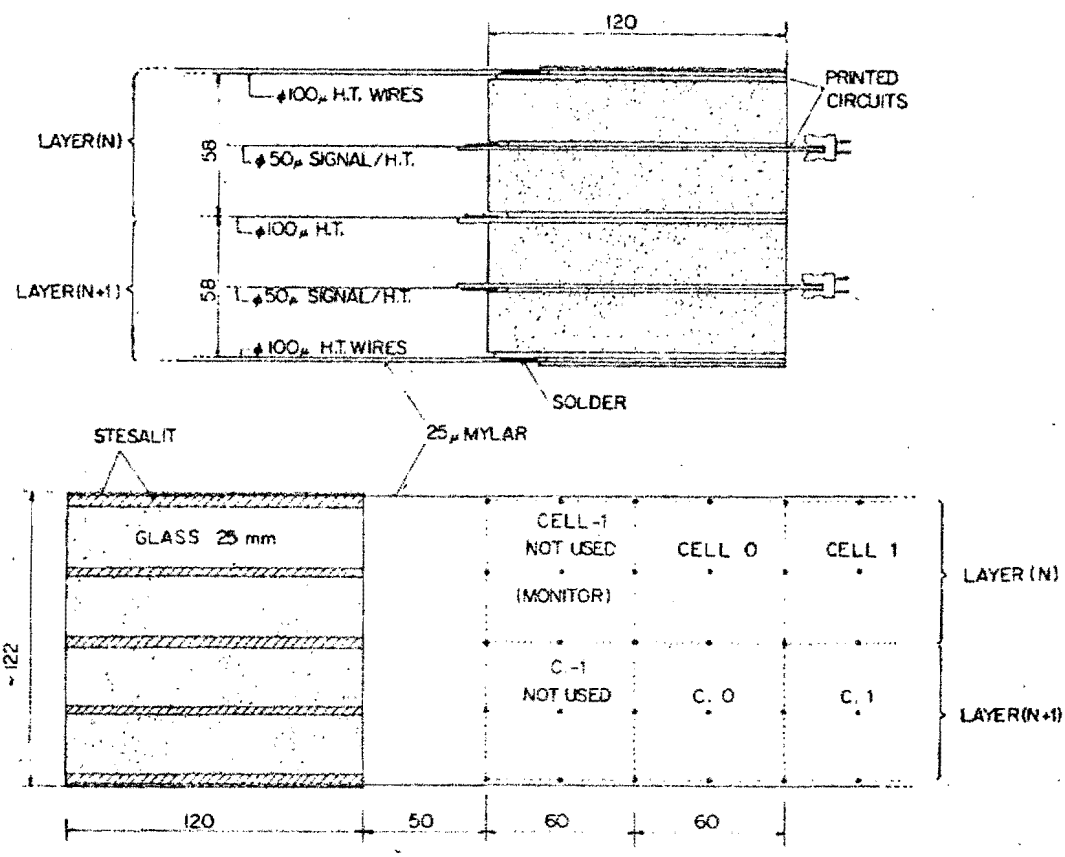

Fig. 1. Construction details of the double-layer module.

The detector, which has a detection surface of 90×192 cm^2 and a total length of about 8 m, will be placed at a distance of 11 m from the center of the bubble chamber. It has been designed to identify those secondary particles having the same charge as the primary beam (leading particle concept). Non-interacting beam particles pass through an insensitive region corresponding to the beam dimensions at one side of the detector (offset beam hole). The rf separated beam[4]) provides for full separation up to 70 GeV/c, the maximum unseparated beam momentum being 150 GeV/c. The spill time is 6 μs (limited by the C-band rf modulator pulse duration). Because the EPI time resolution is longer than the beam spill time, all secondary particles for each accelerator burst must be registered together. The data from the EPI will be read into an on-line computer, compacted and written onto 1600 b.p.i. magnetic tape together with the bubble chamber roll and frame number. To this will be added the track coordinates from multiwire proportional chambers, in front and at the back of the EPI, to enable precise track reconstruction and correlation with the bubble chamber picture in off-line analysis, as well as data from further multiwire proportional chambers which will measure the primary beam particle angles at the bubble chamber entry. The off-line data analysis will include maximum likelihood fitting procedures for the measured ionization values to establish the particle's identity.

2. Construction of modules

Construction details of the double layer modules for the EPI are shown in fig. 1. The assembly has been simplified as much as possible. The individual proportional counters of 6×6 cm^2 section and 101.6 cm length are formed by stretching stainless steel wires with 3 cm spacing on laminated frames. The frames are made of a 12 cm wide sandwich of glass, Stesalit and printed circuits glued together with Araldite and closed at each side by 25 μm thick Mylar foils. Both the outer and the median ht planes have $\varnothing$ 100 μm wires tensioned to 160 g and soldered to the printed circuits. The alternating signal/ht wires are $\varnothing$ 50 μm, tensioned to 40 g which is safely below the breaking point. The electrostatic field of the individual counters is perfectly symmetrical, therefore no forces are exerted on the wires. The deformation of the frames due to the wires and Mylar foils is negligible. Glass, as the principal frame material, was chosen for its surface quality with low outgassing properties as well as for economic reasons. We use glass bars 12 cm wide since narrower ones were not to be obtained, although 8 cm

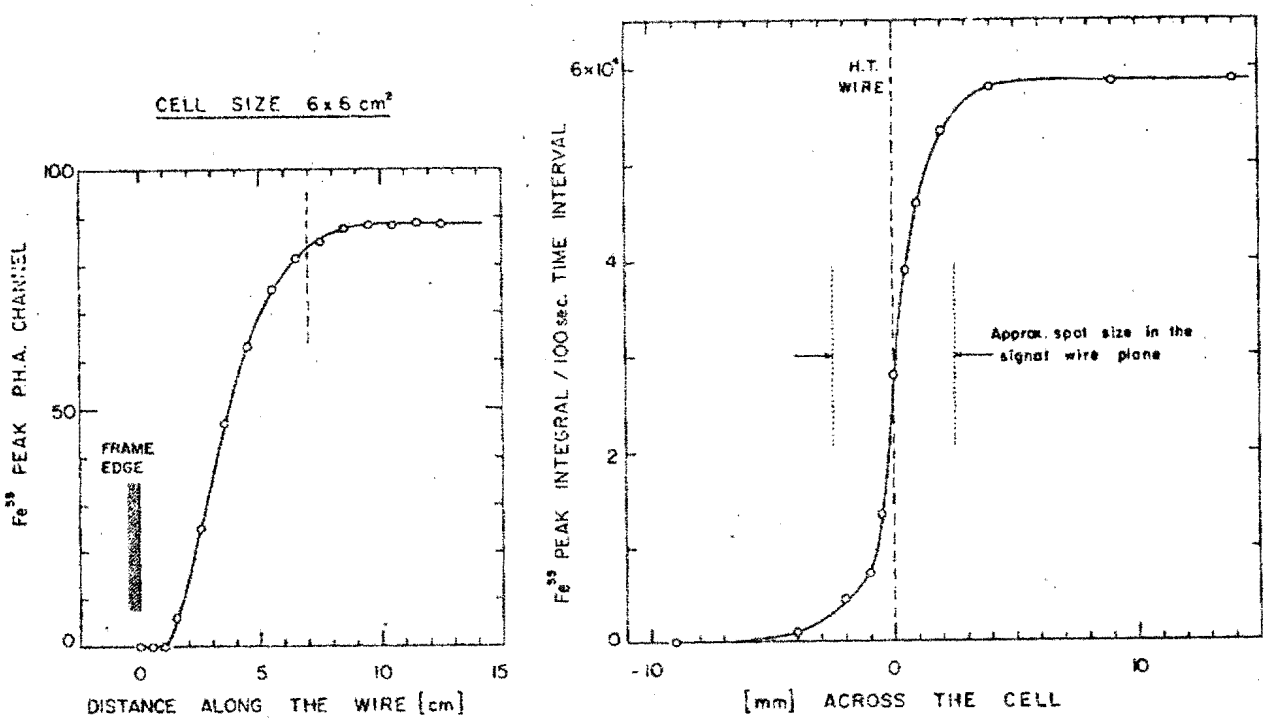

Fig. 2. Edge effect (left) and crosstalk between the adjacent cells (right).

would have been adequate for the frame. The total weight of a double layer module is about 250 kg with electronics. The assembly of one module takes an average of two weeks (27 different operations) and is made in a specially climatised and dust-free workshop. Three modules can be assembled simultaneously.

3. Performance

All important parameters of the EPI were already tested on several prototype modules. The useful height of the detector and the uniformity of the response along the wires has been measured using the 5.9 keV X-rays from an ^{55}Fe source. The result is shown on the left part of fig. 2 for a 6×6 cm^2 cell. At a distance of 5–6 cm from the frame edge the response is already uniform within the acceptable limits of about $\pm 5\%$, giving about 90 cm of effective counter length. Efficiency of the separation between adjacent cells could be estimated from the result presented on the right side of fig. 2. When irradiated by a collimated radioactive source the "uncertain" region is only about 3–4 mm wide, comparable with the source spot size.

Fig. 3 illustrates how the insensitive beam region is produced by covering the appropriate part of the signal wire with a thin insulating layer. Several different materials (e.g. thin metallic tube, Mylar strip, thin coating of paint, coating of Araldite etc.) were tried, but finally a $\varnothing$ 130 μm glass tube was adopted as the most simple and practical solution. As seen from fig. 3 the tube prevents efficiently the charge collection from the desired length of the signal wire with very sharply defined boundaries. With a 4 cm long glass tube the effective insensitive region extends to about 5 cm along the wire.

The long-term stability of the module and necessary gas flushing rate was also tested at constant temperature. After the gas supply was turned off and the internal over-pressure allowed to equalize to the atmospheric pressure, the pulse-height response started to decay due to outgassing, diffusion through the Mylar foils and stratification of the gas filling. As seen in fig. 4, during the first period of about 30 h the decay is most rapid with a rate of about 80 h for a drop to 1/e value due, probably, to penetration of humidity through the Mylar foils, after which it slows to a rate of almost 400 h to 1/e. No corrections were made for atmospheric pressure variations. The resolution for ^{55}Fe was not seriously impaired even after almost 200 h but because of the pulse-height decay it is quite clear that the modules cannot work properly without continuous gas flow.

The behaviour of the detector with respect to the atmospheric pressure changes was also investigated more carefully. Only the reaction to overpressure inside the module was studied. For that purpose it was

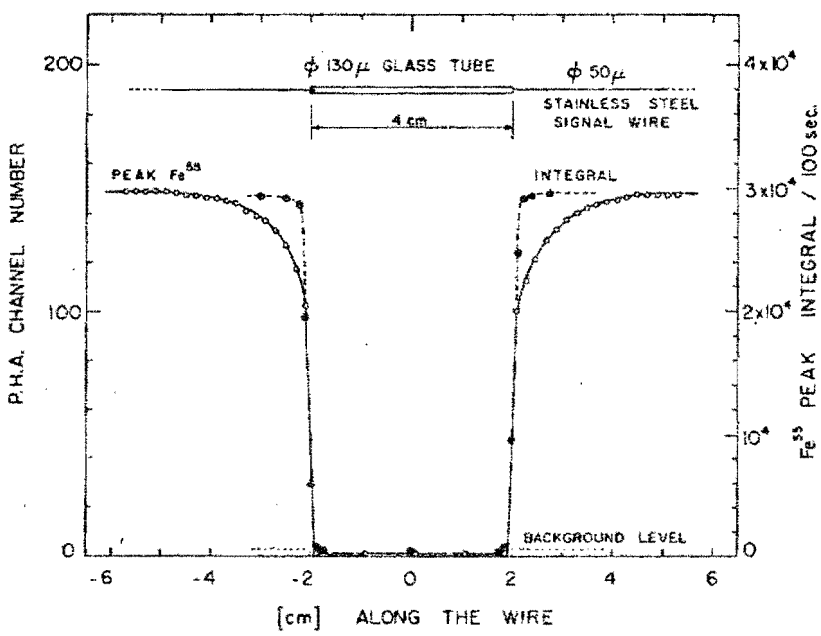

Fig. 3. Beam insensitive region of the signal wire.

TABLE 1

Relativistic rise of the ionization in different gas mixtures.

Gas mixture	π^+/p ionization ratio at 9 GeV/c	Proton peak fwhm (%) (max. likelihood)
Ar + 5% CH_4 [3])	1.21 ± 0.01	10.7
Ar + 5% CH_4 (this exp.)	1.22 ± 0.01	10.5
He + 30% Ar + 10% CH_4 [3])	1.21 ± 0.012	11.3
Ar + 15% Xe + 5% CH_4 (this exp.)	1.23 ± 0.01	12.0
Kr + 5% CH_4 [3])	1.26 ± 0.015	14.9

necessary to cover the Mylar foils with metallic plates in order to protect them from excessive stress and possible rupture. As shown on fig. 5, at the beginning, there is a very steep dependence of the output pulse-height on pressure, which is caused by mechanical settling of the Mylar foils against the supporting metal plates. Starting from about 10 mm H_2O over-pressure the detector pulse-height is reduced by about 2% for a 1% pressure increase in the case of a ^{90}Sr source and by 4.8% in the case of ^{55}Fe. This is explained by the fact that the exp(E/p) term in the gas amplification formula is partially compensated by more ionization deposited by 0.54 MeV relativistic electrons traversing the detector, compared with the 5.9 keV quanta of ^{55}Fe converted locally within a few tenths of a millimetre. Because of that effect, the necessary continuous monitoring of the detector response should be done using energetic β sources.

The deformation of the Mylar foils, responsible for the strong pressure-dependence in the region of the atmospheric pressure variations, will presumably become negligible when all the individual modules are installed inside a pressurized box.

To complement our results using Ar + 5%CH_4 a further gas mixture containing Ar + 15%Xe + 5%CH_4 was tested during the June 1974 run at 9 GeV/c in a 64-layer detector set-up as described in ref. 3. For reference, the Ar + 5%CH_4 mixture was first tested

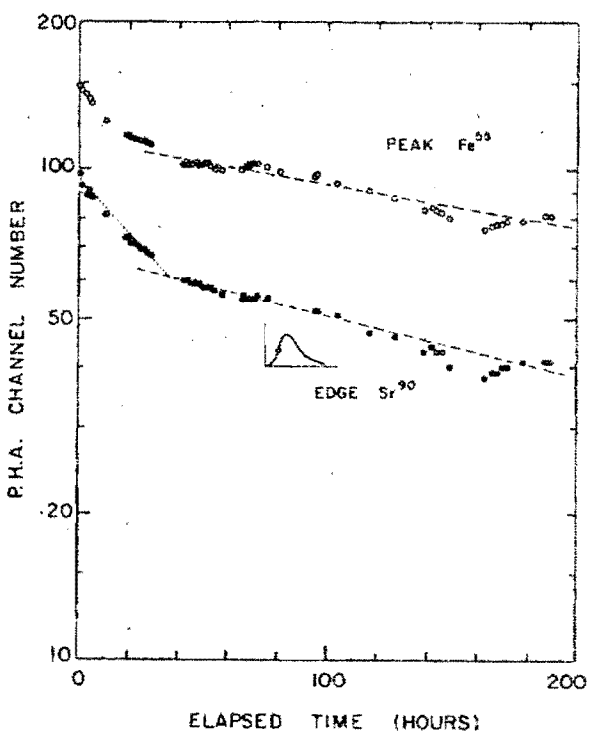

Fig. 4. Long-term stability with the gas supply turned off.

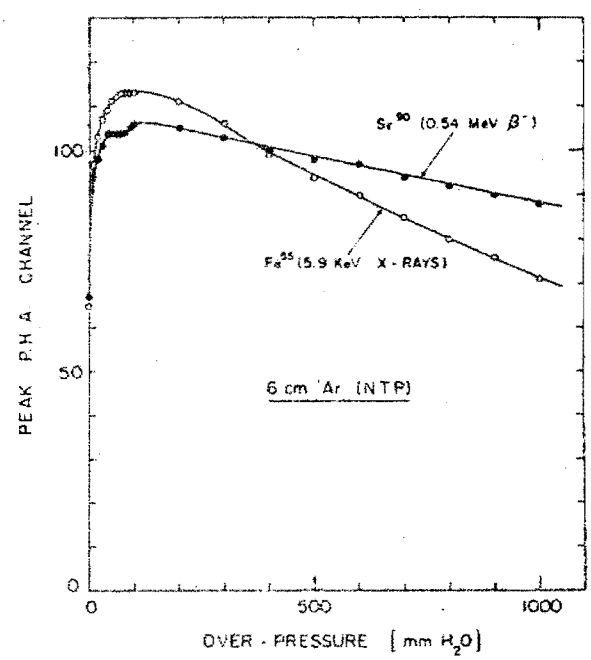

Fig. 5. Pressure dependence of the output pulse height.

again in order to verify the reproducibility of the ionization measurements. The summary of the results is given in table 1 where the ionization ratio for π^+ and protons at 9 GeV/c and the fwhm of the proton peak is listed. The most practical mixture (Ar+5% CH_4) shows a satisfactory relativistic rise and at the same time the best resolution. There is an indication of a slightly steeper relativistic rise for the mixtures containing xenon and for Kr+5%CH_4, an advantage which is, unfortunately, offset by worse resolution. For the runs using the last two mixtures a very limited amount of gas was available (due to high cost) which precluded the attainment of well stabilized conditions. This might be partially responsible for the broadening of the peaks. It is not excluded that, with a closed gas circulation loop and continuous purifying, the next stage of development of the EPI will use the more expensive mixtures. Exact predictions in this field are difficult now, because the values of the Fermi plateau for those mixtures are not known. Nevertheless, it will be certainly attractive to work with a noble gas heavier than argon and at reduced pressure in order to push the onset of the plateau towards higher particle momenta.

4. Electronics

The Data Acquisition (DA) circuit for each one of the 4096 proportional counter cells is shown in fig. 6. It was designed to accept simultaneous and non-simultaneous particles up to a maximum of 10 μs beam spill. At a gas amplification factor of 10^4 the mean charge collected by each cell for each particle is about 3.5×10^{-13} C. The high input-impedance amplifier takes a current from this charge and converts it to a ≈ 1 V output ($-i_{in}=e_0R_f$). This signal then goes to an integrator and to the summing point is added a component of the signal, chosen so that the composite output waveform is flat-topped to within 2% for 10 μs. Provided that the DA gate is open this signal is sampled by an Operational Transconductance Amplifier synchronized by the beam ejection trigger and held when the beam spill ends and the circuits have settled within 1%. The signal is now a dc level which decays about 1% per ms. It is applied to the comparator, assuring a logical "1" at the output, which opens the scaler input gate. About 10 μs after this, 255 clock pulses are generated synchronously with a precision ramp waveform from a digital to analogue convertor. The scaler counts the clock pulses until the ramp voltage equals the acquired signal voltage at which time the comparator switches and stops the scaler counting. Since the clock and the ramp will be common to all channels, the analogue to digital conversion of all 4096 cell signals will be accomplished simultaneously with 8-bit resolution in 250 μs. The measured r.m.s. error for a single channel, based on a most probable signal of 1 V, is $\pm1.5\%$. This comprises the following components: beam spill $\pm1.0\%$, noise $\pm1.0\%$, settling time $\pm0.5\%$, drift $\pm0.25\%$, quantization error $\pm0.4\%$. Overall non-linearity was found to be less than the quantization error. It is not proposed to use close tolerance passive components so each channel will have the facility of adjusting gain, pulse form and zero-set.

At the end of the conversion the Master Control will send the Transfer pulse which parallel loads the data, in the 4096 scalers, into the corresponding cell shift registers, then resets the scalers to zero. This will be followed by eight clock pulses (1 MHz) which operate the cell shift registers which will be arranged (see fig. 7) so that slice 0 data is moved to a separate set of registers, the slice shift registers located at the end of each layer, slice 1 moves to slice 0, slice 2 to 1, etc. The slice shift registers will then be connected serially so that the computer may request the Master Control to shift (at 10 MHz) and transfer slice 0 data via fast data link (as 64 16-bit words) toward the computer. This process is repeated for slices 1, 2, ... 31, the total read-out time constraint from the hardware being $32\times[8+(64\times16\times0.1)]$ μs, or about 4 ms. During the shift process, the DA circuits may accept another beam pulse because the scalers are already cleared. The Master Control will generate all necessary sample, ramp, clock, transfer, reset and shift signals on command from the beam ejection trigger and other hardware or computer timing signals. Extreme care has been taken in keeping the power dissipation of this system, which will be mounted directly on top of the detector modules, to a strict minimum.

The "slice" organised read-out system was chosen since it produces a grouping of cells in the direction of the particle trajectories and thereby eases the pre-evaluation by computer, especially for testing purposes. Furthermore, it lends itself to a direct fast hardware evaluation of a passing test beam for calibration of the EPI. The ionization losses of a particle passing parallel to the detector axis through all 128 layers could be measured with reasonable resolving power using a rather simple hardware wired for "mean of the smallest 40% of 128 values"[3]). A single result per track can be obtained this way, neglecting differences in the individual cell response. The necessary hardware contains essentially a fast random access memory of 256 words of 8 bits. The contents of the 128 channels

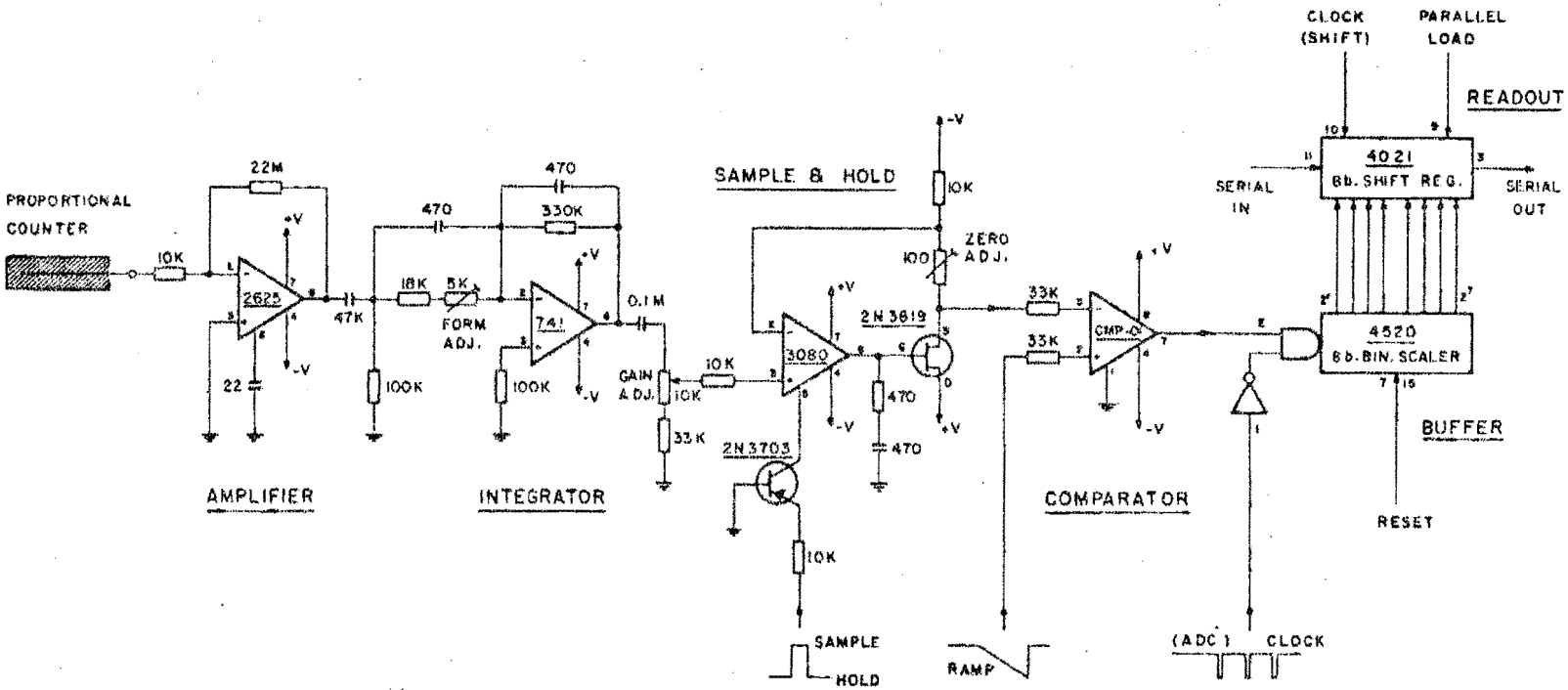

Fig. 6. Data acquisition circuits.

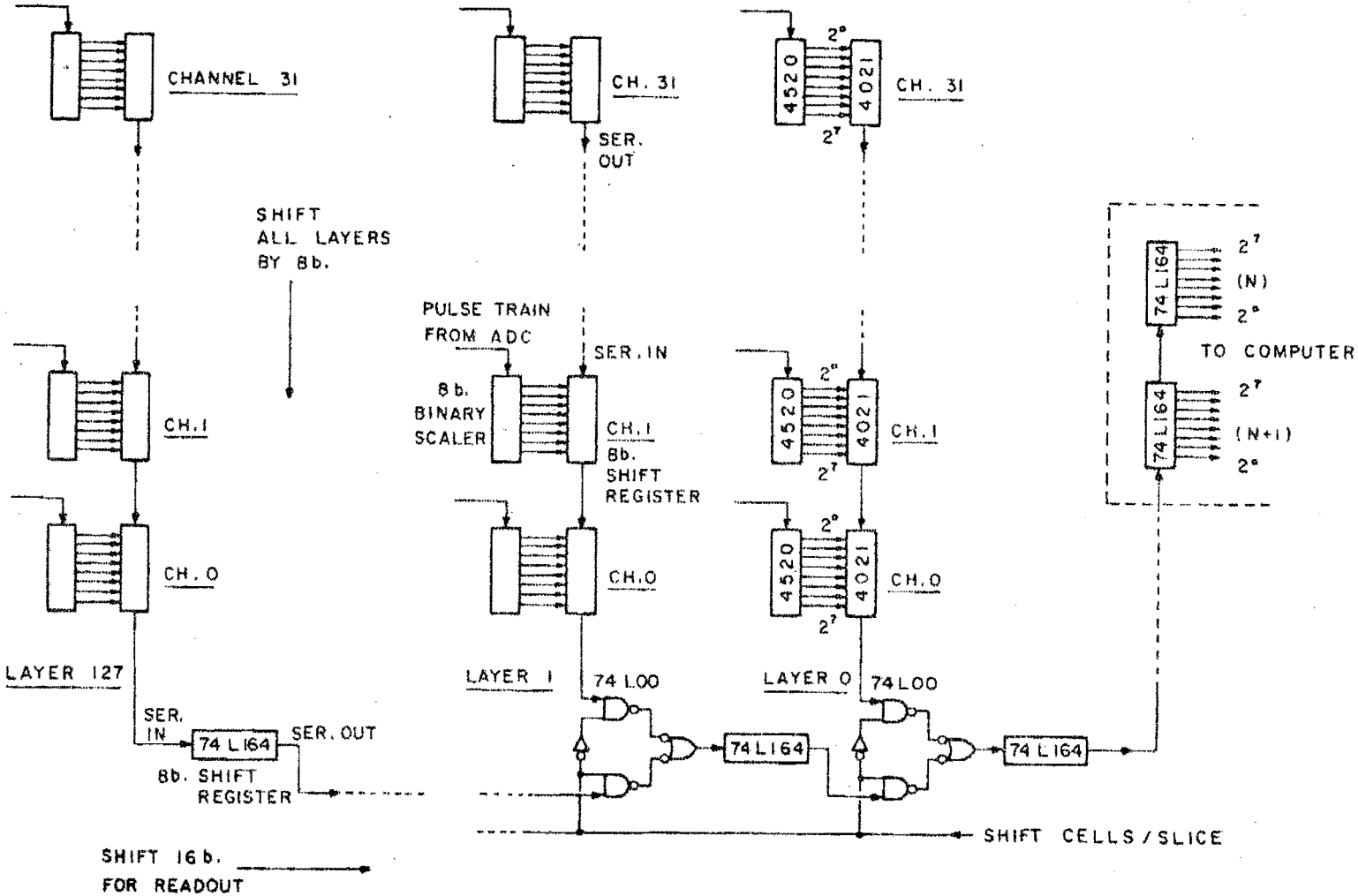

Fig. 7. Shift register read-out structure.

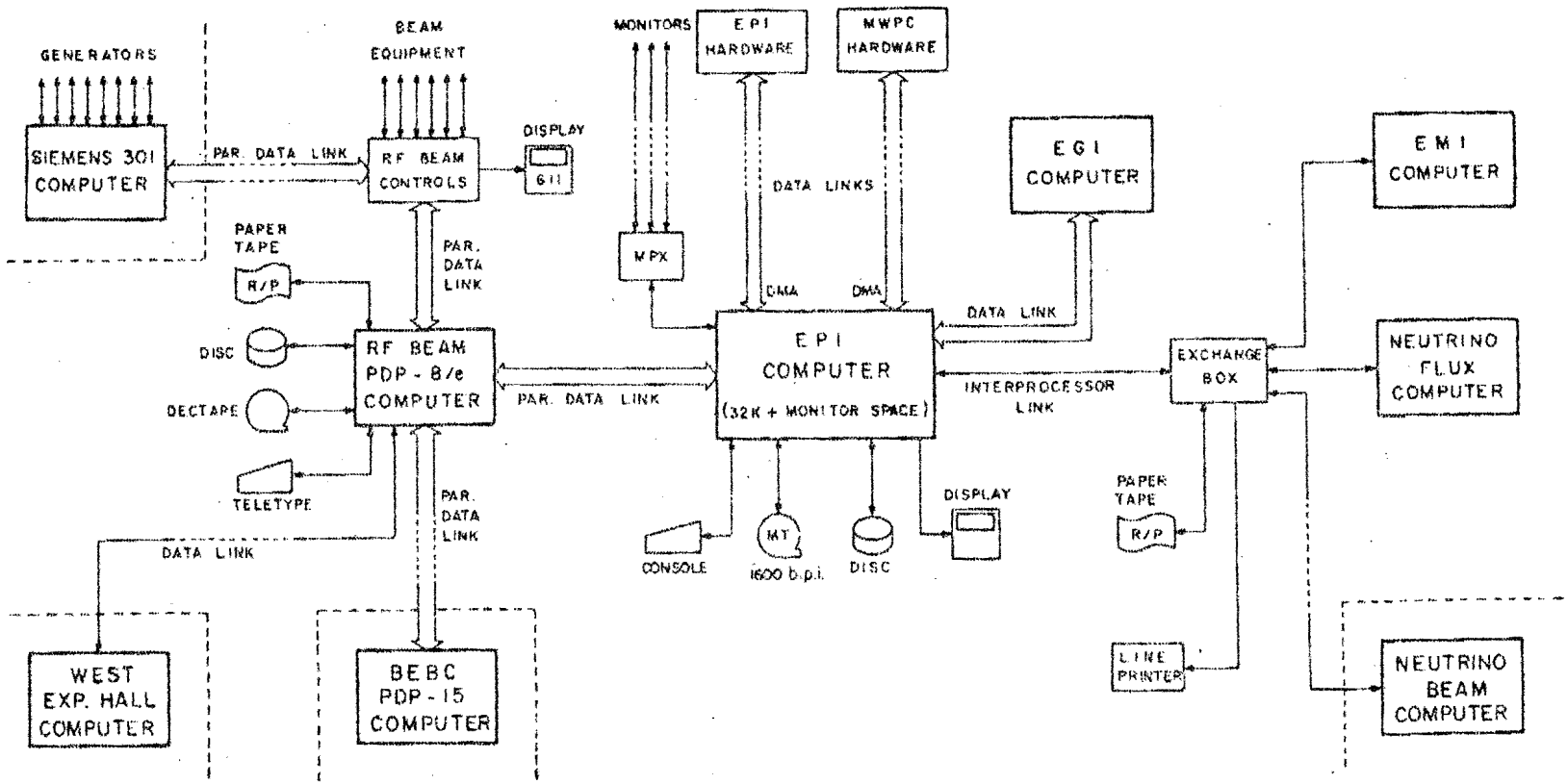

Fig. 8. On-line data handling organisation.

will be scanned through and each time a given value has been found the corresponding address location in the RAM array will be incremented by 1. When all 128 values are processed, the smallest 51 values (i.e. 40%) will be consecutively converted into corresponding pulse trains and summed-up using a modulo-51 scaler. To shift out a full 128 cell slice takes $[8+(128\times 8\times 0.2)]\approx 215\ \mu s$. Writing time into the RAM could be neglected, the serialisation and summing-up would take on the average 650 μs, using a 10 MHz clock. The final result could be made available in less than 1 ms to be visually displayed. For more elaborate testing the on-line computer would be used.

5. On-line data handling facility

The EPI and its associated multiwire proportional chamber system will be serviced by a dedicated computer, which is part of a loosely connected set of data-acquisition and control computers to be used in connection with BEBC and the West Area Neutrino Facility[7]).

The EPI computer (fig. 8) will consist of a ≥ 16 bit machine with 32k words of memory for user programs and data, plus added space for the system monitor. The latter will have full multi-tasking capabilities to allow easy adaption to the real-time environment. A moving head disk of at least 1M word capacity will be incorporated as mass storage for the multi-tasking monitor, user programs, tasks, and overlays as well as for log-files to monitor the long-term efficiency of the apparatus. Data from the experiment will be output via heavy-duty medium speed 1600 b.p.i. 9-track magnetic tape units. As a user interface to communicate with the system a graphics display with keyboard of the storage tube type is foreseen. On-line development of real-time programs, a necessity due to the very extended running periods of the equipment, will be possible from a separate console typewriter, which will also be used as an output device for alarm messages, etc., when appropriate. For large scale alphanumeric, and graphics, output we plan to share a line-printer (plotter) between all involved computers.

Data from the EPI and from the MWPC system before and behind BEBC will be entered via direct memory access transfers after each burst. For the EPI the full 4096 ionization values will be transferred to memory, where they will be compressed by eliminating zero-content cells and then formatted onto the magnetic tape. A similar packing is foreseen for the MWPC output, except that here a hardware feature, described below, will search out the hit wires and the corresponding timing information. To this will be added bubble chamber and beam parameter information as required. With compacting of data it should be possible to run several hours per tape in double expansion mode of the bubble chamber.

Large data regions in memory are foreseen to histogram the overall response of the apparatus over extended periods of time. This is necessary due to the very low intensity of hits per burst, especially for the outer cells. A versatile set of graphics routines will allow operator-requested displays of the efficiencies, response, etc., of numerous subsets of cells. The printer will allow to make hard copies of these displays for easy logging of the results.

Furthermore, an as yet not fully defined set of tasks to control and monitor the important parameters and to allow on-line procedures during setting-up of the equipment will be incorporated. For this a multiplexed digital input/output interface under program control will be used.

Tracing and fitting of sample tracks through the MWPCs and the EPI and ionization determination are aimed at to further monitor the correct functioning. Here again the visual display will play an important role in giving a full picture of the sampled tracks passing through the device. However, the idea of full filtering and reconstruction of all tracks for every burst on an on-line basis and their parametrization has been discarded as unrealistic on a small computer. This will be done at a later stage off-line in connection with the data handling for the bubble chamber pictures.

The EPI computer will be linked to several other computers in the same control area. A parallel link will connect to an already installed PDP-8/e (Disk, Dectape), which controls the rf separated beam equipment. Existing links to the beam controls, the West Generators' Siemens 301 and the BEBC control computer, an extended PDP-15 configuration, will allow the PDP-8/e to transfer all required beam and bubble chamber status information to the EPI computer, or accept commands from it, as needed. To this will be added a parallel link to the computer for the proposed External Gamma Identifier, described in the next chapter, and to the experimental area's computer, a Norsk Data NORD-10.

To enlarge the integration a network of serial links is proposed with the computers for the External Muon Identifier, the Neutrino Flux and the Neutrino Beam Control, which will be of the same type as for the EPI and also run under the same version of the

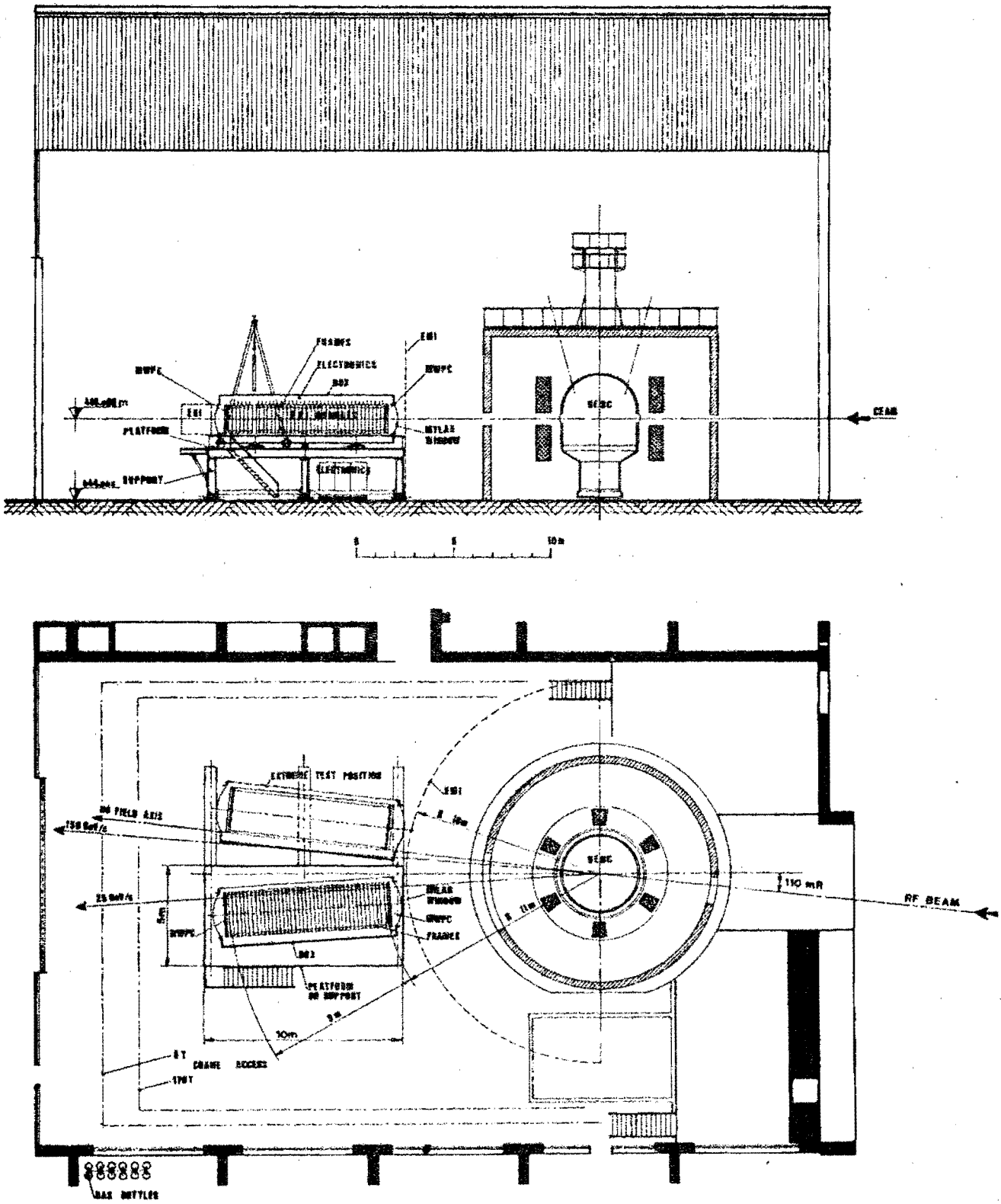

Fig. 9. General layout in the BEBC hall.

7. Efficiency of identification from simulation studies

The EPI has been optimized with respect to a set of constraints, i.e. the BEBC exit geometry, trapping of low momenta secondary particles in the magnetic field, existence of an extra absorber for the EMI which determines the 11 m minimum distance from the BEBC center and limited overall length. Those constraints have formed the basis for a simulation study of the EPI performance in regards to its geometry, the results of which have led to the finalized design as described.

In the simulation a primary beam of a given width and height was directed onto the center of the chamber. The beam, arriving at the shielding window at the angle of 110 mr (see fig. 9), was traced through the stray and main magnetic field, thus forming a curved interaction volume symmetric around the center of the chamber. Inside this volume (for our calculations the full length of the chamber was used) a given number of individual simultaneous secondary tracks of both charges were generated. They were followed through the magnetic field and the downstream shielding window towards the EPI. The distribution of the longitudinal momentum p_l of these secondaries was taken to be uniform between 10 GeV/c and the maximum value (beam momentum). The distribution of the transverse momentum p_t was obtained by using the well known Cocconi formula. Therefore, the generation is based on the assumption

$$\frac{d^2 N}{dp_l\, dp_t^2} \approx \exp\left[-\left(\frac{p_t}{a}\right)^2\right], \quad \text{with } a = 0.4 \text{ GeV}/c.$$

No background from other sources like chamber windows was taken into account. The EPI was aligned so that the beam edge was grazing the outside edge of slice 0 of the detector.

Fig. 11 shows the distribution of momentum p_{total} against the lateral distance from the edge of slice 0, as described above, at the middle plane of the detector (15 m from the BEBC center). The full line shows the

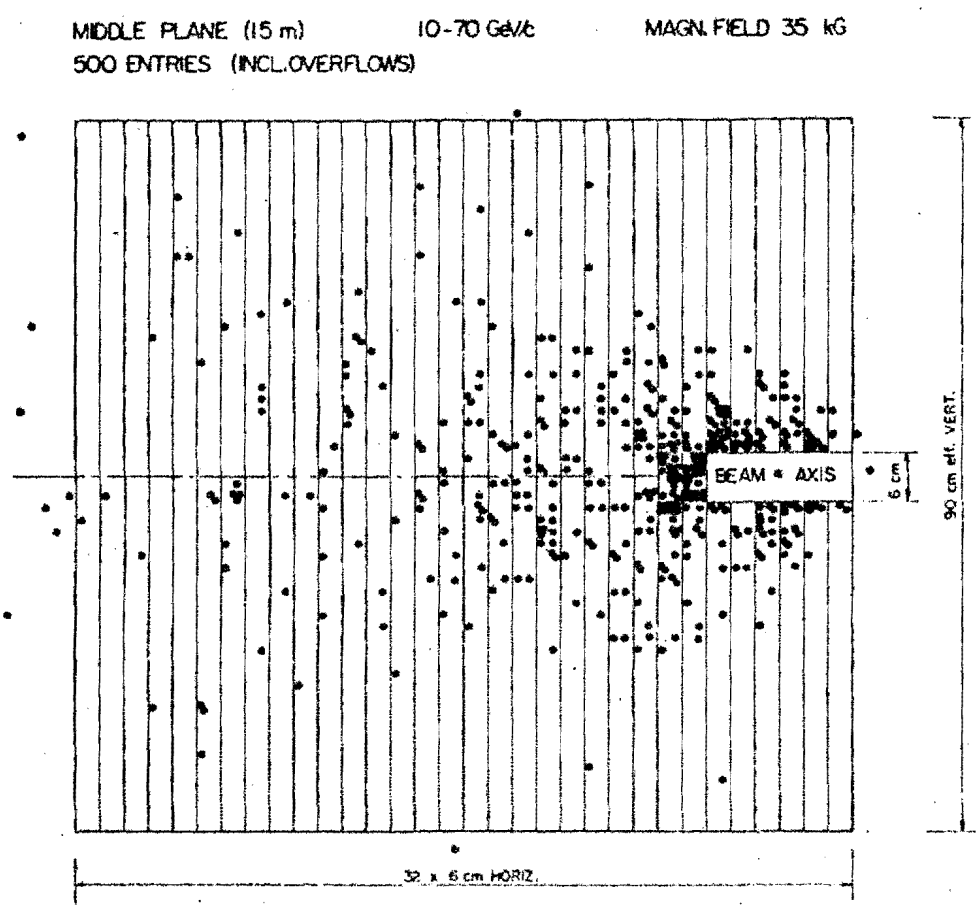

Fig. 12. Spatial distribution of the hits in the middle plane, 10–70 GeV/c, beam-charge secondaries only.

a distance of 11 m behind the BEBC center are listed in table 2 for several beam momenta. The beam enters at −6 m under 110 mr angle directed at the BEBC vertical axis. The errors on the listed angle values are of the order of 1 mr. Note that the vertical beam axis here is 406 cm above the floor level. Two extreme positions of the EPI are shown on fig. 9. One is for "beam-charge secondaries only" mode of operation at 25 GeV/c with the beam passing through the offset hole and the other is the furthest displacement necessary for testing the 32 slices of 128 layers using the beam tracks with BEBC magnet switched off. The necessary local electronics and controls are shown installed under the platform. The battery of the pre-mixed gas bottles must be installed outside the building for safety reasons. The installation of the EPI in the Hydrogen danger zone puts severe constraints on the electric equipment design.

The space occupied by the External Muon Identifier (EMI) [5]) for neutrino physics immediately behind the BEBC magnetic shielding is also shown on fig. 9. Another part of the hybrid BEBC system will at a later stage be the External Gamma Identifier (EGI) [8]) which is localised behind the EPI at a distance of about 20 m from the BEBC center. The EGI is designed for identification of γ's from the fast π^0's in the forward cone when BEBC will be working with a hydrogen track sensitive target in a hydrogen–neon mixture. The proposed detector consists of a sandwich of MWPCs and lead plates followed by an array of lead-glass Cherenkov counters (LGC). This detector is aligned on the neutral axis of the beam. The information from its 100 LGC and the hits from the total of about 10000 wires will be transferred via small dedicated computer to the EPI computer to be added onto the EPI magnetic tape (see fig. 8).

Fig. 10 shows some details of the arrangement of the EPI modules inside the pressurized box, as seen from the back looking towards the bubble chamber. Shown in the cut are 32 "active" cells 6 cm wide, with the grid giving the position of the ht and signal wires. The extra cells at each side are not used except for the ^{90}Sr monitors at the four corners of the detector. The gas enters the modules in the bottom right corners via a distribution system ensuring uniform pressure in all modules. The gas mixture is allowed to escape into the box from the top right corners, the pressure control and common exhaust valve is mounted on the box. The beam insensitive region inside the first group of six active cells (5×36 cm^2) is visible on the left side. The wall of the box on this side will be made as thin and light as possible in order to reduce the interference with the EGI in this region of the neutral beam axis.

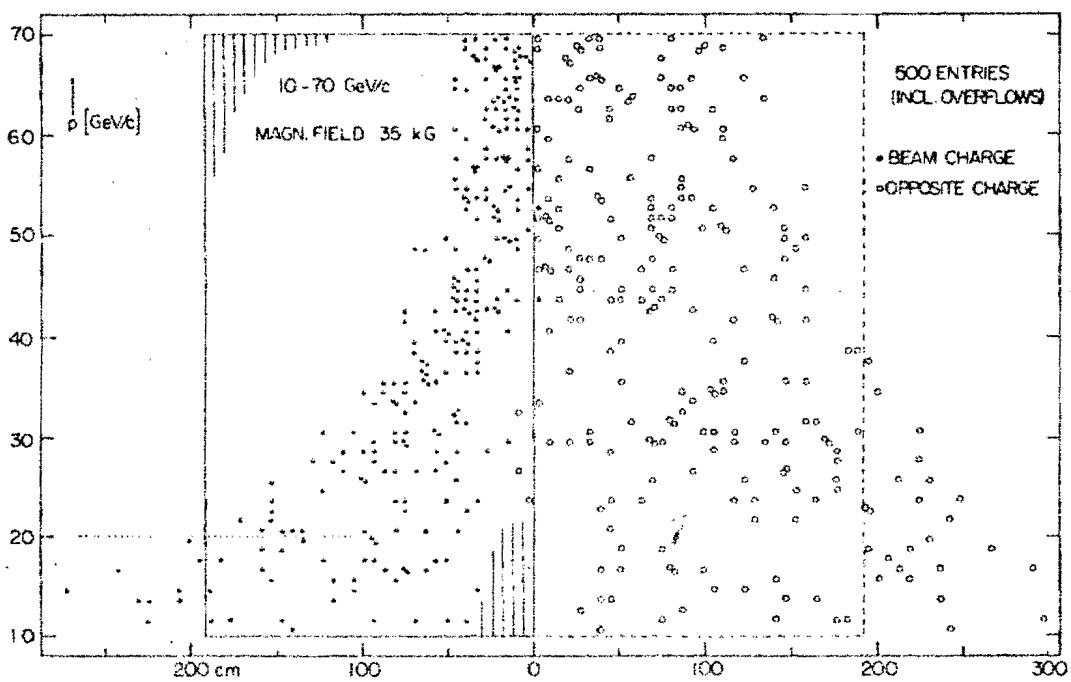

Fig. 11. p_{total} distribution of secondaries across the EPI detection surface.

detector in its normal position, the dashed line shows the double detection surface which would be needed for both positive and negative secondaries. The beam momentum is 70 GeV/c and the BEBC magnetic field is 35 kG. Beam-charge and opposite charge secondary particles in the momentum range of 10 to 70 GeV/c are plotted. For beam-charge particles, some 5–6% of the generated tracks are lost outside the detector, all of them in the 10–20 GeV/c momentum range.

In fig. 12 the spatial distribution of secondary particles in the middle plane of the detector is shown for secondary momenta from 10 to 70 GeV/c and for full magnetic field. The detector is in its normal position, i.e. aligned for maximum efficiency for secondaries having the same charge as the beam particles. Beam particles and the fast secondaries hitting the offset beam hole of 6×36 cm^2 are removed. There are some 13% of fast secondary tracks lost in this beam hole and about 6% are lost outside the detector, most of them in the low momentum range.

We have also studied a symmetric positioning of the EPI for certain experiments. Fig. 13 shows the situation for 10–140 GeV/c secondaries of both charges for full magnetic field of BEBC. In this mode of operation of the EPI a second insensitive beam region would be of interest near the detector center. In this position about 4% of secondary particles are lost in the offset beam hole. Some 6–7% of the lower momentum particles are lost at each side of the detector. If the central beam hole has the same dimensions as the offset hole (i.e. 6×36 cm^2), about 22% of the fast particles will be lost there. With no central beam hole, signals from simultaneous beam particles will cover the signals from the regions above and below the beam, resulting in an additional 10% loss.

Since the central hole will cause disadvantages for experiments, where only beam-like secondaries are of major interest, we feel that the best compromise would be to suppress the central beam hole and, for experiments where both charges are of interest, to reduce the primary beam width to the smallest value still acceptable for the bubble chamber. The same argument is valid for work in the lower momentum region at 10 to 70 GeV/c where it becomes immediately apparent that the BEBC magnetic field would have to be reduced correspondingly to get the same spread.

Two simulated 10-particle events as "seen" by the cell matrix of the EPI are shown on fig. 14. The non-interacting beam tracks and the secondaries within the

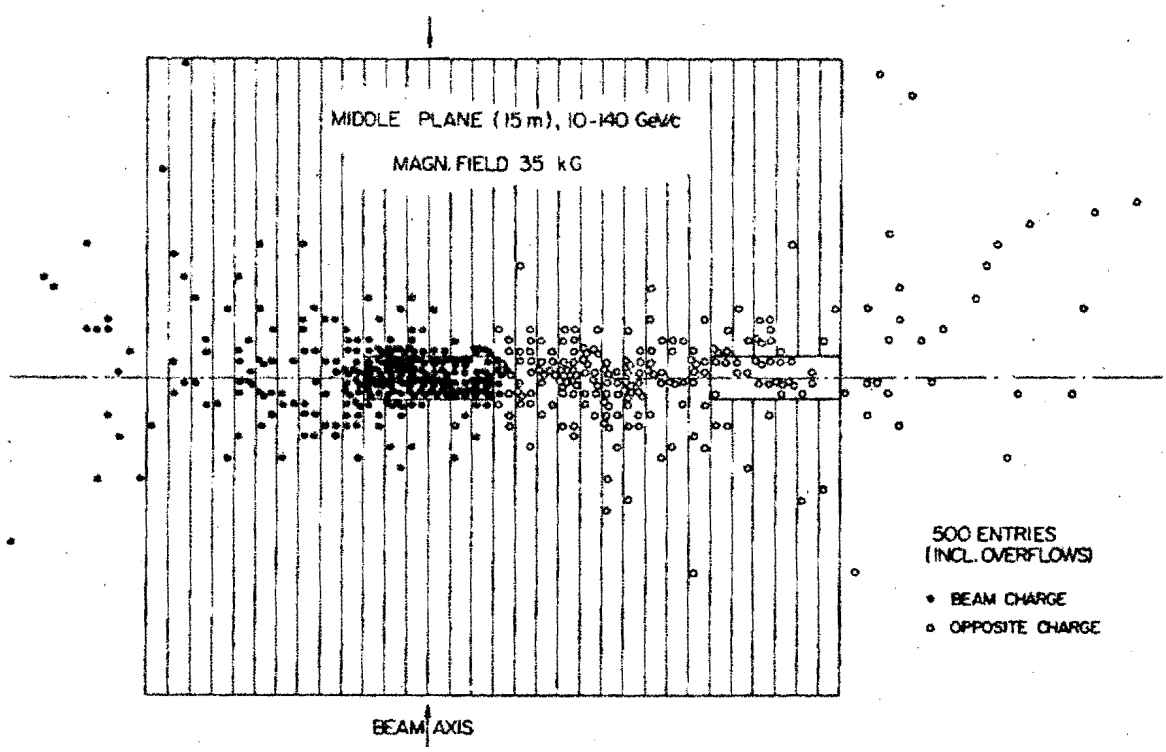

Fig. 13. Spatial distribution for secondaries of both charges.

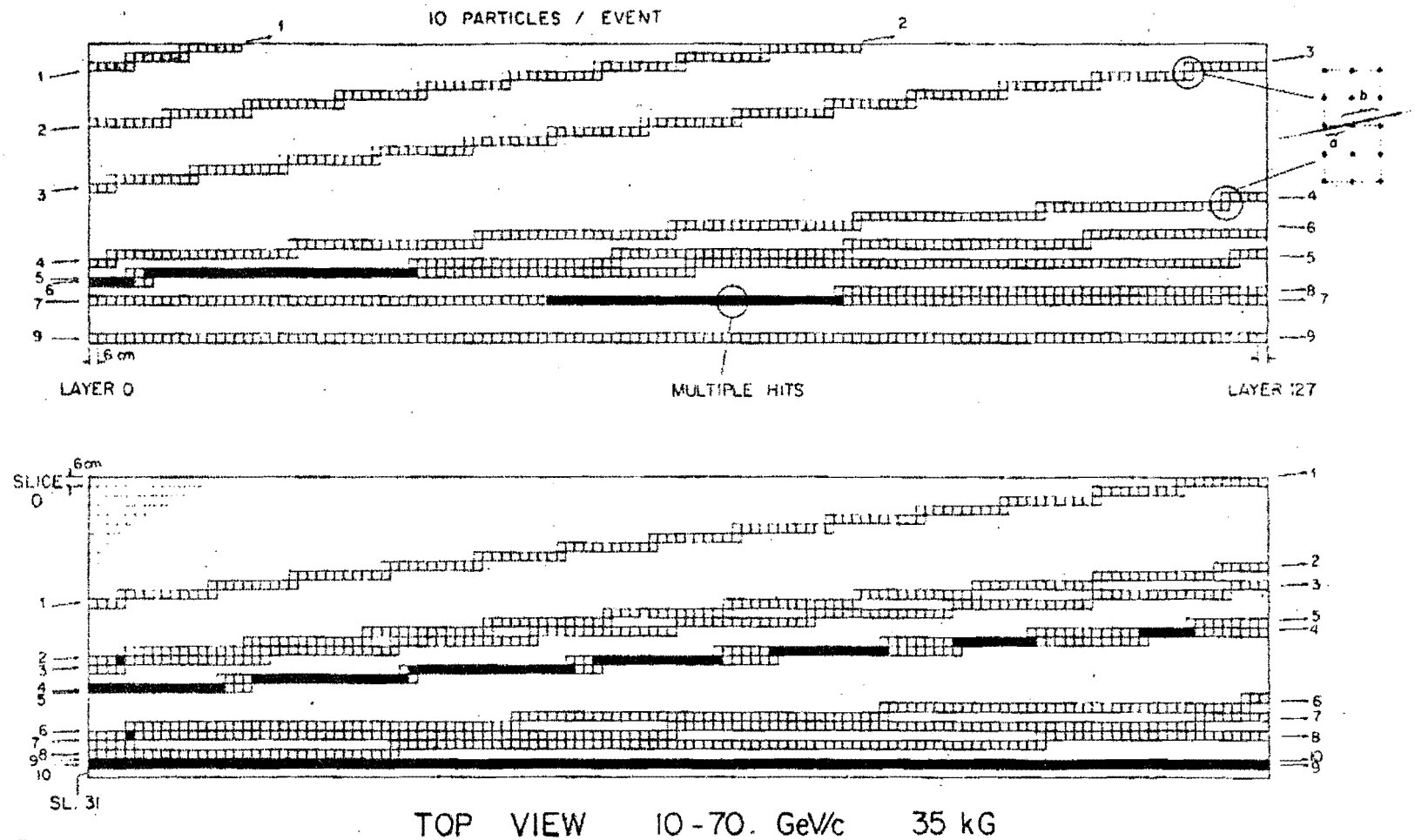

Fig. 14. Two 10-particle events as "seen" by the 32 × 128 cell EPI matrix.

TABLE 3

EPI efficiency for multiple particles.

Number of simultaneous particles	Percentage of clean hits in 128 layers ≥ 100	≥ 64
5	65%	76%
10	46%	62%
15	30%	44%
20	20%	31%

TABLE 4

Losses in the beam hole for different dimensions.

Beam size	Beam hole dimensions	Particles lost (%)
3×10 cm^2	6×12 cm^2	4
3×15	6×18	6
3×20	6×24	10
3×30	6×36	13
3×40	6×42	14
3×50	6×54	16
3×30	4×36	9
	5×36	11
	6×36	13

beam hole were removed, no background tracks were generated. Each square represents one cell hit, the dark squares contain signals from more than one particle and must be considered as lost information. The front layer of the detector is at 11 m from the BEBC, the magnetic field is 35 kG and the secondary particle momenta are 10–70 GeV/c. Note track 8 on the top part of fig. 14, emerging from the beam hole near the middle part of the detector.

The maximum attainable ionization-resolution is obviously a function of the total number of clean (i.e. one particle only) hits per track in the 128-layer detector. In table 3, there is a summary of the proportion of clean hits in more than 64 and more than 100 out of 128 layers respectively, for 5, 10, 15 and 20 simultaneous particles. The secondary particle momenta are 10–70 GeV/c beam-like charge only, 35 kG BEBC magnetic field. The beam size inside BEBC is 3×30 cm^2, the beam hole is 6×36 cm^2. The result is practically independent of the beam size and particle momentum. This multiple hit effect represents the most serious part of the loss in identification efficiency for a given configuration.

Table 4 shows for the front of the detector, the percentage of (mainly fast) secondary tracks lost in the beam hole for 10 simultaneous particles of 10–70 GeV/c momentum and 35 kG magnetic field, for several different beam hole dimensions in both vertical and horizontal planes. The need for the beam width to be as small as possible is evident, but the dimensions of the beam hole in the discussed range have less influence on the losses than the effects of multiple hits.

TABLE 5

Losses in the beam hole for several values of the beam momentum.

p_{max} (GeV/c)	Particles lost (%)
40	5
60	10
80	16
100	20
120	23
140	26

The losses due to the beam hole as a function of maximum secondary particle momentum are shown in table 5, again for 10 simultaneous particles, 35 kG magnetic field, beam-like charge only, beam size 3×30 cm^2 and beam hole dimensions of 6×36 cm^2. In the region of maximum interest the losses are still below 20%.

The combined effect of all factors mentioned above leads, for an "average" experiment, to about 60% identification efficiency. Non-uniform slice width across the detector following the population density of the p_t distribution projection (i.e. narrower slices around the beam region and broader slices at the lower momentum side) does not improve the situation considerably, tends to be experiment and momentum dependent and brings in serious technical difficulties. The same argument is valid for any parallel grouping and variable interconnection of a larger number of narrower slices.

Another specific study of the EPI performance with respect to $K^{\pm}\pi^{\pm}$ ambiguities in K^+p interactions (and taking into account the background influence) arrived at a similar result of about 60% identification efficiency even for a considerable number of simultaneous tracks in the bubble chamber[6]). The $p/K/\pi$ separation efficiencies as presented in ref. (3) have not been folded in.

8. Determination of the secondary particle trajectories

The track reconstruction inside the EPI, the trajec-

tory determination and correlation with the corresponding track on the bubble chamber picture is done using a set of 3 MWPCs. The first chamber should be placed as close to BEBC as possible. The ideal position would be inside the magnetic shielding near the superconducting coils. The other two chambers are located just in front and at the back of the EPI module stack. The horizontal coordinate (x) has 2 mm wire spacing and the other coordinates (u,v) inclined by $\pm 30°$ have $\lesssim 3$ mm spacing. The total number of wires required for the two big EPI chambers of about 200 (H) × 100(V) cm^2 of detection area is 4400. The smaller chamber near BEBC would have another 1600 wires arranged in similar configuration. The two big chambers will be permanently fixed to the EPI box. Extreme care will be taken to prevent the transfer of heat from the MWPC electronics towards the EPI modules. At the same time the strict hydrogen safety rules concerning the gas filling and the electric installation must be complied with.

For the 6 μs beam spill time, and practically simultaneous secondary particles coming from the interactions, the standard MWPC electronics could be used with small modifications only. The bistable memory element and the read-out circuits would be replaced by a shift register which is advanced on every clock pulse by a general clock started by the ejection trigger. Each time when there is a signal on a particular wire a "1" will be strobed into the corresponding time slot, if not, a zero is strobed in. After each accelerator burst the shift register array will be scanned and shifted across to the EPI computer in a way giving the arrays of hit wire addresses for any particular time interval. As a first approximation it seems to be reasonable to envisage a 5 MHz clock rate representing about ± 200 ns uncertainty in the time information. 32-bit shift registers will be adequate for 6 μs beam spill. This read-out scheme is very straightforward and needs only a very small number of interconnections between the chambers and the computer interface. The total hardware read-out time for 6000 wires is of the order of $[(32 \times 0.2) + (6000 \times 0.1)]$ μs $= 610$ μs, to which the switching delays and the computer read-in time should be added. The ambiguities in space and time determination should not represent a serious problem, and some additional useful information could be gained from the 32×128 cell matrix of the EPI.

9. Determination of the angle of entry to BEBC of the beam particles

The last 50 m of the beam line in front of BEBC will be used for precise determination of the entry angle for each individual beam track. At least 3 (x,u,v) MWPC planes will be needed there to keep the ambiguities in pattern recognition at a tolerable level. The first chamber, with 10×10 cm^2 detection area, would be mounted immediately after the last horizontal bend of the beam. The beam, which almost fills the magnet aperture of 8 cm diameter in this place, is then gradually spread horizontally and focused vertically when approaching BEBC. The middle chamber would therefore cover some 25(H) × 10(V) cm^2 and the last one, mounted as close as possible to the BEBC magnetic shielding, would have a detection area about 50(H) × 10(V) cm^2. The wire spacing for the horizontal (x) coordinate is assumed to be 2 mm and for the $\pm 30°$ (u) and (v) planes ≈ 3 mm. The total number of wires will be about $(110+270+$ $+550) = 930$. The electronics and read-out structure is similar to the one already mentioned in the previous paragraph. The total read-out time will be about 100 μs without the computer read-in. The timing of the centrally distributed clock signal must be corrected for the time-of-flight differences between the individual chambers. In order to make full use of the spatial resolution of the system, helium bags would be used in the beam line to reduce the multiple scattering.

10. Setting-up procedures

A certain amount of beam running time should be reserved for essential tests necessary for the determination of the principal EPI parameters. These tests will be performed with or (preferably) without the BEBC magnetic field. Initially the horizontally focused beam, with the intensity reduced to 1 detected particle for every 3–4 SPS bursts, should be directed at the detector aligned parallel to it. It is assumed that the beam could be spread vertically enough in order to get at least part of the beam particles out of the beam hole region of the EPI without additional up/down displacement of the heavy complete assembly. Then by moving the EPI across in 6 cm steps the distributions of the ionization losses for each of the 4096 cells would be accumulated in the computer with sufficient statistics for determination of the individual channel response corrections.

At a fixed position with this set-up the accessible part of the relativistic rise of the ionisation would be established with full 128 layer resolution using positive pions and protons at about 30–40, 50, 70, 100 and 150 GeV/c beam momenta.

Calibration runs, with the BEBC magnet on, for determination of the correlation between the BEBC coordinate frame and the MWPC system of the EPI

should be foreseen. The downstream MWPC's position should be verified using the beam tracks for every different beam momentum.

11. Conclusions

The essential technical parameters of the EPI could be summarized as follows:

- distance of the front plane from BEBC center 11 m,
- inside dimensions of the 12 cm wide frames 104(V) × 214(H) cm,
- effective detection surface 90(V) × 192(H) cm^2,
- number of layers (6 cm thick) 128,
- number of active cells per layer 32,
- cell size 6 × 6 cm^2,
- overall length of the detector 8 m,
- beam insensitive region 5(V) × 36(H) cm^2,
- gas filling (at atmospheric pressure) Ar + 5% CH_4,
- mylar windows 130 μm × 25 μm.

The contradictory demands concerning the interference of the central part of the EMI's additional absorber plugs in case of alternating operation of the rf and neutrino ejections within the same SPS cycle were resolved by finding a resonable compromise. This consists in a variable width opening in the central part of the EMI absorber which will affect only a rather limited fraction of the fast forward-going muons.

The off-line data handling should not cause any fundamental problems. Fig. 14 gives a good impression of the type of procedure, which it will be necessary to follow. For a given event on BEBC film, for which an ambiuity of hypothesis exists, the ambiguous track, and any interfering tracks, will be fitted through the EPI with the help of the stored information from the high resolution MWPCs before and behind the device. This will allow the selection of the ionization measurements along the particle's trajectory. Special care must be taken to filter out and eliminate all double hits resulting from crossing or closely parallel tracks passing through the same cell. In the case of a track crossing a slice boundary, as displayed in the inset of fig. 14, addition of the output from both cells will avoid losing these measurements for the statistical treatment. For all values corrections will be applied for differences in channel response, barometric pressure variations and path length differences of inclined tracks.

Using a maximum likelihood method the clean set of ionization measurements will be fitted by an "ideal" single channel ionization distribution, the latter having been established experimentally during a test run. The momentum of the traversing track would be measured inside BEBC and its precision improved using the MWPC data. For this given momentum the likelihood for the particle to be either a proton, or a kaon, or a pion will be established using the experimentally determined relativistic rise of ionization.

It should be noted here that the ionization measuring devices work most efficiently in cases of exclusive ambiguites of, e.g., the π/K type, but they have rather low rejection efficiency in cases when a very small fraction of wanted particles need to be identified in the presence of high background level.

Also, a fast trigger for the bubble chamber flash cannot be provided for. This is not a serious drawback if the EPI-type device is considered to be used in connection with a big conventional (not rapid-cycling) bubble chamber, which is our case.

The present status of the EPI project should assure its operation with the start of the SPS secondary beams in the West Hall.

References

1) I. Lehraus, Int. Report CERN/D.Ph.II/BEAM 72-1 (15.3.1972) and CERN/ECFA/72-4, Vol. I (July 1972) p. 60.
2) D. Jeanne, P. Lazeyras, I. Lehraus, R. Matthewson, W. Tejessy and M. Aderholz, Nucl. Instr. and Meth. 111 (1973) 287.
3) M. Aderholz, P. Lazeyras, I. Lehraus, R. Matthewson and W. Tejessy, Nucl. Instr. and Meth. 118 (1974) 49.
4) P. Bernard, A. Grant and P. Lazeyras, CERN/EFCA/72-4, Vol. I (July 1972) p. 435.
5) M. Aderholz, R. Böck, H. Burmeister and A. Grant, Int. Report CERN/D.Ph.II/BEAM 73-4 (31.8.1973).
6) N. Elverhaug and A. Grant, Int. Report CERN/D.Ph.II/BEAM 74-2 (22.3.1974).
7) A. Ball, G. Cavallari, D. Jacobs and W. Tejessy, Int. Report CERN/D.Ph.II/GC/fa (5.3.1974).
8) Int. Report CERN/SPSC/I 73-35 (10.8.1973).

APPENDIX B-1

Physics Letters 59B, 299 (1975)

Charged Particle Multiplicities in 100 GeV/c $\bar{p}p$ Interactions

R.E. Ansorge, C.P. Bust, J.R. Carter, W.W. Neale and J.G.Rushbrooke

Cavendish Laboratory, Cambridge, England*

C. Moore, R. Raja, L. Voyvodic and R.J. Walker

Fermi National Accelerator Laboratory, Batavia,Ill 60510,USA**

W. Morris, B.Y. Oh, D.L. Parker, G.A. Smith, J. Whitmore

Michigan State University, E.Lansing, Michigan 48824,USA†

ABSTRACT

Results are presented on the topological cross sections obtained for antiproton-proton interactions from an exposure of the Fermilab 30-inch bubble chamber to a 100 GeV/c negative beam enriched in $\bar{p}$'s. The $\bar{p}p$ inelastic cross section is found to be $\sigma_{inel} = 34.6 \pm 0.4$ mb, and the average inelastic charged particle multiplicity to be $\langle n \rangle = 6.74 \pm 0.05$.

In this letter we present the first results of an investigation of antiproton-proton interactions at 100 GeV/c. From a 98,000 picture exposure of the Fermilab 30-inch hydrogen bubble chamber and wide gap spark chamber hybrid system to a negative beam enriched in $\bar{p}$'s, we have measured the elastic and inelastic topological cross sections in 100 GeV/c $\bar{p}p$ and $\pi^- p$ interactions. The antiproton data comprise the first detailed study of the $\bar{p}p$ collision process above 32 GeV/c.

The enriched beam used in this experiment was obtained from 300 GeV/c primary protons incident on a copper target 1km upstream of the Fermilab 30-inch bubble chamber. Since a negatively charged 100 GeV/c secondary particle beam contains only $\sim 0.02\ \bar{p}/\pi^-$, we used a new technique[1] to achieve a higher $\bar{p}/\pi^-$ ratio. Downstream of the target a bending magnet deflected charged secondary particles out of the beam line acceptance. However, neutral hyperons and kaons decaying in the region beyond the bending magnet yielded some charged secondaries having the correct trajectories for transmission to the bubble chamber. Antiprotons from $\bar{\Lambda}^o$ decay are selected preferentially since the negative pions produced in K_s^o decay have an average transverse momentum double that of the antiprotons. In this way we obtained a beam with 0.20 $\bar{p}$'s/negative particle at the bubble chamber. With the requirement of (a) more than one $\bar{p}$ per pulse or (b) a deflection trigger on a tagged $\bar{p}$ beam particle before taking a picture, we obtained 98,000 pictures containing on average 0.32 $\bar{p}$'s/negative particle, and because of the difference in total cross sections, 50% of the events observed in the bubble chamber were from $\bar{p}p$ interactions.

The results presented here come from a sample of 58,000 pictures scanned for all interactions. After an event was found in the bubble chamber, a measurement of the interacting beam track permitted a comparison[2] between the spatial position of that track and the position reconstructed from upstream multiwire proportional chambers (MWPC) in coincidence with a differential gas Cerenkov counter located 500 m upstream from the bubble chamber. This correlation

between a reconstructed bubble chamber track and a Cerenkov tagged trajectory in the MWPC was possible for ∿ 80% of the events. The remaining 20% represent only a loss of data[2] and do not bias the results in any way. For the remainder of this paper we use only those events that have a positive identification as being due to either a $\bar{p}$ (or π^-). We estimate that the background to identified antiprotons due to inefficiencies of the Cerenkov counter is <2%.

A portion of the film(∿18%) has been rescanned in order to determine the scanning efficiencies for various topologies, and these were used to correct event numbers. All those events (∿1/3% of the total) with an apparent odd number of charged particles have been classified as belonging to the next highest even charged particle topology, on the assumption that a short track was missed. An undetected charged secondary interaction occuring close to the primary vertex could also simulate an odd prong topology, but in view of the very few events in this category a correction for secondary interactions was deemed unnecessary.

In ∿ 1½% of events a Dalitz pair was observed, but because of the uncertainty of identification at the scanning stage the pair was included in the topological count and a statistical correction made. This correction used an estimate of the mean number of π^0's produced per event as a function of charged multiplicity n, which was determined from measurements of observed γ conversions in the bubble chamber. The final Dalitz correction amounted to a shift of events between topologies at a level of $\lesssim$ 3%. A small correction was also made for unseen V^0's and electron pairs from γ conversions. We find no evidence for any bias resulting from use of the deflection trigger. We conclude that the final uncertainty in all these corrections is well within statistical errors.

The major correction applied to the raw data occurs for the two prong topology. All two prong events have been measured and kinematic fits to the $\bar{p}p$ and π^-p elastic[3] hypotheses attempted. Elastic events were corrected for scanning losses, determined as a function of t (the square of the four-momentum

transfer from target to outgoing proton), and then the elastic t distribution was fitted , for $|t| \gtrsim 0.08$ GeV^2, to an exponential form $\frac{d\sigma}{dt} = Ae^{bt}$ to correct for an apparent loss of events below this value of $|t|$. We find a slope parameter of $b = 11.4 \pm 0.6$ (7.7 ± 0.4) $(\text{GeV/c})^{-2}$ for 100 GeV/c $\bar{p}p$ (π^-p) elastic scattering. Inelastic events were corrected independently for scanning losses; we stress that no correction has been made to the inelastic two prong cross section for a loss at small $|t|$ [3].

In Table I we present our measured topological cross sections for 100 GeV/c $\bar{p}p$ interactions, normalized to the total cross-section data for Carroll et al.[4]. The $\bar{p}p$ elastic cross section of $\sigma_{el} = 7.41 \pm 0.38$ mb would appear to be in good agreement with an extrapolation from lower energies. The total inelastic cross section is found to be 34.63 ± 0.38 mb. Our 100 GeV/c π^-p topological cross sections (not shown) agree with previous data[5] within quoted errors.

In Figure 1 we show the variation of the $\bar{p}p$ topological cross sections with the square of the cms total energy s and the beam momentum. The general features of this plot are similar to those observed, for example, in π^-p collisions. In particular, we observe that the 0-prong cross section is falling rapidly and may be parameterized as $\sigma_o(\text{mb}) = 58\ P_{lab}^{-(1.46 \pm .13)}$ between $P_{lab} = 15$ and 100 GeV/c. The 2,4,and 6-prong cross sections are falling at 100 GeV/c while the cross sections for producing 8 or more charged particles are still increasing at 100 GeV/c.

From inelastic cross sections given in Table I, we compute various moments of the $\bar{p}p$ multiplicity distribution (see Table II). We find an average charged particle multiplicity of $\langle n \rangle = 6.74 \pm 0.05$. In Figure 2(a) we show $\langle n \rangle$ as a function of the incident beam momentum for $\bar{p}p$ interactions, compared with the corresponding data obtained from pp interactions. It is seen that at any momentum the $\bar{p}p$ charged multiplicity is greater than the pp value and there is no real indication that they are converging at higher momenta.

In Figure 2(b) we show the ratio of the average multiplicity to the dispersion, $D = [\langle n^2 \rangle - \langle n \rangle^2]^{1/2}$ for the $\bar{p}p$ and pp charged multiplicity distributions. As is well-known, the high energy pp data seem to approach a constant value of $\langle n \rangle / D \simeq 2$. Above $\sim$ 15 GeV/c the $\bar{p}p$ data points are reasonably consistent with this value, though our 100 GeV/c measurement of 2.07 ± 0.03 could be suggestive of an increase with momentum that has important implications for models[6].

We now make a more detailed comparison between the 100 GeV/c $\bar{p}p$ and pp data. First we note that the pp data [7] have an average multiplicity $\langle n \rangle = 6.32 \pm 0.07$, considerably lower than the $\bar{p}p$ value. To investigate this difference in more detail, we show in Figure 3 the inelastic topological cross section for $\bar{p}p$ and pp at 100 GeV/c. The strongest feature is that the possibility of producing a high multiplicity event ($n \gtrsim 8$) is greater in $\bar{p}p$ than in pp collisions. It would appear natural to expect that the dominant cause of this difference lies in the effects of the annihilation channels available in $\bar{p}p$ interactions. This will be examined further in a subsequent paper.

We thank the staff of the FNAL Neutrino Laboratory, M. Johnson and S. Pruss in particular, for helping to obtain the enriched beam used in this experiment.

REFERENCES

* Work supported in part by the Science Research Council, U.K.

** Operated by the Universities Research Association, Inc, under Contract with the Energy Research and Development Administration, U.S.A.

† Work supported in part by the National Science Foundation, U.S.A.

1. W.W. Neale, "Enriched Particle Beams for the Bubble Chambers at FNAL". FN-259 (1974).

2. J. Erwin et al., Phys. Rev. Letters 32, 254 (1974).
V.E. Barnes et al., Phys. Rev. Letters 34, 415 (1975).

3. J. Whitmore et al., "A Study of the Elastic and Inelastic Two Prong Interaction in 100 GeV/c pp and π^-p Collisions", paper in preparation.

4. A. S. Carroll et al., Phys. Rev. Letters 33, 928 (1974) and ibid,932

5. E. L. Berger et al., Nucl. Phys. B77, 365 (1974).

6. J. Whitmore, Physics Reports 10C, 273 (1974).

7. C. Bromberg et al., Phys.Rev. Letters 31, 1563 (1973).

Table I

$\bar{p}p$ Topological Cross Sections at 100 GeV/c

Prong number n	Raw Events	Corrected Events	Cross sections σ_n (mb) (a)
0	11	13	0.061 ± 0.019
2	1876	Elast.1635	7.41 ± 0.38
		Inel. 794	3.60 ± 0.30
4	1664	1777	8.05 ± 0.20
6	1765	1821	8.25 ± 0.20
8	1527	1528	6.93 ± 0.18
10	937	907	4.11 ± 0.13
12	513	484	2.19 ± 0.10
14	215	199	0.90 ± 0.06
16	82	80	0.36 ± 0.04
18	26	26	0.12 ± 0.02
20	9	9	0.041 ± 0.014
22	2	2	0.009 ± 0.006
Total	8626	9275	42.04 ± 0.09 (b)

(a) Errors are statistical only except for 2-prong cross sections.

(b) Input value (ref.4)

Table II

Moments of the 100 GeV/c $\bar{p}p$ Multiplicity Distribution

Moments	All Charges	Negative Charges
$\langle n \rangle$	6.74 ± 0.05	3.37 ± 0.03
$\langle n(n-1) \rangle$	49.25 ± 0.68	10.63 ± 0.16
$\langle n(n-1)(n-2) \rangle$	389 ± 8	32.7 ± 0.8
$\langle n \rangle / D$	2.07 ± 0.03	
$f_2 = \langle n(n-1) \rangle - \langle n \rangle^2$	3.85 ± 0.22	-0.72 ± 0.06
$f_3 = \langle n(n-1)(n-2) \rangle - 3\langle n(n-1) \rangle \langle n \rangle + 2\langle n \rangle^3$	5.8 ± 1.1	1.81 ± 0.14

FIGURE CAPTIONS

Fig.1. Momentum and s dependence of $\bar{p}p$ topological cross-sections. The curves are to guide the eye.

Fig.2. Momentum and s dependence of (a) the average charged multiplicity $\langle n \rangle$, and (b) the quantity $\langle n \rangle / D$, where D is the dispersion of the multiplicity distribution, for $\bar{p}p$ and pp interactions. The curves are to guide the eye.

Fig.3. Comparison of $\bar{p}p$ and pp topological cross sections at 100 GeV/c. The pp data is from ref.[7].

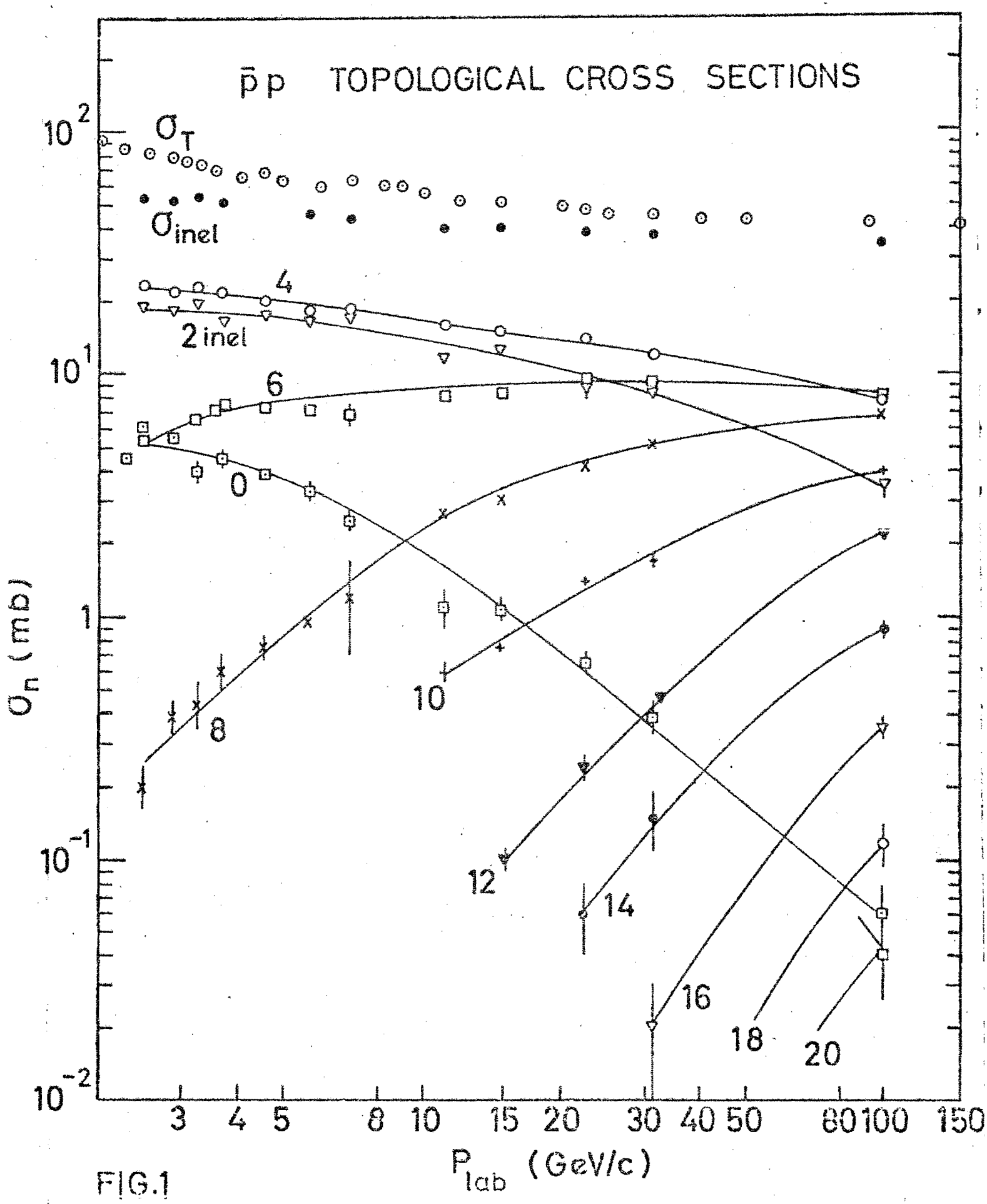
p̄p TOPOLOGICAL CROSS SECTIONS
σT
σinel
4
2 inel
6
0
8
10
12
14
16
18
20
σn (mb)
10^2
10^1
1
10^-1
10^-2
3
4
5
8
10
15
20
30
40
50
80
100
150
Plab (GeV/c)

FIG.1

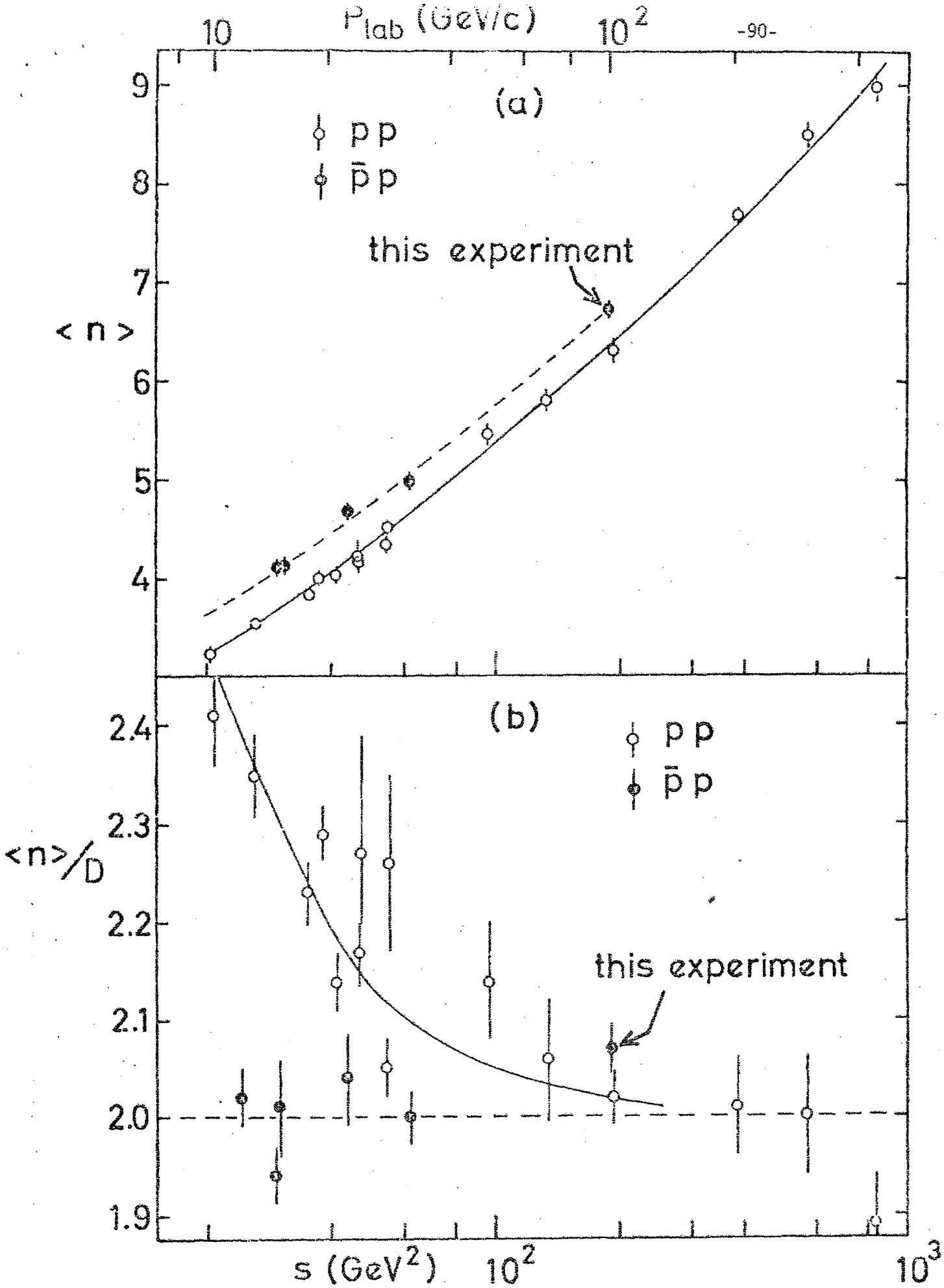
P_{lab} (GeV/c)
10
10^2
(a)
pp
$\bar{p}$p
this experiment
<n>
9
8
7
6
5
4
(b)
pp
$\bar{p}$p
<n>/D
2.4
2.3
2.2
2.1
2.0
1.9
this experiment
s (GeV^2)
10^2
10^3

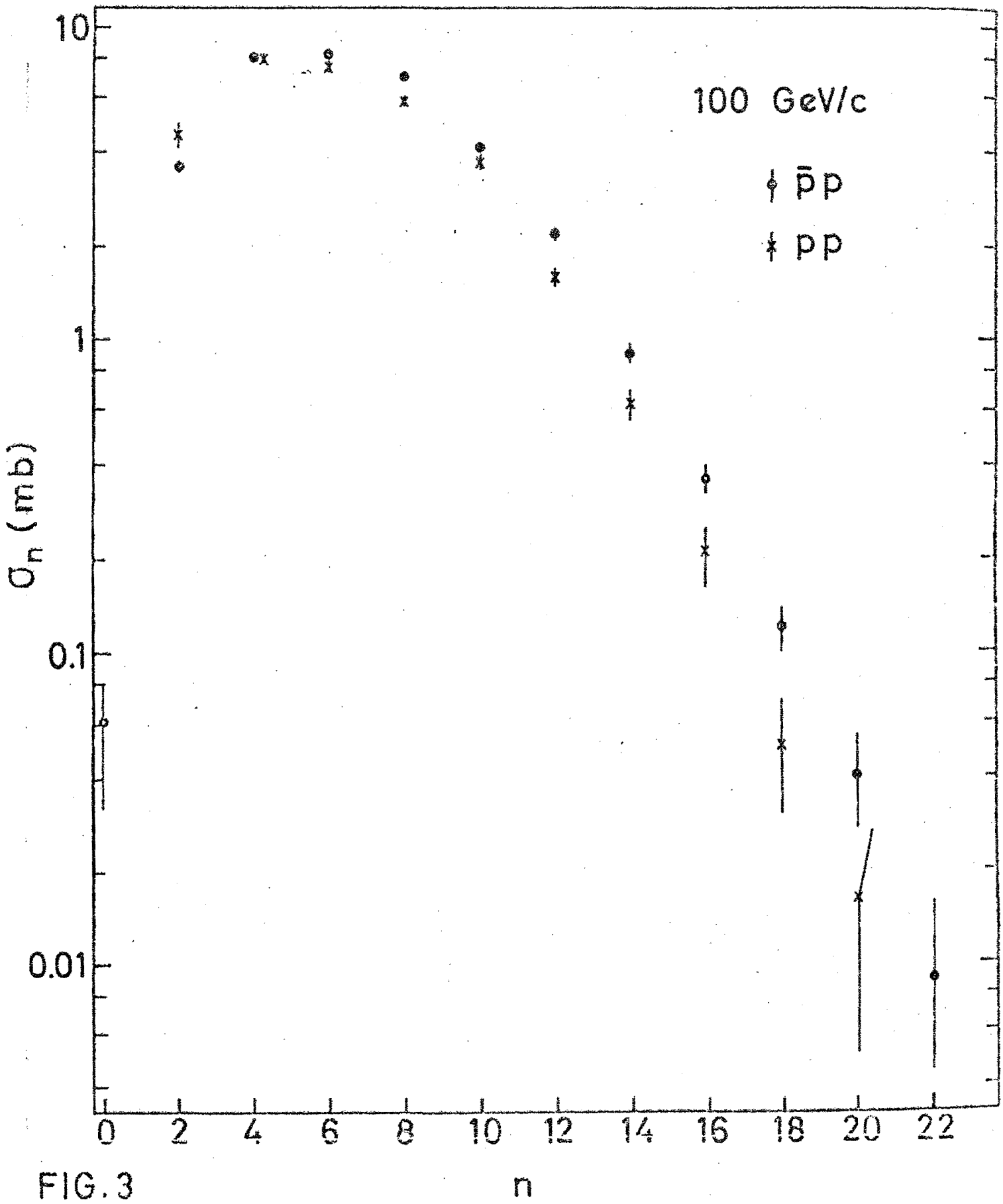

FIG. 3

APPENDIX B-2

Physics Letters 59B, 303 (1975)

On the difference between $\bar{p}p$ and pp topological cross sections up to 100 GeV/c

J.G.Rushbrooke, R.E.Ansorge, C.P.Bust, J.R.Carter and W.W.Neale

Cavendish Laboratory, Cambridge, England*

C.Moore, R.Raja, L.Voyvodic and R.J.Walker

Fermi National Accelerator Laboratory, Batavia, Ill.60510,USA**

W.Morris, B.Y.Oh, D.L.Parker, G.A.Smith and J.Whitmore

Michigan State University, E. Lansing, Michigan 48824,USA†

ABSTRACT

New 100 GeV/c $\bar{p}p$ data is used to find moments of the difference between the $\bar{p}p$ and pp topological cross sections. The mean multiplicity for annihilations at 100 GeV/c is estimated to be 9.06 ± 0.56, and the value of the quantity $\langle n \rangle / D$ to be 2.75 ± 0.33. It is shown that $R_n = \{\sigma_n(\bar{p}p) - \sigma_n(pp)\}/\sigma_n(pp)$ can be fitted to an expression $R_n = s^{-\alpha} \beta^n$ in which α and β appear to be reaching asymptotic values at 100 GeV/c.

* Work supported by the Science Research Council, U.K.

** Operated by the Universities Research Association, Inc. under Contract with the Energy Research and Development Adminstration, USA.

† Work supported in part by the National Science Foundation, USA.

Information on very high energy $\bar{p}p$ interactions has recently become available [1] in the form of topological cross-sections and the moments of the charged multiplicity distribution at 100 GeV/c. Great interest centres on the behaviour with energy of the difference between $\bar{p}p$ and pp interactions, as this may afford insight into the high energy behaviour of the annihilation process, which is known from present data in the 2-10 GeV/c range to possess general properties very different from those of the non-annihilation processes [2]. In this letter we examine the properties of the inelastic topological cross section differences $\sigma_n(\bar{p}p) - \sigma_n(pp)$, where n is the prong number, in the momentum range 9 to 100 GeV/c, compare them with the properties of $\bar{p}p$ annihilation data below 7 GeV/c, and show that the experimental values of the quantity $R_n = \{\sigma_n(\bar{p}p) - \sigma_n(pp)\}/\sigma_n(pp)$ at each momentum can be fitted to an expression $R_n = s^{-\alpha}\,\beta^n$ in which α and β appear to be reaching asymptotic values at 100 GeV/c.

In Table 1 we give various moments of the 100 GeV/c cross-section differences (*) calculated from our $\bar{p}p$ data [1] and from the 102 GeV/c pp data of Bromberg et al [3], and compare them with the moments found for the 102 GeV/c pp data. We see that the mean charged multiplicity of $\langle n\rangle = 9.06 \pm 0.56$ for ($\bar{p}p$ - pp) is much greater than the value 6.32 ± 0.07 for pp interactions. The ratio $\langle n\rangle/D$, where D is the dispersion, is seen to have a value of $2.75 \pm .33$ which is greater than the roughly constant value of ≈ 2 found for pp interactions above $\sim$ 50 GeV/c [4] and for $\bar{p}p$ interactions above 7 GeV/c [1,4].

To study the energy dependence of some of these moments we have interpolated the existing pp data [5] on topological cross sections and subtracted (*) them from those [6] for $\bar{p}p$ interactions at beam momenta of

(*) In the case of the inelastic 2-prong topology a large error is found in the difference between $\bar{p}p$ and pp cross sections, and above 9 GeV/c this difference is always consistent with zero within errors. For this reason at all momenta > 9 GeV/c we used instead an extrapolation of the lower momentum (<7 GeV/c) 2-prong annihilation data. The error on the data points presented in this paper allow for any uncertainty in this procedure.

12,14.75,15,22.4 and 32 GeV/c. In $\bar{p}p$ experiments up to 9 GeV/c [7] the annihilation component of each topological cross section has itself been measured, and these values were used to calculate the multiplicity moments(†).

In Fig.1(a) we show the resulting mean negative multiplicity $\langle n_- \rangle$ versus the square of the cms total energy s and we see that the 2-2½ units excess over the pp value at the same s, probably due to the 2 GeV extra energy from annihilation of the incident hadron rest masses and the absence of strongly leading particles in the final state, is preserved over the full range of s.

The quantity $\langle n \rangle / D$ has been shown [9] to have an approximately constant average value of 2.73 ± .14 for $\bar{p}p$ annihilations below 7 GeV/c. We find that the average value from ($\bar{p}p$ - pp) over the momentum range 9 to 100 GeV/c has increased slightly to 3.07 ± .07.

The correlation integral f_2^{--} for negative tracks is shown as a function of $\langle n_- \rangle$, the mean multiplicity of negative tracks, in Fig.1(b) where it is compared with that for pp interactions. It has been well known for some time that the negative values of f_2^{--} for $\bar{p}p$ annihilations can be understood [2] in terms of a single cluster (or fireball) formation model. Writing f_2^{--} in the form

$$f_2^{--} = b \langle n_- \rangle + c,$$

then b is predicted to have values in the range -0.6 to -0.7 depending on the assumptions made about the way the fireball decays. Values of b in this range are in good agreement with $\bar{p}p$ annihilation data up to 7 GeV/c as may be seen in Fig.1(b). The large positive values of f_2^{--} for pp interactions are then seen [10] as a consequence of multiple cluster formation ; each cluster has its own negative value of f_2^{--} (as with the annihilation fireball) but the effect

---

(†) Below 7 GeV/c the 0-prong annihilation cross section is available and has been used in calculating the moments. On the other hand an apparently large 0-prong cross section from ($\bar{p}p$ - pp) at higher energies is almost certainly mainly composed of non-annihilation states [8], and has been disregarded in calculating the moments.

of averaging over several clusters is to give a positive f_2^{--}. As one goes to sufficiently high energy and more than one cluster is produced, one might then expect to see f_2^{--} for $\bar{p}p$ annihilations turning up to positive values; Miettinen has predicted [2] that this could happen at a beam momentum of 10 - 20 GeV/c. The 100 GeV/c data point for ($\bar{p}p$ - pp) in Fig.1(b) is suggestive of the onset of this type of behaviour, though it does imply that f_2^{--} would probably not become positive until $\gtrsim$ 300 GeV/c.

The existence of KNO scaling for $\bar{p}p$ annihilations below 7 GeV/c has already been demonstrated [9], in the sense that a single function $\psi(z) = \frac{\langle n \rangle \sigma_n}{\sigma_{in}}$, where $z = n/\langle n \rangle$ and σ_{in} is the total annihilation cross section, can fit all the data in this energy interval. This fit is shown as the dashed curve in Fig.2, and is seen to be quite different from Slattery's fit [11] to pp data in the momentum interval 50-300 GeV/c, which is the solid curve. The ($\bar{p}p$ - pp) data points up to 100 GeV/c are shown in Fig.2 to be in fair agreement with the dashed curve, though there is some suggestion of the distribution becoming narrower at higher energies.

To gain further insight into $\bar{p}p$ annihilations at high energy we show in Fig.3(a) experimental values of the quantity

$$R_n = \frac{\sigma_n(\bar{p}p) - \sigma_n(pp)}{\sigma_n(pp)}$$

plotted against n for $n \geq 4$ for data in the momentum interval 6 - 100 GeV/c. We find that at each value of s, R_n can be fitted to an expression of the form

$$R_n = s^{-\alpha} \beta^n .$$

The values of α and β are shown plotted against $\ln s$ in Fig.3(b), and we see signs of these parameters reaching fairly constant values at 100 GeV/c, where we have $R_n = (1.24 \pm 0.02)^n \; s^{-(0.73 \pm 0.04)}$. Eylon and Harari [12], with a duality-diagram model and unitarity considerations, have predicted that R_n should take the form

$$R_n = \beta^n \; s^{2\alpha_B - 2\alpha_M - (1 - \eta_1)\gamma^n} \qquad (1)$$

where α_M (α_B) is the intercept of the leading exchanged meson(baryon) trajectory, η_1 (≤ 1) is some constant, and $\beta(>1)$ and $\gamma(<1)$ are constants which, in a simple form of the model, are 3/2 and 1/2 respectively. Our fit is consistent with a contribution from the first term of eqn(1) only (implying $\eta_1 \approx 1$ or $\gamma \approx 0$), which in the Eylon-Harari model comes from annihilations. Our fit also means that $\alpha_B - \alpha_M = 0.36 \pm 0.02$, which seems plausible, and that $\beta = 1.24 \pm 0.02$, in disagreement with the prediction $\beta = 1.5$. On the other hand, if the duality diagrams in the Eylon-Harari model are interpreted as leading to the production of clusters, rather than charged pseudoscalar mesons, then since the mean number of charged particles in clusters produced in hadronic interactions is about two [13], we should re-interpret the first term in eqn(1) to contain the factor $\beta^{n/2}$, i.e. $(\sqrt{\beta})^n$. This would mean that $\sqrt{1.5} = 1.225$ is the correct prediction, consistent with our findings.

In summary, this analysis of ($\bar{p}p$ - pp) and $\bar{p}p$ annihilation data at momenta up to 100 GeV/c indicates that

(a) The mean charged multiplicity in $\bar{p}p$ annihilations maintains a constant excess over that in pp interactions up to 100 GeV/c.

(b) The ratio $\langle n \rangle / D$ for $\bar{p}p$ annihilations is roughly constant from threshold to 100 GeV/c and greater than the constant value of ≈ 2 achieved by pp interactions above $\sim$ 50 GeV/c.

(c) KNO scaling is fairly well followed in $\bar{p}p$ annihilations from 9 to 100 GeV/c.

(d) The quantity R_n defined above can be represented as $s^{-\alpha} \beta^n$ where α and β appear to be reaching asymptotic values at 100 GeV/c.

We are grateful to B. R. Webber for helpful discussions.

References

1. R. E. Ansorge et al., "Charged Particle Multiplicities in 100 GeV/c $\bar{p}p$ Interactions" , submitted to Physical Review Letters.

2. H. I. Miettinen, Symposium on Antinucleon-nucleon Interactions, CERN Report 74-18,405 (1974).

3. C. Bromberg et al., Phys. Rev. Letters 31 (1973) 1563. In calculating ($\bar{p}p$-pp) topological cross section differences at 100 GeV/c it was found necessary to smooth some of these 102 GeV/c pp cross sections by reference to other pp data (see Ref.5) at neighbouring momenta; the adjustments were in no case greater than 0.2 mb.

4. F. T. Dao, J. Lach and J. Whitmore, Phys. Letters 45B (1973) 513.

5. pp data. E. Bracci et al., Compilation of cross-sections III - p and $\bar{p}$ induced reactions, CERN Report CERN/HERA 73-1; A. Firestone et al., Phys. Rev. D10 (1974) 2080 ; S. Barish et al., Phys. Rev. D9 (1974) 2689.

6. $\bar{p}p$ data. E. Bracci et al., op.cit. ; see compilation in Ref [5] of F. T. Dao et al., op.cit. ; G. A. Akopdjanov et al., Nucl. Phys. B75 (1974) 401 ; CERN Report 74-18, p275, p281 and p501.

7. $\bar{p}p$ annihilation data;see Table 1 of T. Fields et al., Ref [2], p157; H. Muirhead, Ref [2], p488.

8. H. Muirhead op. cit.

9. J. Salava and V. Simak, Nucl. Phys. B69 (1974) 15.

10. T. Fields et al., op. cit. p151.

11. P. Slattery, Phys. Rev. D1 (1973) 2073.

12. Y. Eylon and H. Harari, Nucl. Phys. B80 (1974) 349.

13. C. Quigg, P.Pirila and G. H. Thomas, Phys. Rev. Letters 34 (1975) 290.

Table 1

	$(\bar{p}p - pp)$ (a)	pp (b)
$\langle n \rangle$	9.06 ± 0.56	6.32 ± 0.07
D	3.30 ± 0.29	3.13 ± 0.04
$\langle n \rangle / D$	2.75 ± 0.33	2.02 ± 0.03
$f_2^{--} =$	−1.81 ± 0.62	0.28 ± 0.07
$f_3^{--} =$	3.9 ± 1.6	−0.50 ± 0.16

Moments of multiplicity distributions at 100 GeV/c

(a) From data of Ref. 1 and 3

(b) Data of Ref. 3

FIGURE CAPTIONS

Fig.1 (a) s-dependence of mean negative multiplicity $\langle n_- \rangle$ for $\bar{p}p$ annihilation data below 7 GeV/c (dots), ($\bar{p}p$ - pp) data up to 100 GeV/c (open circles), and for pp data (crosses). The curves are to guide the eye.

Fig.2 Plots of $\sigma_n \langle n \rangle / \sigma_{inel}$ versus $n/\langle n \rangle$ for $\bar{p}p$ annihilation data below 7 GeV/c (dashed curve[9]), and for ($\bar{p}p$ - pp) data at beam momenta up to 100 GeV/c as indicated. The solid curve is Slattery's fit [11] to pp data in the momentum interval 50- 100 GeV/c.

Fig.3 (a) Experimental values of the quantity $R_n = \{\sigma_n(\bar{p}p) - \sigma_n(pp)\}/\sigma_n(pp)$ plotted against n (≥ 4) for data in the momentum interval 6 - 100 GeV/c as indicated. The straight lines are the results of fitting an expression $R_n = s^{-\alpha} \beta^n$, with α and β free parameters, at each momentum.

(b) Values of α and β obtained in the above fit plotted against $\ell n s$. The curves are to guide the eye.

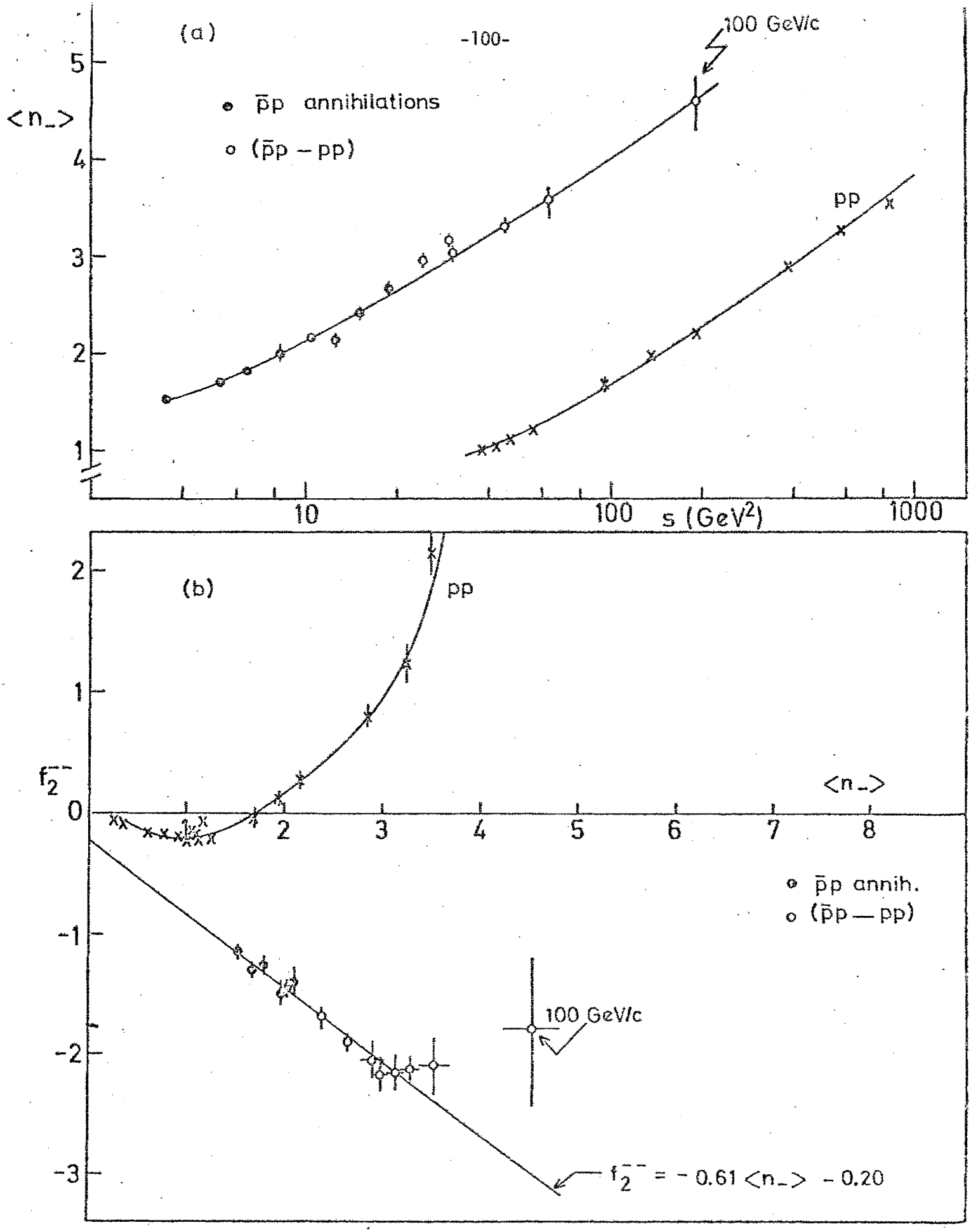
(a)
100 GeV/c
$\bar{p}p$ annihilations
$(\bar{p}p - pp)$
pp
$\langle n_- \rangle$
s (GeV^2)
(b)
pp
f_2^{--}
$\langle n_- \rangle$
$\bar{p}p$ annih.
$(\bar{p}p - pp)$
100 GeV/c
$f_2^{--} = -0.61 \langle n_- \rangle - 0.20$

FIG. 1

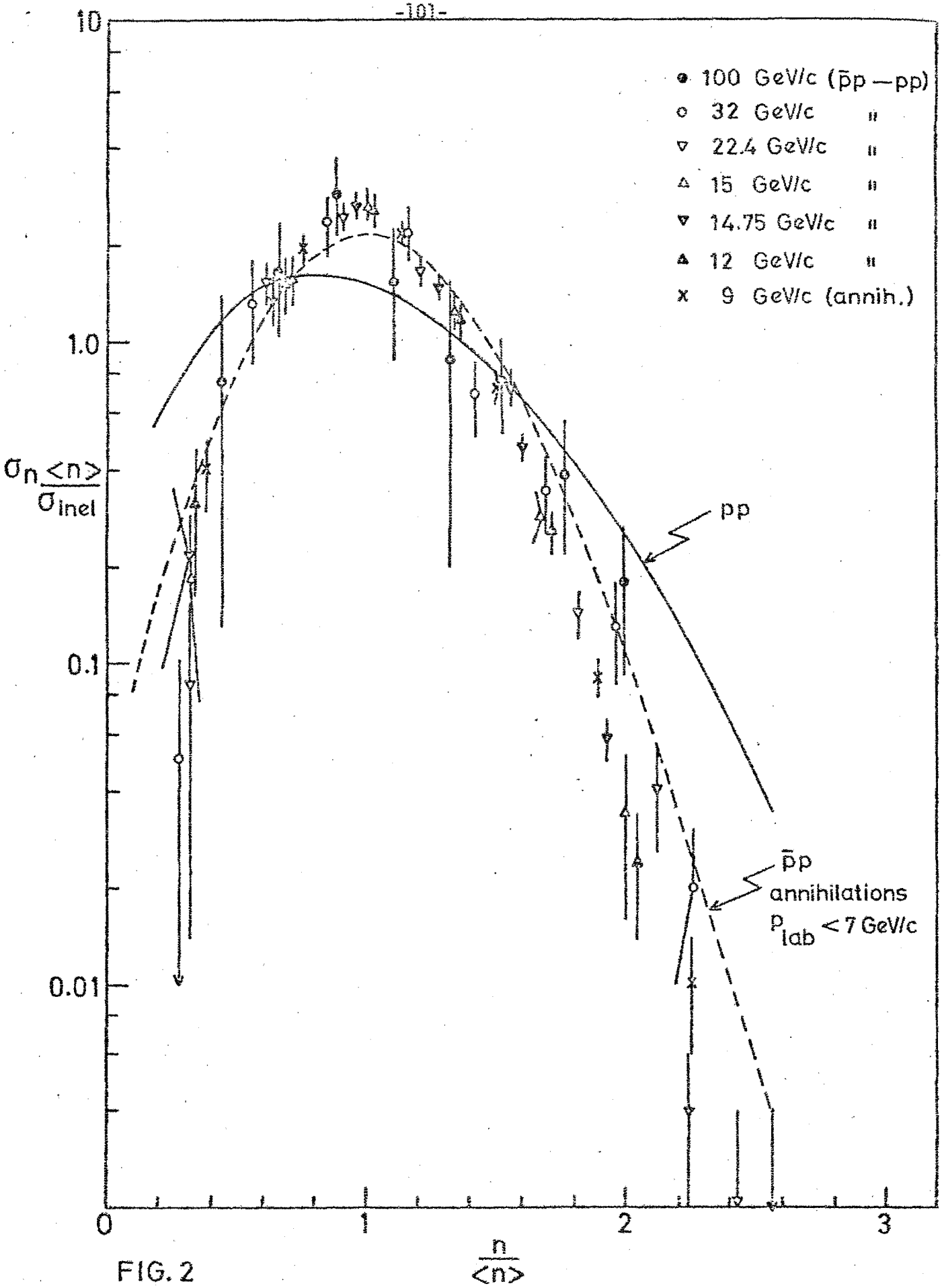
10
1.0
0.1
0.01
$\sigma_n \frac{\langle n \rangle}{\sigma_{inel}}$
0
1
2
3
$\frac{n}{\langle n \rangle}$
100 GeV/c ($\bar{p}p$ — pp)
32 GeV/c "
22.4 GeV/c "
15 GeV/c "
14.75 GeV/c "
12 GeV/c "
9 GeV/c (annih.)
pp
$\bar{p}p$
annihilations
$p_{lab} < 7$ GeV/c

FIG. 2

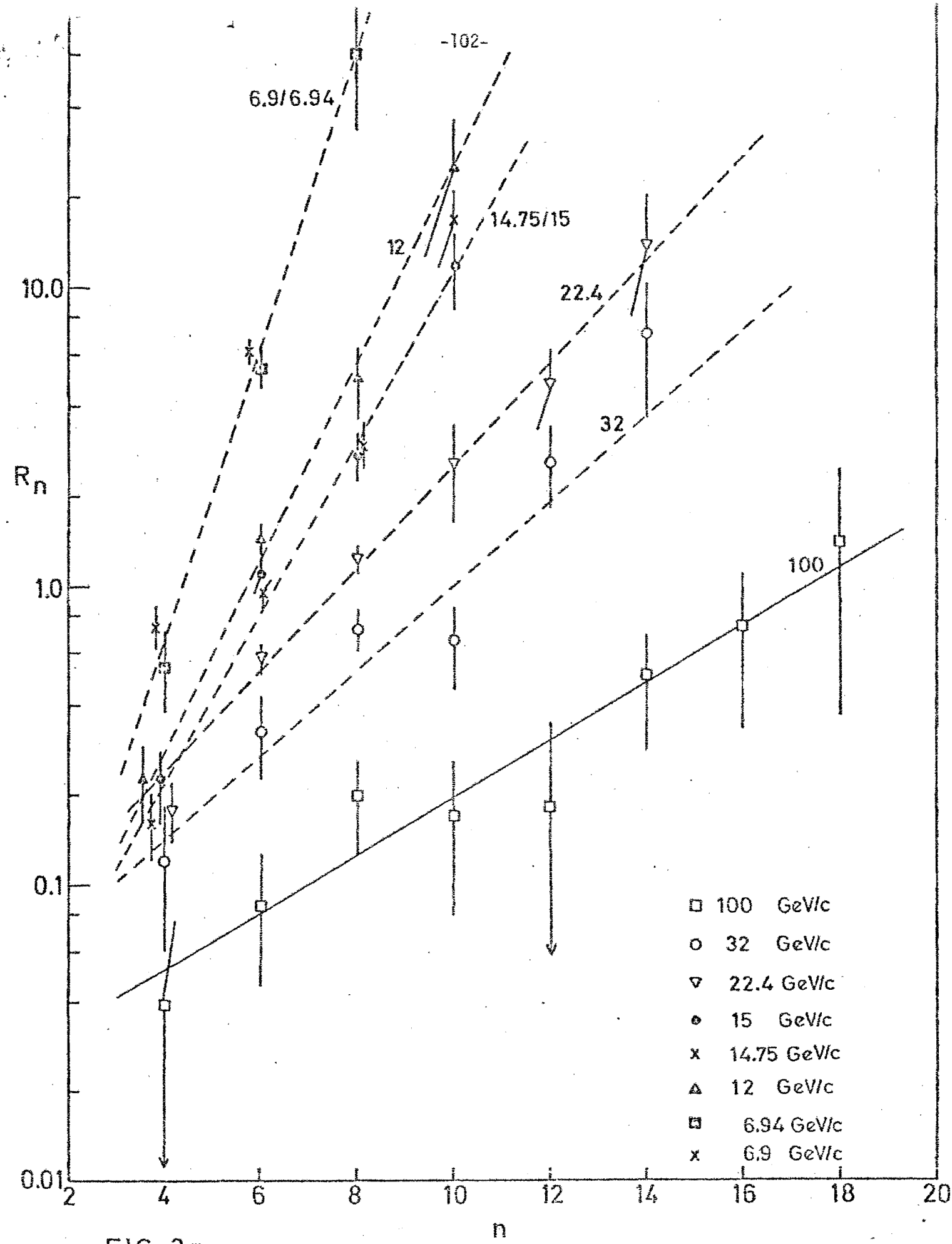
6.9/6.94
12
14.75/15
22.4
32
100
10.0
1.0
0.1
0.01
R_n
2
4
6
8
10
12
14
16
18
20
n
100 GeV/c
32 GeV/c
22.4 GeV/c
15 GeV/c
14.75 GeV/c
12 GeV/c
6.94 GeV/c
6.9 GeV/c

FIG. 3a

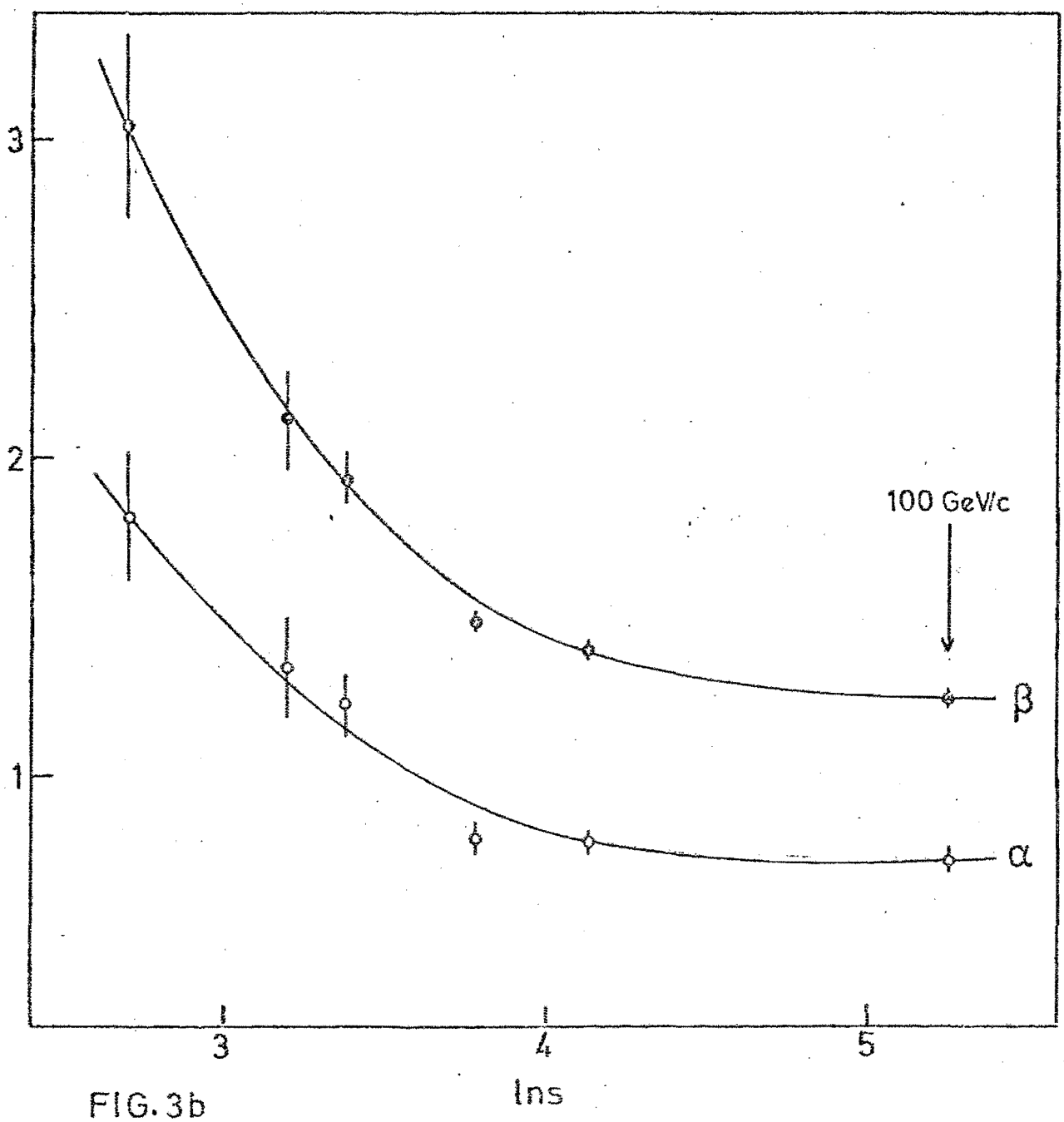

FIG. 3b

APPENDIX B-3

Annihilation effects in neutral particle production in 100 GeV/c $\bar{p}p$ interactions

D.R.Ward, R.E.Ansorge, C.P.Bust, J.R.Carter, W.W.Neale and J.G.Rushbrooke

Cavendish Laboratory, Cambridge, England*

C. Moore, R. Raja, L. Voyvodic and R.J. Walker

Fermi National Accelerator Laboratory, Batavia, Ill.60510, USA**

W.Morris+, B.Y.Oh, D.L.Parker++, G.A.Smith and J.Whitmore

Michigan State University, E. Lansing, Michigan 48824, USA***

November 1975

ABSTRACT

We derive cross-sections for the inclusive production of π^0, K^0_s, and $\Lambda^0/\bar{\Lambda}^0$ of 95.5 ± 8.2 mb, 4.4 ± 0.6 mb and 1.9 ± 0.3 mb respectively, which are all higher than pp cross-sections at this energy. We present evidence that these differences can be attributed to "annihilation" processes.

* Work supported by the Science Research Council, UK.

** Operated by the Universities Research Association, Inc, under Contract with the Energy Research and Development Administration, USA.

+ Presently at General Atomic Company, San Diego, CA 92138, USA.

++ Presently at Department of Physics, Iowa State University, Ames. Iowa, 50010 USA.

*** Work supported in part by the National Science Foundation, USA.

(1) Introduction

We present results on the production of γ, K_s^o, Λ^o and $\bar{\Lambda}^o$ in $\bar{p}p$ interactions at 100 GeV/c. Our principal intention here is to look for differences between pp and $\bar{p}p$ interactions, which one hopes might be ascribed to the effects of "annihilation" reactions. We find that cross-sections for production of neutral particles are in all cases somewhat higher in $\bar{p}p$ interactions than in pp interactions, though the difference is decreasing with momentum up to 100 GeV/c. In the case of γ and Λ^o production, the difference appears to arise mainly in the neighbourhood of $y^* = 0$, characteristic of a central collision process.

The data to be described here come from a 100,000 picture exposure of the 30" bubble chamber at Fermilab to a tagged beam of negative particles. Information on the 100 GeV/c $\bar{p}p$ charged multiplicity distribution [1] and on the difference between $\bar{p}p$ and pp topological cross-sections [2] has already been published. The efficiency for scanning for V^o's was about 90% for singly-scanned film, and after measurement and remeasurement 93% of events had been satisfactorily measured. 1120 V^o's associated to events inside our fiducial volume gave fits to Λ^o, K_s^o, $\bar{\Lambda}^o$ decays or $\gamma \to e^+e^-$ conversion. Ambiguities (affecting about 7% of the events) were resolved by observation of ionization where possible, and otherwise by cuts on the transverse momentum of the decays and on the χ^2 probabilities of the fits.

The data were corrected for scanning and measuring losses, for losses of V^o's converting or decaying outside the fiducial volume, or closer than 3cm (2cm in the case of K_s^o) to the production vertex, and for interactions of the strange particles. The pair production cross section was taken from ref [3], and the strange particle cross-sections were corrected for branching ratios taken from ref [4]. A correction (of 2-3%) was also made for the loss of very slow γ's, using the symmetry of the reaction $\bar{p}p \to \gamma$ in the c.m. system.

(2) Cross-section and multiplicities

In Table 1 we give cross-sections for Λ^o, K_s^o and π^o production, the latter taken to be $\frac{1}{2}\sigma(\bar{p}p \to \gamma)$, normalized to the total number of events in the film. We have used events in both forward and backward hemispheres in the c.m. system for the γ's since there was no asymmetry observed within errors, but have only used events in the backward hemisphere for the K_s^o data because of losses of very fast V^o's, but by C-invariance the cross-sections in forward and backward hemispheres are equal. The $\Lambda^o/\bar{\Lambda}^o$ data are also only from the backward hemisphere, but by C-invariance Λ^o's in the forward hemisphere equal $\bar{\Lambda}^o$'s in the backward hemisphere, hence we lose no information by using only backward data. Table 1 also gives cross-sections for different charged multiplicities at the production vertex (corrected for undetected dalitz pairs and V^o's). We also quote mean associated charged multiplicities for V^o production, and the mean numbers of Λ^o, K_s^o and π^o produced per inelastic collision. For comparison, the corresponding quantities are given for pp interactions. There are pp experiments at 102 GeV/c [5] and also 100 GeV/c [6], and rather than simply average their values, we quote "smoothed" values for π^o and K_s^o cross-sections, taking account of pp data at other energies [7]. Fig 1 (a-c) shows the cross-sections with data at other energies for comparison.

The cross-section for $\bar{p}p \to \pi^o$ is higher by 9.5 mb than in pp interactions, this being due most probably to the effect of annihilations. However, Fig 1(d) shows that $\langle n(\pi^o)\rangle$ as a function of n_{ch} is virtually identical to pp interactions. The implication of this is that the degree of correlation between charged and neutral pions is the same in both cases, and hence has not been significantly affected by the annihilation component. One can also see this in the correlation parameter $f_2^{-o} = \langle n_o n_-\rangle - \langle n_o\rangle\langle n_-\rangle$, which has the value of 1.03 ± .24 for $\bar{p}p$, compared to 1.12 ± .26 in pp interactions.

We can make a rough estimate of the "annihilation" component in $\bar{p}p \to \pi^0$ from the difference ($\bar{p}p$ - pp), by subtracting the cross-sections given in Table 1. The errors are large, but the mean charged multiplicity, 10.4 ± 3.4, is greater than that for the whole sample of π^0 events, 7.49 ± 0.17, as was found to be the case for the ($\bar{p}p$ - pp) multiplicity distribution of all events [2], for which a mean charged multiplicity 9.06 ± 0.56 was obtained.

Fig 1(e) compares the variation of $\langle n(K^0_s)\rangle$ with n_{ch} for $\bar{p}p$ and pp interactions and Fig 1(f) gives the same for Λ^0 and $\bar{\Lambda}^0$ combined. As with the π^0's the $\bar{p}p$ and pp behaviour is very similar, again indicating that the correlation between charged particles and neutrals is much the same in $\bar{p}p$ as in pp interactions. ~~As with π^0's,~~ Also the ($\bar{p}p$ - pp) multiplicity distributions for K^0_s and for $\Lambda^0/\bar{\Lambda}^0$ again show mean multiplicities ∿ 10, though with large errors, which encourages one to identify the differences with annihilations. This interpretation is supported by the single particle distributions presented in the next section.

(3) Single particle distributions

It is of interest to try and localise these differences in cross-sections in terms of single particle distributions. We find the most useful of these to be the centre-of-mass rapidity, y*. Fig 2 (a-c) shows the distributions of $d\sigma/dy^*$ for our Λ^0, K^0_s and γ data, folded about y* = 0 in the latter case, compared with pp data from refs [5,6]. For the sake of clarity the pp data have been represented by curves, drawn by eye, and typically the errors on the curves are comparable to those on our data points.

The $d\sigma/dy^*$ distribution for the γ's, Fig 2(a), has the best statistics, and the indications are that the two points nearest to y* = 0 are rather higher than the pp curves, while for $|y^*| \gtrsim 1.0$ our data points agree very well with pp values. The $d\sigma/dy^*$ distribution for K^0_s, Fig 2(b), suggests that the difference between $\bar{p}p$ and pp cross-sections is not concentrated near y* = 0, but spread over the whole range of rapidity. Possibly we are seeing kaons acting as leading particles in the "annihilation" process, though the statistical errors on this distribution

do not permit any very clear conclusions. Fig 2(c) shows the rapidity distribution for combined Λ^o and $\bar{\Lambda}^o$ data,† and as for the γ's there seems to be a substantial difference between $\bar{p}p$ and pp in the region $|y^*| < 1$, but agreement elsewhere. This observation invites interpretation in terms of processes such as $\bar{p}p \to (\Lambda\bar{Y}) + \pi$'s , $\bar{p}p \to (\Lambda K\bar{N}) + \pi$'s etc, (together with interference contributions with "non-annihilation" processes in the latter case), which, insofar as there are no leading baryons, may be considered as "annihilations", and would be expected to yield hyperons and antihyperons in the central region.

These effects may be described quantitatively by making a direct subtraction of the data of refs [5,6] from our $\bar{p}p$ cross-sections in the regions $|y^*| > 1.0$ and $|y^*| < 1.0$. In these ranges of rapidity we obtain: for $\sigma(\bar{p}p - pp \to \gamma)$, / 0.5 ± 11.7 mb and 18.6 ± 16.5 mb respectively; for $\sigma(\bar{p}p - pp \to K^o_s)$, / 0.20 ± 0.38mb and 0.10 ± 0.52 mb; and for $|\sigma(\bar{p}p - pp \to \Lambda^o/\bar{\Lambda}^o)|$ -0.16 ± 0.21 mb and 0.37 ± 0.28 mb. In the case of γ and $\Lambda^o/\bar{\Lambda}^o$ production the differences are clearly concentrated in the rapidity range $|y^*| \lesssim 1.0$, though it is clear that both $\bar{p}p$ and pp experiments with much improved statistics would be required to observe these effects in any greater detail.

We have also examined the transverse momentum distributions of Λ^o, K^o_s, and γ, but these display no significant differences from pp data in their shape, essentially differing only in their normalization. We derive values for the mean transverse momenta of γ, K^o_s and Λ^o, 0.16 ± 0.01, 0.45 ± 0.03 and 0.50 ± 0.04 GeV/c respectively, which are in agreement with values in pp interactions at similar energies.

---

† The unknown $pp \to \bar{\Lambda}^o$ contribution was estimated by taking the cross-section from ref [6], and adding this uniformly in the range $|y^*|<1$. By making this assumption we are in effect placing a lower limit on the ($\bar{p}p$ - pp) difference in this region.

(4) Summary

We have derived cross-sections for the production of γ, K_s^o and Λ^o in $\bar{p}p$ interactions at 100 GeV/c. In all cases, these cross-sections are higher than in pp experiments at this energy. The difference in cross-sections is associated with higher charged multiplicities on average, which leads us to identify the difference with annihilation processes. In the case of γ and Λ^o production these differences seem confined to the central region, near $y^* = 0$, while for K_s^o production there are indications of a difference at larger $|y^*|$.

n_{ch} Charged Multiplicity	$\sigma(\bar{p}p\to\pi^0)$ (mb)	smoothed $\sigma(pp\to\pi^0)$ (mb)	$\sigma(\bar{p}p\to K^0_S)$ (mb)	smoothed $\sigma(pp\to K^0_S)$ (mb)	$\frac{1}{2}\sigma(\bar{p}p\to\Lambda^0/\bar{\Lambda}^0)$ (mb)	smoothed $\frac{1}{2}\sigma(pp\to\Lambda^0/\bar{\Lambda}^0)$ (mb)
0	0.3±0.3	-	-	-	0.03±0.02	-
2	5.7±1.1	7.2±1.5	0.22±0.07	0.31±0.07	0.23±0.06	0.17±0.06
4	15.7±1.8	14.5±1.0	0.80±0.13	0.77±0.15	0.43±0.07	0.62±0.12
6	24.6±2.4	22.8±4.0	1.09±0.15	1.10±0.15	0.44±0.11	0.37±0.09
8	23.1±2.2	20.3±2.2	1.14±0.16	0.80±0.10	0.43±0.09	0.30±0.09
10	11.5±1.7	10.9±1.0	0.64±0.12	0.65±0.10	0.23±0.07	0.21±0.07
12	8.3±1.2	6.3±1.0	0.34±0.09	0.30±0.07	0.07±0.03	0.02±0.02
14	4.7±1.2	2.5±1.5	0.11±0.05	0.07±0.07	0.06±0.03	-
16	0.4±0.3	1.0±0.4	0.03±0.03	0.04±0.04	-	-
18	1.2±0.7	0.5±0.5	-	0.02±0.02	-	-
Total †	95.5±8.2	86±6	4.39±0.58	4.1±0.3	1.9±0.3	1.7±0.2
$\langle n_{ch}\rangle$	7.49±0.17	7.17±.19	7.28±0.21	7.05±0.24	6.37±0.28	5.80±0.30
$\langle n(V^0)\rangle$	2.76±0.19	2.70±.19	0.13±0.02	0.13±0.01	0.055±0.009	0.053±0.006
Raw no. of $\bar{p}p$ events	553		364		167	

Table 1. Comparison of neutral particle cross-sections in $\bar{p}p$ and pp interactions at 100 GeV/c

† The errors on the total cross-sections include a contribution (of 5%) for the uncertainty in overall normalization.

References

[1] R.E. Ansorge et al., "Charged particle multiplicities in 100 GeV/c $\bar{p}p$ interactions", Physics Letters B (to be published).

[2] J.G. Rushbrooke et al., "On the difference between $\bar{p}p$ and pp topological cross sections up to 100 GeV/c", Physics Letters B (to be published).

[3] T.M. Knasel, DESY report 70/3 (1970) unpublished.

[4] Particle Data Group, Phys. Lett. 50B, (1974) 1.

[5] J.W. Chapman et al., Phys. Lett. 47B (1973) 465.

[6] M. Alston-Garnjost et al., Phys. Rev. Lett. 35 (1975) 142.

[7] V. Blobel et al., Nucl. Phys. B69 (1974) 454.
K. Jaeger et al., Phys. Rev. D11 (1975) 1756.
H. Blumenfeld et al., Phys. Lett. 45B (1973) 525,528.
K. Jaeger et al., Phys. Rev. D11 (1975) 2405.
F. T. Dao et al., Phys. Rev. Lett. 30 (1973) 1151.

[8] F. T. Dao et al., Phys. Rev. 51B (1974) 505.

[9] B. Y. Oh et al., Nuc. Phys. B51 (1973) 57.

Figure Captions

Fig 1. (a-c) Cross-sections for $\bar{p}p \to \pi^o$, K^o_s, $\Lambda^o/\bar{\Lambda}^o$ respectively, with pp data for comparison. The dashed curves through the $\bar{p}p$ points guide the eye. $\bar{p}p$ data at lower energies are taken from refs [8,9].

(d-f) mean numbers of neutrals as a function of charged multiplicity for $\bar{p}p$ and pp interactions at 100 GeV/c.

Fig 2. (a-c) Distributions of $d\sigma/dy^*$ for $\bar{p}p \to \gamma$, K^o_s, $\Lambda^o/\bar{\Lambda}^o$ respectively with pp data for comparison. The dashed curves are drawn through the $\bar{p}p$ data to guide the eye.

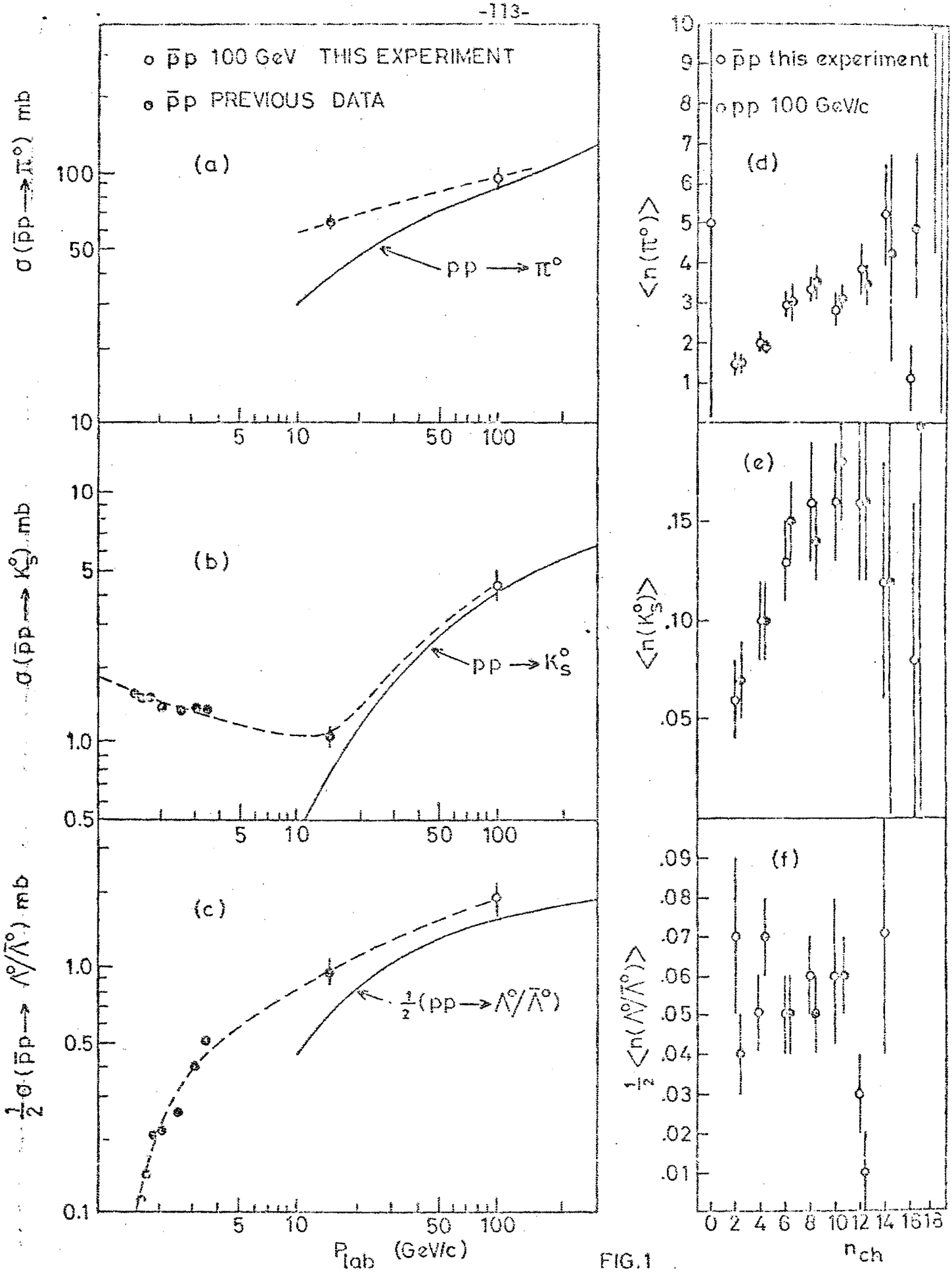
o p̄p 100 GeV THIS EXPERIMENT
o p̄p PREVIOUS DATA
(a)
pp → π°
σ(p̄p → π°) mb
(b)
pp → K°s
σ(p̄p → K°s) mb
(c)
½(pp → Λ°/Λ̄°)
½σ(p̄p → Λ°/Λ̄°) mb
P_lab (GeV/c)
o p̄p this experiment
o pp 100 GeV/c
(d)
<n(π°)>
(e)
<n(K°s)>
(f)
½<n(Λ°/Λ̄°)>
n_ch

FIG.1

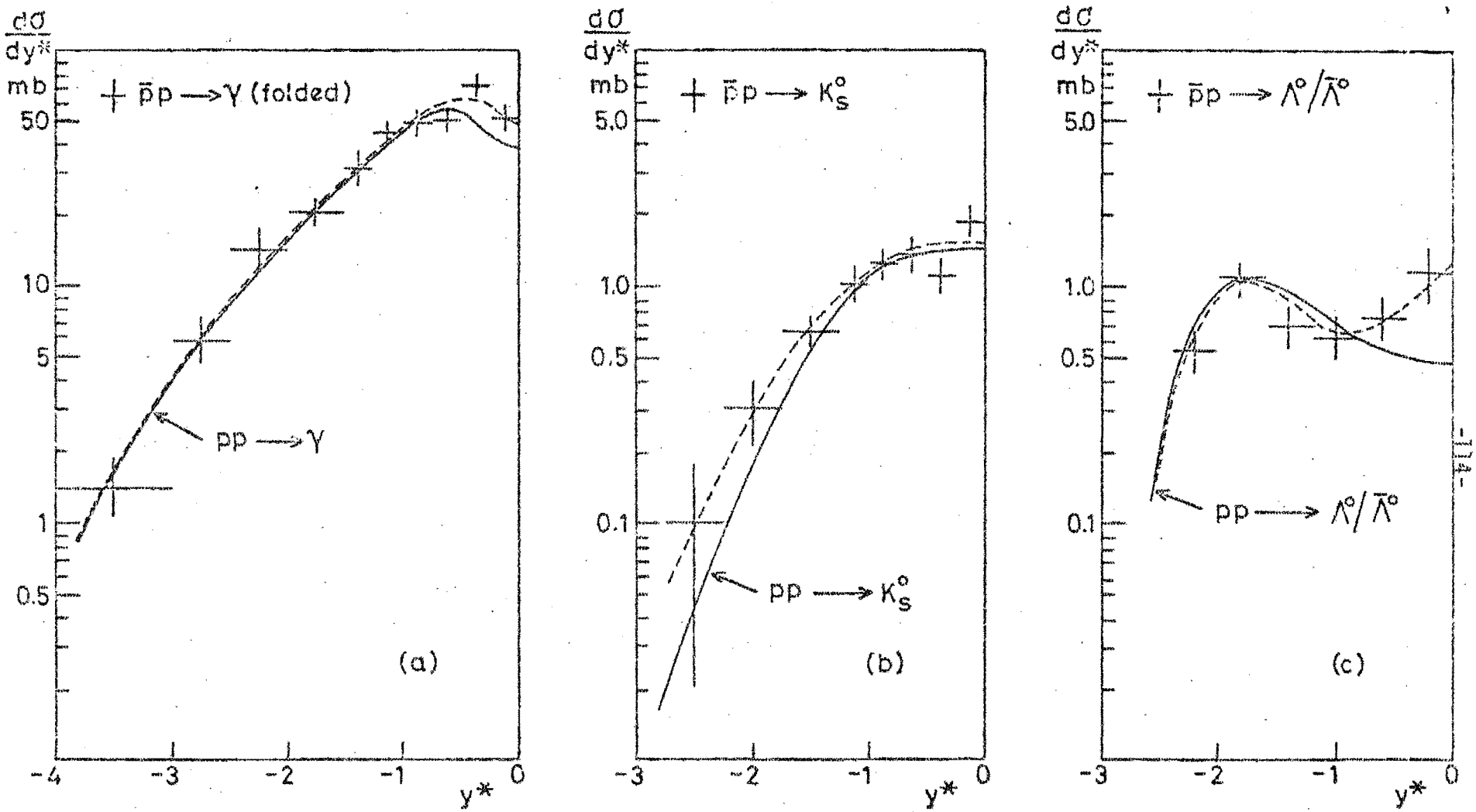

FIG. 2

Spokesman: J. WHITMORE
Department of Physics
Michigan State University
East Lansing, Mich. 48824
517-353-5180

Fermilab Proposal No. 394
(Second Revision)

PROPOSAL FOR A HIGH STATISTICS STUDY OF $\bar{p}p$ ANNIHILATIONS AND COMPARISON OF $\bar{p}p$ AND pp INTERACTIONS AT 100 GeV/c WITH THE FERMILAB 30-INCH HYDROGEN BUBBLE CHAMBER AND DOWNSTREAM PARTICLE IDENTIFIER

R. E. ANSORGE, J. R. CARTER, W. W. NEALE,
J. G. RUSHBROOKE, D. R. WARD and T. W. WHITE
Cavendish Laboratory, University of Cambridge, Cambridge CB3 OHE England

J. LYS, C. MOORE, R. RAJA, L. VOYVODIC and R. J. WALKER
Fermi National Accelerator Laboratory, Batavia, Illinois 60510 U.S.A.

R. A. LEWIS, B. Y. OH, M. PRATAP, G. SIONAKIDES, G. A. SMITH and J. WHITMORE
Department of Physics
Michigan State University, East Lansing, Michigan 48824, U.S.A.

G. EKSPONG, S. O. HOLMGREN, S. NILSSON and N. YAMDAGNI
Institute of Physics, University of Stockholm, S-113 46 Stockholm, Sweden

28 January 1977

TABLE OF CONTENTS

		Page
I.	Summary	1
II.	Abstract	2
III.	Introduction	2
IV.	Beam and Bubble Chamber	4
V.	Downstream Particle Identifier	5
VI.	Neutral Hadron Calorimeter	9
VII.	Physics Justification	11
VIII.	Study of the efficiency for separating Annihilation and Nonannihilation	19
REFERENCES		21
APPENDIX		
A1.	"Charged Particle Multiplicities in 100 GeV/c $\bar{p}p$ Interactions"	47
A2.	"On the Difference Between $\bar{p}p$ and pp Topological Cross sections up to 100 GeV/c"	51
A3.	"Comparison of Neutral Particle Production in 100 GeV/c $\bar{p}p$ and pp Interactions"	56
B.	"Particle Identifiers for Hadron Physics"	60

I. Summary

1. Request:

   2.25×10^6 pictures of $\bar{p}p$ (1.25×10^6) and pp (10^6) interactions in the 30-inch bubble chamber with Downstream Particle Identifier and Hadron Calorimeter, taken in an untriggered, but tagged, mode. These data will permit relatively background-free studies of the $\bar{p}p$ annihilation process and its relation to $\Delta\sigma_T = \sigma_T(\bar{p}p) - \sigma_T(pp)$. As well, we should be able to make detailed comparisons of multiparticle production in $\bar{p}p$ and pp interactions without annihilation.

2. Beam:

   100 GeV/c $\bar{p}$ enriched negative beam (30% $\bar{p}$/70% π^-) and 100 GeV/c positive beam (30% p/10% K^+/60% π^+) to the 30-inch bubble chamber with the standard octuple pulsing tagged by the beam Cerenkov counter(s).

3. Equipment:

   (a) 30-inch bubble chamber with Downstream Particle Identifier (ISIS/Cerenkov counter).

   (b) Antineutron detector (Neutral Hadron Calorimeter) to be provided by the collaboration.

4. Data Analysis:

   (a) Measurements will be done on 4 image plane digitizers (MSU), 3 film plane digitizers and 2 SWEEPNIKS (Cambridge), 2 image plane digitizers and SAMM (Fermilab), and a Spiral Reader (Stockholm).

   (b) Analysis will be done on the MSU CDC6500, Cambridge IBM370-165, Fermilab CDC6600 and Stockholm computers.

   (c) Although this collaboration expects to be able to analyze only the $\bar{p}p$ and pp interactions, it is our understanding that a proposal to analyze the $\pi^{\pm}p$, K^+p events in the film will be submitted shortly by a separate group of collaborating institutions.

II. Abstract

We propose to continue our studies of multiparticle production at high energies by performing complementary high statistics experiments with 100 GeV/c antiproton-proton and proton-proton interactions using the Fermilab 30-inch hydrogen bubble chamber spectrometer with a Downstream Particle Identifier (DPI) for charged $p/K/\pi$ separation. We request 1.25×10^6 pictures with a Cerenkov-tagged $\bar{p}/\pi^-$ secondary beam and 10^6 pictures with a tagged $p/K^+/\pi^+$ beam. The primary goals of these experiments are: (a) a measurement of the $\bar{p}p$ annihilation cross section and a study of multiparticle production in baryon annihilation events; (b) a high statistics comparison between $\bar{p}p$ and pp interactions; (c) a study of $K\pi$ correlations in both $\bar{p}p$ and pp interactions; (d) a study of low cross section processes, such as exclusive channels, neutral particle production, and central region production of $\bar{p}p$ and pp pairs; (e) Resonance (ρ, f, ϕ, K*, etc.) production, and (f) a detailed comparison of $\bar{p}p$ annihilation and $e^+e^- \rightarrow$ hadrons at similar values of $\sqrt{s}$.

Since there will be a large number of π^+p and K^+p interactions in this film, these events will permit a high statistics study of many of the above topics in these interactions. A separate proposal which will guarantee that these data will be analyzed is being submitted by a separate group of collaborating institutions.

III. Introduction

Our collaboration (Cambridge, Fermilab, MSU) completed data taking for E-311 in January, 1975. This experiment was a survey experiment of 10^5 pictures of antiproton-proton interactions at 100 GeV/c using the Fermilab 30-inch bubble chamber-wide gap optical spark chamber hybrid system. The

data analysis has progressed rapidly with all of the ∿12,000 $\bar{p}p$ events having been measured. Three papers on the multiplicity distributions and neutral particle production in $\bar{p}p$ and pp interactions are already published[1-3], and three additional papers on annihilation and nonannihilation effects have been submitted for publication.[4-6] Copies of the three publications may be found in Appendices A1-A3 to this proposal.

On the basis of the current analysis of E-311, as well as other studies of high energy interactions at Fermilab (E-2B, E-281), we are requesting 1.25×10^6 pictures of a 100 GeV/c Cerenkov-tagged enriched $\bar{p}$ beam (30% $\bar{p}$/70% π^-) and 10^6 pictures of a 100 GeV/c Cerenkov-tagged $p/K^+/\pi^+$ (30% p/10% K^+/60% π^+) beam into the 30-inch bubble chamber filled with hydrogen. A novel feature of this proposal is the planned use of both the Downstream Particle Identifier (DPI), in order to identify the antiprotons, protons, and charged kaons which emerge from the chamber, as well as a neutral hadron calorimeter to identify antineutrons and neutrons. With such a system we expect to obtain a highly enriched sample of baryon annihilation events. Another extremely important use of the DPI would be to identify a large fraction of the central region protons and kaons, produced either in annihilation <u>or</u> nonannihilation interactions. With this information, as well as with the neutral kaon detection in the bubble chamber itself, one can study such topics as central region $p/\bar{p}$ production, the rapidity gap distribution for strangeness exchange, and two particle correlations between $K^-\pi^-$, $K^+\pi^\pm$ (and $K\bar{K}$). Since significant like-particle effects have been observed in $\pi^\pm\pi^\pm$ correlations,[7] it would be most interesting to study other combinations such as $K^\pm\pi^\pm$ which are still exotic but do not consist of two identical particles.

Because of the π^+, K^+ content of the beams, there will be approximately 10^5 π^+p and 1.25×10^5 π^-p events in this film. A collaboration consisting of several other groups is submitting a separate proposal to ensure that all of the interactions photographed will be analyzed.

IV. Beam and Bubble Chamber

The results of E-311 have shown that the enriched "halo" $\bar{p}$ beam[8] at 100 GeV/c is perfectly adequate for the current proposal. During that experiment a negative beam containing 20% $\bar{p}$'s at 100 GeV/c was obtained from the target "halo" produced by the decays of $\bar{\Lambda}$'s. By requiring that there be 2 or more $\bar{p}$'s/pulse before taking a bubble chamber picture we took 98,000 pictures containing 0.32 $\bar{p}$'s/negative beam particle. With the collimators wide open a flux of 30-40 $\bar{p}$'s/10^{11} incident protons was obtained, which was more than adequate for the quadruple pulsing mode which was standard for the bubble chamber at that time.

The E-311 exposure was carried out with a 300 GeV incident proton beam. However, 400 GeV protons are now available on a regular basis. In fact, recent $\bar{p}p$ experiments at the 30-inch bubble chamber (E-345, 100 GeV/c $\bar{p}d$; and E-344, 50 GeV/c $\bar{p}p$) and recent beam tests have shown that one can easily obtain a 100 GeV/c 30% $\bar{p}$/70% π^- beam at the 30-inch bubble chamber without triggering the bubble chamber flash with sufficient flux to octuple pulse the chamber with less than 2.5×10^{11} protons on target per accelerator cycle.

The currently existing beam line <u>without any filtering</u> is quite adequate for the proposed positive beam (30% p/10% K^+/60% π^+), although a few shifts of beam time may be necessary to tune the beam for optimal K^+ content. Again, octuple pulsing of the chamber is planned.

We would plan to use the current upstream system of proportional wire chambers and beam Cerenkov counters in Enclosures 106 and 108 to tag each beam track entering the bubble chamber.

In summary, we will no longer need to trigger the bubble chamber flash. Hence the 2.25×10^6 pictures could be taken in $\sim 2.25 \times 10^6$ chamber expansions and $\sim$281 K accelerator cycles, assuming 100% efficient octuple pulsing of the beam line and bubble chamber.

V. Downstream Particle Identifier (DPI)

The primary object of the proposed experiment is to identify as many of the produced particles as possible, i.e., one wants to identify the leading particles (generally p, $\bar{p}$ or π') if they exist, as well as those particles produced in the central region (generally π's and K's).

The system we propose to use is the Downstream Particle Identifier (DPI) (see Fig. 1) which is currently under construction by the PHSC (ISIS) and by the Michigan State University group (Cerenkov counter). At the current time, $40,000 to start the project have already been allocated by Fermilab. It is expected the project will be concluded in FY78 at a total cost of $\sim$\$130,000, with substantial additional support coming from the resources of the PHSC and MSU. Details of this system are described in the July 1976 issue of NALREP, which is included as Appendix B. Basically, the system consists of two elements behind the 30-inch bubble chamber: (a) an ISIS device[9] consisting of a $1 \times 1 \times 1 m^3$ section followed by a $1 \times 1 \times 2 m^3$ section interspersed with drift chambers, and (b) a $2 \times 2 \times 5 m^3$ 8-cell atmospheric pressure N_2-He Cerenkov detector. In the ISIS device, ionization deposited in the detector is sampled by measuring the pulse height from each "cell" hit by the charged particles and, utilizing the relativistic rise effect,

mass identification of particles traversing the device is possible. The circulating gas would be a 80% Ar - 20% CO_2 mixture, which gives a satisfactory relativistic rise. Monte Carlo calculations, substantiated by tests, indicate that one can obtain 7.8% FWHM ionization resolution on a track which passes through the entire device (3m.). With this resolution, it is anticipated that useful particle separation can be achieved up to $\sim$30-40 GeV/c.

To examine the acceptance of the ISIS detector for the proposed experiment, we have used $\sim$4200 inelastic $\bar{p}p$ events (see Fig. 2) obtained from E-311. To investigate the properties of the leading $\bar{p}$ (or p in pp collisions), we have identified slow protons and π's by ionization in the bubble chamber, transformed their laboratory 3-momenta into the center-of-mass system and reversed them, and then transformed them back into the laboratory system. Using these events we find the following:

(a) The acceptance as a function of the laboratory momentum of the produced pions is shown in Table I. Typically $\sim$89% of the forward hemisphere pions from a given event make their way into the ISIS (see Table II). Many slow (backward hemisphere) particles do not traverse the exit aperture of the bubble chamber magnet (see Table I). Typically $\sim$50% of the forward hemisphere particles traverse the entire ISIS device. The acceptance as a function of CM rapidity is shown in Fig. 3.

(b) For a sample of events examined in detail (see Fig. 4 for examples), we estimate that the average resulting resolution on ionization, after folding in the (negligible) probability of more than 1 track entering the same cell, for tracks that traverse the full 3 meters of ISIS is $\sim$7.8% FWHM. For tracks that do not traverse the full 3 meters, the resolution is estimated to be $\sim$11.7% FWHM.

To effectively use the information from ISIS (and the Cerenkov counter) requires that the momentum of the particle be known to $\sim$7% and that one has information on the position of each track entering and leaving the DPI. The proposed use of the drift chambers and the PWC's (Fig. 1) should yield the desired momentum resolution.

The second element of the DPI is the $2x2x5m^3$ atmospheric pressure Cerenkov counter. The thresholds and photoelectron response for different $He-N_2$ mixtures ranging from 100% He to 100% N_2 are shown in Table III. It should be noted that because of the ability to vary the proton (kaon) threshold from 39 (21) to 116 (61) GeV/c, such a detector provides an extremely flexible system to identify the faster particles with momenta above the effective range of ISIS ($\sim$30-40 GeV/c) as well as the ability to identify some of the particles that are also identified by ISIS. Thus the Cerenkov counter is complementary to the ISIS system and by using the information from both systems, the range of mass identification will be increased as will be the confidence one has of unique particle mass identification. In particular, for this proposal the Cerenkov counter plays an essential role in identifying (in a passive veto mode) the fast $\bar{p}$'s with momenta typically above 50 GeV/c from the nonannihilation events.

At the current time the plans are for this Cerenkov counter to have 8 cells, consisting of 2 vertical sets each of four mirrors of size 50, 20, 20, and 50 cm (high) x 70 cm (wide), respectively (see Fig. 5). Acceptance calculations, again using events from E-311, show that the overall acceptance for $\bar{p}$'s, is $\gtrsim$ 99% based on the inversion (in the CM system) of protons with $P_{lab} \lesssim 1.4$ GeV/c which are identified by ionization. Furthermore, 36% of the forward CM hemisphere π's and K's will also hit the Cerenkov mirrors at 11 m. The acceptance as a function of the CM rapidity is also shown in Fig. 3.

Again, this plot shows the complementarity of the $\check{C}$ and ISIS systems. We have also studied the likelihood of two or more particles striking the same mirror (overlap) and find the following: (a) only 3.6% of the $\bar{p}$'s have at least one other track in the same mirror, and (b) only 12% of all π's or K's have at least one other track striking the same mirror. This calculation has taken into account the radius of the cone of the Cerenkov light. For each track we have taken this radius to be the maximum possible radius given the momentum of the track and assuming that the Cerenkov light is produced at the front of the counter (5m from the mirrors) and that the proton threshold is set at 100 GeV/c (see Table III). A track is then considered to have no overlap (i.e. to be unique) if the Cerenkov light from that track strikes a mirror which does not receive light from any other track.

The ranges of particle separation are shown in Fig. 6(a) for the bubble chamber (ionization), ISIS and for two settings of the Cerenkov counter (C_1 has p threshold at 70 GeV/c; C_2 has proton threshold at 100 GeV/c). Fig. 6(b) shows how particles would be identified for each range of momentum. The dotted lines indicate no identification at all and the percentages indicate the % of each type of particle expected in a given momentum range. With such a system one should be able to identify almost all of the antiprotons in addition to $\gtrsim$70% of the slow protons.

VI. Neutral Hadron Calorimeter (Antineutron Detector)

One of the primary considerations of these high statistics exposures is to identify a "clean" sample of annihilation events. To do this, it is necessary to identify as many as possible of the events which have a leading baryon or antibaryon. The slow protons can be identified by ionization in the bubble chamber. The fast antiprotons, whose laboratory momentum spectra is shown in Fig. 7, can only be identified by the Cerenkov counter, since $p/K/\pi$ separation in ISIS is available for $\sim$30-40 GeV/c. Since slow neutrons are difficult to identify, to find all the nonannihilation final states ($\bar{p}pX$, $\bar{p}nX$, $\bar{n}pX$ and $\bar{n}nX$), a necessary ingredient in rejecting nonannihilation events is the detection of forward $\bar{n}$'s. As will be discussed in detail in the next section, a device of cross section 31" x 31" placed immediately behind the Cerenkov counter at 12m will "see" $\sim$90% of the $\bar{n}$'s produced at 100 GeV/c. The expected laboratory angular and momentum distributions of $\bar{n}$'s (total) and those "seen" by the detector (shaded) are shown in Fig. 8.

Since we intend to (passively) veto $\bar{n}$ events, the $\bar{n}$ detector must have high efficiency. Our considerations indicate that a steel-scintillator sandwich neutron counter similar to that discussed by Marshak and Schmuser[10] will do an adequate job. A schematic drawing of our proposed device is shown in Figure 9. Over a large part of the counter's sensitive area, its efficiency is given by[10]

$$\text{Eff.} = (0.95)(1-e^{-x/6.4})(e^{-y/23}),$$

where x is the total length of steel (inches) and y is the amount of steel between any two scintillators (inches). The coefficient 0.95 reflects the probability that the neutron interacted to produce only neutrals that were never detected. With x = 36" and y = 2", we expect an efficiency of $\gtrsim$88%

(since the $\bar{n}$-Fe total cross section is probably 30-50% larger than that for n-Fe, we have stated a lower limit for this value).

As you are aware, the DPI Workshop of May 7-8, 1976 recognized the possibility that other detectors such as a neutral hadron calorimeter might be considered for use behind the Cerenkov counter (see NALREP, July, 1976, Appendix B). The Cambridge-MSU group has been approved for a 9 GeV/c $\bar{p}p$ experiment (BC-64) at the SLAC 40-inch hybrid bubble chamber facility. One of the aims of that experiment is to measure the $\bar{p}p$ annihilation cross section at 9 GeV/c and to aid in that measurement we are currently building a 31" x 31" x 88" antineutron detector. It is our intention to place a similar antineutron detector behind the Cerenkov counter in the 30-inch bubble chamber DPI.

Since the possible presence of γ-rays could simulate antineutrons through electromagnetic showers in the detector, we have made estimates of the $\gamma/\bar{n}$ ratio resulting from nonannihilation interactions in the bubble chamber. Using acceptance calculations based on the simultaneous production of a forward $\bar{p}$ and $\pi^{'}$ in E-311 events, we estimate that $\pi''/\bar{n} \lesssim 7\%$ for $\bar{n}$'s and π°'s "aimed" at the $\bar{n}$ detector. We have not done a detailed calculation of the π° decay; however, it is highly unlikely that both γ's from π° decay will enter the $\bar{n}$ detector. Our best estimate is that $\sim$7% of the $\bar{n}$'s in the detector will be accompanied by a γ. For annihilations, we again estimate that $\sim$7% of the events will yield a γ in the $\bar{n}$ detector. We would consider at least three methods for reducing this background: (1) place a lead filter before the counter, (2) cut on the longitudinal development of the shower (γ showers are preferentially in the front end of the detector), or (3) cut on pulse height (γ's are typically lower in energy). All these have the effect of lowering the $\bar{n}$ efficiency somewhat, however.

In a manner similar to that for estimating the $\pi^0/\bar{n}$ ratio, the ratio $\pi^+/\bar{n}$ is estimated to be $\sim$14% for nonannihilation (this follows from $\pi^0/\bar{n} \approx 7\%$ and $\pi^0 \approx 1/2\ \pi^+$). Hence, in about 14% of the cases an $\bar{n}$ signal may be accompanied by a π^+ interacting in the $\bar{n}$ detector. For this reason we have placed 3 scintillator hodoscopes (5x5 elements, each 6" wide) at depths of $\sim$one radiation length, $\sim$one interaction length and $\sim$three interaction lengths, respectively, in the $\bar{n}$ detector in order to discriminate between π^+/γ and $\bar{n}$ interactions.

As we will see later, the importance of the $\bar{n}$ detector in providing a "clean" sample of annihilation events is dependent upon the ratio of $\bar{p}$'s to $\bar{n}$'s produced in nonannihilation events. Hence, one consequence of having this detector will be a measurement of the ratio of inclusive p/n ($\bar{p}/\bar{n}$) production in 100 GeV/c pp ($\bar{p}p$) interactions.

Acceptances and Detection Efficiencies for $\bar{n}$'s:

An acceptance calculation has been performed for $\bar{n}$'s. For this purpose, we assume a 31" x 31" detector placed immediately behind the Cerenkov counter. Since $\bar{p}p \to \bar{n}$ data are not readily available, we have used neutron production data for $pp \to n(0.2 < p_T < 0.8\ \text{GeV/c})$[11] at ISR energies (invariant cross sections $E\, d^3\sigma/d^3p$ have been assumed to scale to 100 GeV/c) as an approximation to the $\bar{p}p \to \bar{n}$ distribution. Our calculations show that 90% of the $\bar{n}$'s will be "seen" by a 31" x 31" $\bar{n}$ detector (see Fig. 8).

VII. Physics Justification

In our considerations to date of a high statistics experiment yielding "clean" annihilation events, we have established in our minds a considerable

number of exciting and topical studies based on such data. The second primary objective of this experiment is to study central region production of $K^{\pm}$ and $p^{\pm}$ in events with or without annihilation. We have enumerated in the following sections several examples of why we believe this proposed research should be carried out and emphasize that these are just examples of the full range of physics possible in this experiment.

a) $\bar{p}p$ Annihilation and the Difference of $\bar{p}p$ and pp Total Cross Sections

We are interested in carrying out a detailed study of the baryon annihilation component in antiproton-proton interactions at 100 GeV/c incident antiproton momentum. One of the long-standing problems in $\bar{p}p$ annihilation is the possible relationship of $\sigma(\text{ann})$ to $\Delta\sigma_T = \sigma_T(\bar{p}p) - \sigma_T(pp)$. Recently we have published[2] an analysis of the difference between $\bar{p}p$ and pp topological cross sections up to 100 GeV/c, including 100 GeV/c data from our E-311 $\bar{p}p$ experiment. The analysis indicates that good fits may be obtained to the model of Eylon and Harari[12], where the quantity

$$R_n = \frac{\sigma_n(\bar{p}p) - \sigma_n(pp)}{\sigma_n(pp)} \tag{1}$$

is predicted to be of the form

$$R_n = \beta^n s^{2\alpha_B - 2\alpha_M} - (1-\eta_1)\gamma^n , \tag{2}$$

and s is the square of the $\bar{p}p$ C.M. energy, n is the charge multiplicity, $\alpha_M(\alpha_B)$ is the intercept of the leading exchanged meson (baryon) trajectory, $\eta_1(\leq 1)$ is a constant, and $\beta(>1)$ and $\gamma(<1)$ are constants which, in a simple form of the model, are 3/2 and 1/2 respectively. Our fits (shown in Figures 1 and 2 of our paper[2] [included as Appendix A2] with the further definition

$\alpha = 2\alpha_M - 2\alpha_B$) are consistent with a contribution from the first term of Eq. (2) only (implying $\eta_1 \simeq 1$ or $\gamma \simeq 0$). In the Eylon-Harari model the first term of Eq. (2) represents annihilations due to the Pomeron exchange term in the total cross section, whereas the second term represents nonannihilations due to Pomeron and meson exchange terms. Thus, the data support the conjecture that the annihilation component in $\bar{p}p$ interactions is due to the Pomeron and not meson exchange contributions to the total cross section.

The Eylon-Harari model is very much in contradiction with the "classical" approach to the difference in the total cross sections. That is, in Regge terminology one usually writes

$$\sigma_T(\bar{p}p) = \mathrm{Im}(P + \rho + \omega + f + A_2)_{t=0} \tag{3}$$

$$\sigma_T(pp) = \mathrm{Im}(P - \rho - \omega + f + A_2)_{t=0} \tag{4}$$

and hence,

$$\Delta\sigma_T = 2\mathrm{Im}(\rho + \omega)_{t=0} \ , \tag{5}$$

indicating the difference is due to the vector meson exchange part of the total cross section. In fact, the energy dependence of $\Delta\sigma_T$ from Eq. (5) is $s^{\alpha_V(0)-1} \sim s^{-0.5}$, which is a good representation of the data (see Fig. 10). In both the "classical" and Eylon-Harari models as well as related phenomenologies[13,14] it is argued that σ(ann) <u>may</u> equal $\Delta\sigma_T$. To a certain extent this is obviously false, since (1) the $\bar{p}p$ system is an equal mixture of isospin one and zero states, whereas pp is pure isospin one and (2) there are nonannihilation states ($\Lambda^0\bar{\Lambda}^0$ for example) which are available to $\bar{p}p$ but which are not open to pp. Obviously, if the various models discussed above which claim to address the question of annihilations via $\Delta\sigma_T$ are to be proven valid, the experimental relationship of $\Delta\sigma_T$ to σ(ann) must be established.

We propose to do this with a high statistics sample ($\sim$12 K events) of "clean" annihilations.

Somewhat surprisingly, no clean event-by-event identification of annihilation events has been made above $\sim$1-2 GeV/c incident antiproton momentum. This is the result of several factors: (1) the high multiplicity final states in both annihilation and nonannihilation interactions belong to the domain of the bubble chamber technique with its well known high multi-track efficiency; (2) annihilation cross sections are relatively large ($\sim$3.5 mb at 100 GeV/c, see Fig. 10), further lending their study to bubble chambers; (3) ambiguities among $\bar{p}$ and $\pi^-(K^-)$ tracks cannot be resolved in the bubble chamber above $\sim$1.5 GeV/c and (4) neutrons and antineutrons cannot be identified in the bubble chamber. Attempts have been made up to 12 GeV/c to statistically separate the annihilation component.[14-15] These are interesting first steps in isolating annihilations and have been extremely illuminating in their own right. However, they require assumptions which might bias the final result. Clearly better measurements free of possible systematic errors are required.

As mentioned earlier, the Cambridge-MSU collaboration has been approved for a similar $\bar{p}p$ and pp experiment (BC-64) at 9 GeV/c at the SLAC 40-inch hybrid bubble chamber facility. Because of the similarities between these two experiments, we expect to be able to study the energy dependence of many of the annihilation properties by comparing our 9 GeV/c data with the results we would obtain at 100 GeV/c from this proposed experiment.

b) Similarities Between e^+e^- and $\bar{p}p$ Annihilations

Muirhead[16] has pointed out a number of intriguing similarities between the annihilation processes

$$e^+e^- \to \text{hadrons} \tag{6}$$

and

$$\bar{p}p \to \text{hadrons}, \tag{7}$$

where for these purposes "hadrons" is limited to pions or kaons. For example, Figures 11-14 directly compare the $\langle n^- \rangle$, f_2^{--}, $\langle E_{neutral} \rangle / \langle E_{negative} \rangle$ and inclusive cross sections for the two processes. In some cases off-shell (below threshold) low mass $\bar{p}p$ data are obtained by examining virtual $\bar{p}p$ interactions in the u-channel for the reaction $K^-p \to \Lambda^0$ + pions. The similarities in the data are indeed remarkable. With the exception of the lowest energies the $\bar{p}p$ points must be viewed as only approximate since "clean" samples of annihilation events have not been identified in the "bare" bubble chamber experiments. For example, taken at face value the $\bar{p}p$ data of Fig. 13 do not exhibit the "energy crisis" observed in e^+e^- data. On the other hand, a measurement of $\langle E_{neutral} \rangle / \langle E_{negative} \rangle$ at 100 GeV/c (s = 189 GeV^2) with "clean" events free of nonannihilation contamination and comparisons with new data from high energy e^+e^- experiments could be most revealing.

Muirhead[16] has pointed out that the processes most likely responsible for $\bar{p}p$ and e^+e^- annihilation are multiperipheral baryon exchange and one photon exchange respectively, as illustrated in Figures 15(a) and 15(b). Goldberg[17] has shown that the multiperipheral baryon exchange model for $\bar{p}p$ annihilation is, in general, equivalent to vector meson exchange in the t-channel, but on theoretical grounds alone there is no apparent way to connect this process to vector exchange in the s-channel for $\bar{p}p$ annihilation (Figure 15(c)). Hence, it is not clear at the moment what we can learn of fundamental importance (other than what may follow from phase space considerations) from these comparisons. Nevertheless, the potential of a high statistics, "clean" comparison of $\bar{p}p$ and e^+e^- annihilations seems

intriguing to us and could be extended to the details of topological features, specific exclusive channels, resonance production, etc., with the added feature of kaon identification as will be discussed later. It appears to us that the $\sim$ 12,000 annihilation events (based on $\sigma_{ann} \sim 3.5$ mb, see Fig. 10) should be adequate for a preliminary e^+e^-, $\bar{p}p$ annihilation comparison.

c) Multiplicities

The $\bar{p}p$ topological cross sections, shown in papers[1-2] from E-311 that have been included as Appendices A1 and A2, show interesting differences when compared to pp results at 100 GeV/c. The trend seems to be for the low multiplicity $\bar{p}p$ cross sections to be smaller than the pp ones, while the higher charged multiplicity (i.e., $\gtrsim$ 14 prongs) cross sections are significantly larger than the corresponding pp values. This suggests that annihilations occur mainly in the high multiplicity events. (If this is true, it will be difficult to study these events in anything but a bubble chamber.) With an increase in statistics by a factor of 10 for both $\bar{p}p$ and pp, we will be able to study this difference in much greater detail.

d) Neutral and Strange Particle Production

The results[3,4] from E-311, also included in Appendix A3, show that the differences in single particle production spectra occur mainly in the central region suggesting that the annihilation process is a more central collision than the pp reaction. Clearly, a factor of 10 (again for both $\bar{p}p$ and pp) will make such studies more conclusive.

With the identification of K_S^o, $K^{\pm}$, Λ and $\bar{\Lambda}$ in a large number of events (see summary in Table IV) one might expect to study the process of

strangeness exchange in both pp and $\bar{p}p$ interactions. For example, what is the rapidity gap distribution between the two strange particles? How locally is strangeness conserved? The answers to these questions (along with the analogous questions relating to charge exchange) could be most revealing.

With such data it will also be possible to estimate how often annihilations occur which yield K's in the final state and to make a comprehensive search for excited states which decay into a strange particle and one or more pions.

With the additional information of kaon production, it will be possible to attempt a test of Zweig's Rule in 100 GeV/c pp and $\bar{p}p$ interactions following the technique used at 24 GeV/c[18]. Using the identification of at least one charged kaon, one tries all mass combinations with particles of the opposite sign to search for a $\phi \to K^+K^-$ signal. This is quite a reliable method for locating relatively clean ϕ events due to the mass and width of the ϕ. Then one studies the production of extra kaons (charged or neutral). This is particularly interesting in that Blobel et al.[18] find no evidence for a preponderance of K production with ϕ's, in contradiction to Zweig's Rule.

e) Single Particle Inclusive Distributions

With the data that we obtain in this experiment we will be able to make detailed comparisons between $\bar{p}p$ and pp inelastic interactions and between $\bar{p}p$ annihilations and pp interactions. The latter comparison studied as a function of x, y, p_T, etc., should yield detailed information about the annihilation process. It will also be interesting to compare these data with similar $\bar{p}p$ data that already exist at incident momenta below $\sim$20 GeV/c. For example, Fig. 16 shows the CM rapidity distribution for $\bar{p}p \to \pi^+$ + anything, for annihilation and nonannihilation interactions combined, at 4.6, 9.1,

14.8 and 100 GeV/c. In view of the strong energy dependence observed at y=0 it would be most interesting to study such distributions separately for annihilations and nonannihilations. Some preliminary studies[5,6] along these lines using E-311 data have been made.

f) Two-particle Correlations

One of the interesting features observed in $\pi^- p$ and pp interactions at Fermilab energies is the strong dependence of the two particle correlation function on the azimuthal angular separation for a pair of like pions[7]. Figure 17 shows a strong like-particle correlation for $\Delta\phi \sim 0$ and the absence of a correlation for $\Delta\phi \sim \pi$. It would be interesting to learn whether this effect is due to the Bose statistics of two identical particles. One may be able to learn more about such effects by studying $K^{\pm}\pi^{\pm}$ correlations in a similar manner.

Another correlation which has been observed at lower energies is that between neutral and charged pions, Whereas a positive correlation is observed in $\bar{p}p$ interactions at 15 GeV/c where the annihilation-nonannihilation separation was not possible, the correlation for $\bar{p}p$ annihilations at 4.6 GeV/c has been found to be negative. By identifying events with a proton, antiproton or antineutron, we should be able to study the $\pi^{\circ}\pi^{\pm}$ correlation separately for annihilation and nonannihilation at 100 GeV/c.

Interesting results have been obtained from those pp events which have an identified slow proton. With such events, studies have been made of the charged multiplicity of the recoiling system as well as single particle distributions of $\pi^{\pm}$ in the recoiling system. Interpretations of these data have been made in terms of Pomeron-particle interactions. By identifying both a slow proton as well as a fast leading proton or antiproton one may hope to learn about the diffractive excitation of the Pomeron

as well as to study the inclusive double Pomeron exchange process with high statistics.

g) Exclusive Channels

Figure 18 shows a summary of the 4 and 6 body final states in $\bar{p}p$ interactions. By extrapolation to 100 GeV/c, one can estimate the numbers of events expected for various annihilation and nonannihilation final states. These are given in Table IV along with the analogous values for the pp exposure. With the expected numbers of $\bar{p}p\pi^+\pi^-$ and $pp\pi^+\pi^-$ events one will be able to make interesting comparisons at 100 GeV/c. The number of annihilation events expected in the low ($\sim$6) multiplicities will be too small to permit much analysis, but it could be that the cross sections for annihilations to 8π and up will be large enough to permit some interesting studies.

VIII. Study of the Efficiency for Separating Annihilation from Nonannihilation

The efficiencies determined in the previous sections are summarized in Table V. In Table VI we show the separate efficiencies for detecting the four nonannihilation final states: (1) $\bar{p}pX$; (2) $\bar{p}nX$; (3) $\bar{n}pX$ and (4) $\bar{n}nX$. An important input into these considerations is the anticipated relative abundance of these four states. Assuming pp and $\bar{p}p$ (nonannihilation) reactions are factorizable, the results of Bøggild et al.[19] for pp at 19 GeV/c suggest the above reactions should scale in accordance with the ratio $p:n = 0.7:0.3$. We conclude that 97% of the nonannihilations will be identified. Note that a value of $\epsilon(\bar{n}) = 1.0$ would raise the efficiency to 99%, a relatively small gain to be made at the expense of a considerably larger and more expensive $\bar{n}$ detector. On the other hand, $\epsilon(\bar{n}) = 0$ (no $\bar{n}$ detector) gives an efficiency of 85%, demonstrating the important role played by the $\bar{n}$ detector.

REFERENCES AND FOOTNOTES

1. R. E. Ansorge et al., Physics Letters 59B, 299 (1975).
2. J. G. Rushbrooke et al., Physics Letters 59B, 303 (1975).
3. D. R. Ward et al., Physics Letters 62B, 237 (1976).
4. "Neutral Particle Production in 100 GeV/c $\bar{p}p$ Interactions", R. Raja et al., Fermilab Pub 76/79, accepted for publication in Phys. Rev. D (1977).
5. "Properties of Inclusive $\pi^{\prime}$ production in 100 GeV/c Antiproton-proton Interactions", J. Whitmore et al., Michigan State University preprint, (to be submitted to Phys. Rev. Letters) (1977).
6. "Tests of Factorization from Single- and Double-Pion Production in 100 GeV/c $\bar{p}p$ and pp Collisions", J. G. Rushbrooke et al., Cambridge University preprint, (to be submitted for publication) (1977).
7. B. Y. Oh et al., Physics Letters 56B, 400 (1975).
8. W. W. Neale, Fermilab Report FN-259, June, 1974.
9. W. W. M. Allision et al., Nucl. Instr. Methods 119, 499 (1974).
10. M. L. Marshak and P. Schmuser, Nucl. Instr. & Methods 88, 77 (1970).
11. J. Engler et al., Nucl. Phys. B84, 70 (1975).
12. Y. Eylon and H. Harari, Nucl. Physics B80, 349 (1974).
13. H. Muirhead, Proceedings of the Symposium on NN Interactions, Liblice-Prague, CERN 74-18 (1974), p. 488.
14. P. S. Gregory, Proceedings of the Inter. Symposium on $\bar{p}p$ Interactions, Loma-Koli, U. of Helsinki Report No. 103 (1975), p. 256.
15. C. Walck, ibid., p. 65.
16. H. Muirhead, Ref. 13, p. 300.

17. H. Goldberg, Phys. Rev. D6, 2542 (1972).

18. V. Blobel et al., Phys. Letters 59B, 88 (1975).

19. H. Bøggild et al., Nucl. Phys. B27 285 (1971).

20. J. W. Chapman et al., Phys. Letters 47B, 465 (1973); M. Alston-Garnjost et al., Phys. Rev. Letters 35, 142 (1975); J. Erwin et al., Phys. Rev. Letters 32, 254 (1974); C. Bromberg et al., Phys. Rev. Letters 31, 1563 (1973).

Table I

Acceptance as a Function of Momentum for 100 GeV/c $\bar{p}p$

Momentum (GeV/c)	No. of Pions Produced	π's Escaping Magnet		π's Escaping Magnet and Thru $1x1x3m^3$ ISIS	
		No.	% of π's Produced	No.	% of π's Produced
0-5	16135	8389	52.0	691	4.3
5-10	3752	3734	99.5	2034	54.2
10-15	1692	1678	99.2	1522	90.0
15-20	916	910	99.3	887	96.8
20-30	919	913	99.3	910	99.0
30-40	393	390	99.2	389	98.9
40-50	164	159	97.0	159	97.0
50-60	63	61	96.8	61	96.8
60-70	33	30	90.9	30	90.9
70-100	12	10	83.3	10	83.3
Totals	24079	16274	67.6	6693	27.8

Table II

Overall Acceptance for 100 GeV/c $\bar{p}p \rightarrow$ Pions

	No. of Pions Produced	% of Pions Produced	C.M. Hemisphere Backward No.	Backward %	Forward No.	Forward %
Total produced	24079	100.0	12043	100	12036	100
Leave magnet	16274	67.6	4310	35.8	11964	99.4
Enter 1mx1m ISIS at 2.1m	12664	52.6	1987	16.5	10677	88.7
Exit 1mx1m ISIS at 5.3m	6693	27.8	375	3.1	6318	52.5

Table III

Thresholds and Photoelectron Response

Assuming: 1 atmosphere, 5m length, and $N = 2A\,(n-1)[1-(P_T/p)^2]L$
with $A = 100\ Cm^{-1}$.

Thresholds (GeV/c)						# Photoelectrons			
P	K	π	%He-%N_2	$(n-1)\times10^6$	P(GeV/c)	N^{π}_e	N^{K}_e	N^{p}_e	R^{π}_{max}(cm)
116	61.0	17.3	100 - 0	32.7	100	3.2	2.1	0	4.0
					50	2.9			
					20	0.8			
100	52.6	14.9	95.5-4.5	44.02	100	4.4	3.2	0	4.7
					50	4.0			
					25	2.8			
					20	2.0			
70	36.8	10.4	77.5-22.5	89.83	100	8.9	7.8	4.6	6.7
					50	8.6	4.1		
					25	7.4			
					15	4.7			
55	29.0	8.3	55.3-44.7	145.5	100	14.5	13.4	10.2	8.5
					50	14.2	9.7		
					35	13.8	4.6		
					20	12.1			
					10	4.5			
39.3	20.7	5.9	0-100	285	100	28.4	27.3	24.1	11.9
					50	28.1	23.6	10.9	
					25	27.0	9.0		
					15	24.2			
					10	18.8			
					7	8.6			

Table IV

Estimates of Number of Events to be Obtained

	Negative beam[a]	Positive beam[b]
Pictures	1,250,000	1,000,000
Events/μb	$\bar{p}p$ 3.38	pp 2.7
Total events	142,150	103,950
Elastic	25,060	18,700
Inelastic 2 prong	12,180	12,020
" 4 "	27,220	21,130
" 6 "	27,900	20,050
" 8 "	23,440	15,530
" 10 "	13,900	9,860
" 12 "	7,400	4,250
" 14 "	3,040	1,690
" 16 "	1,210	560
" 18 "	400	135
" 20 "	140	43
" 22 "	30	--
K_S^0	2,880	1,820
$\Lambda/\bar{\Lambda}$	1,960	1,180
γ	7,850	5,950
$pp\pi^+\pi^-$	≲3,380	2,228
$pp2\pi^+2\pi^-$	≲1,100	880
$4\pi/6\pi/8\pi$	≲9/34/34	--
Total Annihilation	11,880	--

(a) Based on the data of E-311.
(b) Based on Ref. 20.

Table V

Detection Efficiencies for Individual Particles

Particle	Efficiency	Detector	Value
$\bar{p}$	$\epsilon(\bar{p})$	DPI (Cerenkov)	97%
$\bar{n}$	$\epsilon(\bar{n})$	$\bar{n}$ Detector	90% x 88% = 80%
$\pi^{\pm}$	$\epsilon(\pi)$	DPI (ISIS and Cerenkov)	36% (of forward hemisphere)
		DPI (ISIS)	53% (of forward hemisphere)
p	$\epsilon(p)$	30-inch B.C.	70%

Table VI

Overall Efficiency for Tagging Nonannihilation Events

Reaction	Relative Abundance*	Efficiency X Rel. Abundance
$\bar{p}pX$	0.49	(1-0.03x0.30)0.49 = 0.49
$\bar{p}nX$	0.21	0.97x0.21 = 0.21
$\bar{n}pX$	0.21	(1-0.30x.20)0.21 = 0.20
$\bar{n}nX$	0.09	0.80x0.09 = 0.07
TOTAL	1.00	0.97

*Assuming $\bar{p}:\bar{n}$ = 0.7:0.3.

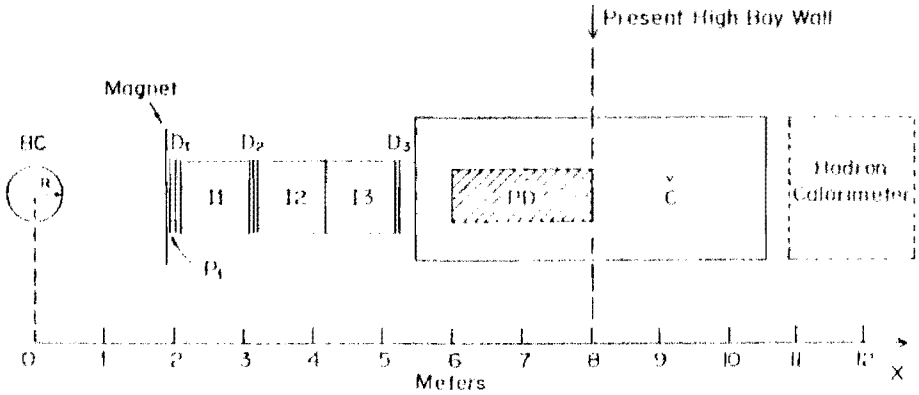

The particle identification system proposed in the recommendations of the workshop for the Fermilab 30-in. bubble chamber hybrid system. I1, I2, and I3 are 1 m × 1 m × 1 m ISIS-type modules; C is a 2 m × 2 m × 5 m multi-cell Cerenkov detector; P_1 is a proportional wire counter; and D_1, D_2, D_3 are drift chambers. The location of the photon detector (PD) and possible location of a future hadron calorimeter are also shown.

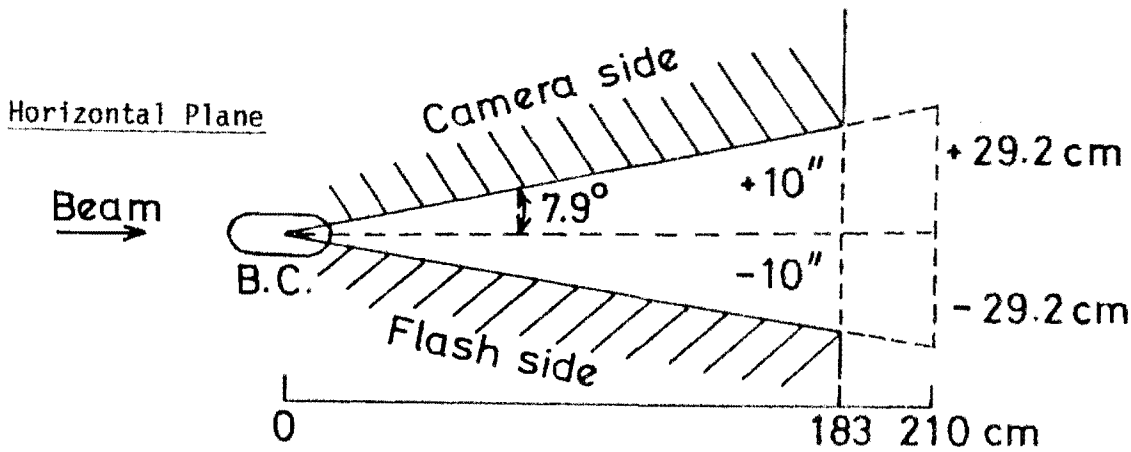

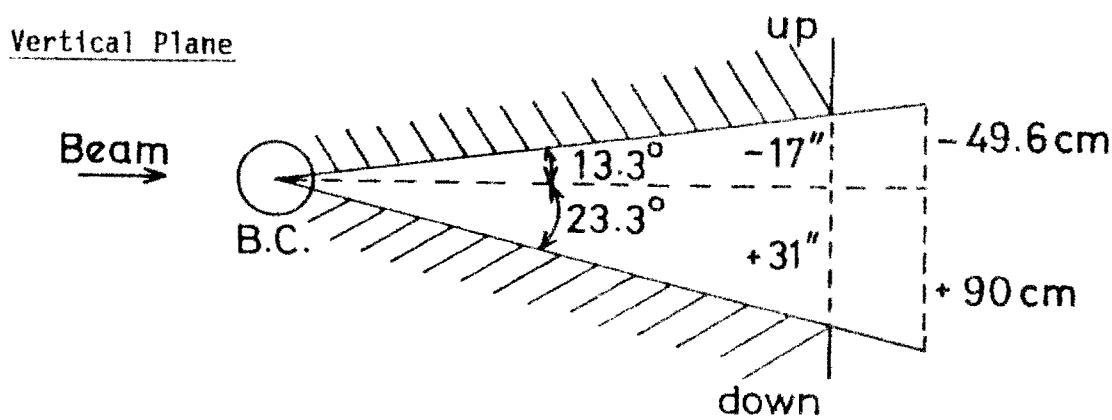

Fig. 1.

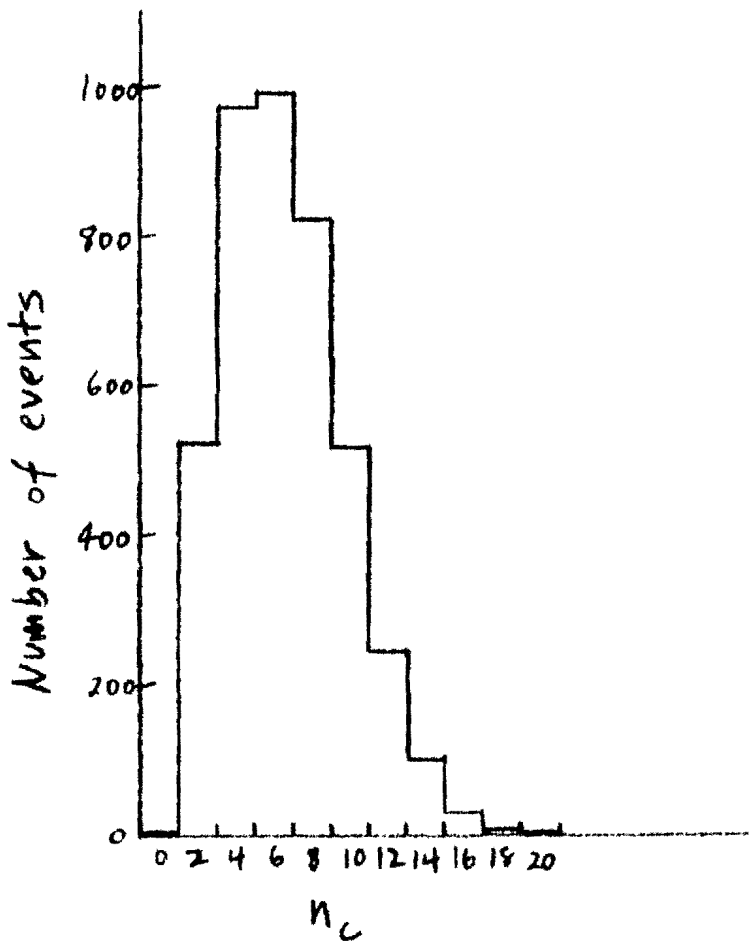

Fig. 2. $\bar{p}p$ Multiplicity distribution of events at 100 GeV/c used for study of the DPI.

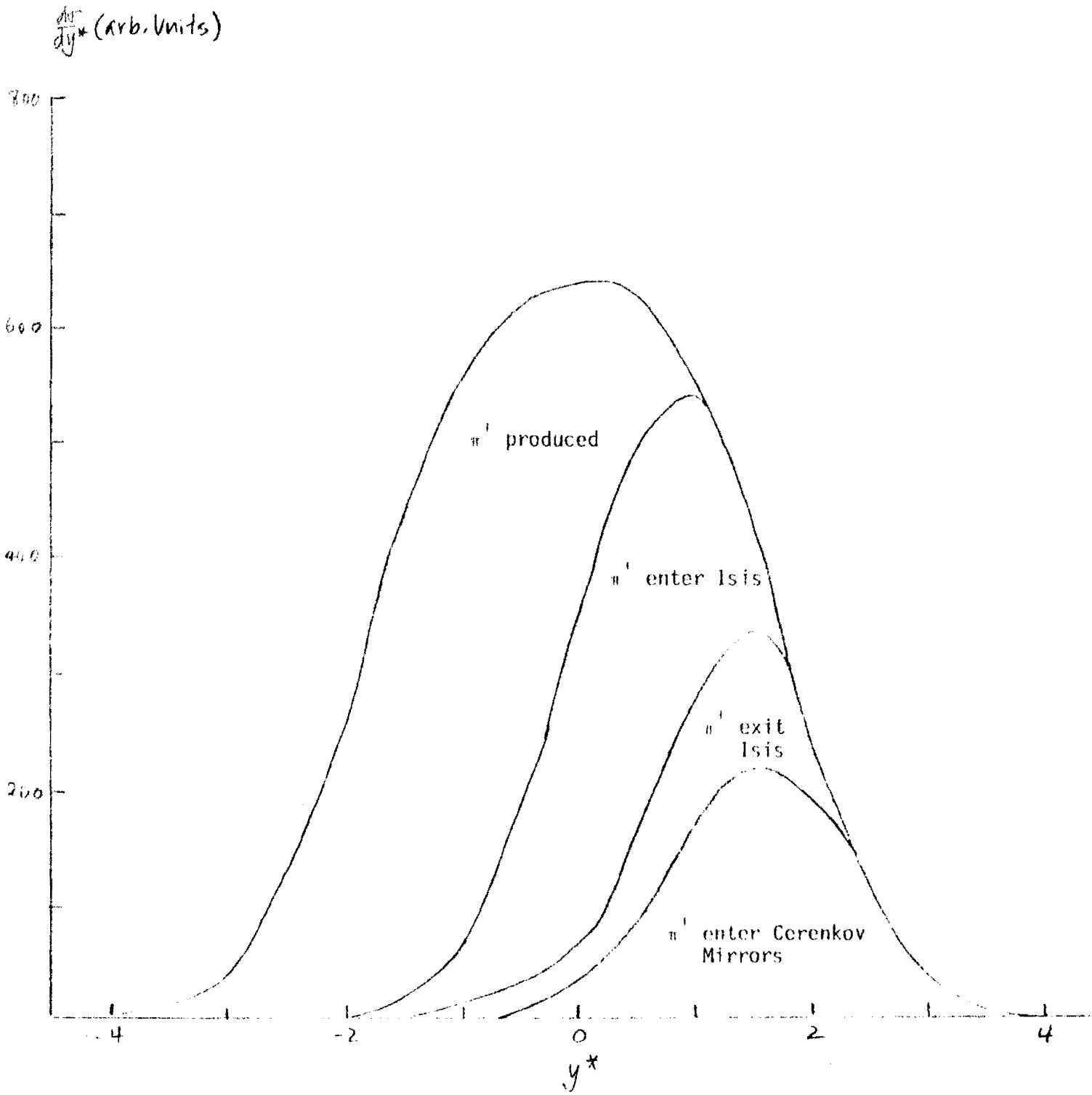
$\frac{d\sigma}{dy^*}$ (Arb. Units)
800
600
400
200
π' produced
π' enter Isis
π' exit Isis
π' enter Cerenkov Mirrors
-4
-2
0
2
4
y^*

Figure 3

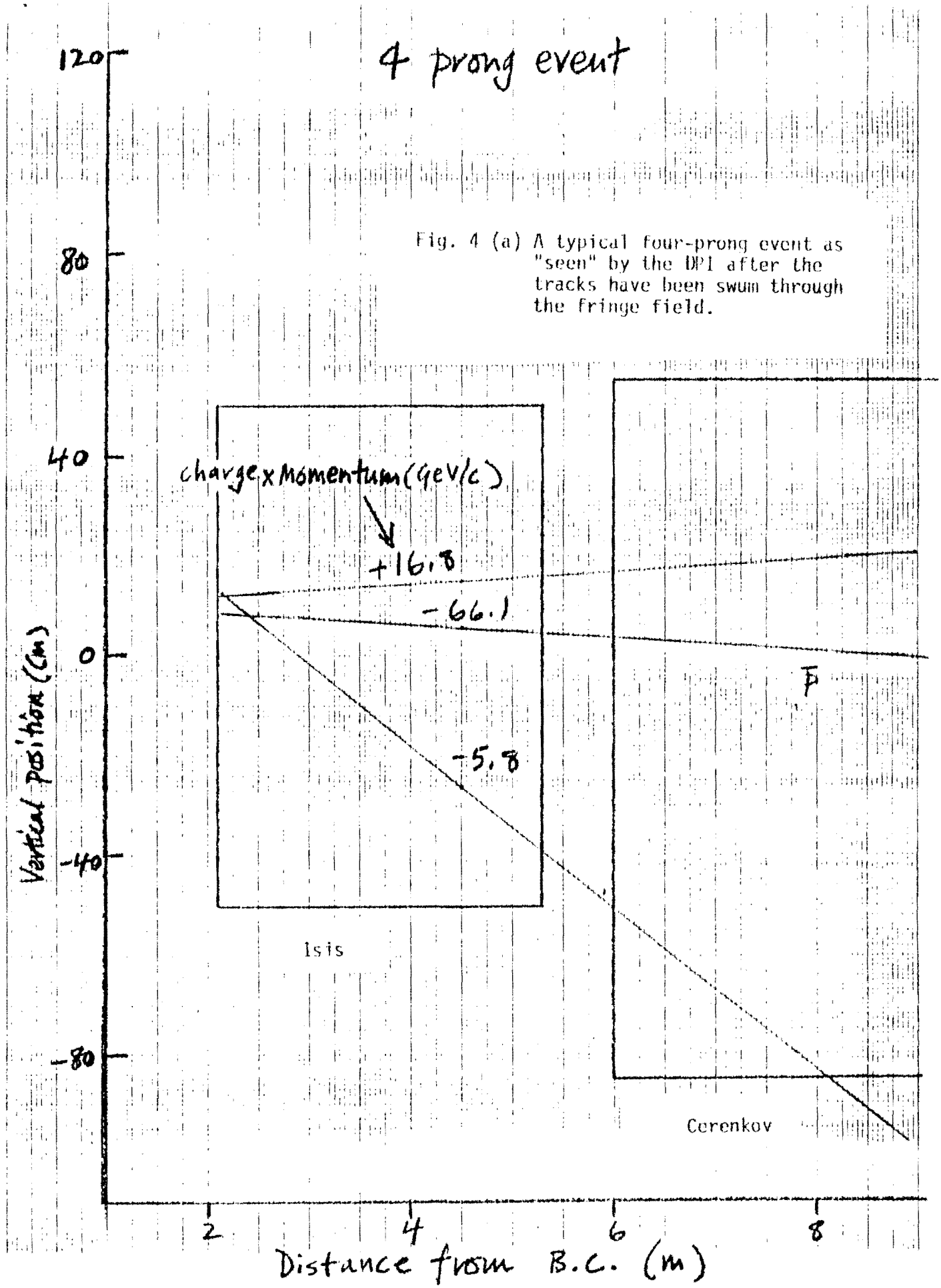

Fig. 4 (a) A typical four-prong event as "seen" by the DPI after the tracks have been swum through the fringe field.

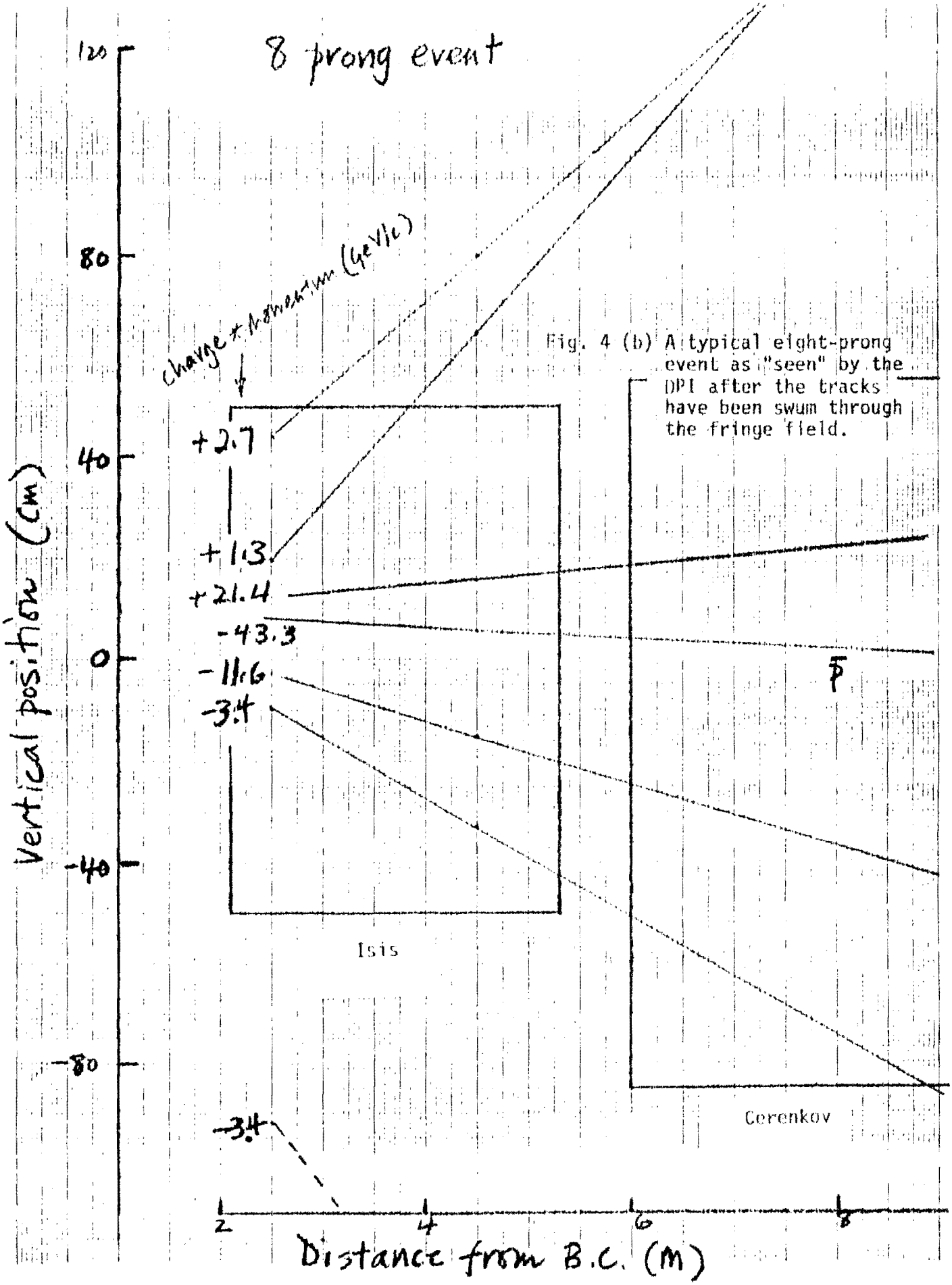

Fig. 4 (b) A typical eight-prong event as "seen" by the DPI after the tracks have been swum through the fringe field.

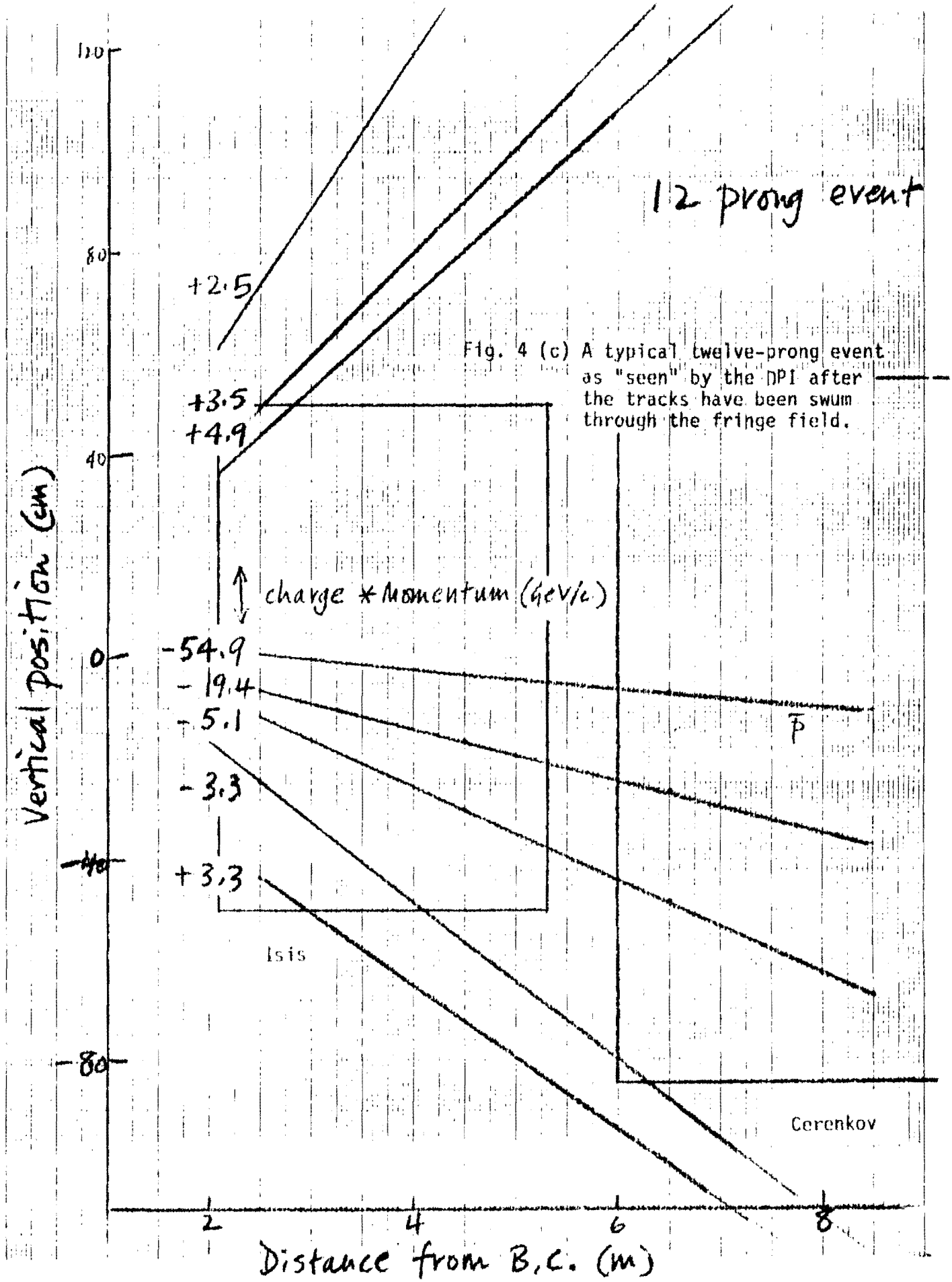

Fig. 4 (c) A typical twelve-prong event as "seen" by the DPI after the tracks have been swum through the fringe field.

Horizontal Plane

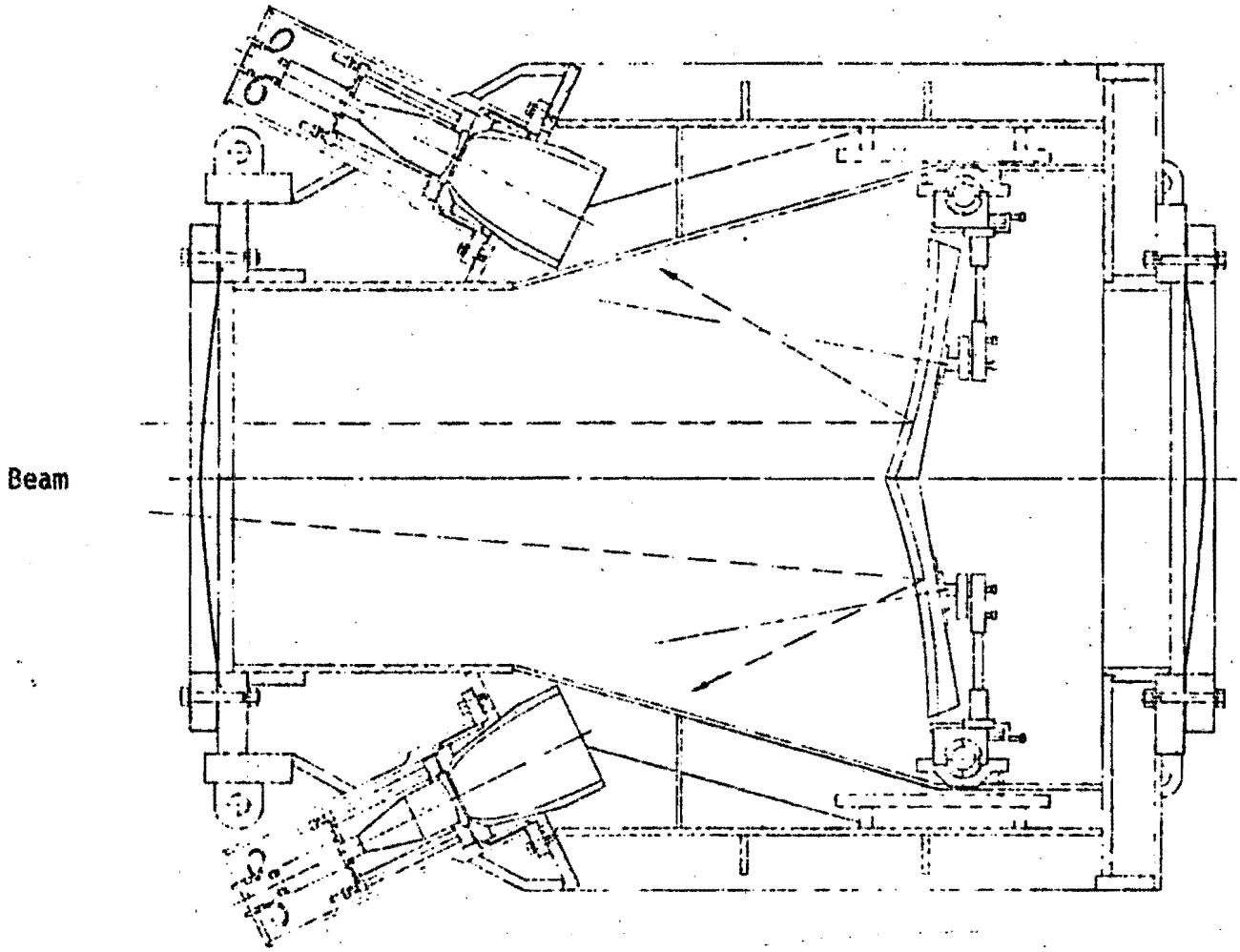

Schematic beam View of Mirrors

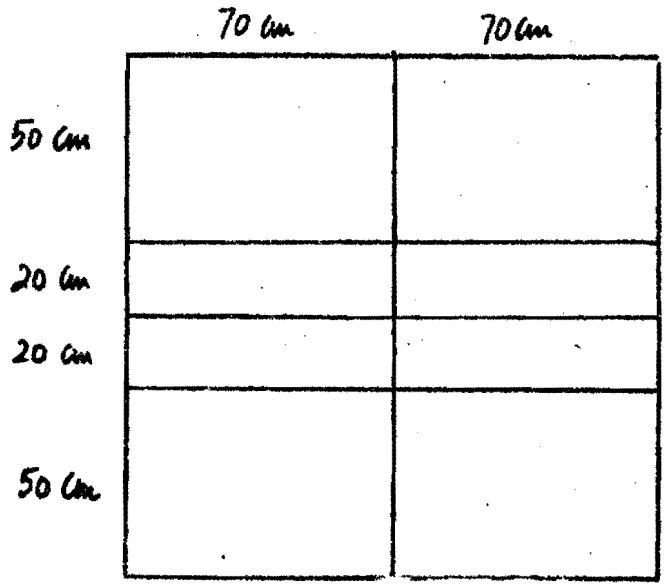

Figure 5

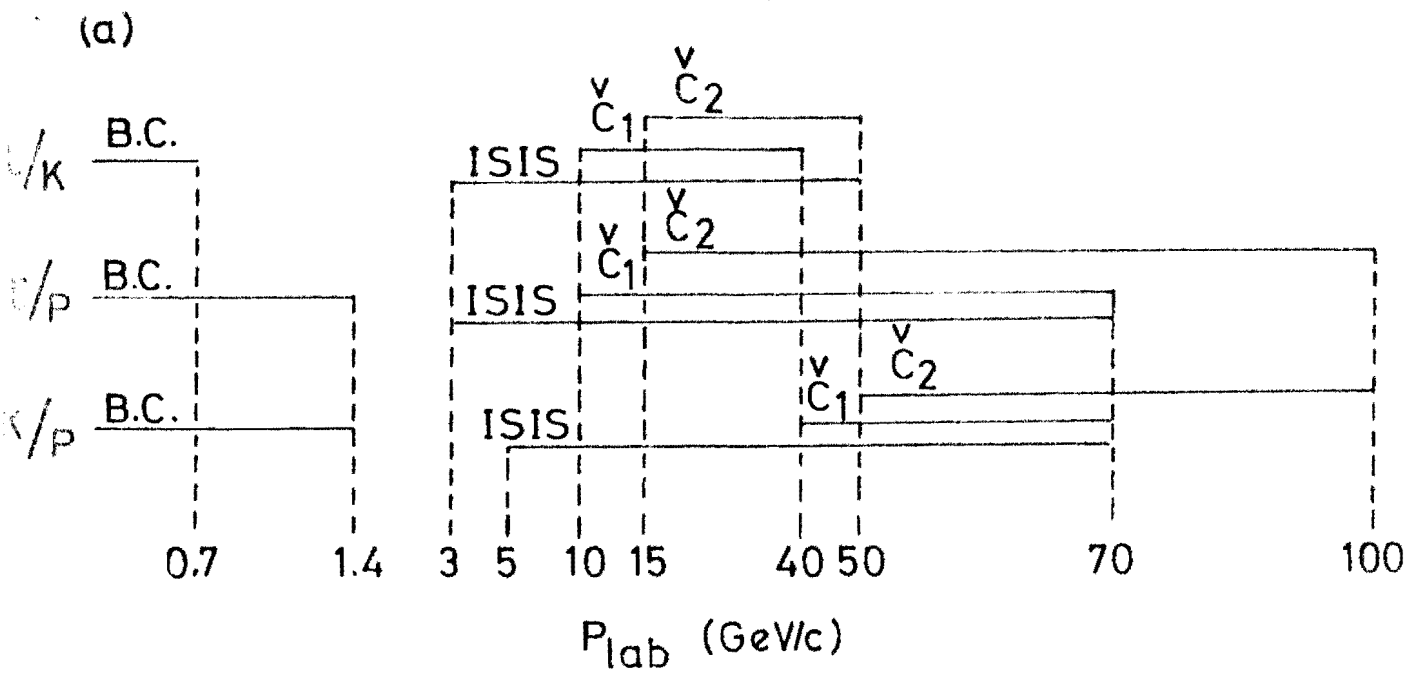
(a)
B.C.
ISIS
C_1
C_2
0.7
1.4
3
5
10
15
40
50
70
100
P_{lab} (GeV/c)

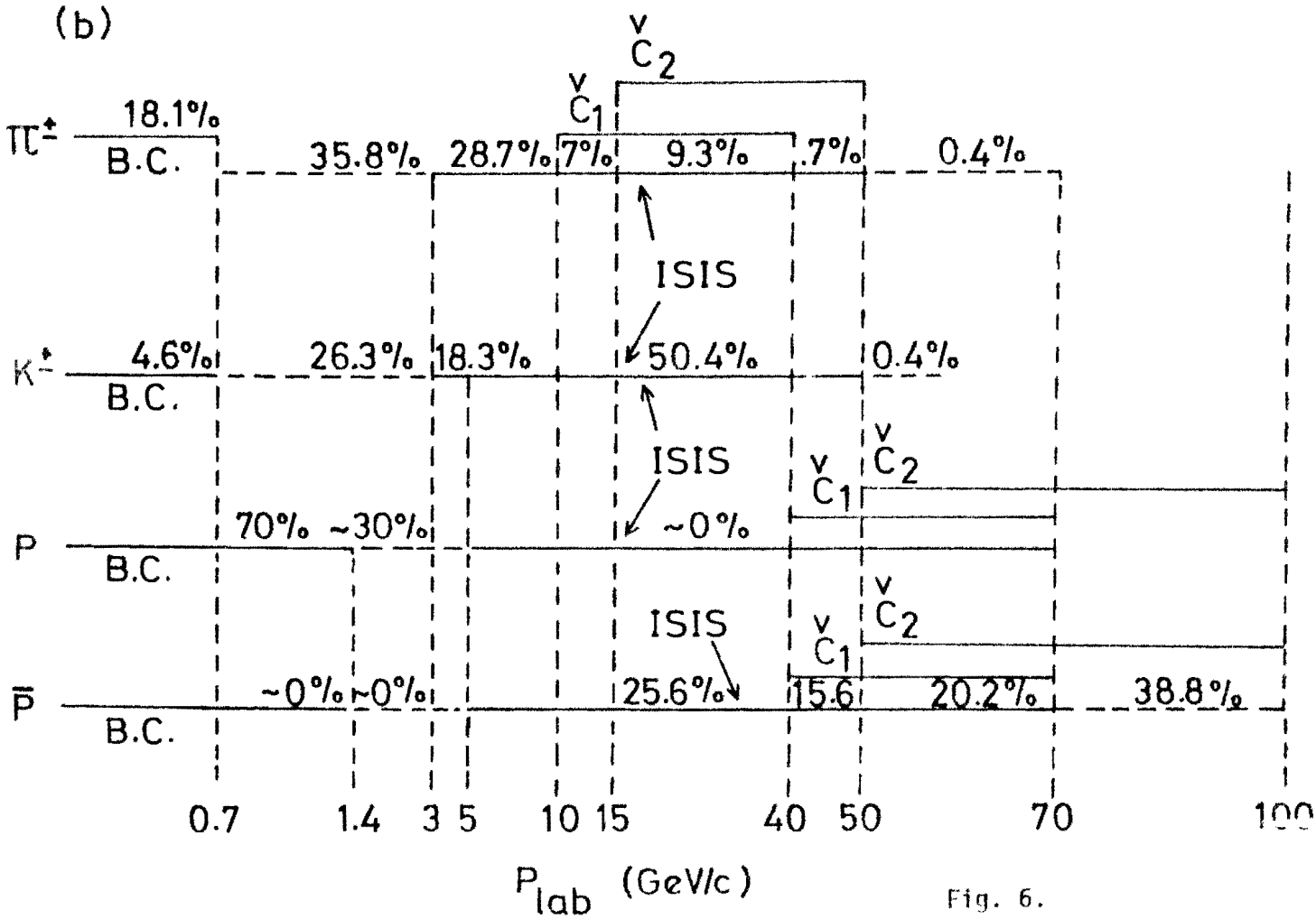
(b)
$\pi^{\pm}$
B.C.
18.1%
35.8%
28.7%
7%
9.3%
.7%
0.4%
ISIS
$K^{\pm}$
4.6%
26.3%
18.3%
50.4%
0.4%
P
70%
~30%
~0%
$\bar{P}$
~0%
~0%
25.6%
15.6
20.2%
38.8%
C_1
C_2
0.7
1.4
3
5
10
15
40
50
70
100
P_{lab} (GeV/c)

Fig. 6.

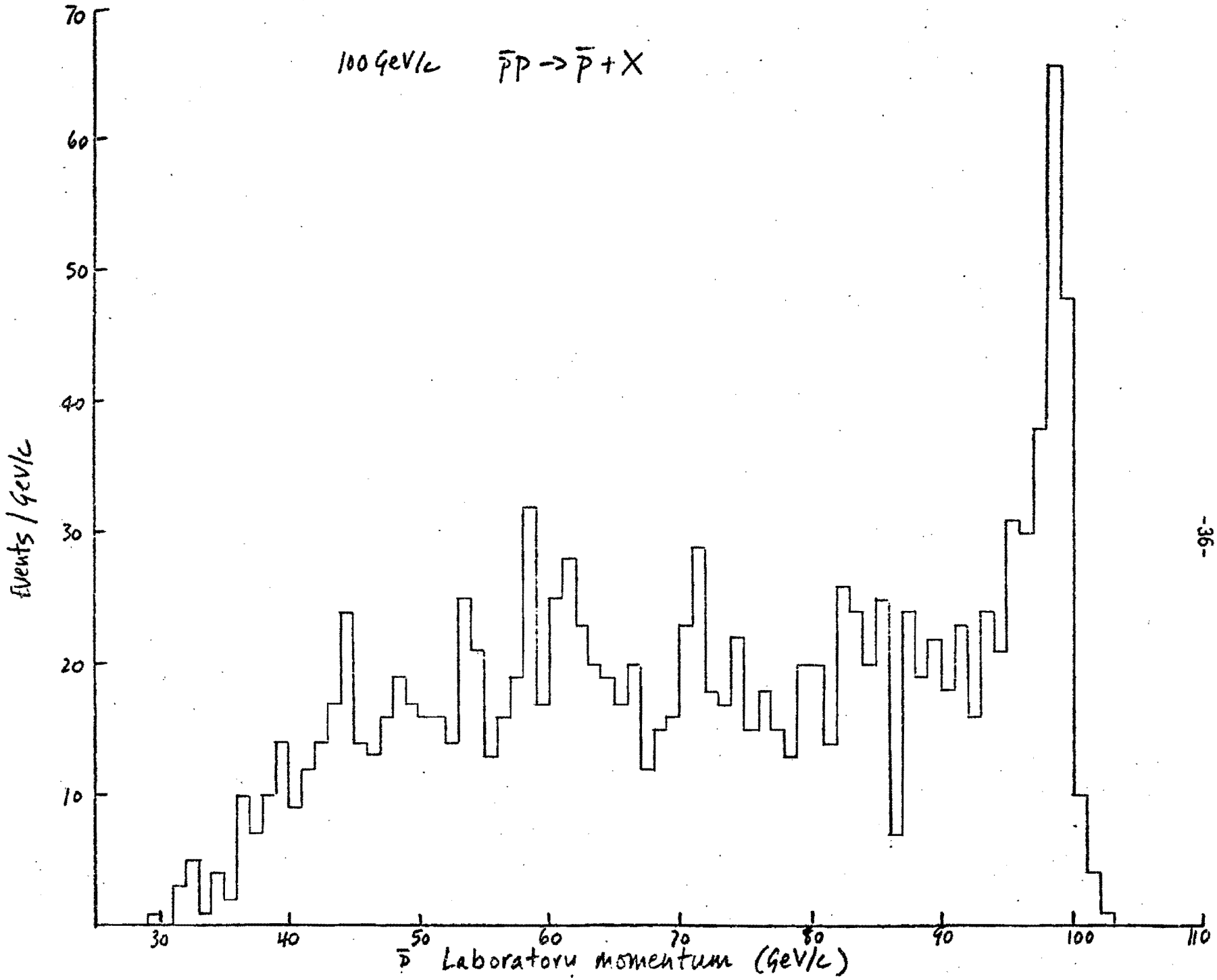
100 GeV/c
$\bar{p}p \to \bar{p} + X$
Events / GeV/c
70
60
50
40
30
20
10
30
40
50
60
70
80
90
100
110
$\bar{p}$ Laboratory momentum (GeV/c)

Figure 7

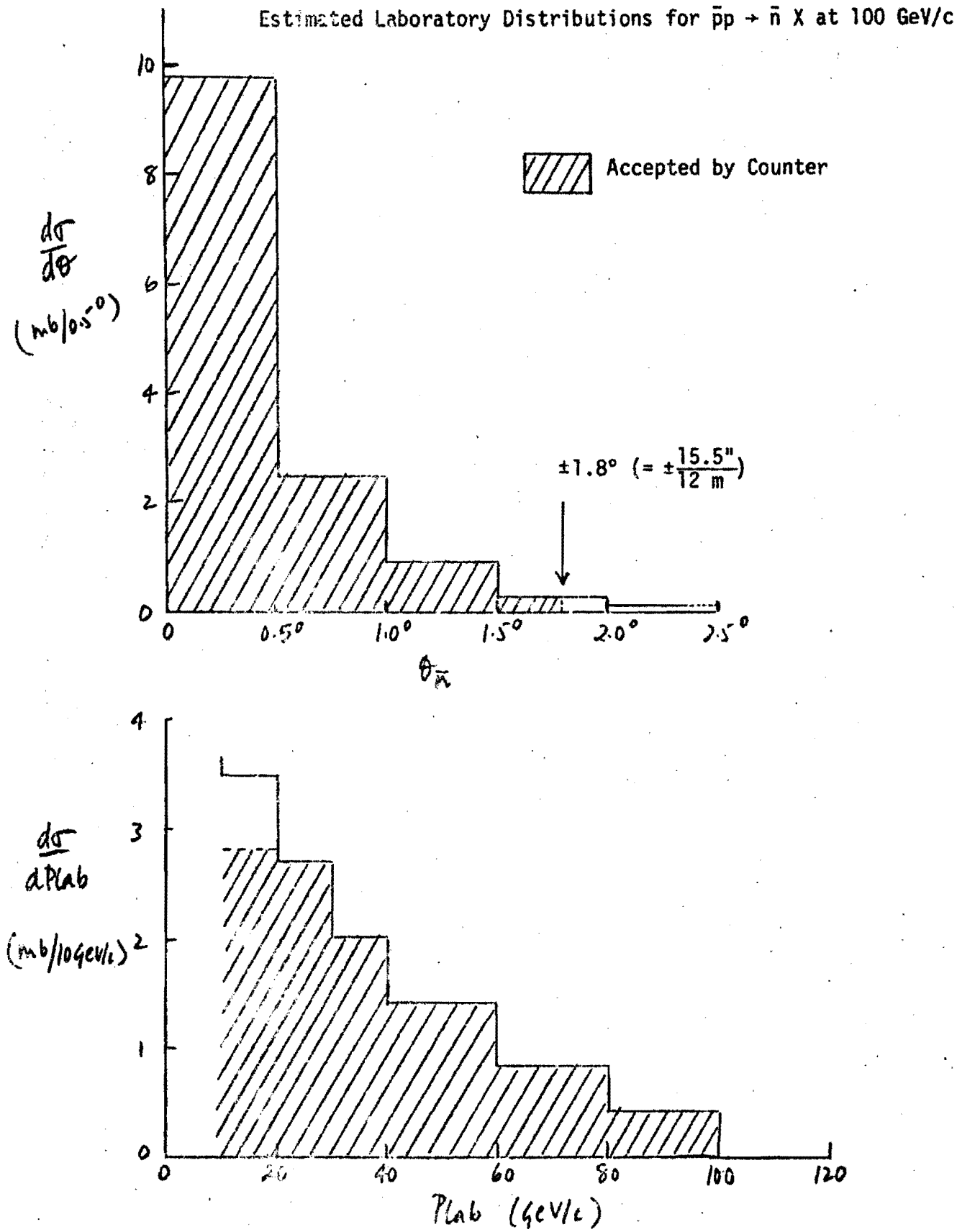
Estimated Laboratory Distributions for $\bar{p}p \to \bar{n}$ X at 100 GeV/c
Accepted by Counter
±1.8° (= ±15.5"/12 m)
dσ/dθ (mb/0.5°)
0
2
4
6
8
10
0
0.5°
1.0°
1.5°
2.0°
2.5°
$\theta_{\bar{n}}$
dσ/dPlab (mb/10GeV/c)
0
1
2
3
4
0
20
40
60
80
100
120
Plab (GeV/c)

Figure 8

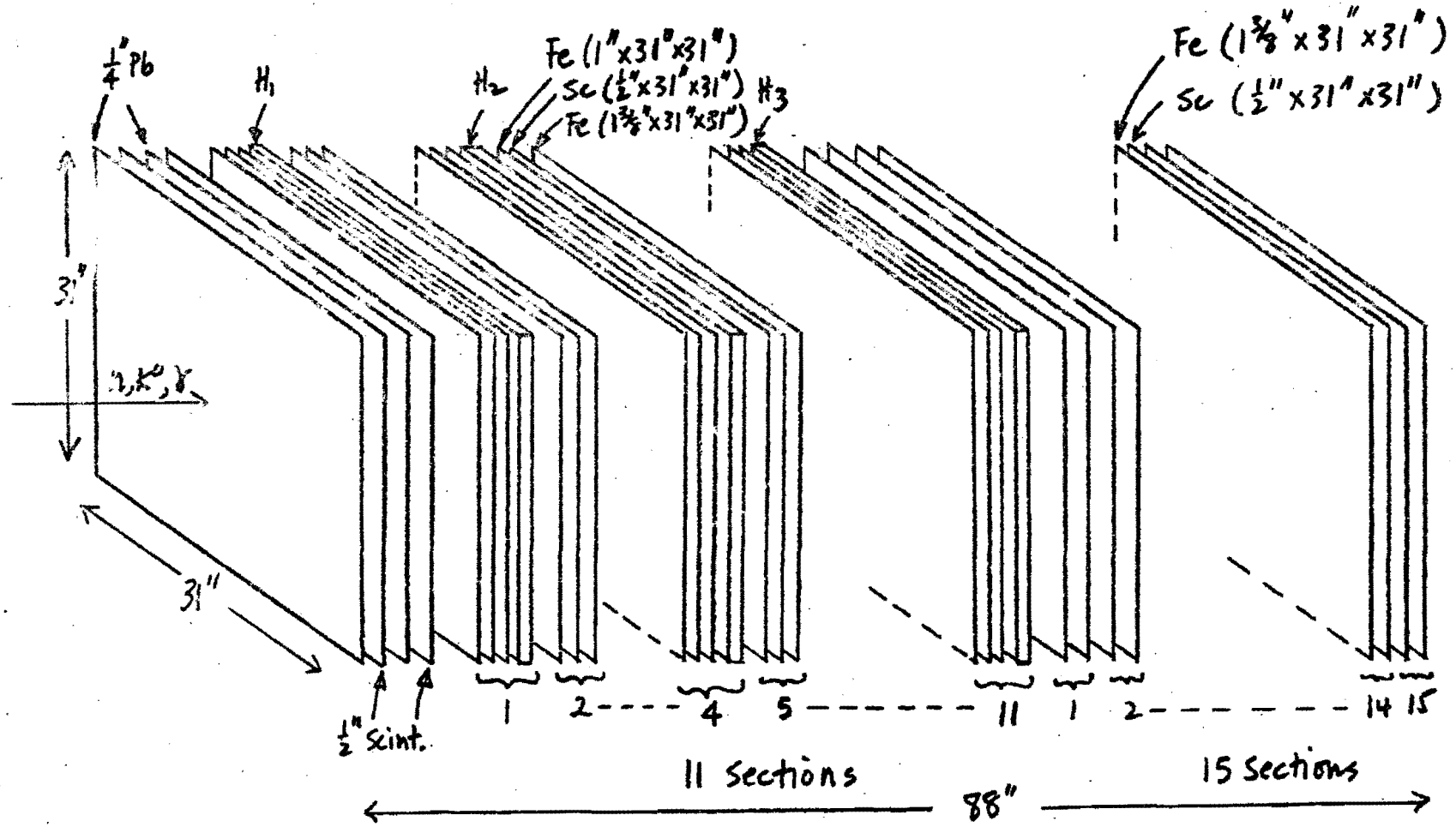

Fig. 9. Schematic view of Neutral Hadron Calorimeter

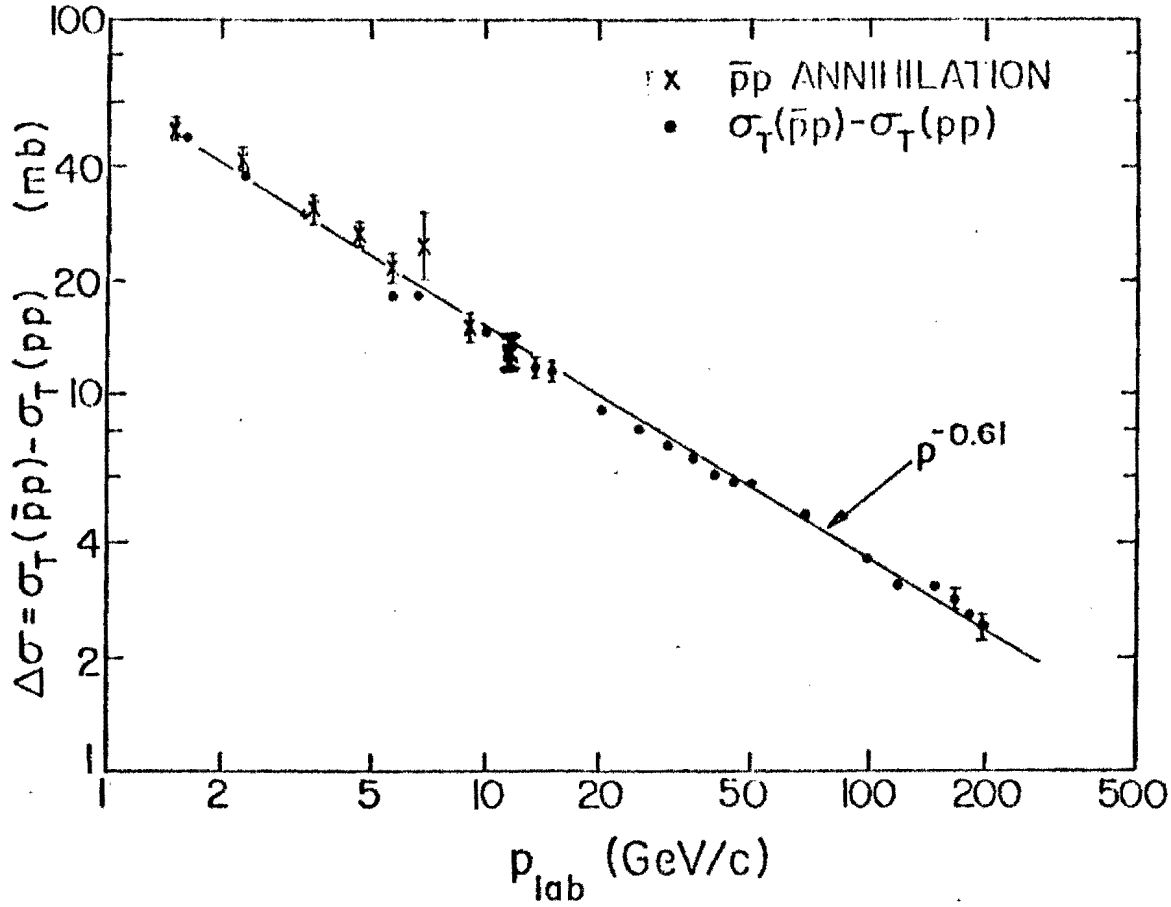

Fig. 10. Difference in total cross section for $\bar{p}p$ and pp interactions as a function of the incident beam momentum. Also shown as the measured annihilation cross section at low energies (see J. Whitmore, proceedings of the APS/DPF Meeting, Seattle, 1975).

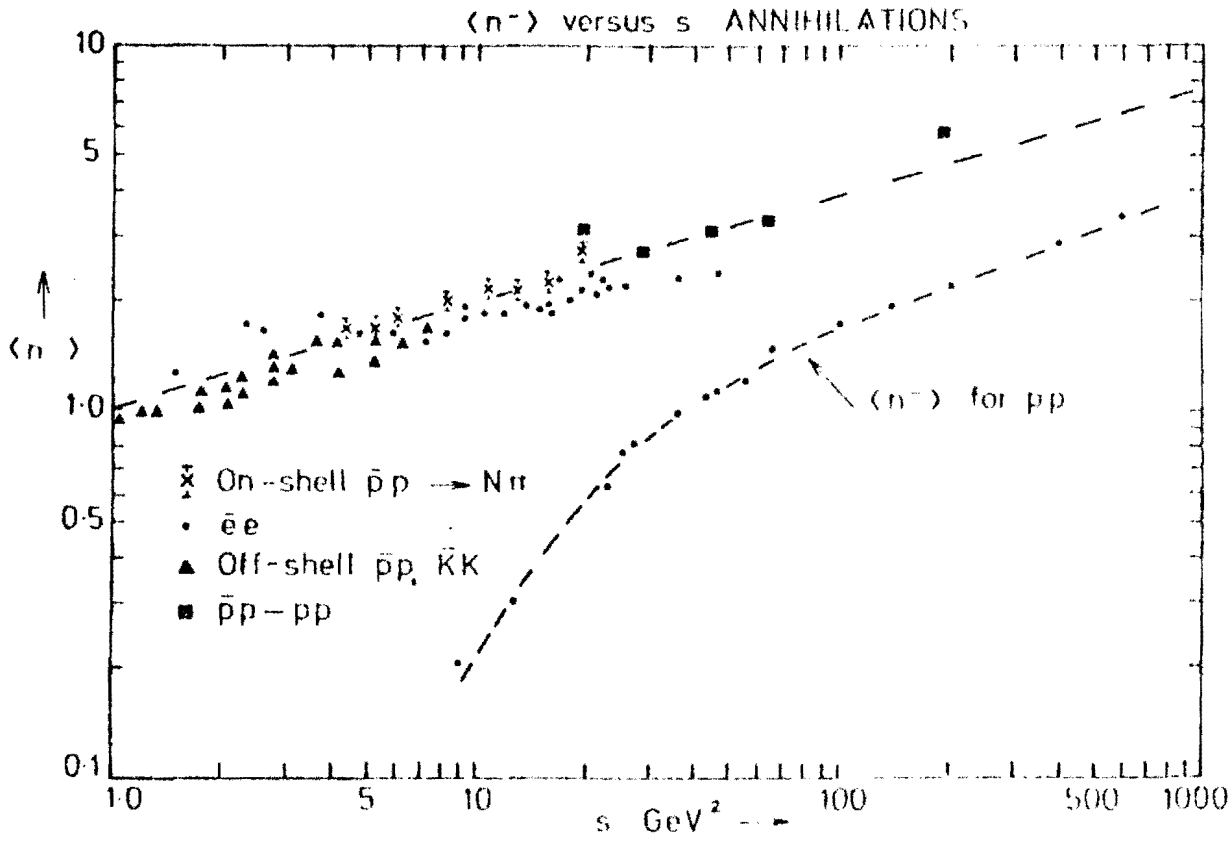
⟨n⁻⟩ versus s ANNIHILATIONS
10
5
1·0
0·5
0·1
⟨n⁻⟩
1·0
5
10
100
500
1000
s GeV²
On-shell p̄p → Nπ
ēe
Off-shell p̄p, K̄K
p̄p − pp
⟨n⁻⟩ for pp

Figure 11

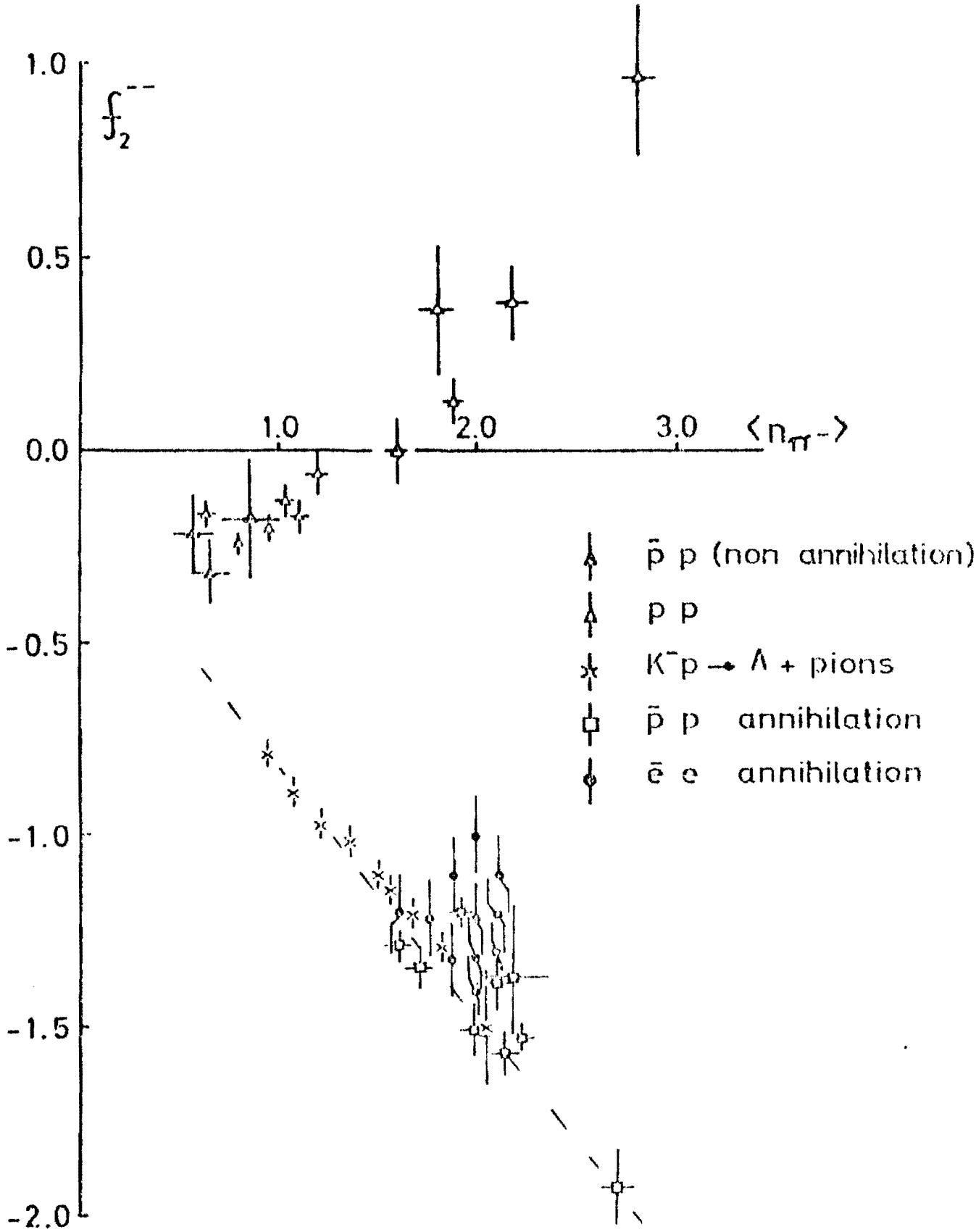
1.0
0.5
0.0
-0.5
-1.0
-1.5
-2.0
f_2^{--}
1.0
2.0
3.0
$\langle n_{\pi^-} \rangle$
$\bar{p}$ p (non annihilation)
p p
$K^- p \rightarrow \Lambda$ + pions
$\bar{p}$ p annihilation
$\bar{e}$ e annihilation

Fig. 12.

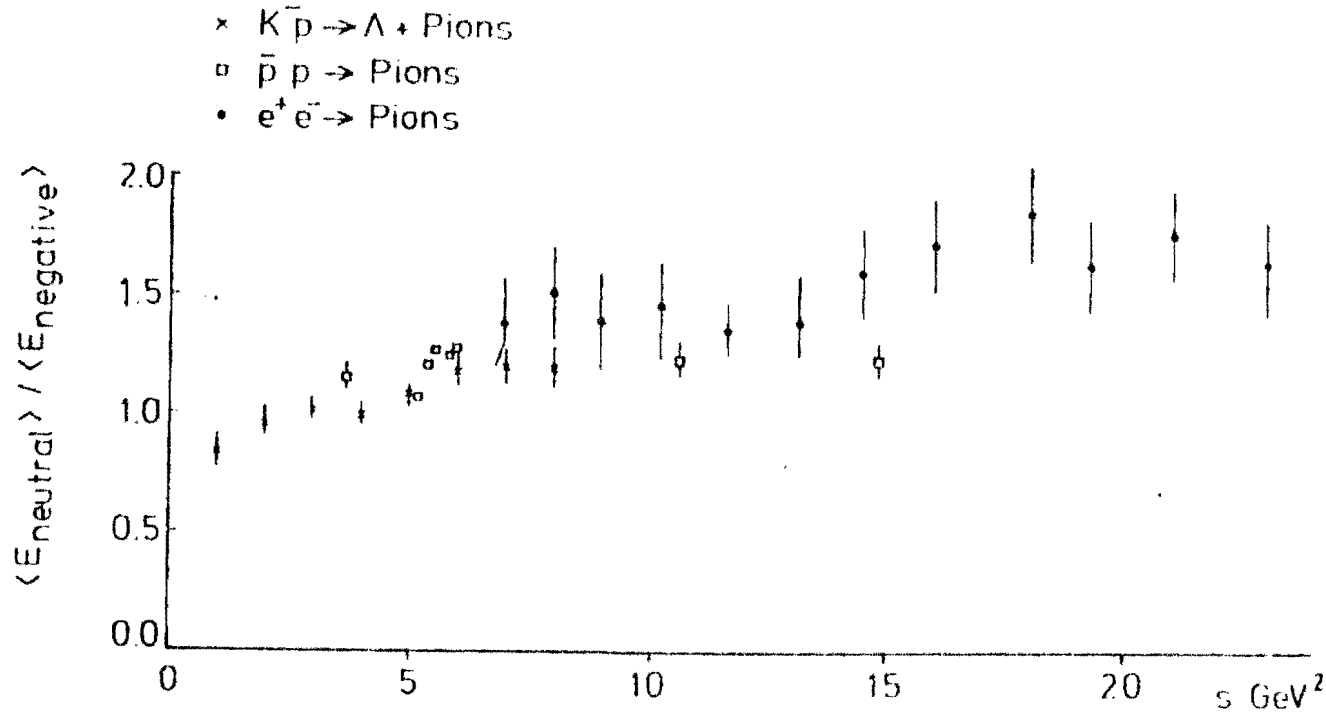
× K⁻p → Λ + Pions
▫ p̄ p → Pions
• e⁺e⁻ → Pions
⟨E neutral⟩ / ⟨E negative⟩
2.0
1.5
1.0
0.5
0.0
0
5
10
15
20
s GeV²

Fig. 13.

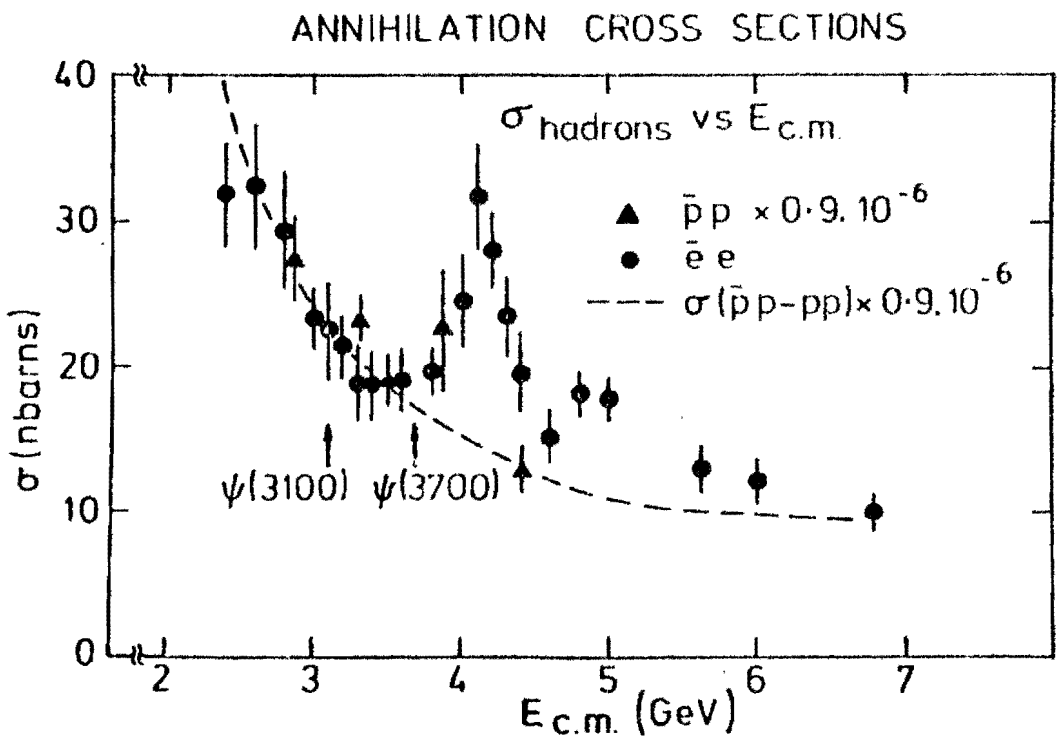
ANNIHILATION CROSS SECTIONS
σ hadrons vs E c.m.
▲ p̄p × 0·9. 10⁻⁶
● ē e
--- σ(p̄p-pp)× 0·9.10⁻⁶
ψ(3100)
ψ(3700)
σ (nbarns)
40
30
20
10
0
2
3
4
5
6
7
E c.m. (GeV)

Fig. 14.

(a)

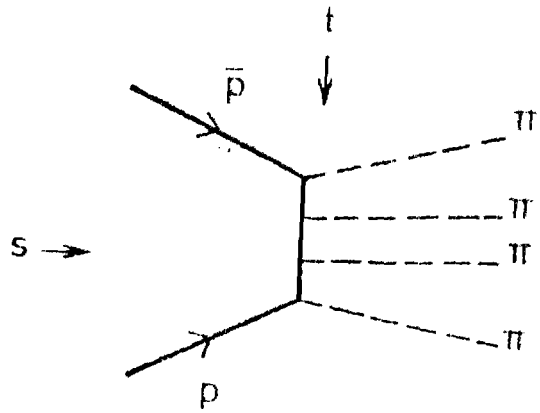

(b)

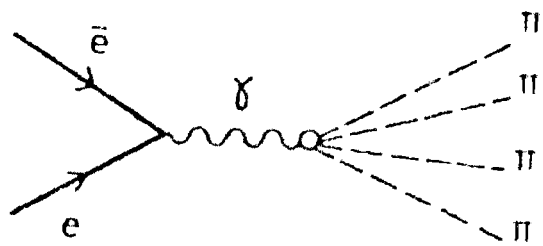

(c)

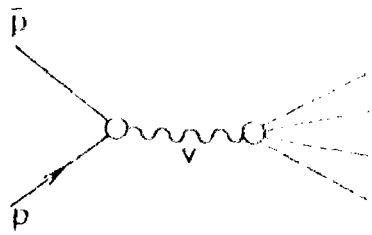

Fig. 15.

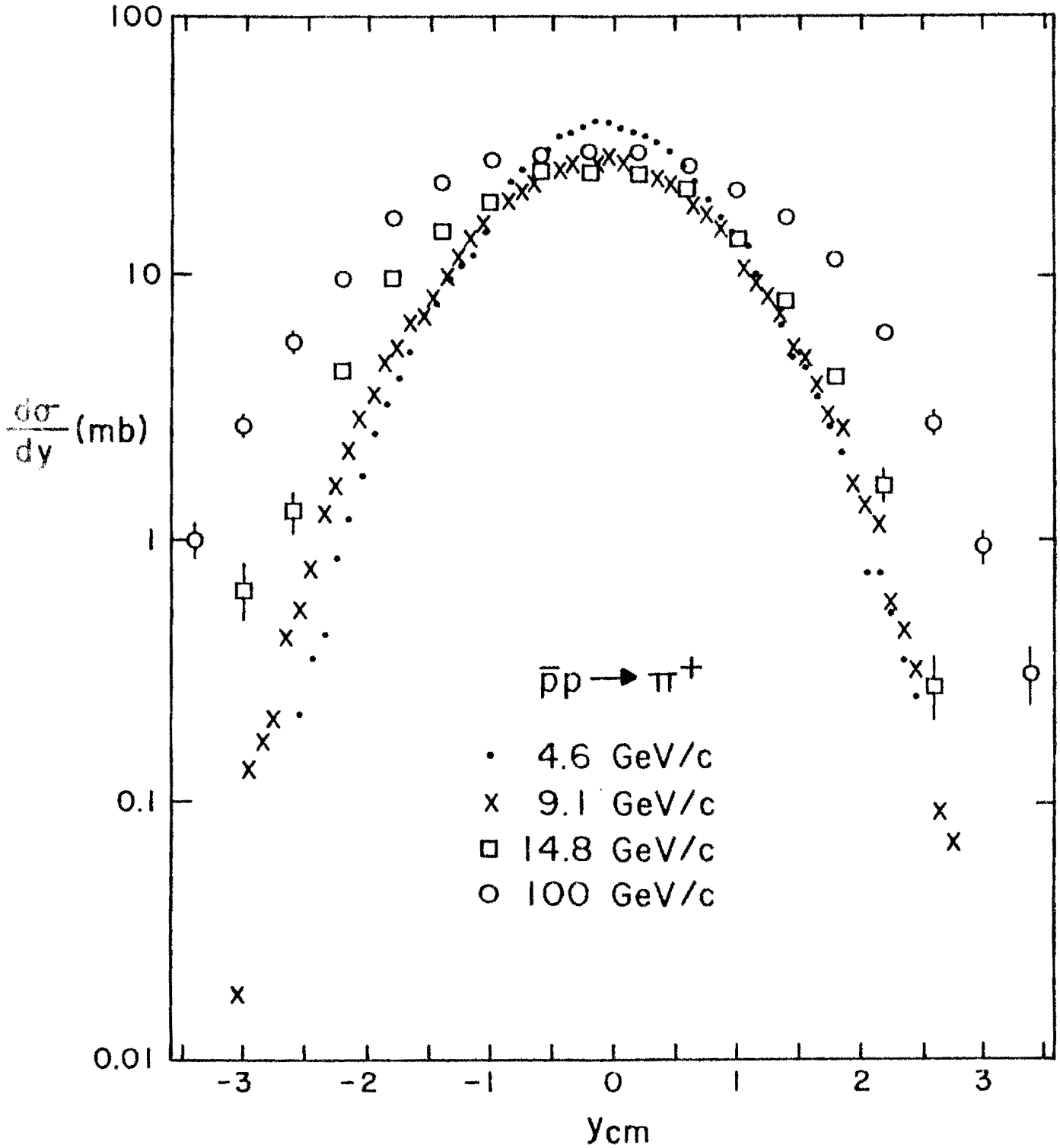

Fig. 16. Center of Mass rapidity distributions for $\bar{p}p \rightarrow \pi^+$ + anything at 4.6, 9.1, 14.8 and 100 GeV/c.

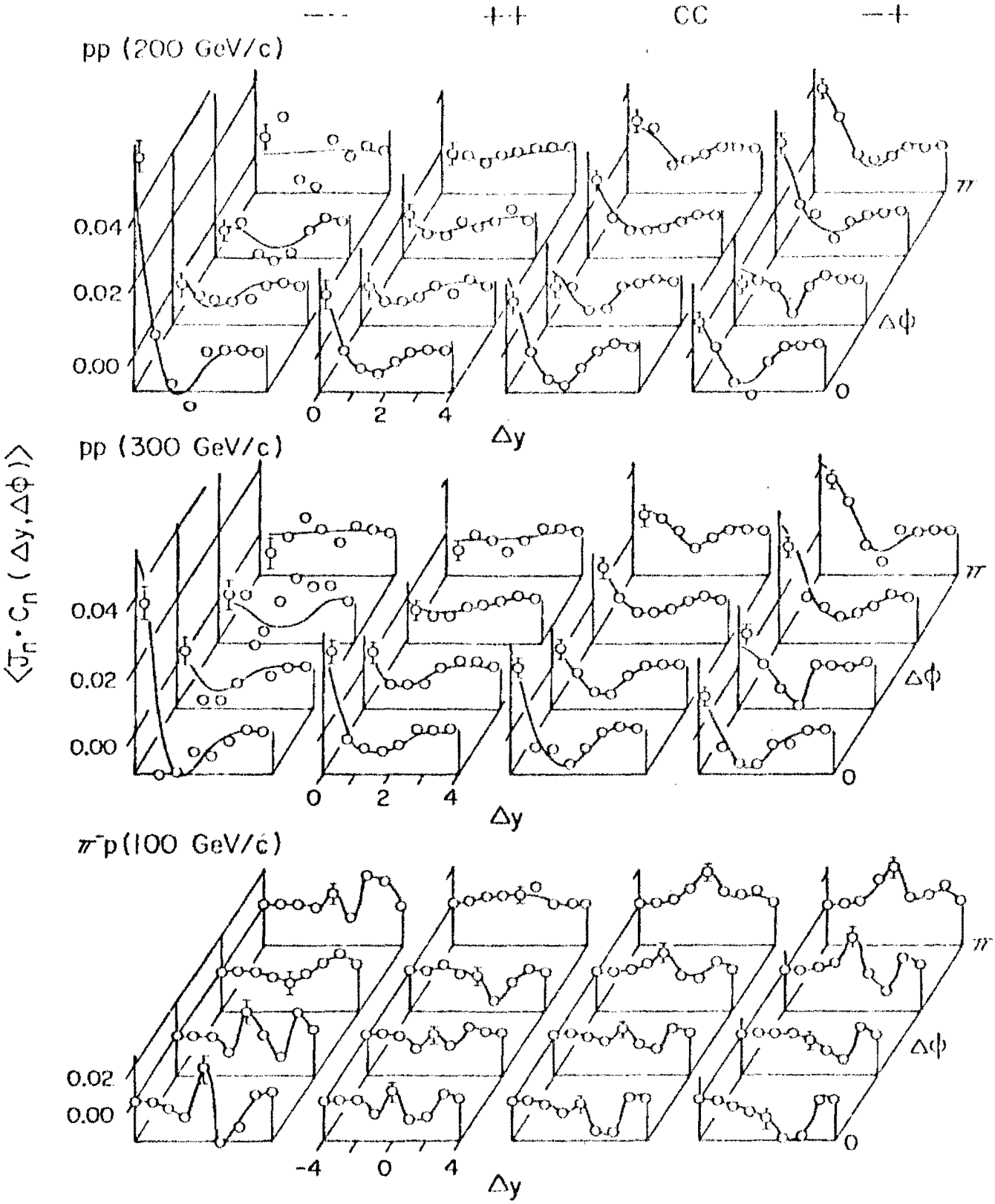

Fig. 17. The two-particle correlation function for various charge combinations from π^-p and pp collisions as a function of the rapidity separation and azimuthal angular separation (Ref. 7).

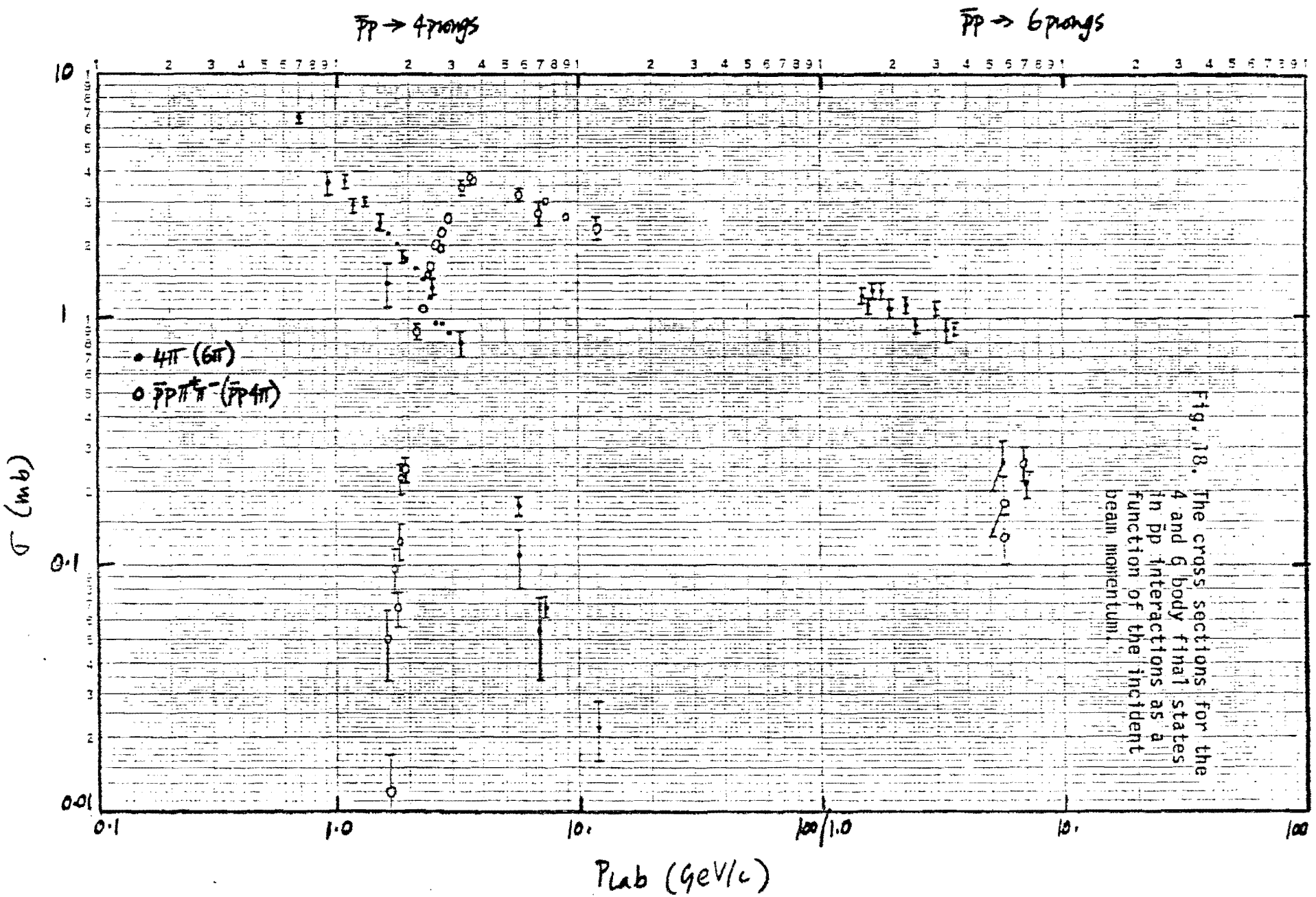

Fig. 18. The cross sections for the 4 and 6 body final states in $\bar{p}p$ interactions as a function of the incident beam momentum.

APPENDIX A1

Volume 59B, number 3 PHYSICS LETTERS 10 November 1975

CHARGED PARTICLE MULTIPLICITIES IN 100 GeV/c $\bar{p}p$ INTERACTIONS

R.E. ANSORGE, C.P. BUST, J.R. CARTER, W.W. NEALE and J.G. RUSHBROOKE
Cavendish Laboratory [1], *Cambridge, England*

C. MOORE, R. RAJA, L. VOYVODIC and R.J. WALKER
Fermi National Accelerator Laboratory [2], *Batavia, Ill. 60510, USA*

W. MORRIS, B.Y. OH, D.L. PARKER, G.A. SMITH, J. WHITMORE
Michigan State University [3], *E. Lansing, Michigan 48824, USA*

Received 15 September 1975

Results are presented on the topological cross sections obtained for antiproton-proton interactions from an exposure of the Fermilab 30-inch bubble chamber to a 100 GeV/c negative beam enriched in $\bar{p}$'s. The $\bar{p}p$ inelastic cross section is found to be $\sigma_{inel} = 34.6 \pm 0.4$ mb, and the average inelastic charged particle multiplicity to be $\langle n \rangle = 6.74 \pm 0.05$.

In this letter we present the first results of an investigation of antiproton-proton interactions at 100 GeV/c. From a 98 000 picture exposure of the Fermilab 30-inch hydrogen bubble chamber and wide gap spark chamber hybrid system to a negative beam enriched in $\bar{p}$'s, we have measured the elastic and inelastic topological cross sections in 100 GeV/c $\bar{p}p$ and $\pi^- p$ interactions. The antiproton data comprise the first detailed study of the $\bar{p}p$ collision process above 32 GeV/c.

The enriched beam used in this experiment was obtained from 300 GeV/c primary protons incident on a copper target 1 km upstream of the Fermilab 30-inch bubble chamber. Since a negatively charged 100 GeV/c secondary particle beam contains only ~ 0.02 $\bar{p}/\pi^-$, we used a new technique [1] to achieve a higher $\bar{p}/\pi^-$ ratio. Downstream of the target a bending magnet deflected charged secondary particles out of the beam line acceptance. However, neutral hyperons and kaons decaying in the region beyond the bending magnet yielded some charged secondaries having the correct trajectories for transmission to the bubble chamber. Antiprotons from $\bar{\Lambda}^0$ decay are selected preferentially since the negative pions produced in K_s^0 decay have an average transverse momentum double that of the antiprotons. In this way we obtained a beam with 0.20 $\bar{p}$'s/negative particle at the bubble chamber. With the requirement of (a) more than one $\bar{p}$ per pulse or (b) a deflection trigger on a tagged $\bar{p}$ beam particle before taking a picture, we obtained 98 000 pictures containing on average 0.32 $\bar{p}$'s/negative particle, and because of the difference in total cross sections, 50% of the events observed in the bubble chamber were from $\bar{p}p$ interactions.

The results presented here come from a sample of 58 000 pictures scanned for all interactions. After an event was found in the bubble chamber, a measurement of the interacting beam track permitted a comparison [2] between the spatial position of that track and the position reconstructed from upstream multiwire proportional chambers (MWPC) in coincidence with a differential gas Cerenkov counter located 500 m upstream from the bubble chamber. This correlation between a reconstructed bubble chamber track and a Cerenkov tagged trajectory in the MWPC was possible for $\sim 80\%$ of the events. The remaining 20% represent only a loss of data [2] and do not bias the results in any way. For the remainder of this paper we use only those events that have a positive identification as being

[1] Work supported in part by the Science Research Council, U.K.
[2] Operated by the Universities Research Association, Inc., under Contract with the Energy Research and Development Administration, U.S.A.
[3] Work supported in part by the National Science Foundation, U.S.A.

due to either a $\bar{p}$ (or π^-). We estimate that the background to identified antiprotons due to inefficiencies of the Cerenkov counter is < 2%.

A portion of the film (~ 18%) has been rescanned in order to determine the scanning efficiencies for various topologies, and these were used to correct event numbers. All those events (~ 1/3% of the total) with an apparent odd number of charged particles have been classified as belonging to the next highest even charged particle topology, on the assumption that a short track was missed. An undetected charged secondary interaction occuring close to the primary vertex could also simulate an odd prong topology, but in view of the very few events in this category a correction for secondary interactions was deemed unnecessary.

In ~ 1.5% of events a Dalitz pair was observed, but because of the uncertainty of identification at the scanning stage the pair was included in the topological count and a statistical correction made. This correction used an estimate of the mean number of π^0's produced per event as a function of charged multiplicity n, which was determined from measurements of observed γ conversions in the bubble chamber. The final Dalitz correction amounted to a shift of events between topologies at a level of $\lesssim$ 3%. A small correction was also made for unseen V^0's and electron pairs from γ conversions. We find no evidence for any bias resulting from use of the deflection trigger. We conclude that the final uncertainty in all these corrections is well within statistical errors.

The major correction applied to the raw data occurs for the two prong topology. All two prong events have been measured and kinematic fits to the $\bar{p}p$ and π^-p elastic [3] hypotheses attempted. Elastic events were corrected for scanning losses, determined as a function of t (the square of the four-momentum transfer from target to outgoing proton), and then the elastic t distribution was fitted, for $|t| \gtrsim 0.08\,(\mathrm{GeV}/c)^2$, to an exponential form $d\sigma/dt = A\exp(bt)$ to correct for an apparent loss of events below this value of $|t|$. We find a slope parameter of $b = 11.4 \pm 0.6\ (7.7 \pm 0.4)(\mathrm{GeV}/c)^{-2}$ for 100 GeV/c $\bar{p}p$ (π^-p) elastic scattering. Inelastic events were corrected independently for scanning losses; we stress that *no* correction has been made to the inelastic two prong cross section for a loss at small $|t|$ [3].

In table 1 we present our measured topological cross sections for 100 GeV/c $\bar{p}p$ interactions, normal-

Table 1
$\bar{p}p$ topological cross sections at 100 GeV/c

Prong number n	Raw events	Corrected events	Cross sections [(a)] σ_n(mb)
0	11	13	0.061 ± 0.019
2	1876	Elast. 1635	7.41 ± 0.38
		Inel. 794	3.60 ± 0.30
4	1664	1777	8.05 ± 0.20
6	1765	1821	8.25 ± 0.20
8	1527	1528	6.93 ± 0.18
10	937	907	4.11 ± 0.13
12	513	484	2.19 ± 0.10
14	215	199	0.90 ± 0.06
16	82	80	0.36 ± 0.04
18	26	26	0.12 ± 0.02
20	9	9	0.041 ± 0.014
22	2	2	0.009 ± 0.006
Total	8626	9275	42.04 ± 0.09 [(b)]

(a) Errors are statistical only except for 2-prong cross sections.
(b) Input value (ref. [4]).

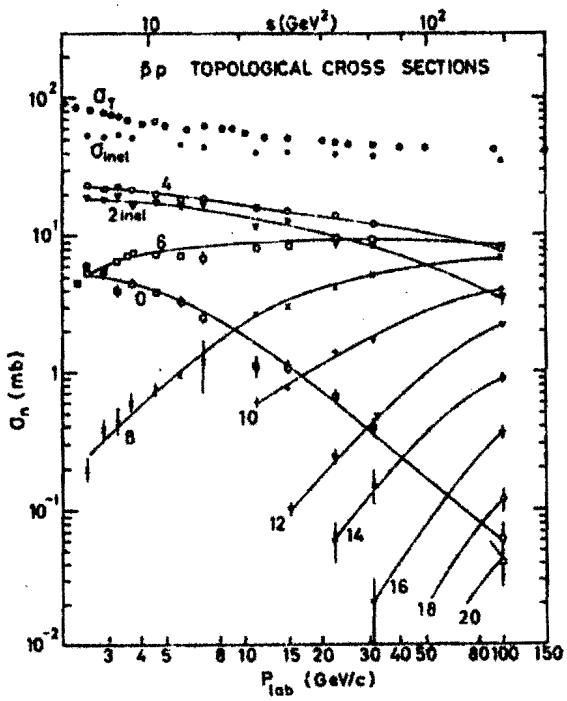

Fig. 1. Momentum and s dependence of $\bar{p}p$ topological cross-sections. The curves are to guide the eye.

Table 2
Moments of the 100 GeV/c $\bar{p}p$ multiplicity distribution

Moments	All charges	Negative charges
$\langle n \rangle$	6.74 ± 0.05	3.37 ± 0.03
$\langle n(n-1) \rangle$	49.25 ± 0.68	10.63 ± 0.16
$\langle n(n-1)(n-2) \rangle$	389 ± 8	32.7 ± 0.8
$\langle n \rangle / D$	2.07 ± 0.03	
$f_2 = \langle n(n-1) \rangle - \langle n \rangle^2$	3.85 ± 0.22	−0.72 ± 0.06
$f_3 = \langle n(n-1)(n-2) \rangle - 3\langle n(n-1) \rangle \langle n \rangle + 2\langle n \rangle^3$	5.8 ± 1.1	1.81 ± 0.14

ized to the total cross-section data for Carroll et al. [4]. The $\bar{p}p$ elastic cross section of $\sigma_{el} = 7.41 \pm 0.38$ mb would appear to be in good agreement with an extrapolation from lower energies. The total inelastic cross section is found to be 34.63 ± 0.38 mb. Our 100 GeV/c $\pi^- p$ topological cross sections (not shown) agree with previous data [5] within quoted errors.

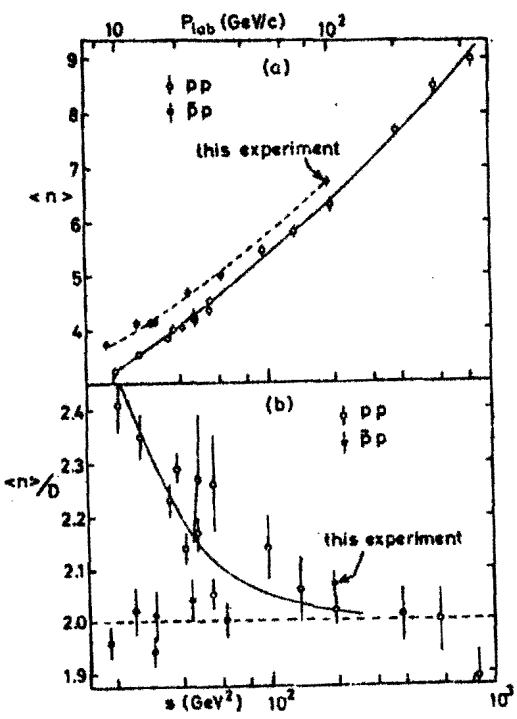

Fig. 2. Momentum and s dependence of (a) the average charged multiplicity $\langle n \rangle$, and (b) the quantity $\langle n \rangle / D$, where D is the dispersion of the multiplicity distribution, for $\bar{p}p$ and pp interactions. The curves are to guide the eye.

In fig. 1 we show the variation of the $\bar{p}p$ topological cross sections with the square of the cms total energy s and the beam momentum. The general features of this plot are similar to those observed, for example, in $\pi\bar{p}$ collisions. In particular, we observe that the 0-prong cross section is falling rapidly and may be parameterized as $\sigma_0(\text{mb}) = 58\, P_{lab}^{-(1.46 \pm 0.13)}$ between $P_{lab} = 15$ and 100 GeV/c. The 2, 4 and 6-prong cross sections are falling at 100 GeV/c while the cross sections for producing 8 or more charged particles are still increasing at 100 GeV/c.

From inelastic cross sections given in table 1, we compute various moments of the $\bar{p}p$ multiplicity distribution (see table 2). We find an average charged particle multiplicity of $\langle n \rangle = 6.74 \pm 0.005$. In fig. 2(a) we show $\langle n \rangle$ as a function of the incident beam momentum for $\bar{p}p$ interactions, compared with the corresponding data obtained from pp interactions. It is seen that at any momentum the $\bar{p}p$ charged multiplicity is greater than the pp value and there is no real indication that they are converging at higher momenta.

In fig. 2(b) we show the ratio of the average multiplicity to the dispersion, $D = [\langle n^2 \rangle - \langle n \rangle^2]^{1/2}$ for the $\bar{p}p$ and pp charged multiplicity distributions. As is

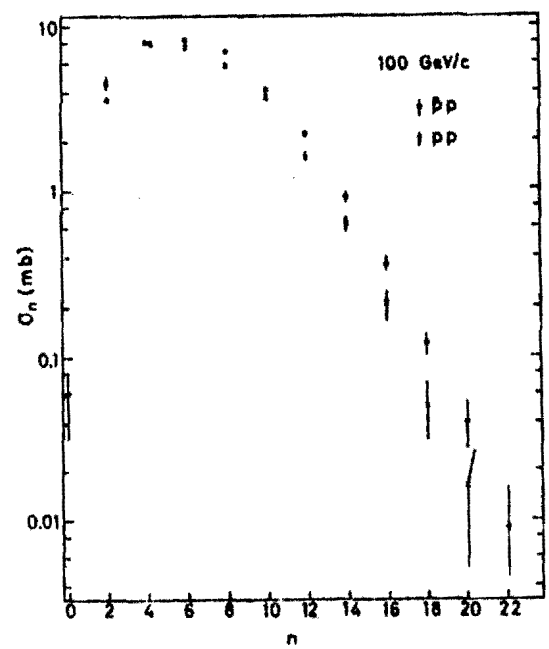

Fig. 3. Comparison of $\bar{p}p$ and pp topological cross sections at 100 GeV/c. The pp data are from ref. [7].

well-known, the high energy pp data seem to approach a constant value of $\langle n \rangle / D \approx 2$. Above ~ 15 GeV/$c$ the $\bar{p}p$ data points are reasonably consistent with this value, though our 100 GeV/c measurement of 2.07 ± 0.03 could be suggestive of an increase with momentum that has important implications for models [6].

We now make a more detailed comparison between the 100 GeV/c $\bar{p}p$ and pp data. First we note that the pp data [7] have an average multiplicity $\langle n \rangle =$ 6.32 ± 0.07, considerably lower than the $\bar{p}p$ value. To investigate this difference in more detail, we show in fig. 3 the inelastic topological cross sections for $\bar{p}p$ and pp at 100 GeV/c. The strongest feature is that the probability of producing a high multiplicity event ($n \gtrsim 8$) is greater in $\bar{p}p$ than in pp collisions. It would appear natural to expect that the dominant cause of this difference lies in the effects of the annihilation channels available in $\bar{p}p$ interactions. This will be examined further in a subsequent paper.

We thank the staff of the FNAL Neutrino Laboratory, M. Johnson and S. Pruss in particular, for helping to obtain the enriched beam used in this experiment.

References

[1] W.W. Neale, Enriched Particle Beams for the Bubble Chambers at FNAL FN-259 (1974).
[2] J. Erwin et al., Phys. Rev. Letters 32 (1974) 254.
V.E. Barnes et al., Phys. Rev. Letters 34 (1975) 415.
[3] J. Whitmore et al., A study of the elastic and inelastic two prong interaction in 100 GeV/c $\bar{p}p$ and $\pi^- p$ collisions, paper in preparation.
[4] A.S. Carroll et al., Phys. Rev. Letters 33 (1974) 928, 932.
[5] E.L. Berger et al., Nucl. Phys. B77 (1974) 365.
[6] J. Whitmore, Physics Reports 10C (1974) 273.
[7] C. Bromberg et al., Phys. Rev. Letters 31 (1973) 1563.

APPENDIX A2

Volume 59B, number 3 PHYSICS LETTERS 10 November 1975

ON THE DIFFERENCE BETWEEN $\bar{p}p$ AND pp TOPOLOGICAL CROSS SECTIONS UP TO 100 GeV/c

J.G. RUSHBROOKE, R.E. ANSORGE, C.P. BUST, J.R. CARTER and W.W. NEALE
Cavendish Laboratory[1], *Cambridge, UK*

C. MOORE, R. RAJA, L. VOYVODIC and R.J. WALKER
Fermi National Accelerator Laboratory[2], *Batavia, Ill. 60510, USA*

and

W. MORRIS[3], B.Y. OH, D.L. PARKER[4], G.A. SMITH and J. WHITMORE
Michigan State University[5], *E. Lansing, Michigan 48824, USA*

Received 15 September 1975

New 100 GeV/c $\bar{p}p$ data are used to find moments of the difference between the $\bar{p}p$ and pp topological cross sections. The mean multiplicity for annihilations at 100 GeV/c is estimated to be 9.06 ± 0.56, and the value of the quantity $\langle n \rangle / D$ to be 2.75 ± 0.33. It is shown that $R_n = \{\sigma_n(\bar{p}p) - \sigma_n(pp)\}/\sigma_n(pp)$ appears at 100 GeV/c to have acquired an asymptotic form, $R_n = s^{-\alpha}\beta^n$, with α and β constant.

Information on very high energy $\bar{p}p$ interactions has recently become available [1] in the form of topological cross-sections and the moments of the charged multiplicity distribution at 100 GeV/c. Great interest centres on the behaviour with energy of the difference between $\bar{p}p$ and pp interactions, as this may afford insight into the high energy behaviour of the annihilation process, which is known from present data in the 2–10 GeV/c range to possess general properties very different from those of the non-annihilation processes [2]. In this letter we examine the properties of the inelastic topological cross-section differences $\sigma_n(\bar{p}p) - \sigma_n(pp)$, where n is the prong number, in the momentum range 9 to 100 GeV/c, compare them with the properties of $\bar{p}p$ annihilation data below 7 GeV/c, and show that the experimental values of the quantity $R_n = \{\sigma_n(\bar{p}p) - \sigma_n(pp)\}/\sigma_n(pp)$, for $n \geqslant 4$, appear to have acquired by 100 GeV/c an aymptotic form $R_n = s^{-\alpha}\beta^n$, with α and β constant.

We firstly estimate various moments of the charged multiplicity distribution for annihilations at 100 GeV/c. For this we have used the cross-section differences $\sigma_n(\bar{p}p) - \sigma_n(pp)$ calculated from our $\bar{p}p$ data [1] and from the 102 GeV/c pp data of Bromberg et al. [3] ‡1, except for the case $n = 2$, where the procedure of removing elastic events would unavoidably lead to a large error in this cross-section difference, even though its value is certainly small. In the case of 2-prongs we have therefore used an extrapolation of the 2-prong annihilation cross section itself, for which measurements [4] have been made up to 7 GeV/c, and which can be represented to sufficient accuracy by the empirical formula $\sigma_{2,\mathrm{ann}}$ (mb) $\approx 1540\, s^{-2.46}$. In calculating annihilation moments we have also disregarded the contribution of 0-prongs, since an apparently large 0-prong cross-section from ($\bar{p}p$ – pp) is almost certainly composed of non-annihilation states [5].

[1] Work supported by the Science Research Council, UK.
[2] Operated by the Universities Research Association, Inc. under Contract with the Energy Research and Development Administration, USA.
[3] Presently at General Atomic Company, San Diego, CA 92138.
[4] Presently at Department of Physics, Iowa State University, Ames, Iowa 50010.
[5] Work supported in part by the National Science Foundation, USA.

‡1 It was found necessary to smooth some of these 102 GeV/c cross-sections by reference to other pp data (see ref. [7]) at neighbouring momenta; the adjustments were in no case greater than 0.2 mb.

$$f_2^{--} = b\langle n_- \rangle + c, \tag{1}$$

then b is predicted to have values in the range −0.6 to −0.7 depending on the assumptions made about the way the fireball decays. Values of b in this range are in good agreement with $\bar{p}p$ annihilation data up to 7 GeV/c as may be seen in fig. 1(b). The large positive values of f_2^{--} for pp interactions are then seen [10] as a consequence of multiple cluster formation; each cluster has its own negative value of f_2^{--} (as with the annihilation fireball) but the effect of averaging over several clusters is to give a positive f_2^{--}. As one goes to sufficiently high energy and more than one cluster is produced, one might then expect to see f_2^{--} for $\bar{p}p$ annihilations turning up to positive values: Miettinen has predicted [2] that this could happen at a beam momentum of 10–20 GeV/c. The 100 GeV/c data point for ($\bar{p}p$ – pp) in fig. 1(b) is suggestive of the onset of this type of behaviour, though it does imply that f_2^{--} would probably not become positive until $\gtrsim$ 300 GeV/c.

The existence of KNO scaling for $\bar{p}p$ annihilations below 7 GeV/c has already been demonstrated [9], in the sense that a single function $\psi(z) = \langle n \rangle \sigma_n/\sigma_{ann}$, where $z = n/\langle n \rangle$ and σ_{ann} is the total annihilation cross-section, can fit all the data in this energy interval. This fit is shown as the dashed curve in fig. 2, and is seen to be quite different from Slattery's fit [11] to pp data in the momentum interval 50–300 GeV/c, which is the solid curve. The ($\bar{p}p$ – pp) data points up to 100 GeV/c are shown in fig. 2 to be in fair agreement with the dashed curve, though there is some suggestion of the distribution becoming narrower at higher energies.

To gain further insight into $\bar{p}p$ annihilations at high energy we show in fig. 3(a) experimental values of the quantity

$$R_n = \frac{\sigma_n(\bar{p}p) - \sigma_n(pp)}{\sigma_n(pp)} \tag{2}$$

plotted against n for $n \geq 4$ for data in the momentum interval 6–100 GeV/c. We find phenomenologically that at each value of s, R_n can be fitted to an expression of the form

$$R_n = A\beta^n. \tag{3}$$

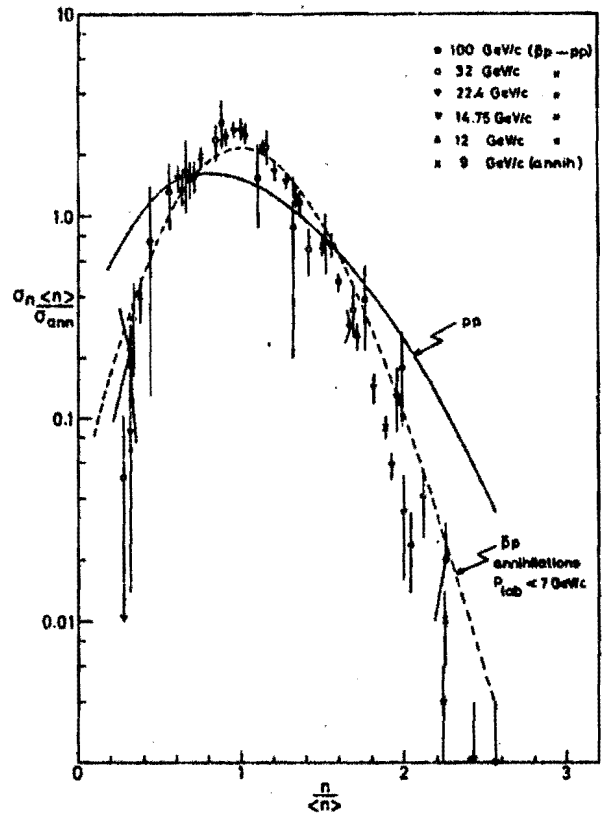

Fig. 2. Plots of $\sigma_n\langle n \rangle/\sigma_{ann}$ versus $n/\langle n \rangle$ for $\bar{p}p$ annihilation data below 7 GeV/c (dashed curve [9]), and for ($\bar{p}p$ – pp) data at beam momenta up to 100 GeV/c as indicated. The solid curve is Slattery's fit [11] to pp data in the momentum interval 50–100 GeV/c.

The values of $\alpha \equiv \ln A/\ln s$ and β are shown plotted against $\ln s$ in fig. 3(b), and we see signs of these parameters reaching fairly constant values at 100 GeV/c, which implies the existence of an asymptotic form

$$R_n \to s^{-\alpha}\beta^n \tag{4}$$

with $\alpha = 0.73 \pm 0.04$ and $\beta = 1.24 \pm 0.02$.

It is interesting to compare this finding with the work of Eylon and Harari [12], who with a duality diagram model and unitarity considerations, have predicted that R_n should take the form

$$R_n = \beta^n s^{2\alpha_B - 2\alpha_M} - (1 - \eta_1)\gamma^n, \tag{5}$$

where $\alpha_M(\alpha_B)$ is the intercept of the leading exchanged meson (baryon) trajectory, $\eta_1(\leq 1)$ is some constant, and $\beta(> 1)$ and $\gamma(< 1)$ are constants which, in a simple

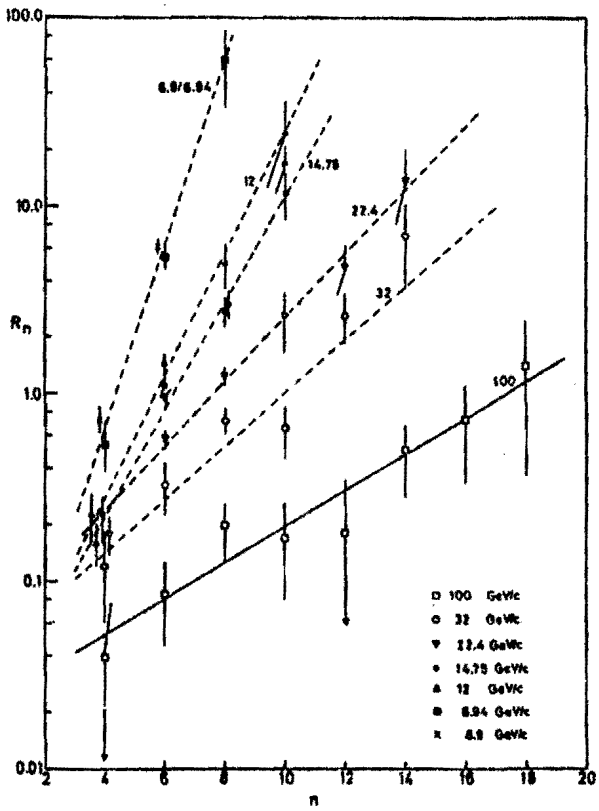

Fig. 3(a). Experimental values of the quantity $R_n = \{\sigma_n(\bar{p}p) - \sigma_n(pp)\}/\sigma_n(pp)$ plotted against $n(\geq 4)$ for data in the momentum interval 6–100 GeV/c as indicated. The straight lines are the results of fitting an expression $R_n = A\beta^n$, with A and β free parameters, at each momentum.

form of the model, are 3/2 and 1/2 respectively. Our fit is consistent with a contribution from the first term of eq. (5) only (implying $\eta_1 \approx 1$ or $\gamma \approx 0$) which in the Eylon–Harari model comes from annihilations. Our fit also gives $\alpha_M - \alpha_B = 0.36 \pm 0.02$, which seems plausible, and $\beta = 1.24 \pm 0.02$, in disagreement with the prediction $\beta = 1.5$[43].

In summary, this analysis of ($\bar{p}p - pp$) and $\bar{p}p$ annihilation data at momenta up to 100 GeV/c indicates that

(a) The mean charged multiplicity in $\bar{p}p$ annihilations maintains a constant excess over that in pp interactions up to 100 GeV/c.

(b) The ratio $\langle n \rangle/D$ for $\bar{p}p$ annihilations is roughly constant from threshold to 100 GeV/c and greater than the constant value of ≈ 2 achieved by pp interactions above ~ 50 GeV/c.

(c) KNO scaling is fairly well followed in $\bar{p}p$ annihilations from 9 to 100 GeV/c.

(d) The quantity R_n defined above appears to be acquiring an asymptotic form $s^{-\alpha}\beta^n$ at 100 GeV/c, with α and β constant.

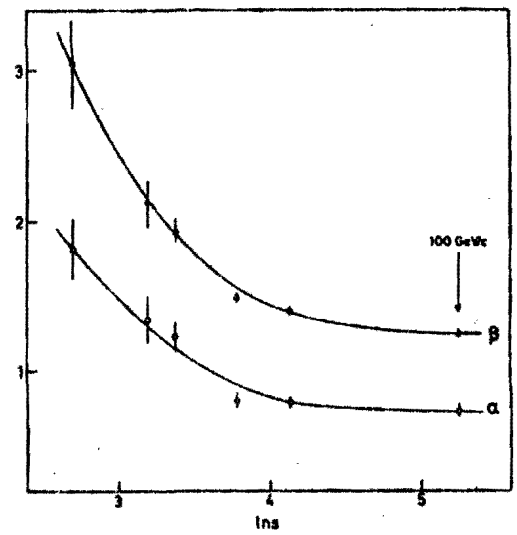

Fig. 3(b). Values of $\alpha = -\ln A/\ln s$ and β plotted against $\ln s$. The curves are to guide the eye.

We are grateful to B.R. Webber for helpful discussions.

[43] On the other hand it is perhaps interesting to observe that if the duality diagrams in the Eylon–Harari model are interpreted leading to the production of *clusters*, rather than charge pseudoscalar mesons, then since the mean number of charged particles in clusters produced in hadronic interactions is about two [13], we should re-interpret the first term in eq. (5) to contain the factor $\beta^{1/2}$, i.e. $(\sqrt{\beta})^n$. This would mean that $\sqrt{1.5} = 1.225$ is the correct prediction, consistent with our findings.

References

[1] R.E. Ansorge et al., Phys Lett. 59B (1975) 299.
[2] H.I. Miettinen, Phenomenology of $\bar{B}B$ interactions, in Symposium on Antinucleon-nucleon Interactions, CERN report 74–18 (1974) p. 405.
[3] C. Bromberg et al., Phys. Rev. Letters 31 (1973) 1563.

[4] $\bar{p}p$ annihilation data; see Symposium on Antinucleon-nucleon Interactions, CERN report 74-88 (1974), p. 157 and p. 488.
[5] H. Muirhead, Inclusive annihilation reactions in symposium on antinucleon-nucleon interactions, CERN report 74-18 (1974) p. 488.
[6] F.T. Dao, J. Lach and J. Whitmore, Phys. Letters 45B (1973) 513.
[7] pp data: E. Bracci et al., Compilation of cross-sections III-p and $\bar{p}$ induced reactions, CERN report CERN/HERA 73-1;
A. Firestone et al., Phys. Rev. D10 (1974) 2080;
S. Barish et al., Phys. Rev. D9 (1974) 2689.
[8] $\bar{p}p$ data: E. Bracci et al., op. cit.;
see compilation in ref [5] of F.T. Dao et al., op. cit.;
G.A. Akopdjanov et al., Nucl. Phys. B75 (1974) 401;
Symposium on Antinucleon-nucleon Interactions, CERN report 74-18, p. 275 and p. 281.
[9] J. Salava and V. Simak, Phys. B69 (1974) 15.
[10] T. Fields et al., Clusters in $\bar{p}p$ annihilation and in pp pionization, in Symposium on Antinucleon-nucleon Interactions, CERN report 74-18 (1974) p. 151.
[11] P. Slattery, Phys. Rev. D1 (1973) 2073.
[12] Y. Eylon and H. Harari, Nucl. Phys. B80 (1974) 349.
[13] C. Quigg and G.H. Thomas, Phys. Rev. Letters 34 (1975) 290.
[14] A.H. Mueller, Phys. Rev. D4 (1971) 150.

APPENDIX A3

Volume 62B, number 2 PHYSICS LETTERS 24 May 1976

COMPARISON OF NEUTRAL PARTICLE PRODUCTION IN 100 GeV/c $\bar{p}p$ AND pp INTERACTIONS

D.R. WARD, R.E. ANSORGE, C.P. BUST, J.R. CARTER, W.W. NEALE and J.G. RUSHBROOKE
Cavendish Laboratory[1], *Cambridge, England*

C. MOORE, R. RAJA, L. VOYVODIC and R.J. WALKER
Fermi National Accelerator Laboratory[2], *Batavia, Ill. 60510, USA*

W. MORRIS[3], B.Y. OH, D.L. PARKER[4], G.A. SMITH and J. WHITMORE
Michigan State University[5], *E. Lansing, Michigan 48824, USA*

Received 12 April 1976

We derive cross-sections for the inclusive production in $\bar{p}p$ interactions at 100 GeV/c of π^0, K^0_s and $\Lambda^0/\bar{\Lambda}^0$ of 91.5±5.7 mb, 5.2±0.4 mb and 4.8±0.4 mb respectively, which are all higher than pp cross-sections at this energy. We find indications that these differences can be attributed to "annihilation" processes.

Introduction. We present results on the production of γ, K^0_s, Λ^0 and $\bar{\Lambda}^0$ in $\bar{p}p$ interactions at 100 GeV/c. We also look for differences between pp and $\bar{p}p$ interactions, which could be ascribed to the effects of "annihilation" processes. Both the present experiment and pp experiments at this energy suffer from limited statistics, but we find that cross-sections for the production of neutral particles are in all cases somewhat higher in $\bar{p}p$ interactions than in pp interactions. In the case of $\Lambda^0/\bar{\Lambda}^0$ production (and possibly γ's) the difference appears to arise mainly in the neighbourhood of $y^* = 0$, characteristic of a central production process.

The data to be described are the first on $\bar{p}p \to$ neutrals above 14.75 GeV/c, and come from a 100 000 picture exposure of the 30" hydrogen bubble chamber at Fermilab to a tagged beam of negative particles. Information on the $\bar{p}p$ charged multiplicity distribution at 100 GeV/c [1] and on the difference between $\bar{p}p$ and pp topological cross-sections [2] has already been published. The efficiency for scanning for V^0's was about 90% for singly scanned film, and after measurement and remeasurement 93% of events had been satisfactorily measured. After all cuts we have 1015 V^0's associated to events inside our fiducial volume giving fits to Λ^0, K^0_s and $\bar{\Lambda}^0$ decays, or $\gamma \to e^+e^-$ conversion. Ambiguities (affecting about 9% of the events) were resolved by observing ionizations where possible, and otherwise by cuts on the transverse momentum of the decays and on the χ^2 probabilities of the fits.

The data were corrected for scanning and measuring losses, for losses of V^0's decaying or converting outside the fiducial volume, or closer than 3 cm (2 cm in the case of K^0_s) to the production vertex, and for interactions of the strange particles. The pair production cross-section was taken from ref. [3], and the strange particle cross-sections were corrected for branching ratios taken from ref. [4]. A correction (~2–3%) was made for the loss of γ's below 40 MeV/c using the symmetry of the reaction $\bar{p}p \to \gamma$ in the c.m. system.

Cross-sections and multiplicities. In table 1 we give cross-sections for $\Lambda^0/\bar{\Lambda}^0$, K^0_s and π^0 production, the latter taken to be $\frac{1}{2}\sigma(\bar{p}p \to \gamma)$. We have used events in both forward and backward hemispheres in the c.m. system for the γ's, since, apart from the loss of very slow γ's, no forward/backward asymmetry was found

[1] Work supported by the Science Research Council, UK.
[2] Operated by the Universities Research Association, Inc., under Contract with the Energy Research and Development Administration, USA.
[3] Presently at General Atomic Company, San Diego, CA 92138, USA.
[4] Presently at Department of Physics, Iowa State University, Ames, Iowa, 50010, USA.
[5] Work supported in part by the National Science Foundation, USA.

Table 1
Comparison of neutral particle cross-sections in $\bar{p}p$ and pp interactions at 100 GeV/c.

Charged Multiplicity n_{ch}	$\sigma(\bar{p}p\to\pi^0)$ mb	Smoothed $\sigma(pp\to\pi^0)$ mb	$\sigma(\bar{p}p\to K^0_s)$ mb	Smoothed $\sigma(pp\to K^0_s)$ mb	$\sigma(\bar{p}p\to\Lambda^0/\bar{\Lambda}^0)$ mb	$\sigma(pp\to\Lambda^0/\bar{\Lambda}^0)$ [c] mb
0	0.65±0.32	–	–	–	0.02±0.02	–
2	4.8 ±0.8	7.2±1.5	0.26±0.11	0.31±0.07	0.48±0.12	0.36±0.14
4	15.4 ±1.6	14.5±1.0	0.97±0.15	0.77±0.15	1.14±0.18	1.32±0.24
6	22.8 ±2.8	22.8±4.0	1.27±0.17	1.1 ±0.15	1.24±0.20	0.80±0.18
8	23.0 ±2.0	20.3±2.2	1.39±0.18	0.8 ±0.1	1.00±0.20	0.64±0.18
10	11.6 ±1.5	10.9±1.0	0.71±0.14	0.65±0.1	0.62±0.14	0.46±0.16
12	6.9 ±1.0	6.3±1.0	0.46±0.11	0.3 ±0.07	0.14±0.06	0.04±0.04
14	5.4 ±1.2	2.5±1.5	0.10±0.05	0.07±0.07	0.16±0.08	–
16	0.2 ±0.2	1.0±0.4	0.03±0.03	0.04±0.04	–	–
18	0.6 ±0.4	0.5±0.5	–	0.02±0.02	–	–
Total [a]	91.5 ±5.7	86 ±6	5.2 ±0.4	4.1 ±0.3	4.8 ±0.4	3.6 ±0.4
$\langle n_{ch}\rangle$	7.45±0.15	7.17±0.19	7.25±0.22	7.05±0.24	6.48±0.24	5.79±0.29
$\langle n(V^0)\rangle$	2.64±0.16	2.70±0.19	0.15±0.01	0.13±0.01	0.14±0.01	0.11±0.01
Raw no. of $\bar{p}p$ events	628		230 (backward only)		157 (backward only)	
Average weight [b]	52.5		1.50		1.80	

[a] The errors on the $\bar{p}p$ cross-sections here include a 5% systematic uncertainty in normalization.
[b] Excluding scanning and measuring losses, and branching ratios. [c] Unsmoothed values from ref. [5], scaled up to allow for $\bar{\Lambda}^0$'s.

within errors. For the K^0_s data, however, we have only used events in the backward hemisphere because of the low detection efficiency for fast V's, but by C-invariance the cross-section in the two hemispheres must be equal. The $\Lambda^0/\bar{\Lambda}^0$ cross-section likewise uses only events in the backward hemisphere, but again C-invariance implies that Λ^0 and $\bar{\Lambda}^0$ distributions are related by a simple reflection about $y^* = 0$ in the c.m. Hence we lose no information on $\Lambda^0/\bar{\Lambda}^0$ by using only the backward hemisphere, and $\frac{1}{2}\sigma(\bar{p}p\to\Lambda^0/\bar{\Lambda}^0) = \sigma(\bar{p}p\to\Lambda^0) = \sigma(\bar{p}p\to\bar{\Lambda}^0)$. Table 1 gives cross-sections for different charged multiplicities at the primary vertex (corrected for undetected dalitz pairs and V^0's). We also quote mean associated charged multiplicities for V^0 production and mean numbers of $\Lambda^0/\bar{\Lambda}^0$, K^0_s and π^0 produced per inelastic collision. For comparison, the corresponding quantities are given for pp interactions. There are pp experiments at 102 GeV/c [5] and 100 GeV/c [6], and rather than simply averaging their values, we quote "smoothed" values for π^0 and K^0_s cross-sections, taking account of pp data at other energies [7]. There are no data on the topological cross-sections for $pp\to\bar{\Lambda}^0$, but this is a small contribution, so we have taken the same topological dependence as for $pp\to\Lambda^0$. Fig. 1 (a–c) shows the cross-sections with data at lower energies [8], and we also show the energy dependence of the pp channels, for comparison.

The cross-section for $\bar{p}p\to\pi^0$ is higher by ~5.5 mb than in pp interactions, though this is less than one standard deviation. Fig. 1(d) shows that $\langle n(\pi^0)\rangle$ as a function of n_{ch} is virtually identical to pp interactions, implying that the degree of correlation between charged and neutral pions is the same in both cases, and has not been significantly affected by any annihilation component, in contrast to the behaviour found at 14.75 GeV/c [8]. This is also indicated by the correlation parameters $f_2^{-0} = \langle n_0 n_-\rangle - \langle n_0\rangle\langle n_-\rangle$, which has the value at 100 GeV/c of 0.94±0.24 for $\bar{p}p$, compared to 1.10±0.26 for pp interactions.

Fig. 1(e) shows the variation of $\langle n(K^0_s)\rangle$ with n_{ch} for $\bar{p}p$ and pp interactions, and likewise fig. 1(f) for $\Lambda^0/\bar{\Lambda}^0$. Again there is no clear difference between $\bar{p}p$ and pp, indicating that correlations between charged particles and neutrals are similar in the two cases. We

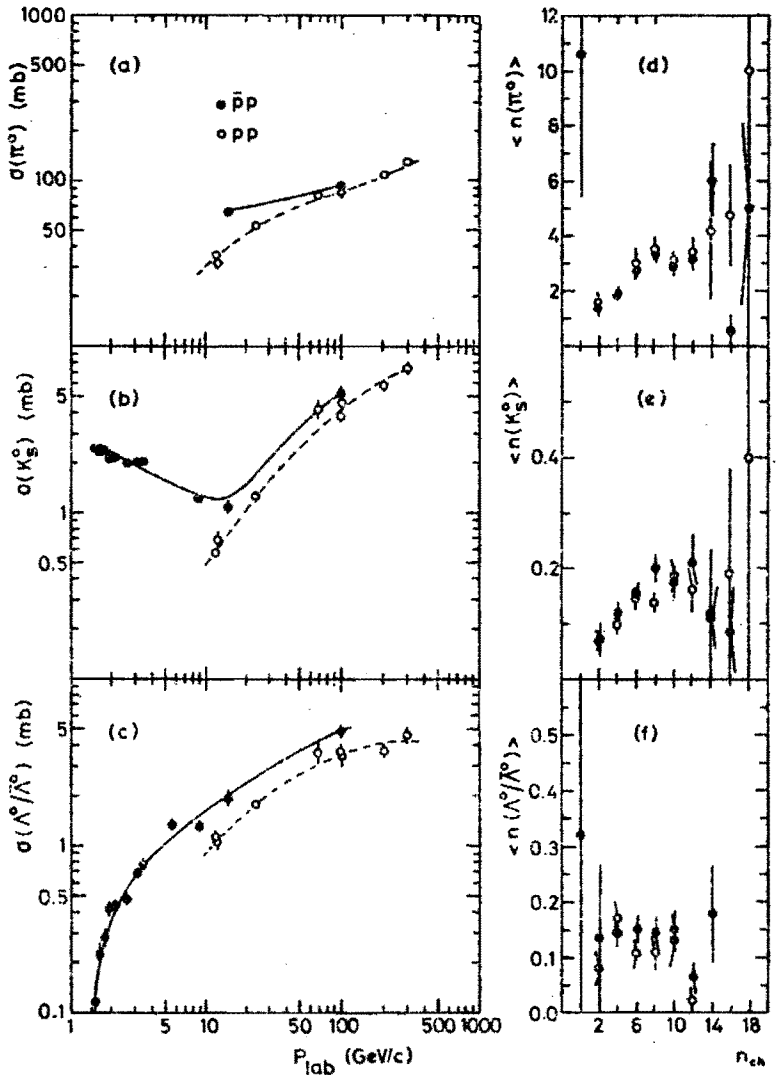

Fig. 1. (a) Cross-section for $\bar{p}p \to \pi^0$ as a function of laboratory momentum, with pp data for comparison. (b) Likewise for K^0_S. (c) Likewise for $\Lambda^0/\bar{\Lambda}^0$. (d) $\langle n(\pi^0)\rangle$ as a function of charged multiplicity, for 100 GeV/c $\bar{p}p$ and pp interactions. (e) likewise for K^0_S. (f) Likewise for $\Lambda^0/\bar{\Lambda}^0$. The curves merely guide the eye.

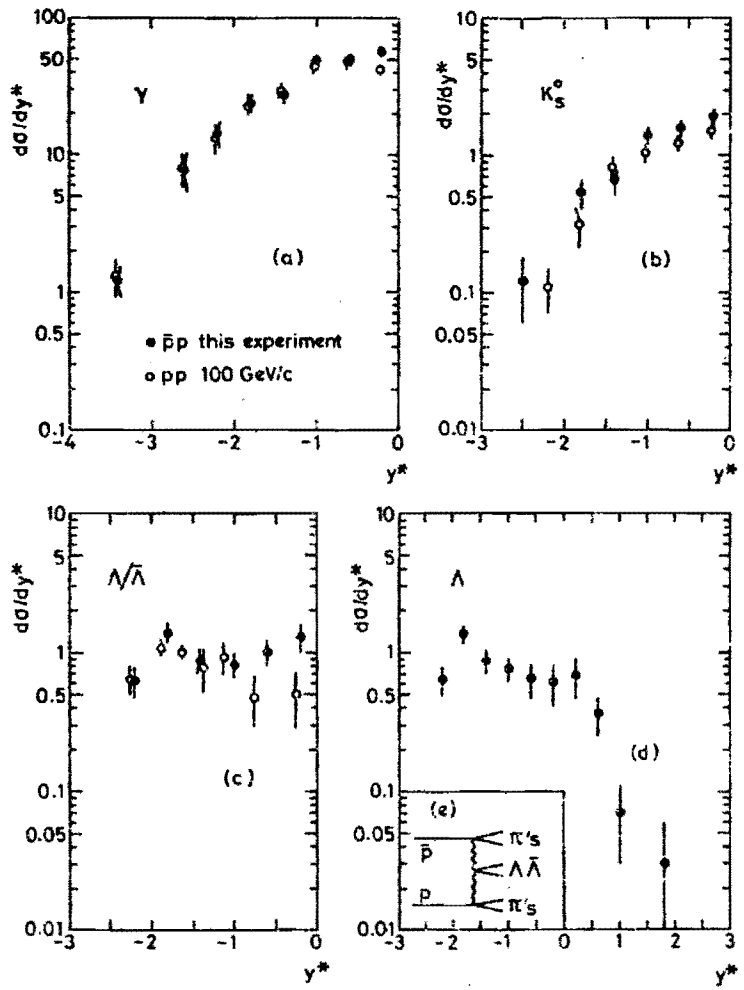

Fig. 2. (a) $d\sigma/dy^*$ vs y^* for $\bar{p}p \to \gamma$ at 100 GeV/c, with pp data (averaged using data of refs. [5,6]) for comparison. Data from both hemispheres are averaged. (b) $d\sigma/dy^*$ for $\bar{p}p \to K^0_S$, compared with pp data at 100 GeV/c. Only backward hemisphere data is used. (c) $d\sigma/dy^*$ for $\bar{p}p \to \Lambda^0/\bar{\Lambda}^0$ at 100 GeV/c compared with pp data [5]. (d) $d\sigma/dy^*$ for $\bar{p}p \to \Lambda^0$ at 100 GeV/c; backward hemisphere Λ^0, and $\bar{\Lambda}^0$ reflected into the forward hemisphere to represent the full Λ^0 distribution. (e) Diagram which could contribute an excess of $\Lambda^0/\bar{\Lambda}^0$ in the central region in $\bar{p}p$ interactions.

can make an estimate of the "annihilation" component in $\bar{p}p \to K_s^0$ and $\bar{p}p \to \Lambda^0/\bar{\Lambda}^0$ from the differences ($\bar{p}p - pp$), subtracting the cross-sections given in table 1. The mean charged multiplicities calculated from these differences are 8.0±1.3 and 8.4±1.6 respectively which are probably both somewhat higher than for the overall samples of K_s^0 and $\Lambda^0/\bar{\Lambda}^0$ events. Such an effect was also seen in the ($\bar{p}p - pp$) multiplicity distribution of all events [2], where a mean charged multiplicity 9.06± 0.56 was found; hence we are encouraged to associate the difference in cross-sections with "annihilations", an interpretation which receives some support from the single particle distributions presented in the next section. The mean charged multiplicity for ($\bar{p}p - pp$) $\to \pi^0$ is also high, ~10, though with large errors.

Single particle distributions. We now try to localise these cross-section differences in terms of single particle distributions. We find the most useful of these to be the centre-of-mass rapidity, y^*. Fig. 2(a–c) shows $d\sigma/dy^*$ for our γ, K_s^0 and $\Lambda^0/\bar{\Lambda}^0$ data, folded about $y^* = 0$ and halved in the former case, compared with pp data from refs. [5,6]. Fig. 2(d) shows the $\bar{p}p \to \Lambda^0$ and $\bar{p}p \to \bar{\Lambda}^0$ data separately (the latter reflected into the forward hemisphere).

The $d\sigma/dy^*$ distribution for the γ's, fig. 2(a), has the best statistics, and indicates that any difference between $\bar{p}p$ and pp cross-sections is mostly coming from the region $|y^*| \leq 1.0$. For $|y^*| > 1$ the agreement is really rather close. For the K_s^0, fig. 2(b), the difference in cross-sections appears to be spread fairly uniformly over the range of y^*, though our statistics do not permit us to say whether the K's are really behaving differently from the γ's. Fig. 2(c) shows the rapidity distribution for combined $\Lambda^0/\bar{\Lambda}^0$ production (the small $pp \to \bar{\Lambda}^0$ contribution was estimated by scaling the distribution at 200 GeV/c [9] to the 100 GeV/c cross-section). Here there is good agreement between $\bar{p}p$ and pp in the proton fragmentation region, $y^* < -1$, but a substantial excess in $\bar{p}p$ in the central region, $y^* > -1$. This observation invites interpretation in terms of processes like $\bar{p}p \to (\Lambda\bar{\Lambda}) + \pi$'s, which cannot occur in pp interactions, and insofar as there are no leading baryons, may be akin to annihilation processes, (see fig. 2(e)), and yield central hyperons and antihyperons [‡1].

The statistical significance of these effects is shown by making a direct subtraction of the data of refs. [5,6] from our $\bar{p}p$ cross-sections. In the regions $|y^*| > 1$ and $|y^*| < 1$ we obtain for $\sigma(\bar{p}p - pp \to \gamma)$: −1.1±7.5 mb and 12.1±11.2 mb respectively, for $\sigma(\bar{p}p - pp \to K_s^0)$: 0.50±0.28 mb and 0.60±0.37 mb, and for $\sigma(\bar{p}p - pp \to \Lambda^0/\bar{\Lambda}^0)$: 0.16±0.36 mb and 1.16±0.42 mb. It is clear that both $\bar{p}p$ and pp experiments with much better statistics are required in order to observe these effects in any greater detail.

The transverse momentum distributions of $\Lambda^0/\bar{\Lambda}^0$, K_s^0 and γ have been examined, and show no convincing differences from pp data in their shape, essentially just differing in normalization. The mean transverse momenta of γ, K_s^0 and $\Lambda^0/\bar{\Lambda}^0$ are 0.16±0.01, 0.46±0.03 and 0.52±0.04 GeV/c respectively, compared to mean values in pp interactions at 102 GeV/c [5]: 0.175± 0.020, 0.42±0.04 and 0.54±0.06 GeV/c [‡2].

Summary. We have derived cross-sections for the production of γ, K_s^0 and $\Lambda^0/\bar{\Lambda}^0$ in $\bar{p}p$ interactions at 100 GeV/c. In all cases the cross-sections are higher than in pp experiments at this energy. The difference in cross-sections tends to be associated with higher charged multiplicities, which inclines us to identify the differences with annihilation processes. In γ and $\Lambda^0/\bar{\Lambda}^0$ production the differences are probably concentrated near $y^* = 0$, while for K_s^0 there may be a difference at larger $|y^*|$ as well.

‡1 In this connection it may be worth noting that we have five events containing both Λ^0 and $\bar{\Lambda}^0$, corresponding to a cross-section ~0.6 mb, compared with the inclusive $pp \to \bar{\Lambda}^0$ cross-section, ~0.2 mb. Further, in four out of these five events the $\Lambda\bar{\Lambda}$ effective mass is small; less than 3.5 GeV/c^2.

‡2 This value is $\langle p_t \rangle$ for Λ^0 alone, and could be slightly affected by the inclusion of $\bar{\Lambda}^0$'s.

[1] R.E. Ansorge et al., Phys. Lett. 59B (1975) 299.
[2] J.G. Rushbrooke et al., Phys. Lett. 59B (1975) 303.
[3] T.M. Knasel, DESY report 70/3 (1970) unpublished.
[4] Particle Data Group, Phys. Lett. 50B (1974) 1.
[5] J.W. Chapman et al., Phys. Lett. 47B (1973) 465.
[6] M. Alston-Garnjost et al., Phys. Rev. Lett. 35 (1975) 142.
[7] V. Blobel et al., Nucl. Phys. B69 (1974) 454. [12,24 GeV/c];
K. Jaeger et al., Phys. Rev. D11 (1975) 1756 [12.4 GeV/c];
H. Blumenfeld et al., Phys. Lett. 45B (1973) 525, 528 [69 GeV/c];
K. Jaeger et al., Phys. Rev. D11 (1975) 2405 [205 GeV/c];
A. Sheng et al., Phys. Rev. D11 (1975) 1733 [303 GeV/c];
[8] F.T. Dao et al., Phys. Lett. 51B (1974) 505 [14.75 GeV/c];
B.Y. Oh et al., Nucl. Phys. B51 (1973) 57 [1.51–3.45 GeV/c].
S.N. Ganguli & B. Sadoulet, Nucl. Phys. B53 (1973) 458 [5.7 GeV/c];
R. Carlsson et al., Nucl. Phys. B99 (1975) 451 [9 GeV/c].
[9] S.J. Barish et al., Phys. Rev. D12 (1975) 1260.

APPENDIX B (Copied from July 1976 Issue of NALREP)

PARTICLE IDENTIFIERS FOR HADRON PHYSICS

Vera Kistiakowsky, Massachusetts Institute of Technology

A workshop was held at Fermilab on May 7-8, 1976, to discuss what system of particle identifiers would be optimum for further studies of hadron collisions with the Fermilab hybrid bubble chamber proportional wire chamber system. The meeting was attended by about 40 physicists from various institutions.

What Can Be Learned?

The bare bubble-chamber experiments and the experiments with the two hybrid systems have already yielded many interesting results concerning hadron physics at Fermilab energies. For example, leading-particle studies have demonstrated the factorization of the Pomeron. Inclusive $\pi^{\pm}p$ studies have shown that the leading particles and clusters retain the charge of the given incoming particle to low Feynman x and studies of the distribution of charge as a function of rapidity have indicated the absence of a central neutral plateau. Studies of two-particle correlations have shown a strong dependence of this correlation on the respective charges and on the azimuthal and rapidity separations of the two particles. The new results on $\bar{p}p$ charged multiplicities and a comparison with pp data have yielded hints of some of the interesting properties of high energy $\bar{p}p$ annihilations.

T. Ludlam (Yale) discussed some of the physics questions pertaining to particles produced in the central region of rapidity. The graph on the next page gives the differential cross sections for various particles from π^-p interactions at 147 GeV/c and it can be seen that, except for elastic scattering and beam and

target fragmentation, most of the particle production is between y = -2 and y = +2. Investigations already being carried out on the charge structure of the particles in the central region of rapidity indicate the presence of short-range correlations and of local conservation of charge and raise the question of whether neutral clusters exist. An obvious extension of charge-transfer studies lies in similar investigations of strangeness. With charged-particle identification it should be possible to study strangeness transfer and it would be very interesting to determine whether the Quigg prediction of local strangeness conservation is verified. Turning to two-body resonances, charged-particle identification would permit investigation of K^*, ϕ, and Y^* production and, together with previous results on ρ^0 and Δ^{++} production, this would again permit an enlightening comparison between charge- and strangeness-dependent effects. Since a photon detector will shortly be part of the hybrid system, this will permit π^0 identification and thus studies of $\rho^\pm$ and ω production. Finally, the recent observation at the ISR that in pp interactions there is apparently a sizable cross section (~1 mb) for events where both protons come almost to rest in the center-of-mass system raises the question whether the pions associated with such events are produced in jets or distributed isotropically. In conclusion, a rich source of information would be

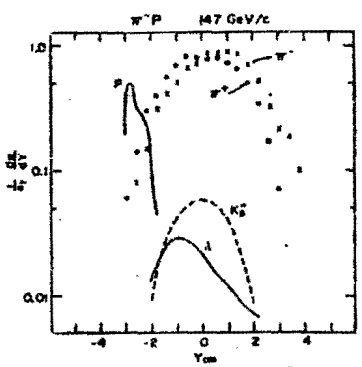

The fractional differential cross section as a function of c. m. rapidity for p, $\pi^\pm$, n, and K_s^0 produced in 147 GeV/c π^-p interactions.

opened up if clean π/K/p separation were possible over most of the central region and if programmatic studies with several incident beams and reasonably good statistics were carried out.

J. Whitmore (Michigan State) emphasized the physics question which could be studied in $\bar{p}p$ and pp interactions, but also mentioned the interest in the central-region physics from the $\pi^\pm$ interactions which could be obtained in the same exposures. One topic of considerable interest is a measurement of the relative contributions of annihilation and nonannihilation final states in $\bar{p}p$ interactions and the study of baryon annihilations at high energy. The study of the annihilation channels is of particular importance since this process has not been studied at all above approximately 12 GeV/c and has not been studied in any detail above approximately 7 GeV/c. It is estimated that for $\bar{p}p$ at 100 GeV/c (P-394) about 97% of the nonannihilation events could be identified by a suitable combination of particle identifiers, and the consequent identification of annihilation events would permit a comparison of the annihilation cross section with the difference between the $\bar{p}p$ and pp total cross sections, as well as a study of the annihilation multiplicity distributions and related topics. $\pi\pi$ correlations and single particle inclusive studies would also be possible and would contribute to a much better understanding of the annihilation channels at high energies. With respect to the central-region physics, in addition to the topics already mentioned, it would be interesting to determine the cross sections for production of $K\bar{K}$ and $N\bar{N}$ pairs in $\bar{p}p$, pp, and πp interactions and to determine the properties of such events. Studies of this variety would require π/K/p separation both for leading particles and in the central region, a neutral-hadron detector, and high-statistics experiments.

W. Walker (Duke) reviewed the results of hadron-nucleus interaction studies, which have shown that the multiplicity, momentum and rapidity distributions are very similar to those for hadron-nucleon collisions. The differences, which are relatively small, indicate that the characteristic time for particle production is considerably longer than the collision time for hadron-nucleus collisions. It is necessary to measure the production spectra for K's, π's and nucleons separately to further illuminate this result.

Fermilab Hybrid System

R. Plano (Rutgers) presented some possible configurations of the Fermilab hybrid system with downstream particle identifiers and described acceptance studies for these systems. The next phase of the hybrid system will include drift chambers and a photon detector, as well as proportional wire chambers. A downstream charged-particle identifier would be the next addition desired, and two possibilities have been considered by the Proportional Hybrid System Consortium (PHSC). The first consists of three 1 m × 1 m × 1 m sections of a relativistic rise detector (ISIS) and the second of a 3 m diam × 3 m tall Cerenkov detector (CANUTE). Both detectors can only separate π/K/p above 5 GeV/c and this corresponds kinematically to a limitation on the region of rapidity for which particle identification is possible. This limitation is less severe at higher incident-particle momenta and thus acceptance studies have been carried out at 300 GeV/c as well as 150 GeV/c, both based on data from the 147-GeV/c $\pi^- p$ (E-154) exposure. The graph at the top of the next page shows the 300 GeV/c distribution of particles with $p > 5$ GeV/c as a function of rapidity which traverse a 3 m ISIS located 2.25 m from the bubble chamber center.

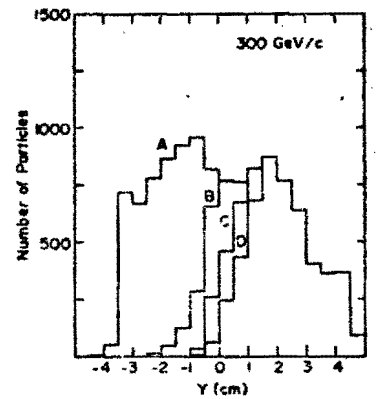

The number of particles from simulated 300 GeV/c π p interactions as a function of rapidity: A) all particles, B) particles which leave bubble chamber magnet, C) particles with $p > 5$ GeV/c which leave bubble chamber magnet and D) which pass through ISIS.

R. Yamamoto (MIT) described the photon detector and the results of recent tests of this device in the N-5 beam. This detector consists of two lead-glass photon converter detectors, each containing five counters, and four shower-energy absorber detectors. A scintillation-counter hodoscope permits an accurate location of the shower vertex. The total energy of the shower is obtained by adding the converter and absorber pulse heights, permitting very good energy resolution ($\Delta E \approx 0.15E^{\frac{1}{2}}$, where E is in GeV). Tests with electrons of various energies have verified

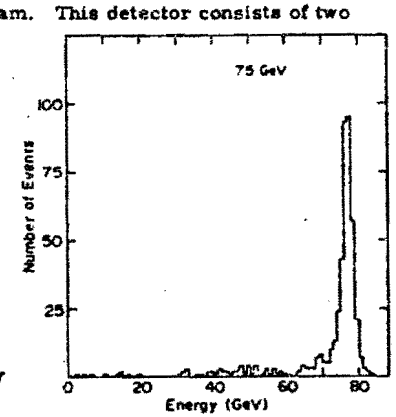

The number of events in the photon detector as a function of energy with 75-GeV electrons incident on the detector.

this prediction. The figure at the bottom of page 17 shows the pulse-height distributions of showers generated by 75-GeV/c particles tagged as electrons by a Cerenkov counter. The events observed at low energies are probably from pions which produce knock on electrons in the Cerenkov counter. This detector is currently being installed and will be used in Experiment 299 as soon as the schedule permits.

Charged-Particle Identifiers

R. Lewis (SLAC) described the Cerenkov counter operating in the SLAC hybrid facility and showed some experimental results on K/π^- separation obtained in a $\pi^+p \to K^+Y^*$ experiment at about 12 GeV/c. The figure below shows the experimental layout and the 3 m diameter by 3 m high cylindrical Cerenkov counter (CANUTE). This is a segmented device with two rows of

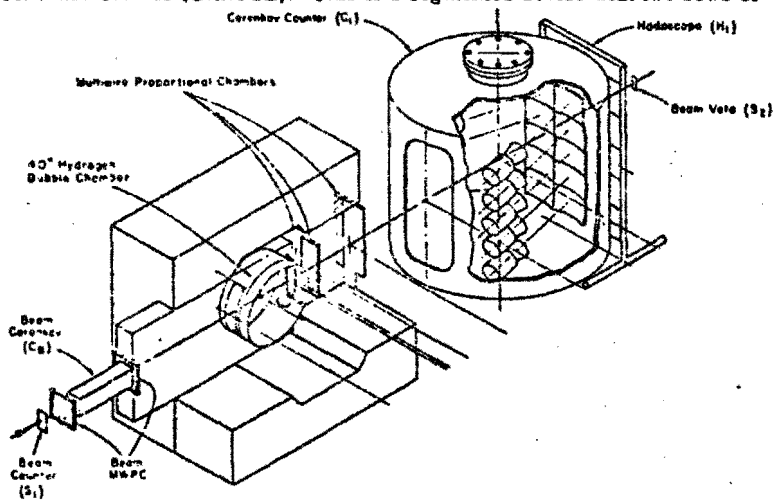

The layout of the SLAC 40-in. bubble chamber hybrid system including the Cerenkov detector (CANUTE).

five 75 cm wide by 50 cm high black lucite mirrors focusing the light on phototubes on either side of the beam line. CANUTE has been designed both mechanically and optically to operate with freon at pressures from slightly above atmospheric up to 4 atmospheres. With a filling of 45 psia of freon 100 photoelectrons are produced by particles with B of order 1 and thus K/π separation by pulse-height analysis is possible. It can be seen from the figure at the right that a good separation of K^+ from π^+ is achieved at 11.6 GeV/c.

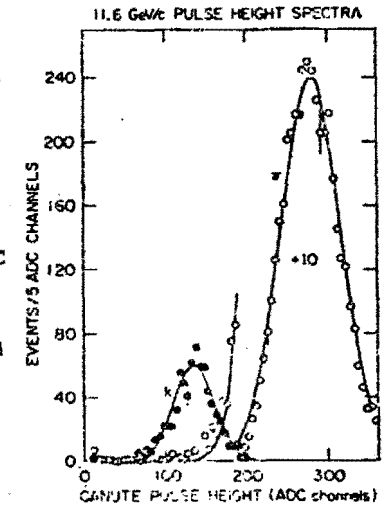

The number of events as a function of pulse height for 11.6 GeV/c π mesons and K mesons in CANUTE.

G. Smith (Michigan State) discussed the particle-identification considerations necessary to a 9 GeV/c $\bar{p}p$ experiment to be carried out at the SLAC 40-in. hybrid facility by a Cambridge-Michigan State collaboration (BC-64) and considered the same questions for the 100 GeV/c $\bar{p}p$ experiment proposed for the Fermilab hybrid spectrometer (P-394). The two essential components of the SLAC experiment are CANUTE and the UCLA neutron detector, suitably modified, used for antineutrons. This device will contain 26 layers of iron alternated with scintillator and three hodoscopes for accurate location of the $\bar{n}$ interaction. This device will have an efficiency of approximately 88% for $\bar{n}$. A possible particle-identification scheme for the Fermilab 100 GeV/c $\bar{p}p$ experiment would involve a CANUTE-type Cerenkov counter to separate $\pi/K/p$ for central-region

physics followed by a multi-cell 2 m × 2 m × 5 m atmospheric pressure Cerenkov counter (C_2) similar to that constructed at Michigan State for E-366, which when filled with approximately 95% helium and 5% nitrogen would permit a $\pi/K/\bar{p}$ separation between 53 GeV/c (K threshold) and 100 GeV/c (p threshold). Acceptance calculations yield a 97% overall detection efficiency for $\bar{p}$ by C_2. An antineutron detector similar to that planned for SLAC would follow the Cerenkov counters and would have about 90% acceptance. This, together with the conversion efficiency, would yield an overall detection efficiency of about 80% for antineutrons. These estimates, together with cross-section information, yield a 73% estimated purity of the annihilation sample. The cost for building C_1 would be approximately $110,000 (based on the construction cost of CANUTE) and for C_2 approximately $30,000 (based on the Michigan State E-366 Cerenkov cost).

V. Kistiakowsky (MIT) discussed the problems associated with using Cerenkov detectors for central-region physics and presented some estimates of the separation expected from a CANUTE-type detector at 150 GeV/c and 300 GeV/c. The graph on the following page gives the laboratory momentum p as a function of laboratory angle θ for K-mesons and protons produced with very low c.m. momenta p' by 300 GeV/c interactions. It is seen that the region where particle separation would be desired stretches from p approximately 3 to 16 GeV/c. For lower incident momenta, these curves are shifted downward in laboratory momentum. Currently attainable K thresholds are ≥ 5.3 GeV/c (4 atmospheres freon) due to safety considerations. Using the experimental results for the number of photoelectrons in CANUTE,

the efficiency for distinguishing $\pi/K/p$ has been estimated. From about 5.5 GeV/c to 11 GeV/c K's can be identified by pulse-height analysis, but there is an overlap between the pulse-height distributions for π, K and p which results in the misidentification of up to 30% of the K-mesons. Another problem which seriously affects the detection efficiency of such a detector is the overlap of Cerenkov light spots from different particles. This cannot be improved by decreasing the CANUTE mirror size, since at 4 atmospheres of freon the size of the spots is comparable to that of the mirrors. At 300 GeV/c, the acceptance of a CANUTE-type detector located 6 m from the bubble chamber would be 46% for particles with momenta 5.5 < p < 11 GeV/c. However, only 43% of the particles accepted would have sufficient separation to permit identification. The advantages of such a device are that it is guaranteed to work and that engineering costs could be minimized by copying CANUTE (estimated cost about $110,000). The disadvantages are the limited region of $\pi/K/p$ separation, the limited particle spatial resolution, and the incompatibility of such a device and the photon detector.

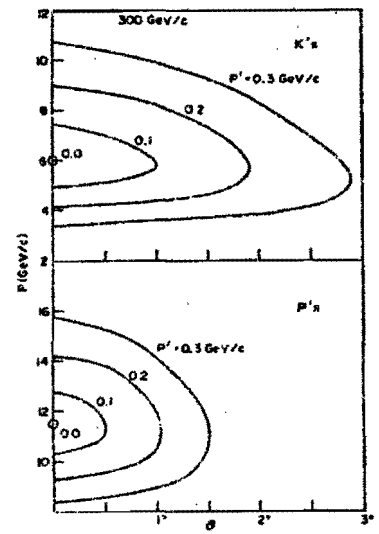

The laboratory momentum p as a function of laboratory angle θ for protons and K mesons produced at various c.m. momenta p' close to zero in 300 GeV/c interactions.

J. Whitmore (Michigan State) described the CERN External Particle Identifier (EPI) and discussed the pros and cons of constructing such a device

for the Fermilab hybrid system. This device is being built (75% completed) for use at BEBC and extensive tests which have been made with prototypes are very promising. This device measures the ionization of the particles in the region (3 to 100 GeV/c) where dE/dx for π, K, and p is different due to the rise at relativistic velocities (see figure below). Since an individual

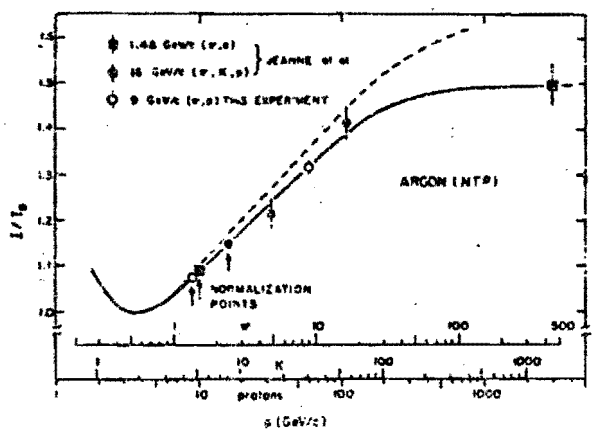

The relative ionization as a function of momentum for π mesons, K mesons, and protons. The dashed line is that calculated by Sternheimer, the solid line is hand drawn through the points which are the results of ex experiments carried out by the group developing the BEBC EPI.

ionization measurement can yield a wide range of values for dE/dx with a probability given by the Landau distribution, the ionization of a given particle must be sampled a large number of times and an average of these measurements (or an equivalent quantity) used to typify the particle. With a large enough number of samples, good resolution can be achieved for the distribution of the average values for a given particle type at a given momentum. The CERN EPI will consist of 128 layers of 32 individual proportional

counters, each of which is 6 cm × 6 cm × 90 cm (see figure below). The active volume of each proportional counter is defined by eight high-voltage wires and the device is filled with 95% A-5% CH_4. Based on experimental studies, 5.5% FWHM resolution is anticipated for 128 6 cm ionization samples suitably analyzed. The acceptance of an EPI located 2.5 m from the bubble chamber center has been estimated using data from a 100 GeV/c $\bar{p}p$ experiment (E-311), and 59.1% of all particles and 97.3% of all forward-hemisphere particles would enter the device. A consideration of the track-overlap problem indicates that in 4-prong events, typically, the information from approximately 31% of the cells must be discarded because of particles passing through the same cell, with a corresponding reduction in resolution to 6.6% FWHM (for 128 layers). In 12-prong events, the loss is approximately 4% with essentially no decrease in resolution. A recent estimate made at CERN for the cost of a 64-layer EPI was $188,000 plus salaries.

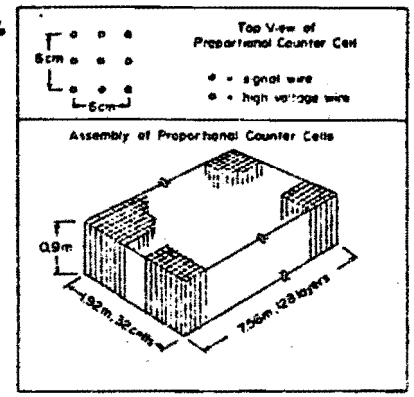

Schematic representation of the BEBC EPI.

W. Bugg (Tennessee) described another relativistic-rise detector and presented some estimates of its anticipated performance with the Fermilab hybrid system. This device is a smaller version of ISIS, the device being developed at Oxford for use with the CERN rapid-cycling bubble-chamber hybrid system. ISIS consists of a 1 m × 4 m × 5 m drift chamber which

contains 330 signal wires with a 1.5 cm spacing (see the illustration below).

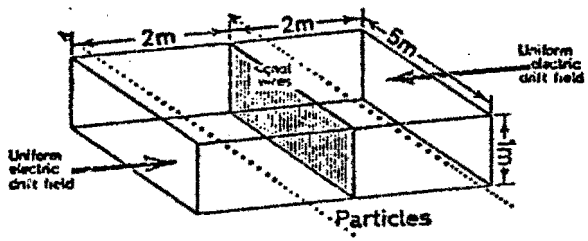

Schematic representation of the Oxford ISIS.

The pulse-height resolution predicted for the mean of the 330 1.5 cm samples is 6.2% FWHM. The time resolution of the signal collection is 250 nsec and thus, with a 2 cm/μsec drift velocity, measurements on tracks within roughly 1 cm of each other cannot be used. A full-scale ISIS has not yet been tested, but extensive studies of both its drift chamber and relativistic-rise aspects have been carried out. There are some stringent constraints on gas purity and field uniformity for operation with a full 2 m drift space, but these disappear if the drift-space dimension is decreased to 50 cm. Such a device could be operated with commercial bottled gas (purity 2 ppm) and an off-the-shelf power supply. Thus it is proposed that three sections of a 1 m × 1 m × 1 m ISIS-type device be constructed, each containing 66 wires at a 1.5 cm spacing, permitting a total of 198 1.5 cm samples of the ionization and a corresponding 7.8% FWHM resolution. The figure at the top of the next page gives the percentage of misidentified K-mesons as a function of particle momentum corresponding to this resolution and this device is seen to give better than 70% K identification from 5 to 30 GeV/c. The figure at the top of page 26 gives the rapidity distribution both for all particles and for those

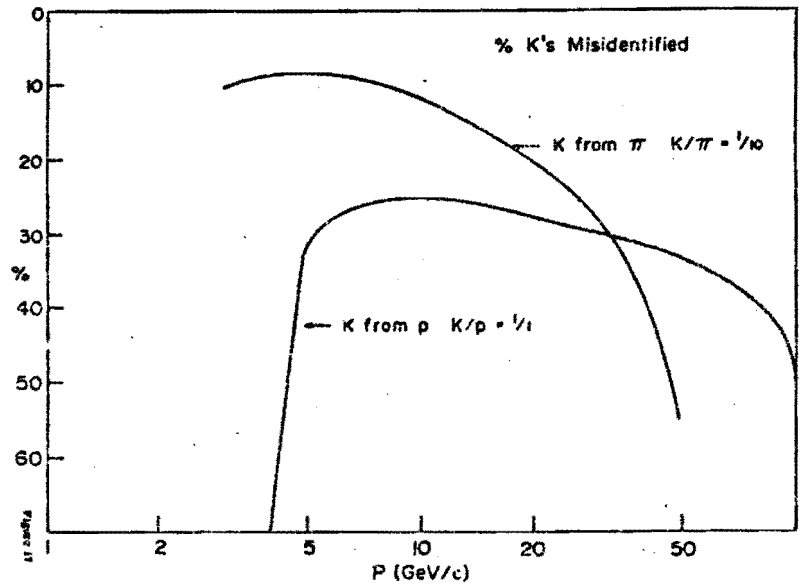

The percentage of K mesons which are misidentified in a relativistic rise detector with 8% FWHM resolution at a function of momentum for π/K/p = 10/1/1.

which both pass through ISIS and have momentum, $5 < p < 40$ GeV/c. At 300 GeV/c, 18% of all particles and 30% of those escaping the magnet satisfy these criteria. One topic of importance to all varieties of particle identifiers is the question of charged-particle background, since a background particle passing through the same cell as a particle from the event renders the information from that cell not useable. A background study has been carried out using the proportional wire counter data for several hundred events chosen at random from E-154 (π^-p at 147 GeV/c) and E-299 (π^+p at 150 GeV/c). The percentage of cells which must be discarded is estimated to be 25% for

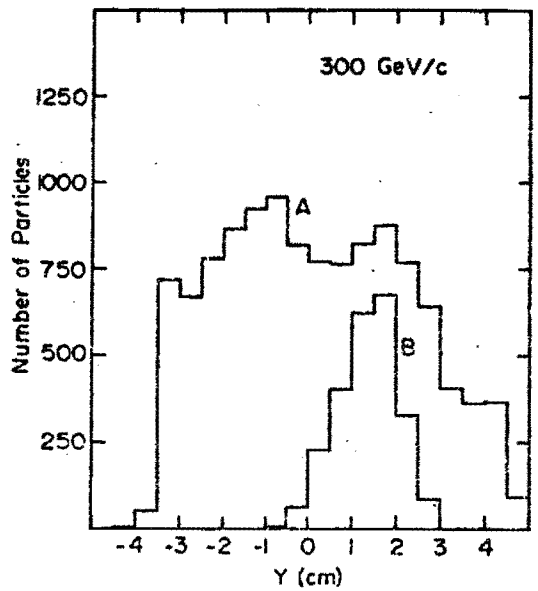

The number of particles as a function of rapidity from simulated 300 GeV/c $\pi^- p$ interactions: A) all particles, B) those particles with $5 < p < 40$ GeV/c which pass through 13 in the figure on page 27.

an ISIS (1 cm cells) and 51% for an EPI (6 cm cells), both located 2 meters from the bubble chamber center, with the current bubble chamber configuration. Improvements in the background could be made by reductions in the amount of matter downstream of the bubble chamber. The cost estimated by the Oxford group for a 1 m × 1 m × 1 m ISIS module is $17,200; thus, including provision for contingencies, a conservative estimate would be $30,000 per module. The first module could be constructed in 6-9 months and the remaining modules could be completed within a year at a total cost of $100,000 plus salaries.

L. Pless (MIT) presented a proposal agreed upon by the workshop for a system which would permit both "central-region" physics (5-50 GeV/c) and "leading-particle" physics (50-100 GeV/c). This system is shown in the figure below and would consist of three elements: an ISIS consisting of three 1 m × 1 m × 1 m sections interspersed with drift chambers (5-50 GeV/c), a 2 m × 2 m × 5 m multi-cell atmospheric pressure N_2-He Cerenkov detector (50-100 GeV/c), and the photon detector. The photon and Cerenkov detectors

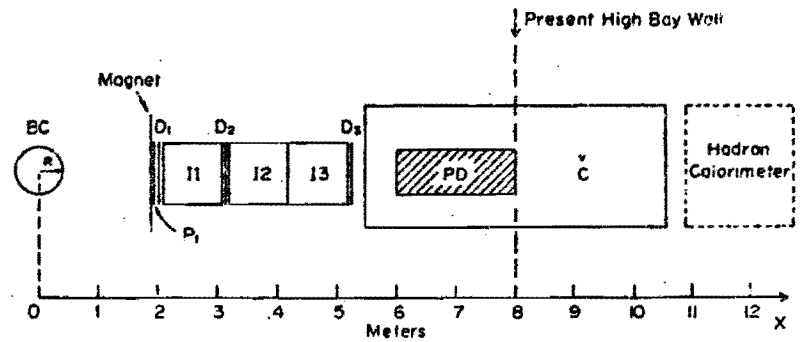

The particle identification system proposed in the recommendations of the workshop for the Fermilab 30-in. bubble chamber hybrid system. I1, I2, and I3 are 1 m × 1 m × 1 m ISIS-type modules; C is a 2 m × 2 m × 5 m multi-cell Cerenkov detector; P_1 is a proportional wire counter; and D_1, D_2, D_3 are drift chambers. The location of the photon detector (PD) and possible location of a future hadron calorimeter are also shown.

could not be used simultaneously and would be mounted on rails for easy interchange. This arrangement would necessitate an addition to the present high-bay area which would accommodate either the Cerenkov or the photon detector when not in use. At a future date, this could be expanded to include a neutral-hadron calorimeter for $n/\bar{n}$ detection. The workshop had been asked to consider 12 aspects of particle identifier systems (NALREP, p. 19,

March, 1976). The proposed system has (1) operating parameters of $\pi/K/p$ separation from 5-100 GeV/c and (2) an acceptance that is reasonably well matched to the geometric profile of the particles leaving the bubble chamber. (3) The background sensitivity is acceptable and (4) the problems of gas handling and purity are minimized since commercially available bottled gas (2 ppm impurity) is satisfactory. (5) The readout electronics can use elements already available and this problem and (6) that of off-line computing are already solved in principle. (7) The system is compatible with photon detection and high-resolution momentum measurements and (8) requires no drift chambers or proportional wire counters other than those already in existence or under construction for the hybrid system. (9) A modest extension of the building will be necessary, but not a crane. (10) The maintenance requirements will be about the same as those of the present system, and (11) the system poses no safety problems. (12) The construction and testing of ISIS would be carried out by the PHSC and that of the Cerenkov detector, by Michigan State University. Conservative estimates of the costs are respectively $100,000 and $30,000. The construction, initial test and installation schedule would involve 6 to 9 months for construction, 1 to 2 months for testing and 3 months for installation, for a total of 12 to 15 months. The PHSC would assume overall responsibility for the integration of these detectors with the proportional hybrid system.